Investigation of Titania and Silica Based Inorganic Ionogels and Eutectogels as Electrolytes for Electrochemical Supercapacitors

A Thesis submitted in partial fulfilment of the requirements

for the degree of

Doctor of Philosophy

in

Chemical Engineering

by

Arindam Dutta

Department of Chemical Engineering
Indian Institute of Technology Guwahati
Guwahati, Assam – 781039, India

School of Molecular and Life Sciences
Curtin University
Perth, WA – 6102, Australia

June 2024

Investigation of Titania and Silica Based Inorganic Ionogels and Eutectogels as Electrolytes for Electrochemical Supercapacitors

A Thesis submitted in partial fulfilment of the requirements

for the degree of

Doctor of Philosophy

in

Chemical Engineering

by

Arindam Dutta

Department of Chemical Engineering
Indian Institute of Technology Guwahati
Guwahati, Assam – 781039, India

School of Molecular and Life Sciences
Curtin University
Perth, WA – 6102, Australia

June 2024

Dedicated to all those navigating the complexities of mental health; may this thesis serve as a beacon of resilience and hope in your journey towards healing and well-being.

Statement

I hereby declare that the content embodied in this thesis entitled **"Investigation of Titania and Silica Based Inorganic Ionogels and Eutectogels as Electrolytes for Electrochemical Supercapacitors"** is the result of investigations carried out by me at the Department of Chemical Engineering, Indian Institute of Technology Guwahati, Guwahati, India under the supervision of **Prof. Tamal Banerjee** and at the School of Molecular and Life Sciences, Curtin University, Perth, Australia under the supervision of **Prof. Debbie Silvester-Dean** and **Prof. San Ping Jiang**.

In keeping with the general practice of reporting scientific observations, due acknowledgements have been made wherever the work described is based on the findings of other investigators.

Arindam Dutta

Guwahati, India
June, 2024

Roll no. (IIT Guwahati): 186107103
Student ID (Curtin University): 20375115

Certificate

It is certified that the work described in this thesis entitled **"Investigation of Titania and Silica Based Inorganic Ionogels and Eutectogels as Electrolytes for Electrochemical Supercapacitors"** by Mr. Arindam Dutta for the award of the degree of Doctor of Philosophy is an authentic record of the results obtained from the research work carried out under our supervision at the Department of Chemical Engineering, Indian Institute of Technology Guwahati (India) and the School of Molecular and Life Sciences, Curtin University (Australia). To the best of our knowledge, this work has not been submitted elsewhere for a degree.

Prof. Tamal Banerjee
Professor
Department of Chemical Engineering
IIT Guwahati, Guwahati
Assam – 781039, India

Prof. Debbie Silvester-Dean
Professor
School of Molecular and Life Sciences
Curtin University, Perth
Western Australia – 6102, Australia

Prof. San Ping Jiang
Professor
WASM: Minerals, Energy and Chemical Engineering
Curtin University, Perth
Western Australia – 6845, Australia

Acknowledgements

"We learned about gratitude and humility – that so many people had a hand in our success."

- Michelle Obama

Today, as I step into the end of the beginning of my journey as a researcher, I am profoundly grateful to the multitude of individuals whose unwavering support and guidance have directly or indirectly helped me thrive. Their collective wisdom, encouragement, and assistance have not only propelled me through the challenges encountered but have also enriched the fabric of my academic pursuit for a doctorate.

To begin with, I extend my deepest gratitude to my esteemed supervisors, **Prof. Tamal Banerjee** (IIT Guwahati), **Prof. Debbie Silvester-Dean** (Curtin University), and **Prof. San Ping Jiang** (Curtin University), for their constant support that has been a guiding light throughout my doctoral journey. Their mentorship has been crucial in shaping the trajectory of my research, providing not only academic guidance but also invaluable personal and professional insights. Their leadership extended beyond the confines of academia, fostering a sense of camaraderie and team-bonding through periodic outings of the research groups at the respective institutes. These gatherings not only provided moments of respite but also nurtured a supportive environment where ideas could flourish and collaborations could thrive. Despite their busy schedules, Prof. Banerjee and Prof. Debbie consistently made time to arrange meetings and address my doubts, offering valuable insights and guidance. Their coordination, efforts, and support were particularly evident in facilitating my visit to Curtin University as a part of the collaborative doctoral program. In a remarkable display of dedication, Prof. Debbie was kind enough to get my air tickets arranged through the School of Molecular and Life

Sciences (MLS) at Curtin, ensuring a seamless transition to and from Australia. I am truly fortunate to have had the opportunity to learn from their expertise and leadership, and I am deeply indebted to them for their invaluable contributions to my academic journey.

I am also sincerely thankful to the members of my Doctoral Committee and Viva-Voce Examination Board, **Prof. Gopal Pugazhenthi** (Chairperson), **Prof. Vaibhav Vasant Goud**, **Assoc. Prof. Manas Das**, **Prof. Mahuya De**, **Assoc. Prof. Prasanna Venkatesh Rajaraman**, **Assoc. Prof. Sreeja Pekkat** at IIT Guwahati, and **Assoc. Prof. Hari Vuthaluru** (Chairperson) at Curtin University. I would also like to thank the external examiners of my doctoral thesis, **Prof. Suryasarathi Bose** of the Indian Institute of Science and **Prof. Matthew J. Panzer** of Tufts University for their time and constructive comments on my thesis. Their insightful feedback, rigorous evaluation, and constructive criticism have been instrumental in refining the quality of my work and successfully complete my PhD.

I also extend my sincere gratitude to my coursework instructors at IIT Guwahati, **Prof. Vijayanand Suryakant Moholkar**, **Prof. Dipankar Bandyopadhyay**, **Prof. Mihir Kumar Purkait**, **Prof. Vaibhav Vasant Goud**, **Assoc. Prof. Pankaj Kalita**, and *the late* **Asst. Prof. Harsh Chaturvedi**. Their insightful lectures, challenging assignments, and valuable feedback have equipped me with the knowledge and skills necessary to excel in my research endeavors. Furthermore, I am grateful to the members of my Comprehensive Examination Committee at IIT Guwahati, **Prof. Vaibhav Vasant Goud** (Chairperson), **Assoc. Prof. Pankaj Kalita**, and *the late* **Asst. Prof. Harsh Chaturvedi** for their rigorous examination of my knowledge in the field. Their probing questions, insightful feedback, and constructive criticism challenged me to articulate my understanding of the subject matter with clarity and precision. Special thanks to my Teaching Assistant (T.A.) supervisors, **Asst. Prof. Omkar Suresh Deshmukh**, **Prof. Tamal Banerjee**, **Assoc. Prof. Anandalakshmi Ramalingam**, and **Prof. Ashok Kumar**

Dasmahapatra for their mentorship and support. However, I was deeply saddened by the untimely demise of Dr. Chaturvedi in 2023 and I extend my heartfelt condolences to his family, friends, and colleagues he was survived by. His presence and contributions will be sorely missed.

I am deeply appreciative of the staff at the two institutes for their dedication in ensuring the smooth functioning of various pertinent departments and facilities during the timeframe of my research. These include the **office** and **analytical laboratory** of **Chemical Engineering** (CL), **Centre for the Environment**, **Finance and Accounts**, **Academic Affairs** (AA), **Students' Affairs** (SA), **Store and Purchase**, **Alumni and External Relations** (AER), **Central Instruments Facility** (CIF), the **PARAM-ISHAN** and **PARAM-KAMRUPA** supercomputing facilities, the **Lakshminath Bezbaroa Central Library,** and **Cores 3 and 4** at IIT Guwahati, as well as **MLS**, the **Western Australian School of Mines: Minerals, Energy and Chemical Engineering** (WASM), and the **Graduate Research School** at Curtin University. In the face of unprecedented challenges posed by the global pandemic, their constant endeavors are worth reiterating. The agility with which they adapted to the changing circumstances during COVID-19, ensuring continuity in academic and administrative processes, has been truly commendable. Their efforts not only facilitated the progression of my research but also created a supportive environment that allowed me to navigate those challenging times with resilience.

In this regard, I would particularly like to mention the assistance extended to me in IIT Guwahati by **Prof. Kaustubha Mohanty** (Head, CL), **Prof. Anugrah Singh** (former Head, CL), **Prof. Bishnupada Mandal** (former Head, CL), **Prof. Chandan Das** (former acting Head, CL), **Prof. Tamal Banerjee** (former acting Head, CL), **Prof. Vaibhav Vasant Goud** (former acting Head, CL), **Prof. Rakhi Chaturvedi** (former Dean, AER), **Prof. Mihir Kumar Purkait**

(former Dean, AER), **Prof. Chitralekha Mahanta** (former Dean, AA), **Prof. Kanduru Venkata Krishna** (Dean, AA), **Prof. Bulu Pradhan** (Assoc. Dean, AA), **Mr. Wanshai Shynret** (Asst. Registrar), **Mr. Harsaraj Biswanath** (Technical Officer Grade I), **Mr. Ariful Hoque** (Junior Technical Superintendent), **Mr. Deep Jyoti Sinha** (Senior Assistant), **Ms. Chinmayee Pathak** (Senior Assistant), **Mr. Riju Mahato** (Junior Assistant), and **Mr. Paragjyoti Sharma** (Senior Assistant) and in Curtin University by **Prof. Abhijit Mukherjee** (Dean International South Asia), **Prof. Garry Allison** (Associate Deputy Vice Chancellor – Research Training), **Dr. Catherine Boisvert** (Director of Graduate Research, MLS), **Mr. Marcus Tey** (Administrative Officer, MLS), **Mr. Peter Chapman** (Senior Technical Officer), and **Assoc. Prof. Hussein Znad** (former Director of Graduate Research, WASM) in their respective capacities during their tenures.

Moreover, I am indebted to **Prof. Dipankar Bandyopadhyay** (IIT Guwahati) and **Prof. Damien Arrigan** (Curtin University) for kindly letting me use the potentiostats in their laboratories to conduct electrochemical experiments. I thank **Assoc. Prof. Partho Sarathi Gooh Pattader** (IIT Guwahati) for kindly allowing the conduction of goniometric measurements in his laboratory. Furthermore, **Prof. George Zheng Chen** of the University of Nottingham deserves a special mention for his patience and selfless dedication in addressing my academic inquiries on multiple occasions over emails and ResearchGate. I am thankful to **Asst. Prof. Biraj Kumar Kakati** (Tezpur University) for imparting his knowledge on energy storage technologies to me. I also acknowledge the **Indian Institute of Science**, Bangalore for permitting the conduction of thermal analysis and the **Vikram Sarabhai Space Centre**, India for the kind donation of the exfoliated electrodes utilized in this research. I extend my sincere thanks to the **Indian Ministry of Education** and **Curtin University** for supporting my research with a Doctoral Fellowship and a Curtin International Postgraduate Research

Scholarship (CIPRS). **Global Reach, Guwahati** is thanked for their kind assistance with the Australian visa process.

The roles of my preceding academic institutes, **Assam Engineering College** (AEC, Gauhati University) and the **Australian National University** (ANU), where I completed my Bachelors and Masters, are immense, as they built my base and garnered in me the confidence to pursue higher education. In this context, I would like to thank **Prof. Amrita Ganguly** (AEC), **Dr. Fiacre Rougieux** (University of New South Wales), **Dr. Fiona Beck** (ANU), and **Dr. Andrew Thomson** (Squadron Energy, Australia) for being my referees in the PhD application processes for IIT Guwahati and Curtin University. I would not have been writing this thesis today, had their supportive recommendations not help the applications make the cut. **Assoc. Prof. (Retd.) Farhana Parveen** (AEC) deserves special mention for her constant motivation since my baccalaureate days.

I express my deepest appreciation to my academic mentors, mates, and the collaborative spirit of the research community at the two institutes. I am grateful to **Dr. Debashis Kundu** for introducing me to the fundamentals of experimental processes. Special thanks to **Dr. Jinesh Subhash Machale** for guiding me through the application process of the collaborative doctoral program. My gratitude extends to **Dr. Upasana Mahanta** and **Dr. Pyarimohan Dehury** specifically for conceptualizing the design of the coin cell used in this research**.** I am also thankful to **Dr. Papu Kumar Naik**, **Dr. Shirsendu Mitra**, **Dr. Dhirendra Kumar Mishra**, **Dr. Venkateswara Rao Chebrolu**, and **Dr. Nikhil Kumar** for their guidance and assistance at various stages. I acknowledge **Dr. Nabendu Paul**, **Mr. Nipu Kumar Das**, and **Mr. Sai Dileep Kumar Seera** for their ever-ready attitude to help and for contributing to my research by assisting in various experimental and computational analyses. I am also thankful to **Mr. Prathu Raja Parmar** and **Mr. Nayan Moni Baishya** for their kind assistance with Raman

and X-ray diffraction characterization. I shall be forever indebted to **Dr. Surbhi Sharma** and **Mr. Wade Millar** for their tremendous assistance with the electrochemical experiments. Furthermore, I am thankful to **Mr. Harish Kumar Bhupathi**, **Ms. Sambita Choudhury**, **Ms. Swetha Thimirishetty**, **Ms. Diksha Jaiswal**, **Mr. Raghibul Hussain**, **Ms. Mitali Basak**, **Mr. Pratyay Singh**, **Mr. Harsh Singh Thakur**, **Mr. G. Harish**, **Mr. Uday Mhapsekar**, **Ms. Anushka Raj Lakshmi**, **Mr. Rajib Nandi**, **Mr. Mangal Singh**, **Mr. Hrishikesh Sarma**, **Mr. Shamim Reza Hussain**, **Ms. Antaripa Saha**, **Mr. Mohammad Kalim Khan**, **Dr. Yunxiao Zhang**, **Ms. Natasha Hoffmann**, **Ms. Sarah Linden**, **Mr. Jesse Mullen**, **Ms. Rabia Jamil**, **Mr. Hum Lamichhane**, **Mr. Hasim Munawar**, **Ms. Stephie Uzice**, **Mr. Mitchell Newbert**, **Mr. Ahmed Matan**, **Mr. Jack Arnold**, **Mr. Dylan Palmer**, and all fellow researchers of CL (IIT Guwahati) and Building 500 (Curtin University) for various assistances and providing a cooperative research environment. It has been a wonderful experience sharing the same work space with them and getting to connect with some of them and their families at a personal level.

I would like to acknowledge the contributions of the wardens, staff, security personnel, and fellow residents of **Brahmaputra Hostel** (IIT Guwahati) and **St Catherine's College** (Curtin University) in creating a safe, warm, and welcoming environment during my stay. Their dedication to ensuring a comfortable living experience and fostering a sense of community within these residential settings have provided a sense of belonging that has enriched my academic experience. I extend my heartfelt appreciation to all those who contributed to making my time at the two residences memorable and enjoyable.

Treading through the roads to a doctorate can be accompanied by moments of challenge and introspection, both personally and academically. It is during these gloomy times that the support of mentors, colleagues, friends, and family becomes even more crucial. In this context, I am deeply grateful for the exceptional support provided by **Ms. Pallabita Barooah**

Chowdhury, my student mental-health counsellor at IIT Guwahati. Her empathetic guidance and understanding played a pivotal role in helping me overcome challenges, providing a safe space to discuss personal and academic concerns. Ms. Chowdhury's contribution to my well-being during these times has been immeasurable, and her encouragement has been a beacon of light during the darker days of my academic journey. I am also grateful for the friendship extended to me by **Mr. Jiwajyoti Mahanta**, **Mr. Sumantra Chaudhuri**, **Mr. Prabhakar Choudhary**, and **Mr. Anil Kumar Tripathy** in the form of immense support, encouragement, helpful suggestions, and patience in bearing with me during troubled and dilemmatic times. **Dr. Sampreet Kalita**, my first cousin and a fellow researcher, deserves special mention for backing me throughout the entire journey. The contributions of my colleagues and friends, **Mr. Nikhil Rahul Dhongde**, **Ms. Sayani Adhikari**, **Mr. Vinod Babasaheb Vanarse**, **Mr. Mrinal Roy**, **Mr. Gaffer Ahmed**, **Dr. Sneha Acharya**, **Ms. Adity Bora**, **Ms. Panchali Borthakur**, **Ms. Trinakshee Sarmah**, and **Mr. Bharat Terang** cannot be pretermitted. Beyond academia, my friends, **Ms. Dipanyta Datta**, **Ms. Snigdha Brahma**, **Ms. Dhanya Varshini Elangovan**, **Mr. Mayank Singh,** and **Ms. Fortune Tormeti** have had an immense role in enriching my life in numerous ways. I thank the entire team of ***Bohagor Duwardolit*** for making my doctoral journey lively and memorable.

A special mention goes to my parents, **Mrs. Mayashree Kalita Dutta** (mother) and **Mr. Utpal Dutta** (father), who have been my pillars of strength throughout this journey. Their unconditional love, unflinching support, and endless sacrifices have been the driving force behind my pursuit of knowledge. Not only have they provided emotional and moral support, but their financial assistance during challenging times has been a lifeline, enabling me to focus on my academic pursuits without added stress. **Mr. Hemango Akshay Hiwale**, a special friend and a constant source of encouragement, deserves special recognition for his unwavering support. I have been fortunate to have him always standing by me as a source of solace during

challenging times. His companionship, motivation, affection, and care have been my strength that fueled my determination to overcome obstacles. I will always be indebted to my *late* ***Didun*** (paternal grandmother), ***Aaita*** (maternal grandmother), **relatives**, **teachers**, **cousins**, **friends**, and **well-wishers** for their love and keeping me in their prayers. Last, but not the least, I offer heartfelt gratitude to the **Almighty**, whose guidance and blessings have illuminated my path and sustained me through every challenge and triumph.

Arindam Dutta

Abstract

As countries and regions establish stringent goals for embracing renewable and sustainable technologies, there has been a dramatic surge in global demand for energy storage solutions. Supercapacitors, in particular, are acclaimed for their high power density, good cycling capacity, and comparatively safer design and operation with minimal environmental impacts. Currently, novel materials and new storage chemistry solutions are being explored to realize storage technologies for the next generation, which include all-solid-state supercapacitors. This step-change includes fundamental research in the design of new electrolytes. In this context, ionogels and eutectogels derived respectively from ionic liquids (ILs) and deep eutectic solvents (DESs) are gaining popularity because of their ability to overcome the drawbacks of their liquid counterparts, while retaining certain beneficial qualities of the latter.

This doctoral thesis explores and compares three primary types of gel electrolytes obtained from a simple sol-gel physical confinement of ILs, natural DESs (NADESs), and an IL-based hybrid DES into an inorganic matrix of titania or silica. The properties of the gels are studied via different characterization techniques which primarily include field emission scanning electron microscopy (FESEM), field emission transmission electron microscopy (FETEM), rheology, Fourier transform infrared (FTIR) spectroscopy, X-ray diffraction (XRD), and thermogravimetric analysis (TGA). Furthermore, their compatibility with symmetric supercapacitors based on reduced graphene oxide (rGO) electrodes is investigated using cyclic voltammetry (CV) and electrochemical impedance spectroscopy (EIS).

For the ionogels, seven different ILs are chosen and confined separately into TiO_2, yielding seven viscoelastic amorphous gels with evident porosity and unaffected structural integrity. However, a reduced thermal stability is observed in each case due to weak non-

bonded interactions between titania surface and IL molecules. Nevertheless, the stability windows are sufficient for potential moderate to high-temperature applications, with the ionogels containing the anion bis(trifluoromethylsulfonyl)imide ($[TFSI]^-$) exhibiting the best thermal stability among all. All the seven ionogels demonstrate a double-layer capacitive behavior within a wide potential window of 4 V, underscoring their compatibility with rGO electrodes and excellent stability in electric double-layer capacitors (EDLCs). Of them, the ionogel based on the IL 1-ethyl-3-methylimidazolium trifluorotris(pentafluoroethyl)phosphate ([EMIM][FAP]) exhibits the best electrochemical performance, delivering the highest specific capacitance (11.5 F g^{-1} or 277.7 mF cm^{-2}), lowest equivalent series resistance (ESR) (36.2 Ω), and highest ionic conductivity (1.3 mS cm^{-1}) at room temperature. The values of maximum energy and power delivered by the system stand at 25.4 W h kg^{-1} and 6.4 kW kg^{-1}. Moreover, the ionogel is able to maintain its operating potential window (OPW) and EDLC characteristics at controlled temperatures of 25 and 50 °C, while showing an increase in specific capacitance and ionic conductivity by factors of 1.6 and 5.9 respectively, at the latter temperature.

Subsequently, eight amorphous and porous eutectogels are obtained from four carboxylic-acid- and DL-Menthol-based NADESs by immobilizing each DES into solid matrices of TiO_2 and SiO_2. Again, in each case, the structural integrity of the DESs remain intact, however their thermal stability is altered after immobilization. A difference in the interactive nature of the two matrices with the DESs is revealed by the variation in the vibrational shifts and degradation temperatures of the titania- and silica-tethered eutectogels. The gels exhibit EDLC characteristics within an impressively wide voltage window of 4 V, a rare feat for DES gels. This ensures their excellent compatibility and stability with rGO-based EDLCs. However, specific capacitance and specific energy values reaching only up to 0.9 mF g^{-1} (86.8 µF cm^{-2}) and 2.2 mW h kg^{-1} are obtained due to high intrinsic resistance in the systems, as confirmed from EIS analyses. Consequently, maximum values of ionic conductivity and

power achieved are only 0.03 mS cm^{-1} and 65.4 mW kg^{-1}, respectively. Interestingly, introducing an IL to the gels significantly reduces the internal resistance, escalating the maximum capacitance and conductivity to 47.7 F g^{-1} (2087 mF cm^{-2}) and 16.3 mS cm^{-1}.

Finally, two IL-based eutectogels anchored with TiO_2 and SiO_2 are prepared using the hybrid DES comprising of the IL 1-butyl-3-methylimidazolium methanesulfonate ([BMIM][$MeSO_3$]) and *N*-methylacetamide (NMAc). These eutectogels, like their two other counterparts, retain the structural integrity of their parent solvent whilst possessing porous and amorphous characteristics. An alteration in the thermal stabilities of the DES constituents is also observed after gelation on account of the interactions between the DES and the matrices. These gels confirm the different interactive natures of the two matrices through differences in vibrational shifts and degradation temperatures. The hybrid DES is able to maintain its double-layer capacitive behavior and 3 V OPW after confinement into either matrix, again highlighting the suitability of the gels with EDLCs and rGO electrodes. Between the two, the titania-based gel delivers higher specific capacitance (16.3 F g^{-1} or 395.8 mF cm^{-2}) and specific energy (20.4 W h kg^{-1}) with a lower ESR (39.6 Ω) and higher ionic conductivity (1.3 mS cm^{-1}), allowing the device to deliver a power of 3.3 kW kg^{-1}. The same gel also maintains its OPW and EDLC properties across controlled temperatures of 25, 50, and 80 °C, exhibiting notable improvement in specific capacitance and ionic conductivity by factors of 3 and 4.4 respectively, at 80 °C.

A schematic representation of the objectives and some of the important findings of the thesis is depicted in **Figure A**.

Keywords: *deep eutectic solvent, electrochemical energy storage, electrochemistry, eutectogel, ionic liquid, ionogel, operating potential window, solid electrolyte, supercapacitor*

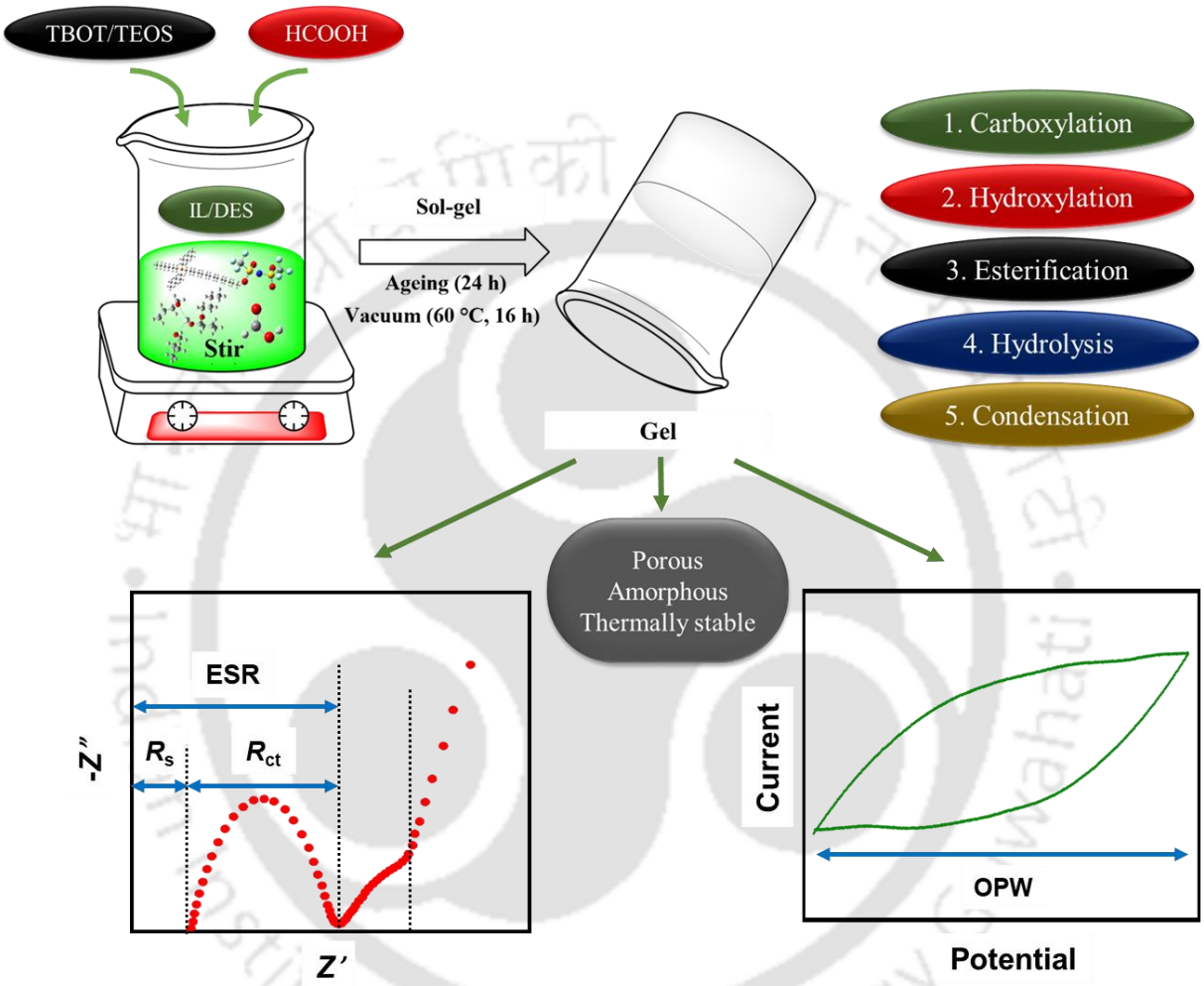

Figure A. Graphical abstract of the thesis work.

Table of Contents

List of Figures

भारतीय प्रौद्योगिकी संस्थान गुवाहाटी
Indian Institute of Technology Guwahati

List of Tables

Glossary

Abbreviations

AA	Acrylic Acid
AC	Activated Carbon, Alternating Current
AM	Acrylamide
AN	Acetonitrile
APS	Ammonium Persulfate
BET	Brunauer-Emmett-Teller
BPO	Dibenzoyl Peroxide
CA	Carbon Aerogel
CCD	Charge-Coupled Device
CE	Counter Electrode
ChCl	Choline Chloride
CNT	Carbon Nanotube
C-PVA	Crosslinked Polyvinyl Alcohol
CV	Cyclic Voltammetry
DBS	1,3:2,4-Dibenzylidene-d-sorbitol
DC	Direct Current
DEM	Deep Eutectic Monomer
DES	Deep Eutectic Solvent
DEX	Dexamethasone
DFT	Density Functional Theory
DoE	Department of Energy

DMAA	*N*,*N*-dimethylacrylamide
DMDMS	Dimethyldimethoxysilane
DMSO-d_6	Deuterated Dimethyl Sulfoxide-d6
DSC	Differential Scanning Calorimetry
DSSC	Dye-Sensitized Solar Cell
EC	Ethylene Carbonate
EDL	Electric Double Layer
EDLC	Electric Double-Layer Capacitor
EG	Ethylene Glycol
EIS	Electrochemical Impedance Spectroscopy
ESPW	Electrochemical Stability Potential Window
ESR	Equivalent Series Resistance
EV	Electric Vehicle
FA	Formic Acid
FESEM	Field Emission Scanning Electron Microscopy
FETEM	Field Emission Transmission Electron Microscopy
FRA	Frequency Response Analyzer
FTIR	Fourier Transform Infrared
GCD	Galvanostatic Charge-Discharge
HBA	Hydrogen Bond Acceptor
HBD	Hydrogen Bond Donor
HEMA	2-Hydroxyethyl Methacrylate
HEV	Hybrid Electric Vehicle
IL	Ionic Liquid
ITO	Indium Tin Oxide

LIB	Lithium-Ion Battery
LMWOG	Low Molecular Weight Organogelators
LVE	Linear Viscoelastic
MA	Maleic Acid
MBAA	Methylene-bis-acrylamide
MD	Molecular Dynamics
MOF-C	Metal-Organic-Framework-Carbon
MWCNT	Multi-Walled Carbon Nanotube
NADES	Natural Deep Eutectic Solvent
NEC	Nippon Electric Company
NMAc	*N*-Methylacetamide
NMR	Nuclear Magnetic Resonance
OCP	Open Circuit Potential
OFET	Organic Field-Effect Transistor
OPW	Operating Potential Window
Or	Orcinol
PA	Phenylacetic Acid
PAA	Polyacrylic Acid
PAAM	Polyacrylamide
PC	Propylene Carbonate
PEGDA	Poly(Ethylene Glycol) Diacrylate
PEGMA	Poly(Ethylene Glycol) Methacrylate
PEO	Polyethylene Oxide
PHEMA	Poly(Hydroxyethyl Methacrylate)
PHEV	Plug-in Hybrid Electric Vehicle

PP	Polypropylene
PTFE	Polytetrafluoroethylene
PVDF	Polyvinylidene Fluoride
PVDF-HFP	Poly(Vinylidene Fluoride-co-Hexafluoropropylene)
QC	Quantum Chemical
rGO	Reduced Graphene Oxide
RTIL	Room Temperature Ionic Liquid
SDG	Sustainable Development Goal
sIPN	semi-Interpenetrating Polymer Network
SOHIO	Standard Oil Company, Cleveland, Ohio
SPEEK	Sulfonated Poly(Ether Ether Ketone)
SPME	Solid-Phase Microextraction
TBOT	Titanium Butoxide / Tetrabutyl Orthotitanate
TCW	Transparent and Conductive Wood
TEOS	Tetraethyl Orthosilicate
TGA	Thermogravimetric Analysis
THEDES	Therapeutic Drug-Eluting Stent
TMOS	Tetramethoxysilane
VACNT	Vertically Aligned Carbon Nanotube
WE	Working Electrode
XRD	X-Ray Diffraction

English Symbols

A	Ampere
A	Cross-sectional area of active portion
Al	Aluminum
Ar	Argon
B	Boron
c	Centi
C	Carbon
C	Capacitance
C_c	Contact capacitance
C_d	Double-layer capacitance
C_{sp}	Specific capacitance
Cl	Chlorine
Co	Cobalt
Cr	Chromium
Cu	Copper
°C	Degree Celsius
d	Interplanar crystal spacing
E	Energy
E_{sp}	Specific energy
eV	Electron volt
F	Farad, Fluorine
Fe	Iron
g	Gram

G'	Storage modulus
G''	Loss modulus
Ga	Gallium
h	Hour
H	Hydrogen
Hz	Hertz
I	Current
In	Indium
k	Kilo
K	Kelvin, Potassium
L	Liter
Li	Lithium
m	Milli, Meter
m	Consistency index, Mass of electrode
M	Mega
min	Minute
n	Nano
n	Integer, Power law index
N	Nitrogen
Na	Sodium
Ni	Nickel
O	Oxygen
P	Phosphorus
P	Power
Pa	Pascal

ppm	Part per million
Q	Charge
R^2	Square of correlation coefficient
R_{ct}	Charge-transfer resistance
R_s	Solution resistance
s	Second
S	Siemen, Sulfur
Si	Silicon
Sn	Tin
t	Thickness of electrolyte pellet or distance between electrodes
$T_{5\%}$	Temperature at which 5 % of mass is lost
T_{cd}	Temperature at which complete decomposition occurs
T_g	Glass-transition temperature
T_m	Endothermic melting point
Ti	Titanium
V	Volt
V	Voltage / Potential
V_a	Initial voltage
V_b	Final voltage
W	Watt
wt%	Weight percent
Z	Impedance
Z'	Real component of impedance
Z''	Imaginary component of impedance
Z_w	Warburg impedance

Zn	Zinc

Greek and Swedish Symbols

Å	Angstrom
σ	Ionic conductivity
θ	Incident angle
μ	Micro
Ω	Ohm
ν	Scan rate, Vibration
δ	Scissoring
γ	Shear rate
η	Viscosity
λ	X-ray wavelength

Ionic Liquids

[AMIM][TFSI] / IL4	1-Allyl-3-methylimidazolium bis(trifluoromethylsulfonyl)imide
[BMIM][BF_4]	1-Butyl-3-methylimidazolium tetrafluoroborate
[BMIM][I]	1-Butyl-3-methylimidazolium iodide
[BMIM][$MeSO_3$]	1-Butyl-3-methylimidazolium methanesulfonate
[BMIM][PF_6]	1-Butyl-3-methylimidazolium hexafluorophosphate
[BMIM][TFSI]	1-Butyl-3-methylimidazolium bis(trifluoromethylsulfonyl)imide
[BTMA][TFSI] / IL7	Butyl(trimethyl)ammonium bis(trifluoromethylsulfonyl)imide
[C_{16}MIM][TFSI]	1-Hexadecyl-3-methylimidazolium

	bis(trifluoromethylsulfonyl)imide
[DEIM][TFSI]	1,2-Dimethyl-3-ethoxyethylimidazolium bis(trifluoromethylsulfonyl)imide
[EMIM][BF_4]	1-Ethyl-3-methylimidazolium tetrafluoroborate
[EMIM][Br]	1-Ethyl-3-methylimidazolium bromide
[EMIM][FAP] / IL5	1-Ethyl-3-methylimidazolium trifluorotris(pentafluoroethyl)phosphate
[EMIM][TFSI]	1-Ethyl-3-methylimidazolium bis(trifluoromethylsulfonyl)imide
[EMIM][TCB]	1-Ethyl-3-methylimidazolium tetracyanoborate
[HMIM][BF_4] / IL3	1-Hexyl-3-methylimidazolium tetrafluoroborate
[HMIM][I]	1-Hexyl-3-methylimidazolium iodide
[MPIM][I]	1-Methyl-3-propylimidazolium iodide
[P_{66614}][DCA] / IL2	Trihexyl(tetradecyl)phosphonium dicyanamide
[PIP13][FSI]	*N*-methyl-*N*-propylpiperidinium bis(fluorosulfonyl)imide
[PMIM][TFSI] / IL6	1-Propyl-3-methylimidazolium bis(trifluoromethylsulfonyl)imide
[P_{66614}][TFSI] / IL1	Trihexyl(tetradecyl)phosphonium bis(trifluoromethylsulfonyl)imide
[PY14][FSI]	*N*-butyl-*N*-methylpyrrolidinium bis(fluorosulfonyl)imide
[PYR1,2o1][TFSI]	*N*-methoxyethyl-*N*-methylpyrrolidinium bis(trifluoromethanesulfonyl)imide
[PY13][TFSI]	*N*-methyl-*N*-propylpyrrolidinium bis(trifluoromethylsulfonyl)imide
[PY14][TFSI]	*N*-butyl-*N*-methylpyrrolidinium bis(trifluoromethylsulfonyl)imide
[TEA][BF_4]	Tetraethylammonium tetrafluroborate
[TEAPS][TFSI]	Triethylammonium propanesulfone bis(trifluoromethylsulfonyl)imide

Ionogels	
TIGel1	IL1 + Titania (TiO_2)
TIGel2	IL2 + TiO_2
TIGel3	IL3 + TiO_2
TIGel4	IL4 + TiO_2
TIGel5	IL5 + TiO_2
TIGel6	IL6 + TiO_2
TIGel7	IL7 + TiO_2

Deep Eutectic Solvents	
DES1	DL-Menthol + Decanoic acid
DES2	DL-Menthol + Lauric acid
DES3	DL-Menthol + Myristic acid
DES4	DL-Menthol + Palmitic acid
DES5	[BMIM][$MeSO_3$] + NMAc

Eutectogels	
TEGel1	DES1 + TiO_2
SEGel1	DES1 + Silica (SiO_2)
TEGel2	DES2 + TiO_2
SEGel2	DES2 + SiO_2
TEGel3	DES3 + TiO_2

SEGel3	DES3 + SiO_2
TEGel4	DES4 + TiO_2
SEGel4	DES4 + SiO_2
TIEGel	DES5 + TiO_2
SIEGel	DES5 + TiO_2

Chapter 1

Introduction, Literature Review, and Objectives of the Research

CHAPTER 1

Introduction, Literature Review, and Objectives of the Research

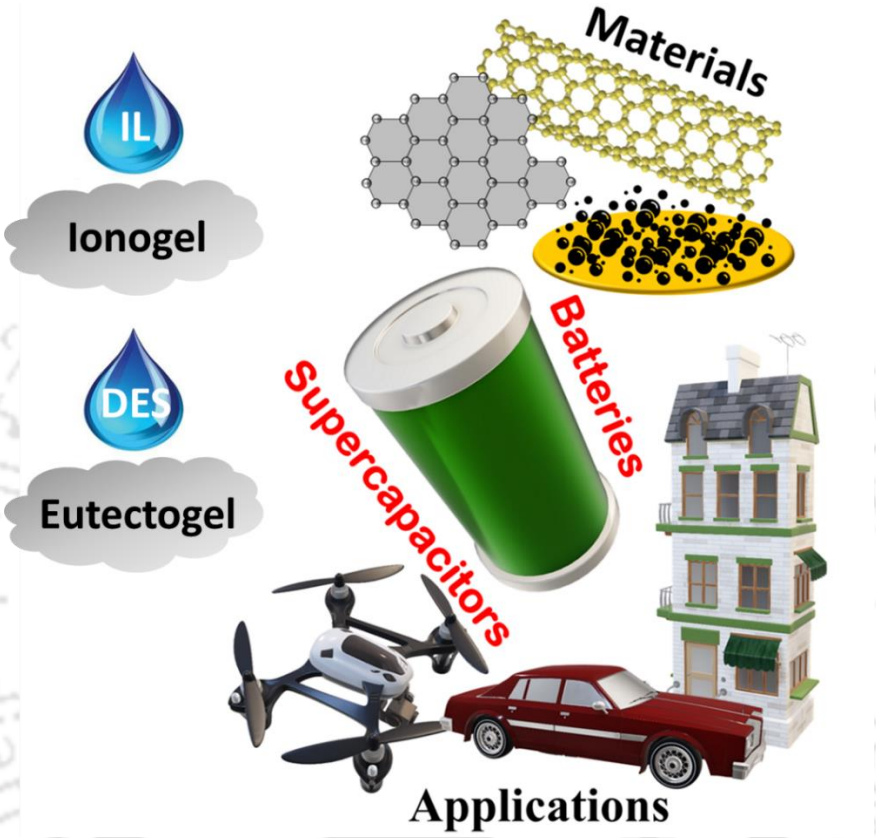

List of publications from Chapter 1:

(1) **Dutta, A.**; Mahanta, J.; Banerjee, T. Supercapacitors in the Light of Solid Waste and Energy Management: A Review. *Adv. Sustain. Syst.* **2020**, *4* (12), 2000182. https://doi.org/10.1002/adsu.202000182

(2) **Dutta, A.**; Mitra, S.; Basak, M.; Banerjee, T. A Comprehensive Review on Batteries and Supercapacitors: Development and Challenges since Their Inception. *Energy Storage* **2022**, *5* (1), No. e339. https://doi.org/10.1002/est2.339

1.1. Introduction

This chapter provides an in-depth background for the doctoral research, furnishing a comprehensive overview of supercapacitors and the diverse electrolytes associated with them. Additionally, the chapter introduces ionogels and eutectogels, derived from ionic liquids (ILs) and deep eutectic solvents (DESs), respectively. It critically examines some of the essential electrochemical characteristics of previously reported ionogels and eutectogels, highlighting the precursor materials and synthesis mechanisms employed in their preparation. The subsequent section briefly explores applications extending beyond the realm of energy storage. Following this, knowledge gaps and research problems are identified, and the objectives, scope, and organization of the thesis are delineated.

1.2. Background of the Research

The global demand for energy is steadily increasing in the contemporary society, raising concerns about the depletion and pollution caused by extensive usage of fossil fuels. In response to this challenge, significant research and technological advancements have been achieved in areas such as renewable energy, alternative energy sources, energy storage devices, and energy extraction from waste materials. Solar energy,[1,2] tidal energy,[3,4] and wind energy[5,6] are attractive alternatives for power generation among renewable sources of energy. However, the intermittent and unpredictable nature of these energy sources makes electricity economically viable only with the concurrent development of reliable and efficient energy storage systems. The extraction of power from any source necessitates the need for storage facilities to gather energy for intermittent use.[7–11] Furthermore, the storage of power is crucial for fulfilling immediate power needs and providing electricity to distant locations. Batteries and supercapacitors are dominant in the field of energy storage among the numerous electrochemical technologies available today. They are widely used in the energy sector.

Furthermore, they are highly intriguing in terms of their practicality and the exploration of fundamental scientific concepts through research and development endeavors. Over time, these disciplines have significantly developed in terms of both design and efficiency.

Recently, the transportation sector has emphasized the necessity of finding a balance between the energy and power density demands in storage systems. This has led to the development of hybrid electric vehicles (HEVs), plug-in hybrid electric vehicles (PHEVs), and full-electric vehicles (EVs). Batteries and supercapacitors are at the forefront of energy storage technologies, being utilized in a wide array of applications ranging from simple portable electronics to complex power grid networks.[12,13] Nevertheless, both of these technologies are incapable of satisfying all needs autonomously. A Ragone plot is an essential tool for evaluating the most appropriate energy technology for a particular application by comparing the energy and power densities of various storage/harvesting devices.[11] According to **Figure 1.1**, batteries are known for their high specific energy (W h kg^{-1}) or energy density (W h L^{-1}), while supercapacitors have higher specific power (W kg^{-1}) or power density (W L^{-1}).[14]

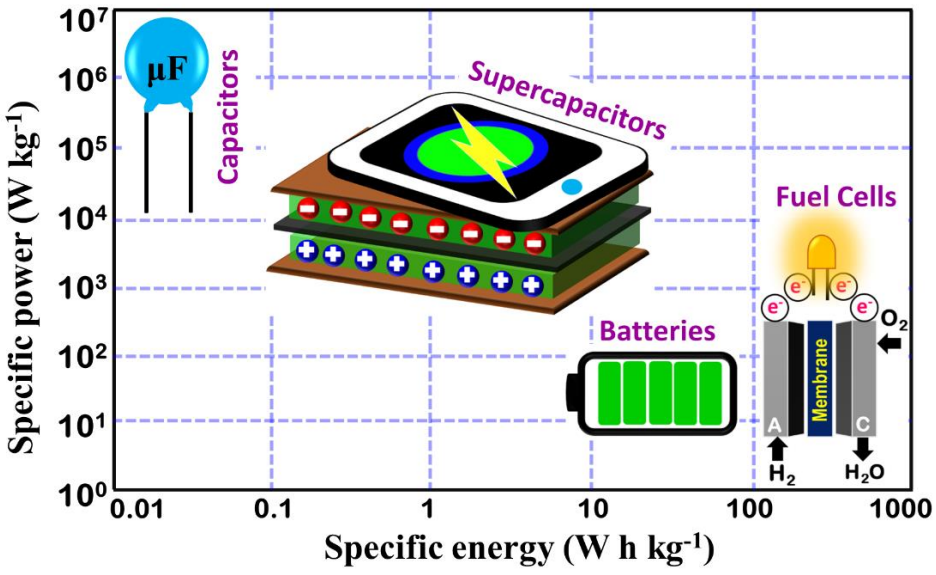

Figure 1.1. A Ragone plot illustrating the typical specific energy (W h kg^{-1}) and specific power (W kg^{-1}) ranges of fuel cells, batteries, supercapacitors, and conventional capacitors.

The United Nations' General Assembly approved the Sustainable Development Goals (SDGs) with the aim of creating a sustainable future for the planet.[15] According to existing laws, there is an anticipated 6 % rise in energy-related CO_2 emissions, projected to climb from 33 Gt in 2015 to 35 Gt by 2050. In order to align with the 2 °C target of the Paris Agreement, the emissions must decrease significantly to 9.7 Gt by 2050. In relation to the frameworks established by these regulations, numerous countries have established ambitious goals to attain sustainability by adopting alternate methods for generating and storing energy. Research has demonstrated that when combined with the electrification of end-use activities, renewable energy and energy efficiency are responsible for 94 % of the decrease in emissions. It is projected that the proportion of renewable energies in the total primary energy supply would increase from 14 % in 2015 to 63 % in 2050. This growth is mainly driven by a significant 60 % increase in the power sector. In order to achieve this, a yearly growth rate of 1.4 ppt per year is necessary, which is six times higher than the growth rate observed in previous years. Consequently, this has led to extensive global research on the advancement of effective energy storage technologies, particularly in the form of batteries and supercapacitors.

In addition to conventional systems, contemporary research is focused on advancing novel and more efficient batteries and supercapacitors. Continuous research aims to achieve optimal performance, cost-effectiveness, and environmental sustainability in these technologies. Novel materials and storage chemistries are being explored to develop the next generation of batteries and supercapacitors.[7,16] This step-change largely focuses on conducting fundamental research to develop novel electrodes and electrolytes for delivery purposes. The advancement of electrolyte and electrode materials has pushed the technological limitations of these technologies even farther, due to increasing competition.[17] Carbon electrodes are favored for supercapacitors due to their cost-effectiveness, superior electrical conductivity, high capacitance, exceptional porosity, favorable electrochemical stability, extensive specific

surface area, and convenient waste disposal.[16,18–23] Graphene, with a 2D structure consisting of a single layer of atoms, is highly regarded for its strong electrical conductivity, exceptional chemical stability, and remarkably large surface area of up to 2630 m^2 g^{-1}.[24] The effective surface area of graphene-based electrodes remains unaffected by the arrangement of pores in the solid state, unlike conventional materials. Conversely, the number of layers in graphene directly affects its characteristics. Graphene with only one or a few layers and minimal clumping has a larger specific surface area, resulting in superior performance as a supercapacitor.[25]

Electrolytes are essential in evaluating the efficiency of an energy storage device. In recent times, there has been a growing interest in solid-state devices as a way to address issues related to the dissolution of electrolytes, leakage, portability, and flammability that are commonly found in conventional systems using liquid electrolytes.[26] These devices utilize typical electrode materials like their conventional counterparts, but what sets them apart is the inclusion of a solid electrolyte that facilitates the passage of ions between the electrodes. The typical preparation approach of such electrolytes entails trapping a solvent within a solid matrix, enabling the solvent to attach to the matrix either through physical or chemical means, depending on the synthesis technique employed. Promising characteristics have been observed in solid electrolytes made from ubiquitous aqueous, organic, ionic liquid (IL), and/or deep eutectic solvent (DES) electrolytes.

1.3. Supercapacitors

1.3.1. Introduction to Supercapacitors

Supercapacitors, or ultracapacitors, are electrochemical devices designed to store significant quantities of electrical energy. Supercapacitors utilize double-layer capacitance and/or

pseudocapacitance techniques to store energy, rather than using a conventional dielectric. Put simply, they integrate the operational principles of conventional capacitors (electrostatic) with those of a regular battery (electrochemical). Since the 19th century, it has been recognized that electrical energy can be stored by forming an electric double layer (EDL) at the interface between an electrolyte and a solid material. The first electrochemical capacitor device was patented by General Electric in 1957. Despite its capability for double-layer charge storage, the requirement for its immersion in an electrolyte pool made this device unsuitable for widespread usage. Thereafter, the first electric double-layer capacitor (EDLC) was introduced in 1961 by the Standard Oil Company, Cleveland, Ohio (SOHIO).[27,28] The invention was rendered inoperable owing to insufficient sales, nevertheless, the prototype was granted a license by Japan-based Nippon Electric Company (NEC) in 1971.[29] In 1975, NEC introduced the first commercially feasible EDLC for memory backup purposes, which was marketed as the supercapacitor. Subsequently, the widespread adoption of telephones and telegraphs prompted other institutions to gradually create their own EDLC prototypes. In 1992, the US Department of Energy (DoE) started the DoE Ultracapacitor Development Program at Maxwell Laboratories, with the aim of using them in HEVs, almost thirty years after their first development. Supercapacitors are currently in high demand for various applications because to their outstanding features, including high power density, extended shelf life, excellent cyclability, large capacitance, minimal environmental effect, and inherently safe design and operation.[30–32]

The energy (E) of supercapacitors is determined by the capacitance (C) and the operating potential window (OPW, V), as described by **equation 1.1**.[33] Furthermore, the specific power (P) is also influenced by the OPW and may be calculated using **equation 1.2**. In this equation, the ESR represents the equivalent series resistance, and m represents the mass of the active electrode.

$$E = \frac{1}{2}CV^2 \quad \textbf{(1.1)}$$

$$P = \frac{V^2}{\text{ESR}\times m} \quad \textbf{(1.2)}$$

1.3.2. Taxonomy of Supercapacitors

Supercapacitors are classified into three main types based on their mechanism of storing energy: EDLC, pseudocapacitor, and hybrid capacitor.[34,35] Each of these categories can be further divided into multiple classes based on the type of electrodes they utilize (**Figure 1.2**). **Figure 1.3** represents the schematic depiction of the different components and operational mechanisms of the three main types of supercapacitors.

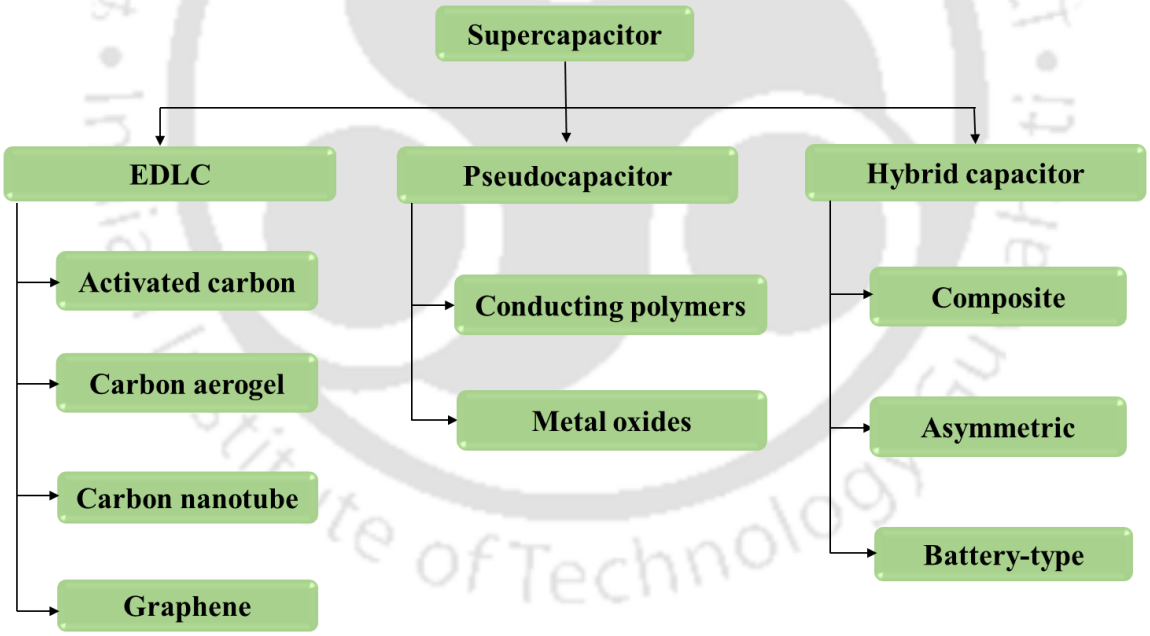

Figure 1.2. Classification and sub-classification of supercapacitors based on their mechanism of energy storage and on some of the most common types of electrodes utilized with them.

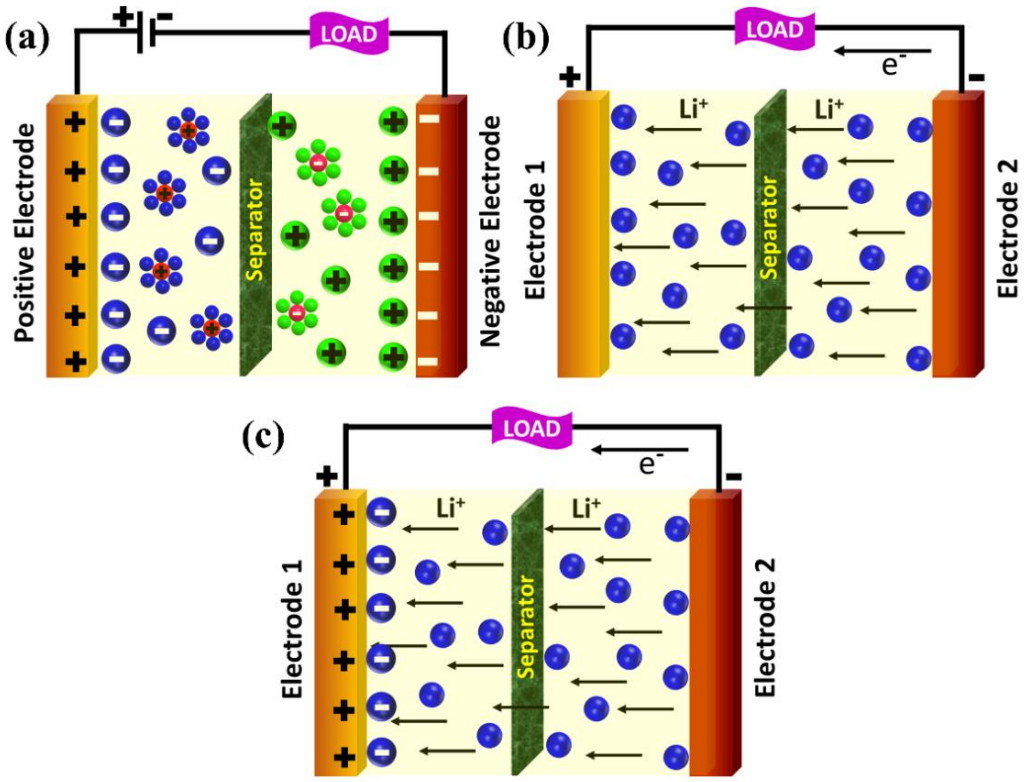

Figure 1.3. Schematic illustration of the three categories of supercapacitors: (a) electric double-layer capacitor (EDLC), (b) pseudocapacitor, and (c) hybrid capacitor.

1.3.2.1. Electric Double-Layer Capacitor

A typical EDLC consists of at least two permeable electrodes and an electrolyte, separated from each other by a separator. Similar to traditional capacitors, EDLCs store energy through electrostatic means, without any transfer of charges between the electrodes and the electrolyte. However, EDLCs utilize an electric double layer of charge to store energy. Upon the application of voltage, electric charge accumulates on the surfaces of the electrodes. The movement of ions in the electrolyte solution occurs via traversing the separator via electrode pores, driven by the inherent force of attraction between opposite charges. The electrodes are engineered to inhibit ion recombination. Consequently, a dual layer is produced on each electrode. By reducing the space between the electrodes and increasing the double-layered surface area, EDLCs are able to achieve greater energy densities than traditional capacitors and

better power densities than batteries. The non-Faradaic approach does not necessitate any chemical or structural alterations because there is no charge transfer between the electrolyte and electrode. Consequently, the retention of charges in EDLCs is exceptionally reversible, resulting in the potential for achieving remarkable cycling stabilities. EDLCs have demonstrated stable performance characteristics across a significant number of charge-discharge cycles, frequently reaching up to 1,000,000 cycles. In contrast, electrochemical batteries can only achieve approximately 1,000 cycles. Due to their versatile cycling capabilities, EDLCs are well-suited for use in places that are not easily accessible to users, such as deep seas or mountains.[36,37] EDLCs predominantly utilize carbon-based electrodes because of their exceptional electrical conductivity, favorable capacitance, substantial porosity, extensive electrochemical stability range, and significant specific surface area.[38] Activated carbon (AC), carbon aerogel (CA), carbon nanotube (CNT), and graphene are the most prevalent types of carbon utilized in EDLCs.[25]

1.3.2.2. Pseudocapacitor

While EDLCs store energy electrostatically, pseudocapacitors utilize the Faradaic mechanism to enable the transfer of charges between the electrodes and the electrolyte. This may be achieved through electrosorption, redox reactions, and intercalation typically resulting in higher capacitances and energy densities than those of EDLCs.[39–41] However, they distinguish themselves from conventional batteries by employing surface redox reactions, while batteries experience redox events within the bulk of the electrode materials. Nonetheless, during repeated cycles of charging and discharging, pseudocapacitors have been reported to experience a more rapid decline in their capacity compared to EDLCs. Pseudocapacitors employ conventional electrolytes seen in EDLCs, however they typically utilize conducting polymers and metal oxides as electrodes.[42]

1.3.2.3. Hybrid Capacitor

Hybrid capacitors aim to optimize their performance by mitigating the inherent limitations of both EDLCs and pseudocapacitors, resulting in enhanced output characteristics.[34] This particular category of supercapacitors employs a combination of Faradaic and non-Faradaic methods to store energy, resulting in increased energy and power densities compared to EDLCs. Additionally, they offer improved cycling stability and affordability when compared to pseudoapacitors. The three varieties of hybrid capacitors are distinguished by their electrode configurations: composite type, asymmetric type, and battery type. Compared to its two counterparts, however, this type of supercapacitor is still in its infancy.

1.3.3. Electrolytes Used with Supercapacitors

The performance attributes of supercapacitors are primarily contingent upon the specific electrolyte employed. The focus is currently on enhancing the energy and power densities of high-performance supercapacitor electrodes. These properties are predominantly influenced by the characteristics of the electrolyte.[43] An effective electrolyte for supercapacitors should possess a wide OPW, high ionic conductivity, substantial charge-storage capacity, and the ability to induce a high power density. Supercapacitors can be used with a wide spectrum of electrolyte systems, including aqueous electrolytes, organic solvent-based electrolytes, unconventional solvents such as ILs and DESs, and quasi-solid or solid electrolyte systems.[44]

1.3.3.1. Aqueous Electrolytes

Aqueous electrolytes have been widely employed in electrochemistry, particularly for supercapacitors, owing to their convenient handling and lower expenses in comparison to organic and IL electrolytes. Aqueous electrolytes have a higher ionic conductivity compared to organic electrolytes and ILs, which gives them an advantage. This leads to a decrease in ESR

and improves the power density. These electrolytes are also acclaimed for their reduced minimum pore-size requirements. Nevertheless, the primary limitation identified in the literature for aqueous electrolytes is their reduced OPW due to the premature decomposition of water. This limitation restricts the energy density and consequently makes them unsuitable for commercial supercapacitors.[45] Aqueous electrolytes primarily comprise of diverse inorganic salts at varying concentrations in water. The selection of cations and anions is determined by their sizes in both unbound and hydrated states,[45] which ultimately governs ion transport. Furthermore, the selection of the electrolyte has an impact on electrochemical stability. Aqueous electrolytes can be classified into three categories: acid, alkaline, and neutral electrolytes. The greater ionic conductivity of H_2SO_4 at various molar concentrations in water makes it a preferred choice of acidic electrolyte. KOH and Na_2SO_4 are often the chosen electrolytes for alkaline and neutral solutions. However, the reduced OPW of such electrolytes limits the energy storage of the device despite an increase in specific capacitance. A recent work conducted by Tomiyasu et al. revealed that a saturated aqueous solution of sodium perchlorate can remain stable up to a voltage of 3.2 V in a graphite-based capacitor.[46] Nonetheless, it is exceedingly uncommon to find such instances using aqueous electrolytes.

1.3.3.2. Organic Electrolytes

Organic electrolytes are frequently used in commercial supercapacitors owing to their broader OPW (2.5–2.8 V) compared to that of aqueous electrolytes.[45] This wider potential window can lead to improved energy and power densities. Nevertheless, the diminished ionic conductivity of organic electrolytes leads to a decrease in specific capacitance. To add to that, the manufacturing cost of supercapacitors using organic electrolytes is higher than that of those using aqueous electrolytes. Tetraethylammonium tetrafluroborate ([TEA][BF_4]) is the predominant organic salt employed in supercapacitors. [TEA][BF_4] dissolved in acetonitrile

(AN) has been widely preferred as an electrolyte throughout the last decade or so.[45,47] This is generally employed to assess the efficiency of new electrode materials for supercapacitors. Similar to aqueous electrolytes, when selecting organic electrolytes for supercapacitors, the important elements to consider are ion size, ion-solvent interaction, ionic conductivity, and viscosity of the solution. The primary benefit of organic electrolytes compared to aqueous electrolytes is their broader electrochemical stability. The existing literature supports this conclusion, notwithstanding their findings of a reduced specific capacitance. Furthermore, the extent of capacitance is mostly influenced by the structure of the electrode rather than the specific characteristics of the electrolyte. Although organic electrolytes have a broader OPW compared to aqueous electrolytes, research on alternative electrolytes began to address the safety concerns associated with their inferior thermal stability. Organic electrolytes exhibit lower ionic conductivity compared to that of aqueous electrolytes,[45] which is yet another drawback of such electrolytes.

1.3.3.3. Ionic Liquid Electrolytes

ILs are molten salts consisting of ions, specifically an organic cation and an organic or inorganic anion. These compounds have melting temperatures below 100 °C.[45] The versatility in the combination of cations and anions leads to a diverse range of ILs. The majority of ILs possess a melting point below room temperature, which is why they are also referred to as room temperature ILs (RTILs). ILs are renowned for their inherent non-flammability, little volatility, thermal and chemical stability, rendering them suitable for a broad spectrum of applications. Additionally, the appealing characteristics of ILs or RTILs specifically for their application in electrochemical energy storage devices are their substantial ionic conductivity and extended electrochemical stability potential window (ESPW).[48] Reported literature have extensively examined the ambit of ILs as a material for energy storage in supercapacitors.[49,50]

Extensive research has been conducted on ILs that consist of imidazolium and pyrrolidinium cations. The size and type of cations and anions have an impact on the ESPW, ionic conductivity, and thermal conductivity, that form some of the key characteristics of an electrolyte for supercapacitors.[49] The literature proposed the following order for cations in terms of reduction stability: piperidinium > pyrrolidinium > ammonium > imidazolium > pyridinium. Frequently employed anions include BF_4, PF_6, and bis(trifluoromethylsulfonyl)imide (TFSI). 1-ethyl-3-methylimidazolium (EMIM), with its reduced cation size, has garnered significant attention from researchers globally. The subsequent choice of imidazolium cation has been 1-butyl-3-methylimidazolium (BMIM), which provides increased resistance due to its larger size. The most extensively studied supercapacitor electrode materials are pure [EMIM][TFSI] and [EMIM][BF_4], mainly because of the lower size of the cationic core.[33,50] In general, imidazolium cations have superior ionic conductivity compared to phosphonium cations, but phosphonium offers a wider ESPW.[45] The latter is comparatively inexpensive and has been noted to exhibit several other benefits, including good ionic conductivity, low volatility, and low combustibility. Phosphonium ILs have been widely studied as electrolytic mediators for electrochemical devices such as Li-ion batteries (LIBs) and supercapacitors.[51–55] ILs with ammonium cations are also recognized for their favorable electrochemical and thermal stabilities.[56] A large potential window leads to increased energy storage, as indicated by **equation 1.1**. Conversely, high ionic conductivity and low viscosity limit the ESR by allowing for faster charge-discharge processes, hence facilitating faster release of stored energy. Thus, the distinct characteristics of the cationic core have varying impacts on the supercapacitor's efficiency.

Additionally, the electrochemical stability and ionic conductivity of the ILs are also influenced by the type of anion.[57] It is important to mention that, according to established protocol, the reduction potential is equivalent to the cathodic limit. The oxidation potential,

however, is determined by the anodic limit. Nevertheless, existing evidence indicates that the positively charged core can experience oxidation before the negatively charged component. The hydrophobic ILs belonging to the TFSI family have demonstrated superior resistance to hydrolysis, exceptional thermal stability even at temperatures exceeding 500 °C, and reduced viscosity.[58,59] Furthermore, their immiscibility with water allows them to be easily produced in forms that do not contain halogens. The anions BF_4 and dicyanamide (DCA) exhibit enhanced ionic conductivity due to their favorable wettable properties and smaller sizes,[60,61] with DCA offering the additional benefit of being considerably more cost-effective.[62] Increased water content amplifies the diffusive characteristics of the ions, leading to enhanced ionic conductivity by decreasing the ionic interactions.[63] Interestingly, ILs with the anion trifluorotris(pentafluoroethyl)phosphate (FAP) are observed to possess good ionic conductivity despite being highly hydrophobic.[56,62,64]

1.3.3.4. Deep Eutectic Solvent Electrolytes

DESs are a newly-emerging class of solvents that are gaining significant interest from the scientific and industrial communities due to their appealing physicochemical characteristics. DESs consist of a combination of two or more components that form a eutectic mixture. In the case of two components, the DES is obtained by mixing a eutectic mixture of a hydrogen bond acceptor (HBA) and a hydrogen bond donor (HBD) in a specified molar ratio.[65] These components are linked together through hydrogen bond interactions. The newly-created phase exhibits a freezing point that is below the fusion or melting temperatures of the constituent materials. The disparity in temperatures is referred to as the reduction in freezing point of a DES. Similar to ILs, these solvents are likewise recognized for their low volatility, non-flammability, ion-dense composition, and moderate ionic conductivity.[63] However, they cannot be classified as ILs since they do not consist solely of ions. Unlike ILs, DES systems are

produced through ion complexation with Brönsted or Lewis acids and bases.[66] As a result, this process generates large unsymmetrical ions, which in turn lowers the lattice energy and causes a fall in melting temperatures. In addition, it is also possible to synthesize DESs using non-ionic species.[65] The majority of investigations on DESs have mostly examined quaternary ammonium or imidazolium salts as the HBA, in combination with a hydrated metal salt or a suitable HBD such as amides, alcohols, glycols, or carboxylic acids.[66] According to literature, choline chloride (ChCl) has been the predominant choice as an HBA.[66] **Table 1.1** illustrates the standard categories of DESs as proposed by Smith et al.[66]

Table 1.1. Classification of DESs

Type of DES	**General Notation**	
Type I	$Cat^+X^- zMCl_x$	M= Zn, Sn, Fe, Al, Ga and In
Type II	$Cat^+X^- zMCl_x. yH2O$	M= Cr, Co, Cu, Ni and Fe
Type III	$Cat^+X^- zRZ$	Z= $CONH_2$, COOH and OH
Type IV	$MCl_X + RZ$	M= Al, Zn and Z= $CONH_2$, OH

Apart from the four categories listed in **Table 1.1**, recent research has unearthed a new category of DESs. These DESs, referred to as natural deep eutectic solvents (NADESs) or type-V DESs, consist of naturally occurring benign compounds in the form of HBAs and HBDs.[67,68] Among such DESs, carboxylic-fatty-acid-based NADESs have become popular due to their desirable properties. These DESs, besides being facile, less volatile, biodegradable, and facilitating reduced waste generation, are also highly stable in water, making them sustainable for various applications in the field of chemistry. Specifically, DESs prepared with DL-Menthol as the HBA and decanoic acid, lauric acid, myristic acid, and palmitic acid as the HBDs are known for their high hydrophobicity, lower cost, low viscosity, and good thermal

stability. They have been successfully utilized in the area of liquid-liquid separation.[69–72]

The utilization of DESs as electrolytes in supercapacitors has only been thoroughly investigated in recent years. Their restricted application as energy-efficient electrolytes is a result of the elevated viscosities and diminished ionic conductivities of the majority of quaternary ammonium salt-based DESs.[63] In order to address this disadvantage, DESs were created using alkali metal salts as the HBA, resulting in a substantial decrease in viscosity and a substantially greater level of ionic conductivity. Boisset et al. extensively investigated DESs consisting of acetamide and lithium TFSI salt (LiTFSI) in combination with capacitors and LIBs.[73–75] However, the OPW of these DESs is smaller compared to that of most RTILs. The ESPW of DESs against glassy carbon electrodes may be comparable to that of ILs. However, it is rare to achieve such a high ESPW for practical applications. In order to retain the advantageous electrochemical characteristics of ILs while limiting the cost of synthesis, hybrid DESs that incorporate ILs have been introduced. Nevertheless, these DESs have only been tested in a limited number of application domains thus far, yet they have demonstrated significant potential and a wide range of opportunities to explore. Mahanta et al. introduced the IL-based DESs, which consist of *N*-methylacetamide (NMAc) or ethylene glycol (EG) as the HBD, and the IL 1-butyl-3-methylimidazolium methanesulfonate ([BMIM][$MeSO_3$]) as the HBA.[63] [BMIM][$MeSO_3$] exhibits a strong tendency for hydrogen bond formation with proton-donating groups, whereas NMAc and EG serve as readily accessible and cost-effective HBDs. The Type III DESs displayed a capacitive behavior with reduced graphene oxide (rGO) electrodes, revealing OPWs of 3 V and 2 V, and room-temperature ionic conductivities of 2.7 mS cm^{-1} and 4.1 mS cm^{-1}, respectively. The devices yielded moderate values of specific capacitance (55–67 F g^{-1}) and specific power (0.6−1.3 kW kg^{-1}). The NMAc-based DES demonstrated a higher specific energy of around 84 W h kg^{-1}, which was attributed to its broader OPW, making it stand out as the better electrolyte candidate for supercapacitors as

compared to its EG-based counterpart.

1.3.3.5. Solid and Quasi-Solid Electrolytes

As previously stated, the majority of conventional electrolytes have inherent limitations. Organic electrolytes have a high ESR and low power density, making them less suitable for device applications. Additionally, the extensive use of ILs can be cost-intensive.[45] Moreover, certain commonly used aqueous and organic solvents like H_2SO_4, KOH, and AN can be harmful to the human skin.[76] While ILs are non-flammable and can help reduce atmospheric pollution due to their low vapor pressure, some hydrophilic ILs are highly soluble in water.[77–79] This increases the risk of environmental contamination if accidentally discharged. As such, another drawback of such electrolytes is their liquid state, which poses hazards in terms of packaging, portability, and leakage. In order to address this challenge, researchers are intensively studying the compatibility of novel solid and/or quasi-solid electrolytes with electrochemical systems as alternatives to their liquid counterparts.[80] Various studies have documented the process of transforming various types of liquid electrolytes into a gel or solid state by immobilizing them onto solid matrices made of polymeric and/or inorganic materials. These solutions have demonstrated their potential as excellent options for use as electrolytes in supercapacitors. Ongoing research is being conducted to create cost-effective, environmentally friendly, and high-performing electrolytes that can be used in supercapacitors and other electrochemical devices.

Supercapacitors have been tested with electrolytes made from covalently crosslinked hydrogels formed by polymerizing aqueous solutions.[81] In addition to aqueous and organic solvents, ILs and DESs, because of their better electrochemical stability and relative benignity, have been used as templates for synthesizing solid and quasi-solid electrolytes.[82] These electrolytes are commonly referred to as ionogels and eutectogels, respectively. In this context,

efforts are also being made to enhance the eco-friendly nature of solid electrolyte-based supercapacitors by exploring the use of polymer electrolytes derived from biowastes such as egg white, rice husk, and potato husk.[83–85] However, research on the properties of such electrolytes and their correlation is at a very nascent stage. Due to their easy portability, eco-friendliness, stability, and flexibility, solid electrolytes have the potential to expand the range of applications for supercapacitors.

1.4. Ionogels and Eutectogels

1.4.1. Introduction to Ionogels and Eutectogels

In the context elucidated earlier, despite their attractive characteristics, the predominant challenge in utilizing ILs and DESs for solid-state systems lies in their liquid nature, posing risks of component corrosion and leakage during packaging and transportation. A remedy to these challenges is found in the adoption of a novel class of solid or quasi-solid electrolytes known as ionogels, replacing conventional solvents in energy storage devices and various electrochemical applications.[86] This substitution not only enhances user-convenience but also broadens the scope, durability, and overall sustainability of the system. Ionogels are composite materials resulting from the immobilization of ILs within a solid matrix via crosslinking.[87] They exhibit substantial stability even under reduced pressure, eliminating leakage risks while retaining favorable properties inherited from the parent ILs.[26] In parallel, akin to ionogels, eutectogels have emerged as a prospective category of solid electrolytes, wherein a DES is confined within a solid matrix. Notably, eutectogels offer facile processing at lower costs compared to IL-based counterparts.[88] Despite their promising attributes, eutectogels are still in their nascent stage, necessitating exploration for additional novel properties and applications.

1.4.2. Classification of Ionogels and Eutectogels

1.4.2.1. Classification of Ionogels

Sahrash et al. has classified ionogels into three major classes based on the type of confining matrix: inorganic ionogels, organic ionogels, and hybrid ionogels (**Figure 1.4**).[89]

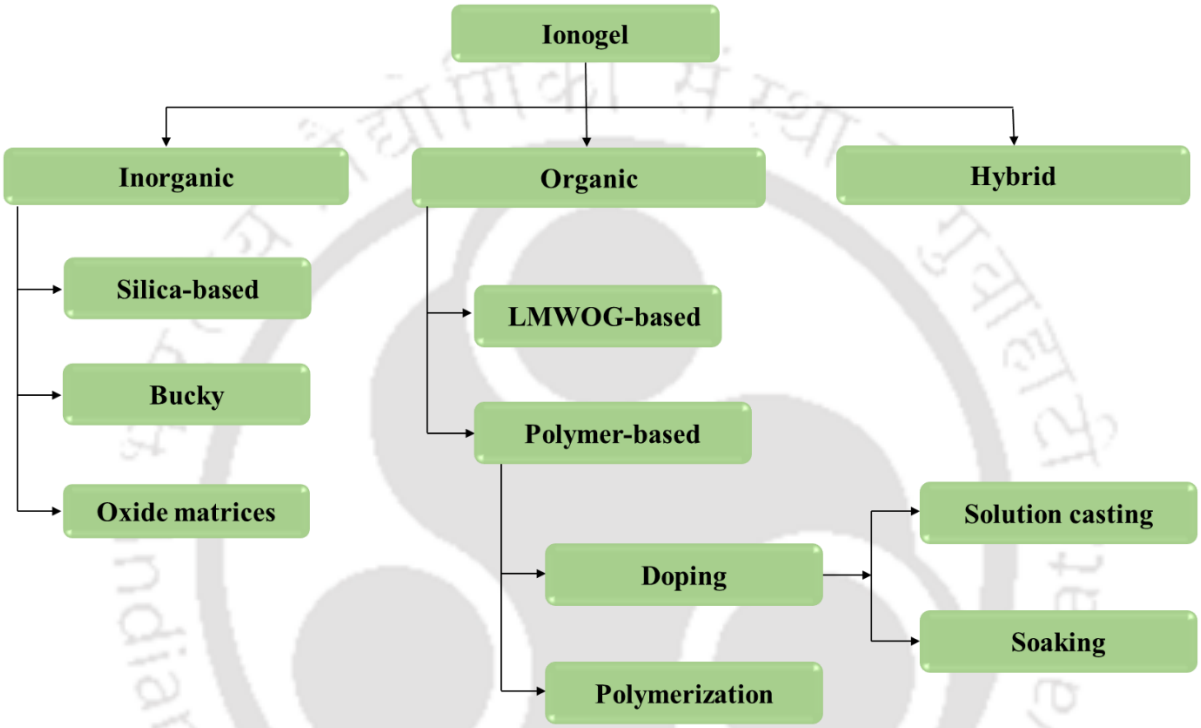

Figure 1.4. Classification of ionogels. [89,93]

1.4.2.1.1. Inorganic Ionogels

Inorganic ionogels are synthesized through the gelation of ILs with silica or by confining ILs within conducting or oxide matrices.[87]

Silica-based ionogels are prepared using either the sol-gel method or by dispersing silica nanoparticles for synthesis.[87] Notably, Brachet et al. and Horowitz et al. utilized [EMIM][TFSI] for synthesizing silica-based ionogels, demonstrating commendable mechanical properties.[90,91]

Bucky gels, characterized as soft gel-like materials, consist of ILs and CNTs, with the formation attributed to π–cation and π–electronic interactions.[89] The dispersion of CNTs in ILs, driven by inter-ionic interactions, establishes physical crosslinks, resulting in the formation of these gels. The synthesis involves grinding in an agitate mortar or sonicating the CNTs and ILs together.

Confinement of ILs in nanoporous oxide matrices, such as SnO_2, TiO_2, etc., yields inorganic ionogels. These oxides act as gelating agents in the synthesis, typically employing the sol-gel method with metallic precursors. Liu et al. reported an ionogel based on [BMIM][BF_4] and titania (TiO_2), utilized in actuators capable of functioning in harsh temperature environments.[92]

1.4.2.1.2. Organic Ionogels

Organic ionogels result from the immobilization of ILs either in polymer matrices or through the use of low molecular weight organogelators (LMWOGs).[93]

LMWOGs, which induce gelation in liquids, cause physical gelation at elevated temperatures when added in small quantities. The incorporation of LMWOGs in ILs at an increased temperature, followed by cooling, leads to the formation of ionogels. An example includes the use of the LMWOG N-benzyloxy-carbonyl-1-isoleucyl and the IL 1-hexyl-3-methylimidazolium iodide ([HMIM][I]) by Kubo et al., revealing high conversion efficiency for quasi-solid-state dye-sensitized solar cells with imidazolium-based ILs.[94]

Polymer-based ionogels employ diverse polymeric materials, such as polyvinylidene fluoride (PVDF), polytetrafluoroethylene (PTFE), polypropylene (PP), etc. for their synthesis.[89] These ionogels are obtained through doping or polymerization methods.[93] The doping approach encompass the solution-casting method (solvent blending), where a polymer

and IL are dissolved in a volatile solvent, followed by casting and drying of the homogeneous mixture obtained to remove the solvent. Another strategy to obtain ionogels using the doping approach is the soaking method (impregnation). This method involves the swelling of a polymer in IL or the formation of microporous polymer membranes, followed by soaking of the as-obtained membranes with the IL. On the other hand, the polymerization method is an in-situ process based on the polymerization or crosslinking of monomers dissolved in the IL. Winterton et al. emphasize IL functionality in ionogel synthesis, providing a medium for polymerization or acting as functional agents when incorporated into a polymer.[95] Yan et al. reported polymer/IL-based ionogel membranes using protic ILs, exhibiting thermal and chemical stability, transparency, and flexibility.[96]

1.4.2.1.3. Hybrid Ionogels

Hybrid ionogels arise from the confinement of ILs within a combination of inorganic and organic matrices, with preparation methods encompassing physical blending, the sol-gel method, or the incorporation of a latent organogelator.[89]

Physical blending involves the amalgamation of polymer electrolyte, IL, and inorganic nanofiller. Wang et al. employed this method in synthesizing electrolytes, utilizing poly(vinylidene fluoride-co-hexafluoropropylene) (PVDF-HFP), silica nanoparticles, and the IL 1-methyl-3-propylimidazolium iodide ([MPIM][I]). The process entailed straightforward mixing, heating, and sonication.[97]

The sol-gel method, a widely adopted approach for hybrid ionogel preparation, begins with suspending desired solid particles in a liquid medium to form a sol. Subsequently, methods like dipping, coating, or spinning are employed for sol deposition on a substrate. The sol transforms into a gel through incorporation of an initiator or evaporation followed by heating.[98] This method of synthesis has been detailed in section 1.4.3 of this thesis.

Synthesis of hybrid ionogels via the introduction of a latent organogelator results in a new class termed latent gel electrolyte precursors. These latent organogelators induce abrupt gelation at elevated temperatures.[89]

1.4.2.2. Classification of Eutectogels

Eutectogels, on the other hand, have been roughly divided into three types by Wang et al. based on the role of the DES in gel formation: polymer gels in which DESs only act as solvents (Eutectogels-S), polymer gels in which DESs act as solvents and polymerized monomers (Eutectogels-P), and supramolecular gels in which DESs act as solvents (Supramolecular Eutectogels) (**Figure 1.5**).[99]

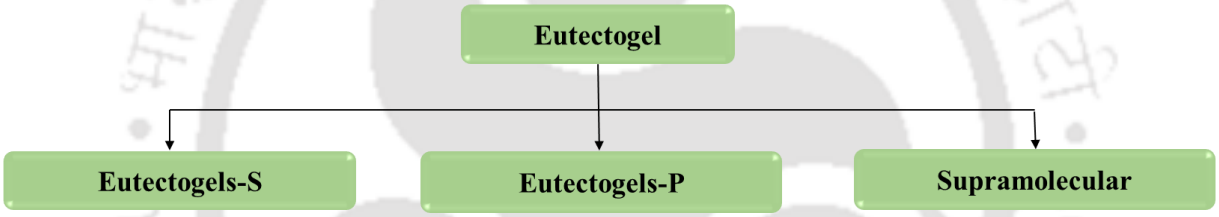

Figure 1.5. Classification of eutectogels.[99]

1.4.2.2.1. Eutectogels-S

In 2017, Qin et al. incorporated 2-hydroxyethyl methacrylate (HEMA) and poly(ethylene glycol) diacrylate (PEGDA) into a DES composed of ChCl and EG. The DES gel electrolyte was synthesized through in-situ UV copolymerization.[100] This groundbreaking study laid the foundation for the development of diverse DES gel electrolytes, catering to the requirements of safe, non-toxic, and cost-effective flexible electronics. Hong et al. extended these efforts by formulating a ternary DES system utilizing ChCl as the HBA and urea, and glycerol as HBDs.[101] In their approach, acrylamide (AM) was dissolved in the ChCl-urea-glycerol DES, initiating free radical polymerization through ammonium persulfate (APS). The resulting gel

exhibited excellent flexibility and mechanical strength due to the establishment of a coherent hydrogen bond network between the DES and the polymer. In 2021, Wang et al. employed betaine and EG as the DES solvent, with acrylic acid (AA) serving as the monomer.[102] Utilizing the dual catalytic system of $FeCl_3$ and vitamin C, they successfully obtained an ultra-stretched DES gel at room temperature. These gels demonstrated commendable electrical conductivity and temperature stability.

1.4.2.2.2. Eutectogels-P

Here, polymerized monomers function as HBAs or HBDs to yield DESs, subsequently undergoing direct polymerization within the DESs to form gels. In 2013, Mota-Morales et al. employed ChCl as the HBA and AA as the HBD, initiating polymerization of monomers with dibenzoyl peroxide (BPO) to synthesize a polyacrylic acid (PAA) eutectogel.[103] Similarly, in 2016, Isik et al. introduced the concept of deep eutectic monomers (DEMs).[104] They utilized quaternary ammonium salt as the HBA and various HBDs, such as citric acid, terephthalic acid, and amidoxime. DESs were then fabricated through free radical polymerization or polycondensation. This innovative approach led to the synthesis of new polymers with diverse applications, thoroughly characterized, including their application in carbon dioxide adsorption. Recently, Li et al. utilized ChCl as the HBA, while AA and maleic acid (MA) collectively acted as HBDs. Polymerization was initiated by UV light, resulting in the preparation of a self-healing, conductive, and transparent gel.[105]

1.4.2.2.3. Supramolecular Eutectogels

The integration of supramolecular gels into materials science research has gained prominence due to their distinctive characteristics and diverse applications. In recent years, researchers have turned their attention to DES-based supramolecular gels. In 2018, Marullo et al. pioneered the concept of supramolecular eutectogels by introducing supramolecular elements into a DES

composed of ChCl and phenylacetic acid (PA) in a 1:2 molar ratio.[106] Utilizing l-amino acids isoleucine and tryptophan as chelating agents, they prepared all-natural eutectogels through a gel-sol transition route. Notably, these gels exhibited high mechanical resistance and environmental friendliness, positioning them as promising candidates for applications requiring superior performance and environmental protection. Coincidentally, in the same year, Florindo et al. reported a novel supramolecular DES gel containing metal ions.[107] They strategically selected a hydrophobic DES, combining adodecanoate sodium salt as a HBA and carboxylic acid as an HBD. The addition of a small amount of water as an anti-solvent led to the gradual precipitation of DES, forming a supramolecular gel. The presence of sodium ions imparted distinctive performance to the gel, showcasing great potential in biomedical applications and wastewater treatment. Recently, Ruiz-Olles et al. introduced the cost-effective and environmentally friendly 1,3:2,4-dibenzylidene-d-sorbitol (DBS) into a DES composed of ChCl and alcohol/urea.[108] Through intermolecular noncovalent interactions, they crafted a new type of supramolecular DES gel. Importantly, these DES supramolecular gels exhibited electrical conductivity similar to liquid DES. The addition of Li^+, Mg^{2+}, and Ca^{2+} ions did not affect gel formation, resulting in similar conductivity between the prepared gels and electrolytes directly dissolved in DES. This strategy positions gels with such characteristics as having great potential in energy and catalysis applications.

1.4.3. Sol-gel Approach for Synthesis of Ionogels and Eutectogels

The synthesis of gels from ILs or DESs and matrices can be achieved through physical or chemical confinement.[26] Physical confinement is particularly appealing due to its ability to preserve the inherent bulk properties of solvents and conveniently modulate those properties by altering the structure and composition of both solvent and matrix. Furthermore, it offers an easy recovery of porous materials and solvents. In physical confinement, the weak interactions

arising from hydrogen bonds, π–π bonds, or hydrophobic associations play a crucial role. This is accomplished through sol-gel or postimpregnation methods. Physical confinement through sol-gel or postimpregnation methods relies on weak interactions such as hydrogen bonds, π–π bonds, or hydrophobic associations. The immobilization of ILs or DESs on porous matrices by covalent anchoring involves chemical reactions between the matrix surface and IL cations with specific functional groups, such as the trimethoxysilyl group. However, it is essential to note that once the IL is bound to a solid matrix, the cation–anion pair no longer constitutes a true IL, leading to a loss of solubility and ionic conductivity. The sol-gel strategy stands out as a popular method for gel synthesis, allowing for the one-step formation of the matrix in the presence of the solvent. The resulting matrix possesses a high specific surface area and homogeneity. In this approach, the solvent permeates the matrix pores through hydrolysis and condensation, creating more intimate biphasic structures compared to those obtained through postimpregnation of matrices.[26,109,110]

The non-hydrolytic route is the most widely used process for the synthesis of gels for electrolyte applications.[26,111] Herein, just two reagents are used: an acidic reagent such as formic acid (FA) and a metal or non-metallic alkoxide. The alkoxide, FA, and IL are first mixed. Consequently, gelation occurs after several hours. The gel thus obtained is kept at room temperature for a couple of days following ultrasound treatment.

The chemical reactions in the sol–gel method can be distributed into the two steps of hydrolysis and condensation as shown in **equations 1.3** through **1.7** below:

Hydrolysis

$$M–(OR)_4 + H_2O + HCOOH \Leftrightarrow H_2O{:}M–(OR)_4 \rightarrow (RO)_3–M–OH + ROH + HCOOH \quad \textbf{(1.3)}$$

$$(RO)_3–M–OH + H_2O + HCOOH \Leftrightarrow H_2O{:}(RO)_3–M–OH \rightarrow (RO)_2–M–(OH)_2 + ROH +$$

HCOOH **(1.4)**

$(RO)_2–M–(OH)_2 + H_2O + HCOOH \Leftrightarrow H_2O:(RO)_2–M–(OH)_2 \rightarrow RO–M–(OH)_3 + ROH +$ HCOOH **(1.5)**

$(RO)–M–(OH)_3 + H_2O + HCOOH \Leftrightarrow H_2O:RO–M–(OH)_3 \rightarrow M–(OH)_4 + ROH + HCOOH$ **(1.6)**

Condensation

$2X\text{-}M\text{-}OH \rightarrow M\text{-}O\text{-}M + H_2O$ **(1.7)**

Here, R is the alkyl group and M is the metal or non-metal atom. Alkoxy precursors are hydrolysed due to their nucleophilic substitution with acid. The hydrolysis of the first alcoholic group is usually a rapid reaction as compared to that of the hydrolysis reactions that follow thereafter. The condensation reaction is considered to be the decisive step for determining the rate of the sol-gel process. It is usually accomplished sometime between a few hours to a few days. The condensation of the X–M–OH groups accompanied by the accumulation of particles results in solid 3D networks.

The ILs behave only as a solvent in the reaction and do not take part in the reactions involving sol-gel transition. However, the type of the IL and the loading amount have significant roles to play in the time for gelation and the structure of the solid matrix. The gelation time is proportional to the percentage of IL content in the precursor mixture. A low percentage of IL increases the rate of reaction leading to an unstable dispersion of colloids. On the other hand, the dilution effect results in distinct and convenient separation of particles when IL is present in a higher percentage.[112,113] In fact, the volume ratio of FA:Alkoxide as well as the volume percentage of IL are jointly responsible for the time of gelation and the structure of the pores. A high IL content and a low FA:Alkoxide result in the slowest gelation times. Both

fast and slow gelation processes significantly influence the microstructures of the confining matrices. If TBOT is the crosslinker, the resulting ionogel exhibits liquid-like characteristics as the IL:Ti ratio increases. Increasing IL:Ti improves the ion-transporting ability and increases the ionic conductivity of the ionogel.[114,115]

Due to its exceptional charge transfer and separation properties, low toxicity, good thermal stability, high-temperature decomposition, and non-volatility, TiO_2 has garnered significant attention as a crosslinking element.[26,116,117] Three classes of titania precursors have been employed in the sol–gel methods for synthesizing TiO_2-based ionogels: inorganic titanium salts, titanium alkoxides, and metatitanic acid. It may be noted that titanium alkoxides are known for their high hydrolysis and condensation rates, and hence exhibit high reactivity. Nevertheless, stable gels based on TiO_2 derived from a titanium butoxide (TBOT) precursor can be achieved by adjusting the reaction rate between TBOT and the FA catalyst in solvents.[114,116] The first sol–gel synthesis of TiO_2-based ionogels was reported in 2009, involving the sonication of a mixture comprising inorganic titanium salts ($TiCl_4$), methanol, FA, and [BMIM][TFSI] at 25 °C.[118] The resulting electrolytes displayed high ionic conductivity (10^{-2} S cm^{-1}) in the intermediate temperature range of 100–200 °C, attributed to the self-assembled ionic transport channels. SiO_2, derived from tetramethoxysilane (TMOS) or tetraethyl orthosilicate (TEOS), serves as another popular matrix material due to its large surface area, mechanical stability, and high thermal stability.[26] In 2000, the first application of ILs to develop SiO_2-based ionogels was demonstrated, using TMOS as the precursor, [EMIM][TFSI] as the solvent, and FA as a catalyst.[119] However, the first eutectogel supported by a SiO_2 scaffold derived from TEOS was introduced only in 2018 as an electrolyte for LIBs, wherein the DES was composed of LiTFSI and NMAc.[88]

1.4.4. Ionogels and Eutectogels as Electrolytes

1.4.4.1. Ionogels as Electrolytes

Research on ionogels as potential electrolyte candidates for LIBs and supercapacitors has been carried out since the beginning of this century.[26,61] A breakthrough was achieved in 2011 with the synthesis of a novel type of ionogel, by confining the IL *N*-butyl-*N*-methylpyrrolidinium bis(trifluoromethylsulfonyl)imide ([PY14][TFSI]) within a non-metallic oxide (SiO_2). This material was successfully tested as a quasi-solid electrolyte in a Li/$LiFePO_4$ battery.[120] Thereafter, ionogels have been tested in a diverse spectrum of energy storage applications. Horowitz and Panzer acquired inorganic ionogels from the sol-gel confinement of [EMIM][TFSI] into TMOS-derived SiO_2. The gels showed a maximum ionic conductivity of 9.3 ± 0.5 mS cm^{-1}, a double-layer capacitance of 7.5 ± 0.4 μF cm^{-2}, and an ESPW of 2.5 V against glassy carbon blocking electrodes.[91] The same ionogel, with Ni-mediated vertically aligned carbon nanotube (VACNT) electrodes showed a specific capacitance of 430 μF cm^{-2} at a scan rate of 100 mV s^{-1} with an OPW of 3 V.[121] The areal energy density calculated for the fabricated device was 0.1–0.5 W h cm^{-2}, with a maximum power density of about 10 mW cm^{-2}. Bideau's group reported a supercapacitor based on carbon electrodes and the same ionogel.[90] The EDLC could be operated up to 2.5 V with a specific capacitance of 20 F g^{-1} at 20 ºC and 2 mV s^{-1}. The gel had an ionic conductivity of ~1.5 mS cm^{-1}. The same group also obtained an ionogel through the confinement of the same IL (~80 wt%) in a hybrid matrix formed by the co-condensation of TMOS and dimethyldimethoxysilane (DMDMS).[122] The ionogel, possessing an ionic conductivity of 3 mS cm^{-1}, was tested as a potential electrolyte in a microsupercapacitor with silicon nanowire electrodes, delivering an OPW of 2.5 V and a specific capacitance of 4 F g^{-1}. Su and team used fumed silica nanopowder and [EMIM][BF_4] to prepare an ionogel to be used with a supercapacitor with electrodes comprising AC and

MnO_2 deposited onto 3D Ni nanocone arrays.[123] The supercapacitor could reach an OPW of 2.5 V along with an energy density of 2.7 mW h cm^{-3} at a power density of 3.5 mW cm^{-3}. Wang et al. demonstrated a micro-supercapacitor fabricated using photoresist-derived porous carbon electrodes and an ionogel electrolyte also obtained from fumed silica and [EMIM][TFSI].[124] The device showed a double-layer capacitive behavior within a potential window of 2 V and a specific capacitance value of 600 μF cm^{-2} at 10 mV s^{-1}. The maximum energy and power density obtained were about 3 mW h cm^{-3} and 26 W cm^{-3}, respectively. They later compared two ionogels acquired from the same IL and SiO_2.[125] One was generated by sol-gel in-situ immobilization of the IL into TMOS-derived SiO_2, while the other was made by mixing fumed silica nanopowder with the IL. The former showed higher specific capacitance (14.2 μF cm^{-2} at 1000 mV s^{-1}) against a glassy carbon electrode. MacFarlane's group prepared an ionogel by sol–gel synthesis using TEOS in [BMIM][BF_4].[126] The gel possessed a room-temperature ionic conductivity of 3.1 mS cm^{-1} with 3 wt% SiO_2. Another ionogel electrolyte was prepared via solution casting of [EMIM][TFSI], PVDF-HFP, and SiO_2 which evinced an ionic conductivity of 1.5 mS cm^{-1} at 20 ºC.[127] The same was tested in conjunction with core-shell $TiNb_2O_7$@MoS_2/C and AC electrodes for an asymmetric supercapacitor. The cyclic voltammetry (CV) profiles exhibited a deviated rectangle shape with obvious redox peaks and shake-up peaks at 2.5–4 V due to the existence of hybrid electrochemical processes. The maximum specific capacitance, energy, and power obtained at a higher temperature of 60 ºC were 68.3 F g^{-1} (1 A g^{-1}), 147.2 W h kg^{-1} (1 A g^{-1}), and 21.9 kW kg^{-1} (10 A g^{-1}). Zhu and co-workers used a sol-gel-obtained [EMIM][TFSI]-SiO_2 ionogel as electrolyte in a supercapacitor with mesoporous carbon monolith as the working electrode.[128] The system behaved as an EDLC within a potential window of 2.5 V while giving a specific capacitance of 75 F g^{-1} at 10 mV s^{-1} per electrode. Nègre et al. reported an inorganic ionogel with ionic conductivity 4.7 mS cm^{-1} at 20 ºC based on sol-gel association of TMOS and TEOS, and [EMIM][TFSI].[129] An

EDLC supported by the electrolyte and AC electrodes led to a specific capacitance of 80 F g^{-1} at 5 mV s^{-1} and an OPW of 3 V. In another unique attempt, the same authors used two ILs, *viz.* *N*-methyl-*N*-propylpiperidinium bis(fluorosulfonyl)imide ([PIP13][FSI]) and [PY14][FSI] (1:1) to prepare an ionogel via a sol-gel route with TMOS and TEOS as the confining agents.[130] The gel revealed a room-temperature ionic conductivity of 5.5 mS cm^{-1}. A supercapacitor based on the ionogel electrolyte and AC electrodes delivered specific capacitance of 91 F g^{-1} at 20 ºC and 5 mV s^{-1}. However, the utilization of two crosslinking agents and/or two ILs renders the systems more expensive relatively.

A novel electro-active actuator based on nanocomposite ionogel electrolyte has also been reported, wherein this time the ionogel was obtained via TiO_2-nanoparticles-inititated UV polymerization of [BMIM][BF_4] and HEMA.[92] The gel had an ionic conductivity of 1.4 mS cm^{-1} at room temperature. Similarly, a sol-gel-derived TiO_2-confined ionogel electrolyte (room-temperature ionic conductivity 0.7 mS cm^{-1}) based on the IL *N*-methoxyethyl-*N*-methylpyrrolidinium bis(trifluoromethanesulfonyl)imide ([PYR1,2o1][TFSI]) and LiTFSI was observed to demonstrate an ESPW of 4.6 V when tested in lithium metal batteries with Li and stainless steel electrodes.[114] Kim's group developed a lithium ion conducting ionogel, consisting of [PY14][TFSI], LiTFSI, and TiO_2 nanoparticles, which resulted in an ionic conductivity of 1.5 mS cm^{-1} at 20 ºC and an ESPW of 4.8 V.[86] Chen et al. reported a rigid-flexible hybrid ionogel obtained from the sol-gel confinement of *N*-methyl-*N*-propylpyrrolidinium bis(trifluoromethylsulfonyl)imide ([PY13][TFSI]) and LiTFSI into TBOT-derived TiO_2 and PVDF-HFP.[131] The ionogel, with an ionic conductivity of 7.4 mS cm^{-1}, showed an ESPW of 5.5 V *versus* Li/Li^+. Wu et al. presented an ionogel for lithium battery prepared similarly using the same IL-LiTFSI electrolyte and TBOT.[116] The ionogel possessed an ionic conductivity of 2.93 mS cm^{-1} at room temperature and achieved an ESPW of 5.2 V (*vs* Li/Li^+). The same authors also reported another sol-gel-acquired ionogel obtained from the

immobilization of [EMIM][TFSI] and LiTFSI into TiO_2.[115] This time, however, the gel manifested an ionic conductivity of 1 mS cm^{-1}, proving the influence of IL ions on the properties of corresponding ionogels.

Liu et al. developed elastic ionogel electrolytes with aligned porous structures for flexible supercapacitors.[37] The IL [BMIM][PF_6] was confined onto TiO_2 nanoparticles and PEGDA-containing poly(ethylene glycol) methacrylate (PEGMA). The ionogel was obtained through UV cryopolymerization. It had an ionic conductivity of 1.46 mS cm^{-1}. The device with carbon nanocage electrodes showed a specific capacitance of 172 F g^{-1} at 1 A g^{-1}. Later, the same authors reported a novel cotton mask impregnated hybrid ionogel formed by UV polymerization of [BMIM][BF_4] with TiO_2 nanoparticles, *N*,*N*-dimethylacrylamide (DMAA), and methylene-bis-acrylamide (MBAA).[132] A supercapacitor based on this ionogel and AC electrodes displayed a specific capacitance of 143 F g^{-1} at 1 A g^{-1}. The ionic conductivity of the ionogel was 3.5 mS cm^{-1} at room temperature. They further used directional freezing (self-initiated cryopolymerization) followed by a solvent replacement method to prepare an aligned nanocomposite ionogel comprising [BMIM][BF_4], TiO_2 nanoparticles, clay nanosheets, DMAA, and water.[133] While the gel retained its ionic conductivity, the specific capacitance was increased to 176 F g^{-1} for the same current density. In all cases, the ionogels showed a stable capacitive behavior up to a voltage of about 3 V. Nonetheless, only limited research has focused on supercapacitors based on simple and facile sol-gel-derived TiO_2-confined ILs.

A polymer-based ionogel electrolyte was reported by Pandey and Hashmi, wherein the process involved the entrapment of [EMIM][FAP] into PVDF-HFP copolymer via a solution-cast method.[134] The gel possessed an ESPW of 4.4 V and an ionic conductivity of ~2 mS cm^{-1} at room temperature. A supercapacitor with HNO_3-treated multi-walled carbon nanotube (MWCNT) electrodes showed an OPW of 2 V and a specific capacitance value of ~76 F g^{-1},

which corresponded to the specific energy of ~17.2 W h kg^{-1} and specific power of ~18.9 kW kg^{-1} at 3 mA cm^{-2}. Traces of pseudocapacitance was observed due to the reaction of the IL with the oxygen-containing functional groups. Visentin and Panzer examined the dependence of the ionic conductivity, double layer capacitance, and elastic modulus of polymer-supported ionogels on the weight fraction of polymer matrix in the gel.[135] The ionogels were formed via UV-initiated crosslinking of PEGDA (4.9 to 44.7 wt%) inside the IL [EMIM][TFSI]. While low-frequency capacitive behavior of the ionogels was not strongly influenced by polymer content, the ionic conductivity reduced with increasing content of PEGDA, with the value standing at just 0.47 mS cm^{-1} for 44.7 wt% of PEGDA. In another work, they highlighted the importance of IL selection on the performance of in-situ crosslinked polymeric ionogels, especially considering their potential use in electrochemical energy-conversion or storage devices.[64] For the three different EMIM-based ILs with the anions FAP, TFSI, and tetracyanoborate (TCB), increasing IL viscosity by changing the anion identity decreased the minimum amount of PEGDA required to realize a non-flowing gel; however, this came at the cost of lower ionic conductivity of the gels. Of them, the ionogel based on [EMIM][TCB] that has the lowest viscosity, achieved the highest ionic conductivity value of 13.1 mS cm^{-1} with 7.2 wt% PEGDA at room temperature. Xing et al. introduced an ionogel formed from the solution casting of [EMIM][BF_4] and NaTFSI into PVDF-HFP.[136] A hybrid supercapacitor with molybdenum disulfide anode and CNT cathode manifested the coexistence of faradaic and non-faradaic mechanisms within a voltage range of 0–3.8 V and delivered a specific capacitance of ~37 F g^{-1} at 1 A g^{-1} and 20 ºC. Further, the system was able to achieve a maximum specific energy of 115.7 W h kg^{-1} at a specific power of 2.1 kW kg^{-1} at 70 ºC. However, the ionic conductivity of the gel stood at ~0.7 mS cm^{-1} at 20 ºC. The same IL was used by Yang et al. to prepare an ionogels with increased ionic conductivity (25 mS cm^{-1}) and 3.5 V ESPW by exploiting PVDF-HFP as the polymer matrix and graphene oxide as the ionic

conducting promoter.[137] The specific energy of an ionogel-laden AC-electrode-based supercapacitor reached as high as 32.4 W h kg^{-1} at a specific power 6.6 kW kg^{-1} at 10 A g^{-1}. A DMAA-, PEGDA-, and [EMIM][BF_4]-based ionogel reported by Song et al. was able to deliver a potential window of 3.5 V and a specific capacitance of 48.4 F g^{-1} at 0.5 A g^{-1} with N, O co-doped honeycomb carbon electrode.[138] Further, the supercapacitor gave maximum specific energy and power of 94.1 W h kg^{-1} and 17.5 W kg^{-1}. In another study, a radically polymerized polymer-matrix was fabricated using crosslinked polyvinyl alcohol (C-PVA) and coarsely crosslinked HEMA.[139] MBAA, potassium persulfate ($K_2S_2O_8$), and [EMIM][BF_4] were used as the crosslinker, initiator, and IL, respectively. The double-networked ionogel film with 60 wt% IL loading possessed an ionic conductivity of 1.8 mS cm^{-1} and an ESPW of 3 V against Au blocking electrodes at 30 ºC. A flexible supercapacitor with the double-networked electrolyte and rGO electrodes achieved an OPW of 2 V with maximum specific capacitance, energy, and power of 31 F g^{-1} (0.1 A g^{-1}), 17.2 W h kg^{-1} (0.1 A g^{-1}), and 13.1 kW kg^{-1} (2 A g^{-1}) respectively, at the same temperature. At 180 ºC, the capacitance, energy, and power of the device increased to 88 F g^{-1}, 51 W h kg^{-1}, and 18.8 kW kg^{-1} for the same corresponding current densities. Zhang et al. used [EMIM][TFSI] to prepare an ionogel with PVDF-HFP, possessing ionic conductivity 0.4 mS cm^{-1} at 25 °C.[140] Used as electrolyte cum membrane, the ionogel showed an OPW of 2.5 V along with an EDL specific capacitance of 119 F g^{-1} at 1.0 A g^{-1} against AC electrodes. The specific energy reached as high as 21.9 W h kg^{-1} at a power density of 6.25 kW kg^{-1} and a current density of 10 A g^{-1}. Simotwo et al. demonstrated a solid-state supercapacitor prepared by incorporating [EMIM][TFSI] and methyl cellulose into 3D AC nanofiber electrodes.[141] The device demonstrated a specific capacitance of 153 F g^{-1} at 20 mV s^{-1}, corresponding to a specific energy of 65 W h kg^{-1} and a specific power of 1.2 kW kg^{-1} with an OPW of 3.5 V. The ionogel exhibited an ionic conductivity of 5.7 mS cm^{-1} at 25 °C.

1.4.4.2. Eutectogels as Electrolytes

In recent years, the emergence of eutectogels has spurred extensive research, particularly in the field of electrochemistry, to explore their properties and suitability for applications in electrochemical energy storage including supercapacitors. Mukesh et al. reported a HEMA-supported eutectogel based on a DES containing ChCl and orcinol (Or).[142] The gel was utilized in supercapacitor prototypes with a metal-organic-framework-carbon (MOF-C) nanocomposite electrode, exhibiting a specific capacitance of 44.6 F g^{-1} at a scan rate of 10 mV s^{-1}. The maximum specific energy and power were 33 W h kg^{-1} and 5.9 kW kg^{-1} at 1 A g^{-1}, respectively. However, the gel possessed a room-temperature ionic conductivity of just 0.24 mS cm^{-1}. As mentioned earlier, Qin and Panzer later reported a chemically crosslinked polymer-based eutectogel derived from a DES comprising ChCl and EG.[100] The scaffold was formed through in-situ UV copolymerization of HEMA and PEGDA. The resulting gel exhibited double-layer capacitive behavior within a voltage range of 3 V, with an ionic conductivity of 5.7 mS cm^{-1}. The system served as a combined electrolyte/separator layer in a supercapacitor prototype with flexible AC fabric electrodes, providing a specific capacitance of 33.3 F g^{-1} and a specific energy of 15.8 W h kg^{-1} at 0.01 A g^{-1}. Hong et al. developed a cellulose-reinforced eutectogel with an ionic conductivity of ~0.6 mS cm^{-1}.[101] The gel was prepared by free radical polymerization of AM in a DES composed of ChCl, urea, and glycerol. The resulting supercapacitor based on the gel and activated carbon electrodes exhibited a specific capacitance of 76.6 F g^{-1} at 1 A g^{-1}, along with a specific energy of 10.6 W h kg^{-1} and a specific power of 0.5 kW kg^{-1}.

Joos and co-workers reported an inorganic eutectogel for LIBs, obtained by sol–gel immobilization of a lithium salt-based DES within a solid matrix of SiO_2.[88] The gel achieved an ionic conductivity of ~1.5 mS cm^{-1}, besides being characterized with good thermal stability

of up to 130 °C. They further proposed a modified eutectogel supported by a solid amide-based polymer, resulting in enhanced mechanical flexibility.[143] However, the ionic conductivity was reduced to 0.78 mS cm^{-1}. In each case, an ESPW over 4.5 V was obtained. In another attempt, Gu's team successfully developed a novel eutectogel membrane based on PVDF-HFP and a DES consisting of LiTFSI and NMAc.[144] The LIB tested with the eutectogel exhibited a room-temperature ionic conductivity of ~0.4 mS cm^{-1} and an ESPW of 5 V.

The same group later reported an eutectogel for supercapacitors, immobilizing a DES composed of urea, EG, ChCl, and zinc chloride ($ZnCl_2$) on a silk protein backbone.[145] The resulting gel manifested an ionic conductivity of 12.3 mS cm^{-1}, an electrochemical stability of 2.2 V, and an OPW of 1.4 V. The Zn | AC hybrid device exhibited a specific capacitance of 342.8 F g^{-1} at 0.2 A g^{-1} and a specific energy of 93.3 W h kg^{-1}. Wu et al. also proposed an eutectogel derived from perchlorate-ion- (ClO_4^-)-initiated radical polymerization of a ternary DES comprising $Zn(ClO_4)_2$, AM, and H_2O.[146] The gel displayed a supercapacitive behavior with an ionic conductivity of 51.7 mS cm^{-1} and a potential window extended up to 2.2 V. A specific capacitance of 194.7 F g^{-1} was obtained at 0.8 A g^{-1} with Zn and N-rGO electrodes, along with a specific energy and power of 117.5 W h kg^{-1} and 0.8 kW kg^{-1}. Similarly, an eutectogel was prepared by absorbing a DES comprising $Zn(ClO_4)_2$ as the HBD, and EG and H_2O as HBAs into a sequence of semi-interpenetrating polymer network (sIPN) hydrogels based on polyacrylamide (PAAM) and sulfonated poly(ether ether ketone) (SPEEK).[147] The system maintained an ionic conductivity of 7.3 mS cm^{-1} even at a low temperature of -40 °C. However, the OPW was limited to 1.7 V. Furthermore, a Zn | AC asymmetric supercapacitor supported by the gel electrolyte reported a specific capacitance of 150.1 F g^{-1} at 0.3 A g^{-1} and a specific energy of 66.8 W h kg^{-1} at a power of 0.2 kW kg^{-1}.

1.4.5. Other Applications of Ionogels and Eutectogels

Besides the realm of energy storage, ionogels and eutectogels find application almost everywhere, wherein IL and DES can be used in a solid form while preserving almost all desirable characteristics but fluidity of the latter.[93,99,148]

1.4.5.1. Other Applications of Ionogels

In recent years, based on their desirable properties, applications of ionogels have also been widely investigated beyond the realm of batteries and supercapacitors. This includes applications in the areas of thermoelectric technologies, adhesives, sensors and soft electronics, separation, extraction, catalysis, and bio-medication.[148]

In 2019, Zhao et al. reported the inaugural findings on the thermoelectric capabilities of ionogels.[149] Thus far, a number of thermoelectric devices utilizing ionogel have been documented.[150–153] In 2020, Sun and colleagues presented a strong ionogel prepared using a poly(ureaurethane) network and 1,2-dimethyl-3-ethoxyethylimidazolium bis(trifluoromethylsulfonyl)imide ([DEIM][TFSI]).[154] The ionogel-based manufactured ionic skin successfully and accurately detected human movement with exceptional sensitivity and dependability. In 2022, Song's team developed a photoluminescent ionogel that can be 3D-printed.[155] This ionogel demonstrated exceptional mechanical durability across a broad spectrum of temperatures. An ionic skin was developed using the ionogel, enabling it to function as a wireless remote control for a robot, allowing for precise control of its movements even in challenging environments. In 2020, Yamada and Toshiyoshi developed a single-use temperature sensor using a water-soluble ionogel.[156]

Ionogels possessing minimal vapor pressure, high ionic conductivity, and a broad range of operating temperatures have demonstrated remarkable potential in applications such as

organic field-effect transistors (OFETs), fuel cells, and solar cells.[93,148] Syairah et al. employed polyethylene oxide (PEO) as the polymer, ethylene carbonate (EC) and propylene carbonate (PC) as the solvents, and NaI as the salt to prepare various ionogel electrolytes using the ILs [MPIM][I], [BMIM][I], and [HMIM][I].[157] Dye-sensitized solar cells (DSSCs) were fabricated utilizing polymeric ionogel electrolytes and examined under a solar simulator. A remarkable power conversion efficiency of 9.35 % was achieved using the ionogel based on [MPIM][I]. Wang and co-workers created an ionogel adhesive by incorporating a [EMIM][Br] solvent into a network of poly(hydroxyethyl methacrylate) (PHEMA).[158] In 2021, Yu and Wu documented the development of a hydrophobic ionogel that functions as an electrode for underwater electrocardiography sensors.[159] The ionogel electrode demonstrated superior adhesion, conductivity, and stability in an underwater environment when compared to commercial electrodes. Ionogels have also been utilized for the fabrication of microstructures using inkjet printing.[160]

Ionogels have been utilized for the fabrication of solid-phase microextraction (SPME) fiber coatings, exhibiting exceptional durability, reusability, and stability.[161] The ionogel-based SPME fiber coatings demonstrated exceptional extractability for a wide range of volatile organic pollutants. Pang et al. fabricated an ionogel fiber coating by utilizing a 1-hexadecyl-3-methylimidazolium-bis(trifluoromethylsulfonyl)imide- ([C_{16}MIM][TFSI])- confined SiO_2-based network. This coating demonstrated efficient extraction of organophosphorus pesticides from wine and juice.[162] Ionogel fiber coatings offer distinct benefits and can be applied to effectively detect and extract organophosphate esters in environmental water samples.[163] Ionogel membranes can be utilized for gas separation, including the separation of CO_2, owing to their exceptional gas solubility, excellent design flexibility, and strong mechanical stability.[164] Fu et al. synthesized ionogels by incorporating [EMIM][TFSI] into supramolecular polymer networks that were crosslinked using imine bonds.[165] These ionogels were designed

to effectively separate CO_2.

Ionogels can also serve as novel heterogeneous catalysis systems. In 2015, Marr and colleagues prepared a reusable ionogel catalyst by trapping an acid-functionalized IL triethylammonium propanesulfone bis(trifluoromethylsulfonyl)imide ([TEAPS][TFSI]) within a SiO_2 gel.[166] This catalyst was capable of facilitating the dehydration of rac-1-phenyl ethanol. ILs, known for their bactericidal activities, also confer good bactericidal characteristics to some ionogels.[167] An instance of this was the utilization of diimidazolium-based organic salts that contain peptides or amino acids as anions to create ionogels using [BMIM][BF_4] and [BMIM][PF_6] as solvents.[168] The ionogels exhibited remarkable antibacterial efficacy against both gram-negative and gram-positive bacteria. Another potential application of ionogels is in drug delivery systems, with the aim of reducing drug degradation and loss, preventing adverse side effects, and enhancing drug bioavailability[169–171] and as biocompatible biomaterials.[172]

1.4.5.2. Other Applications of Eutectogels

Eutectogels are comparatively much newer as compared to ionogels and unlike the latter, not many literatures could be found that have reported their performance beyond the realm of energy storage. Nevertheless, the ones that have, reveal promising results of these materials in certain disciplines other than the domain of electrochemical applications.[99] In a recent study, Silva et al. discovered a novel form of therapeutic drug-eluting stents (THEDES) that are composed of ChCl and ascorbic acid.[173] DES exhibits exceptional solubility, allowing for efficient dissolution of dexamethasone (DEX) inside it. Consequently, DES enhances both the diffusion and penetration properties of DEX. In addition, the presence of hydrogen bond interaction between ascorbic acid and ChCl allowed for the preservation of the antioxidant activities of ascorbic acid for a duration exceeding 6 months. The versatility and flexibility of the study has significant potential for application in the pharmaceutical business and tissue

engineering. Due to its little ecological footprint, eutectogels have emerged as very suitable substances for environmental remediation. Marullo et al. synthesized a supramolecular eutectogel using ChCl and phenylacetic acid as the main components, and l-amino acids as the gelators.[174] The gel possesses a highly effective water purifying capability and can be utilized for a minimum of 9 cycles without any decline in efficacy. Furthermore, by applying the gel to the column for the purpose of removing color from the fluid, an impressive removal efficiency of 85 % was attained in just 10 min. Additionally, the gel could be reused for a minimum of 4 cycles. This study demonstrated the practical usefulness of eutectogels in the process of cleanup.

DESs have been utilized in conjunction with other materials for the fabrication of novel ionic gels. Li et al. developed a conductive paper using polymerizable DESs through in-situ polymerization using a conventional screen-printing technique.[175] The entire method was ecologically sustainable, uncomplicated, and convenient, making it suitable for large-scale manufacturing. The paper that was made exhibited flexibility and the ability to be folded, as well as transparency and conductivity. Origami-based 3D circuits can be readily controlled for input/output purposes. This approach generated novel perspectives on the development of adaptable electrical devices. Wang et al. prepared a DES-based translucent wood through the process of in-situ UV light activation of DES polymerization.[176] The as-acquired wood exhibited favorable levels of transparency, extensibility, and conductivity. The presence of a hydrogen bond between the cellulose and DES in the woods contributed to the transparent woods having favorable mechanical properties. Hence, the utilization of transparent and conductive woods (TCWs) was employed to effectively track subtle variations in pressure and human motions. This study has introduced a novel approach for creating functional composite materials, which holds significant potential for applications in the realm of flexible wearable devices and sensing.

1.5. Knowledge Gap and Motivation for the Study

The fast depletion of conventional sources of energy and the inclination towards alternative resources has tremendously surged up the demand for efficient energy storage technologies and the need for unearthing high-performing novel energy materials. In this context, supercapacitors have been acclaimed for their high power density, high capacitance, low environmental impact, and intrinsically safe design and operation. Solid-state electrolytes have gained great interest in the recent past since they are leak-proof and have the advantage of easy packaging and fabrication. Moreover, solid electrolytes can act as the ion-transport media and electrode separators simultaneously.[45] As seen from **Figure 1.6**, research on solid electrolytes has witnessed an almost steady rise over the past couple of decades from 21,674 scientific articles published in 2004 to 106,761 in 2023 with 19,425 articles already published by February 2024. However, of them, studies focusing on supercapacitors are relatively much lower, with the figure standing at 22,627 in 2023. An extensive survey of the available literature has shown that a major portion of the research on solid electrolytes has been directed towards lithium batteries. Particularly, the application of ionogels and eutectogels as electrolytes in supercapacitors is still at a very nascent stage. During the same time, only about 991 and 151 articles reported studies on supercapacitors exclusively with ionogels and eutectogels, respectively.

Researchers face several challenges throughout the synthesis process of solid electrolytes. The complexity of the systems, ensuring the purity of precursors, adapting to extreme operating conditions, and achieving usability in a cost-effective and energy-conducive manner present significant hurdles. These challenges hinder efforts to explore diverse potential strategies and implement an efficient experimental framework for the development of inorganic solid electrolytes. Overcoming these obstacles is crucial to advancing the understanding and

utilization of inorganic solid electrolytes in various electrochemical applications.

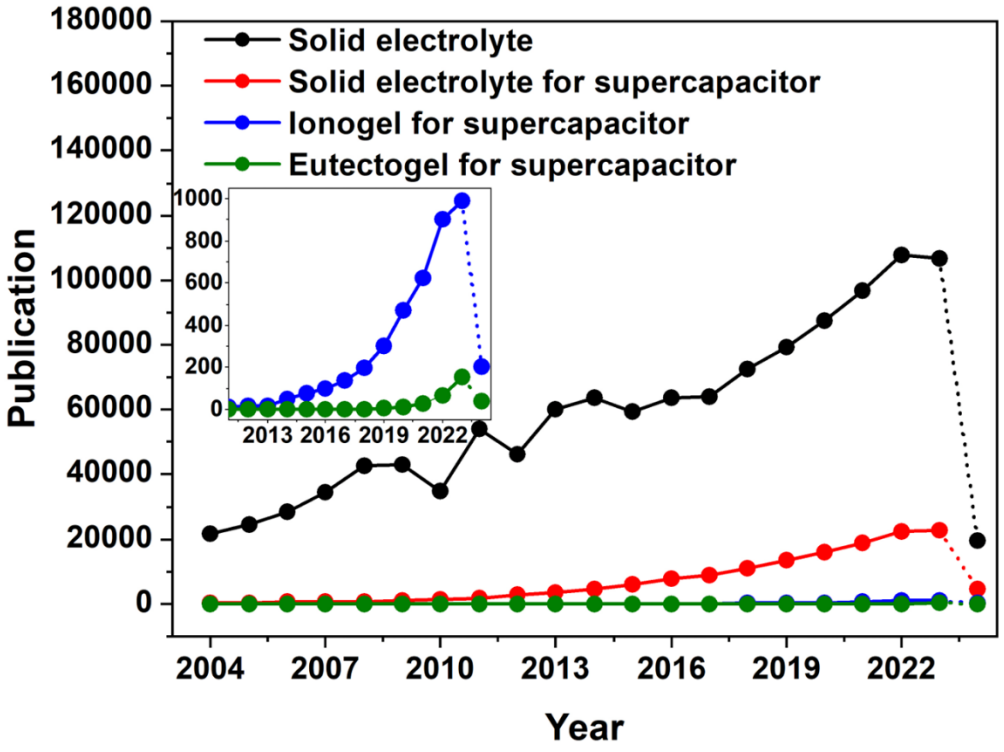

Figure 1.6. Plot depicting the number of scientific articles on solid electrolytes and solid, ionogel (inset), and eutectogel (inset) electrolytes for supercapacitors published between January 2004 and February 2024 (Source: http://app.dimensions.ai; keywords for the search were: solid electrolyte, solid electrolyte for supercapacitor, ionogel for supercapacitor, and eutectogel for supercapacitor; accessed on February 20, 2024).

The prevailing research landscape in solid electrolytes primarily revolves around polymer-based electrolytes, leaving solid electrolytes supported by inorganic materials relatively unexplored. Within the realm of ionogels, imidazolium, pyrrolidinium, and piperidinium IL-based ionogels have been extensively examined for electrochemical applications. In this regard, authors have focused predominantly on some specific ILs for supercapacitors, which include [EMIM][TFSI], [EMIM][BF_4], [BMIM][BF_4], and

[PY14][TFSI]. However, the compatibility of electrochemical supercapacitors with inorganic ionogels formed from phosphonium, ammonium, or other imidazolium cations and different anions largely remain undeciphered. Moreover, despite their favorable characteristics, there is limited comprehensive research on TiO_2-based inorganic ionogels in supercapacitor applications. Similarly, the majority of reported eutectogels have been immobilized into solid matrices derived from polymers. While the properties and feasibility of some of these eutectogels have been studied and tested in supercapacitors, there is a notable gap in the literature regarding an extensive investigation into the physical and electrochemical properties of inorganic supramolecular eutectogels developed from non-toxic and cost-effective NADESs. Additionally, works focusing on inorganic gels prepared from the electrochemically more attractive IL-based DESs are few and far between. This highlights a potential avenue for further research and development in the field of inorganic solid electrolytes for electrochemical applications.

1.6. Aim and Objectives of the Study

Based on the lacunae presented in section 1.5, this research has been aimed towards the development and study of the viability of novel inorganic ionogels and eutectogels for application as electrolytes in electrochemical supercapacitors.

The **principal objectives** of the research are as follows:

1.6.1. Synthesis and characterization of novel inorganic **ionogels** based on the immobilization of **ionic liquids (ILs)** into a solid matrix of TiO_2 through a one-step sol-gel method followed by the examination of their electrochemical characteristics and assessment of their viability as potential electrolytes for supercapacitors.

1.6.2. Synthesis and characterization of novel inorganic **eutectogels** based on the

immobilization of **deep eutectic solvents (DESs)** into solid matrices of TiO_2 and SiO_2 through a one-step sol-gel method followed by the examination of their electrochemical characteristics and assessment of their viability as potential electrolytes for supercapacitors.

1.6.3. Synthesis and characterization of novel inorganic **eutectogels** based on the immobilization of an **IL-based DES** into solid matrices of TiO_2 and SiO_2 through a one-step sol-gel method followed by the examination of their electrochemical characteristics and assessment of their viability as potential electrolytes for supercapacitors.

1.7. Outline of the Thesis

To address the aforementioned objectives, this doctoral thesis has been organized in the following six chapters:

Chapter 1 (Introduction, Literature Review, and Objectives of the Research): This chapter presents a comprehensive background of the research, offering a general overview of supercapacitors and the different types of electrolytes used with them. The chapter further introduces ionogels and eutectogels derived from ILs and DESs respectively, and critically analyzes some of the important electrochemical characteristics of different types of ionogels and eutectogels reported previously, emphasizing the precursor materials and synthesis mechanisms used to obtain them. The subsequent section briefly touches upon some of their applications beyond the domain of energy storage. Thereafter, the knowledge gaps and the research problems have been identified and the aim and objectives of this thesis have been delineated along with its scope and organization. This comprehensive introduction sets the stage for the subsequent research findings and analyses.

Chapter 2 (Materials and Methods): This chapter serves as a repository of essential information regarding the materials utilized in the experimental studies, along with their respective sources. It provides a detailed account of the synthesis procedures employed for the ionogels, DESs, and eutectogels. Additionally, the chapter sheds light on the diverse techniques of characterization and the associated equipment, outlining sample preparation methods. Furthermore, it elucidates the experimental procedures employed to evaluate the various properties of the DESs and gels. This comprehensive overview offers transparency into the methodologies and tools leveraged in the research, establishing a foundation for understanding the subsequent findings and analyses.

Chapter 3 (TiO_2-Mediated Ionic-Liquid-Based Inorganic Ionogels): This chapter is dedicated to the characterization of seven novel ionogels, synthesized by physically confining seven ILs into a solid matrix of TiO_2. The results derived from morphological, spectroscopical, interfacial, thermal, and electrochemical analyses conducted on these ionogels are thoroughly discussed. Additionally, a comparative analysis is presented, aligning the findings with relevant results reported by other researchers. The chapter also includes a report on the electrochemical properties of the ionogel electrolyte that exhibited the most promising performance at room temperature, further examined at controlled temperatures. This comprehensive examination aims to provide valuable insights into the distinctive features and performance of the studied ionogels, contextualized within the existing body of research.

Chapter 4 (TiO_2- and SiO_2-Mediated Natural-Deep-Eutectic-Solvent-Based Inorganic Eutectogels): This chapter is centered on examining the characteristics of eight novel eutectogels, generated through the physical confinement of four NADESs, within a solid matrix of either TiO_2 or SiO_2. The discussion encompasses the results obtained from analyses of

morphological, structural, thermal, and electrochemical properties of these two categories of eutectogels. A comparative analysis is conducted, not only between the TiO_2 and SiO_2 eutectogels but also with relevant findings reported by other researchers. This comprehensive approach aims to provide insights into the distinctive features of the studied eutectogels and their performance relative to existing research in the field.

Chapter 5 (TiO_2- and SiO_2-Mediated Inorganic Eutectogels Developed from an Ionic-Liquid-Based Deep Eutectic Solvent): This chapter delves into a comprehensive discussion and comparison of the morphological, structural, thermal, and electrochemical characteristics of two distinct types of eutectogels. These eutectogels are produced through the physical immobilization of an IL-based DES within an inorganic solid matrix of TiO_2 or SiO_2. The properties of these two eutectogels are systematically compared, not only with each other but also with relevant findings from other works reported previously. Additionally, the chapter includes a report on the controlled-temperature electrochemical properties of the eutectogel electrolyte that exhibited the most promising results at room temperature. This comprehensive analysis aims to contribute valuable insights into the distinctive features and performance of the studied eutectogels, offering a broader context within the existing body of research.

Chapter 6 (Research Conclusions and Future Scopes): This concluding chapter serves to underscore the principal discoveries of the research. It involves a comparative analysis of the three primary types of gel electrolytes investigated in this work and provides insights into their potential applicability in the realm of supercapacitor energy storage technologies. The conclusions drawn are based on the results and discussions presented in the preceding chapters. The thesis concludes by contemplating future directions for this research, offering perspectives on potential avenues for further exploration and advancement in the field.

References

(1) Rehman, S.; Bader, M. A.; Al-Moallem, S. A. Cost of Solar Energy Generated Using PV Panels. *Renewable and Sustainable Energy Reviews* **2007**, *11* (8), 1843–1857. https://doi.org/10.1016/j.rser.2006.03.005.

(2) Timilsina, G. R.; Kurdgelashvili, L.; Narbel, P. A. Solar Energy: Markets, Economics and Policies. *Renewable and Sustainable Energy Reviews* **2012**, *16* (1), 449–465. https://doi.org/10.1016/j.rser.2011.08.009.

(3) O'Rourke, F.; Boyle, F.; Reynolds, A. Tidal Current Energy Resource Assessment in Ireland: Current Status and Future Update. *Renewable and Sustainable Energy Reviews* **2010**, *14* (9), 3206–3212. https://doi.org/10.1016/j.rser.2010.07.039.

(4) Neill, S. P.; Hashemi, M. R.; Lewis, M. J. Tidal Energy Leasing and Tidal Phasing. *Renew Energy* **2016**, *85*, 580–587. https://doi.org/10.1016/j.renene.2015.07.016.

(5) Saidur, R.; Islam, M. R.; Rahim, N. A.; Solangi, K. H. A Review on Global Wind Energy Policy. *Renewable and Sustainable Energy Reviews* **2010**, *14* (7), 1744–1762. https://doi.org/10.1016/j.rser.2010.03.007.

(6) Islam, M. R.; Mekhilef, S.; Saidur, R. Progress and Recent Trends of Wind Energy Technology. *Renewable and Sustainable Energy Reviews* **2013**, *21*, 456–468. https://doi.org/10.1016/j.rser.2013.01.007.

(7) Wang, L.; Han, Y.; Feng, X.; Zhou, J.; Qi, P.; Wang, B. Metal–Organic Frameworks for Energy Storage: Batteries and Supercapacitors. *Coord Chem Rev* **2016**, *307*, 361–381. https://doi.org/10.1016/j.ccr.2015.09.002.

(8) Guan, M.; Liao, W.-H. On the Energy Storage Devices in Piezoelectric Energy Harvesting; Clark, W. W., Ahmadian, M., Lumsdaine, A., Eds.; 2006; p 61690C. https://doi.org/10.1117/12.658402.

(9) Guan, M. J.; Liao, W. H. Characteristics of Energy Storage Devices in Piezoelectric

Energy Harvesting Systems. *J Intell Mater Syst Struct* **2008**, *19* (6), 671–680. https://doi.org/10.1177/1045389X07078969.

(10) Vullers, R. J. M.; van Schaijk, R.; Doms, I.; Van Hoof, C.; Mertens, R. Micropower Energy Harvesting. *Solid State Electron* **2009**, *53* (7), 684–693. https://doi.org/10.1016/j.sse.2008.12.011.

(11) Richards, P. D.; Myers, R. J.; Swinton, S. M.; Walker, R. T. Exchange Rates, Soybean Supply Response, and Deforestation in South America. *Global Environmental Change* **2012**, *22* (2), 454–462. https://doi.org/10.1016/j.gloenvcha.2012.01.004.

(12) Tarascon, J.-M.; Armand, M. Issues and Challenges Facing Rechargeable Lithium Batteries. *Nature* **2001**, *414* (6861), 359–367. https://doi.org/10.1038/35104644.

(13) Simon, P.; Gogotsi, Y. Materials for Electrochemical Capacitors. *Nat Mater* **2008**, *7* (11), 845–854. https://doi.org/10.1038/nmat2297.

(14) Simon, P.; Gogotsi, Y.; Dunn, B. Where Do Batteries End and Supercapacitors Begin? *Science (1979)* **2014**, *343* (6176), 1210–1211. https://doi.org/10.1126/science.1249625.

(15) Gielen, D.; Boshell, F.; Saygin, D.; Bazilian, M. D.; Wagner, N.; Gorini, R. The Role of Renewable Energy in the Global Energy Transformation. *Energy Strategy Reviews* **2019**, *24*, 38–50. https://doi.org/10.1016/j.esr.2019.01.006.

(16) Bruce, P. G.; Freunberger, S. A.; Hardwick, L. J.; Tarascon, J.-M. Li–O2 and Li–S Batteries with High Energy Storage. *Nat Mater* **2012**, *11* (1), 19–29. https://doi.org/10.1038/nmat3191.

(17) Scrosati, B.; Garche, J. Lithium Batteries: Status, Prospects and Future. *J Power Sources* **2010**, *195* (9), 2419–2430. https://doi.org/10.1016/j.jpowsour.2009.11.048.

(18) Hall, P. J.; Bain, E. J. Energy-Storage Technologies and Electricity Generation. *Energy Policy* **2008**, *36* (12), 4352–4355. https://doi.org/10.1016/j.enpol.2008.09.037.

(19) Pandolfo, A. G.; Hollenkamp, A. F. Carbon Properties and Their Role in

Supercapacitors. *J Power Sources* **2006**, *157* (1), 11–27. https://doi.org/10.1016/j.jpowsour.2006.02.065.

(20) Zhang, L. L.; Zhao, X. S. Carbon-Based Materials as Supercapacitor Electrodes. *Chem Soc Rev* **2009**, *38* (9), 2520. https://doi.org/10.1039/b813846j.

(21) Kumar, R.; Singh, R. K.; Vaz, A. R.; Savu, R.; Moshkalev, S. A. Self-Assembled and One-Step Synthesis of Interconnected 3D Network of Fe_3O_4/Reduced Graphene Oxide Nanosheets Hybrid for High-Performance Supercapacitor Electrode. *ACS Appl Mater Interfaces* **2017**, *9* (10), 8880–8890. https://doi.org/10.1021/acsami.6b14704.

(22) Gao, Y.-P.; Zhai, Z.-B.; Huang, K.-J.; Zhang, Y.-Y. Energy Storage Applications of Biomass-Derived Carbon Materials: Batteries and Supercapacitors. *New Journal of Chemistry* **2017**, *41* (20), 11456–11470. https://doi.org/10.1039/C7NJ02580G.

(23) Miao, Z.; Huang, Y.; Xin, J.; Su, X.; Sang, Y.; Liu, H.; Wang, J.-J. High-Performance Symmetric Supercapacitor Constructed Using Carbon Cloth Boosted by Engineering Oxygen-Containing Functional Groups. *ACS Appl Mater Interfaces* **2019**, *11* (19), 18044–18050. https://doi.org/10.1021/acsami.9b04426.

(24) Arbizzani, C.; Mastragostino, M.; Meneghello, L. Polymer-Based Redox Supercapacitors: A Comparative Study. *Electrochim Acta* **1996**, *41* (1), 21–26. https://doi.org/10.1016/0013-4686(95)00289-Q.

(25) Gamby, J.; Taberna, P. L.; Simon, P.; Fauvarque, J. F.; Chesneau, M. Studies and Characterisations of Various Activated Carbons Used for Carbon/Carbon Supercapacitors. *J Power Sources* **2001**, *101* (1), 109–116. https://doi.org/10.1016/S0378-7753(01)00707-8.

(26) Chen, N.; Zhang, H.; Li, L.; Chen, R.; Guo, S. Ionogel Electrolytes for High-Performance Lithium Batteries: A Review. *Advanced Energy Materials*. Wiley-VCH Verlag April 25, 2018. https://doi.org/10.1002/aenm.201702675.

(27) Dănilă, E.; Lucache, D. D. HISTORY OF THE FIRST ENERGY STORAGE SYSTEMS. In *3RD INTERNATIONAL SYMPOSIUM ON THE HISTORY OF ELECTRICAL ENGINEERING AND OF TERTIARY-LEVEL ENGINEERING EDUCATION* ; Iaşi, 2010.

(28) Namisnyk, A.; Zhu, J. G. A Survey of Electrochemical Super-Capacitor Technology. In *Australian Universities Power Engineering Conference*; Christchurch, 2003.

(29) Burke, A. Ultracapacitors: Why, How, and Where Is the Technology. *J Power Sources* **2000**, *91* (1), 37–50. https://doi.org/10.1016/S0378-7753(00)00485-7.

(30) Kötz, R.; Carlen, M. Principles and Applications of Electrochemical Capacitors. *Electrochim Acta* **2000**, *45* (15–16), 2483–2498. https://doi.org/10.1016/S0013-4686(00)00354-6.

(31) Frackowiak, E.; Béguin, F. Carbon Materials for the Electrochemical Storage of Energy in Capacitors. *Carbon N Y* **2001**, *39* (6), 937–950. https://doi.org/10.1016/S0008-6223(00)00183-4.

(32) Pettersson, F.; Keskinen, J.; Remonen, T.; von Hertzen, L.; Jansson, E.; Tappura, K.; Zhang, Y.; Wilén, C.-E.; Österbacka, R. Printed Environmentally Friendly Supercapacitors with Ionic Liquid Electrolytes on Paper. *J Power Sources* **2014**, *271*, 298–304. https://doi.org/10.1016/j.jpowsour.2014.08.020.

(33) Brandt, A.; Pohlmann, S.; Varzi, A.; Balducci, A.; Passerini, S. Ionic Liquids in Supercapacitors. *MRS Bull* **2013**, *38* (7), 554–559. https://doi.org/10.1557/mrs.2013.151.

(34) Halper, M. S.; Ellenbogen, J. C. Supercapacitors: A Brief Overview. *The MITRE Corporation*. March 2006, pp 1–34.

(35) Vangari, M.; Pryor, T.; Jiang, L. Supercapacitors: Review of Materials and Fabrication Methods. *Journal of Energy Engineering* **2013**, *139* (2), 72–79.

https://doi.org/10.1061/(ASCE)EY.1943-7897.0000102.

(36) Phadke, S.; Amara, S.; Anouti, M. Gas Evolution in Activated-Carbon-Based Supercapacitors with Protic Deep Eutectic Solvent as Electrolyte. *ChemPhysChem* **2017**, *18* (17), 2364–2373. https://doi.org/10.1002/cphc.201700621.

(37) Liu, X.; Wang, B.; Jin, Z.; Wang, H.; Wang, Q. Elastic Ionogels with Freeze-Aligned Pores Exhibit Enhanced Electrochemical Performances as Anisotropic Electrolytes of All-Solid-State Supercapacitors. *J Mater Chem A Mater* **2015**, *3* (30), 15408–15412. https://doi.org/10.1039/C5TA03184B.

(38) Shi, H. Activated Carbons and Double Layer Capacitance. *Electrochim Acta* **1996**, *41* (10), 1633–1639. https://doi.org/10.1016/0013-4686(95)00416-5.

(39) Frackowiak, E.; Khomenko, V.; Jurewicz, K.; Lota, K.; Béguin, F. Supercapacitors Based on Conducting Polymers/Nanotubes Composites. *J Power Sources* **2006**, *153* (2), 413–418. https://doi.org/10.1016/j.jpowsour.2005.05.030.

(40) Xia, H.; Lai, M. O.; Lu, L. Nanostructured Manganese Oxide Thin Films as Electrode Material for Supercapacitors. *JOM* **2011**, *63* (1), 54–59. https://doi.org/10.1007/s11837-011-0014-5.

(41) Wang, G.-X.; Zhang, B.-L.; Yu, Z.-L.; Qu, M.-Z. Manganese Oxide/MWNTs Composite Electrodes for Supercapacitors. *Solid State Ion* **2005**, *176* (11–12), 1169–1174. https://doi.org/10.1016/j.ssi.2005.02.005.

(42) Xie, X.; Gao, L. Characterization of a Manganese Dioxide/Carbon Nanotube Composite Fabricated Using an in situ Coating Method. *Carbon N Y* **2007**, *45* (12), 2365–2373. https://doi.org/10.1016/j.carbon.2007.07.014.

(43) Laforgue, A.; Simon, P.; Fauvarque, J. F.; Mastragostino, M.; Soavi, F.; Sarrau, J. F.; Lailler, P.; Conte, M.; Rossi, E.; Saguatti, S. Activated Carbon/Conducting Polymer Hybrid Supercapacitors. *J Electrochem Soc* **2003**, *150* (5), A645.

https://doi.org/10.1149/1.1566411.

(44) Burke, A. R&D Considerations for the Performance and Application of Electrochemical Capacitors. *Electrochim Acta* **2007**, *53* (3), 1083–1091. https://doi.org/10.1016/j.electacta.2007.01.011.

(45) Zhong, C.; Deng, Y.; Hu, W.; Qiao, J.; Zhang, L.; Zhang, J. A Review of Electrolyte Materials and Compositions for Electrochemical Supercapacitors. *Chem Soc Rev* **2015**, *44* (21), 7484–7539. https://doi.org/10.1039/C5CS00303B.

(46) Tomiyasu, H.; Shikata, H.; Takao, K.; Asanuma, N.; Taruta, S.; Park, Y.-Y. An Aqueous Electrolyte of the Widest Potential Window and Its Superior Capability for Capacitors. *Sci Rep* **2017**, *7* (1), 45048. https://doi.org/10.1038/srep45048.

(47) Pal, B.; Yang, S.; Ramesh, S.; Thangadurai, V.; Jose, R. Electrolyte Selection for Supercapacitive Devices: A Critical Review. *Nanoscale Adv* **2019**, *1* (10), 3807–3835. https://doi.org/10.1039/C9NA00374F.

(48) MacFarlane, D. R.; Forsyth, M.; Howlett, P. C.; Kar, M.; Passerini, S.; Pringle, J. M.; Ohno, H.; Watanabe, M.; Yan, F.; Zheng, W.; Zhang, S.; Zhang, J. Ionic Liquids and Their Solid-State Analogues as Materials for Energy Generation and Storage. *Nat Rev Mater* **2016**, *1* (2), 15005. https://doi.org/10.1038/natrevmats.2015.5.

(49) Watanabe, M.; Thomas, M. L.; Zhang, S.; Ueno, K.; Yasuda, T.; Dokko, K. Application of Ionic Liquids to Energy Storage and Conversion Materials and Devices. *Chem Rev* **2017**, *117* (10), 7190–7239. https://doi.org/10.1021/acs.chemrev.6b00504.

(50) Eftekhari, A. Supercapacitors Utilising Ionic Liquids. *Energy Storage Mater* **2017**, *9*, 47–69. https://doi.org/10.1016/j.ensm.2017.06.009.

(51) Kundu, D.; Chakma, S.; Pugazhenthi, G.; Banerjee, T. Ionic Liquid Facilitated Dehydrogenation of *Tert* -Butylamine Borane. *ACS Omega* **2018**, *3* (2), 2273–2281. https://doi.org/10.1021/acsomega.7b01781.

(52) Khazalpour, S.; Yarie, M.; Kianpour, E.; Amani, A.; Asadabadi, S.; Seyf, J. Y.; Rezaeivala, M.; Azizian, S.; Zolfigol, M. A. Applications of Phosphonium-Based Ionic Liquids in Chemical Processes. *Journal of the Iranian Chemical Society* **2020**, *17* (8), 1775–1917. https://doi.org/10.1007/s13738-020-01901-6.

(53) Benito-Lopez, F.; Byrne, R.; Răduţă, A. M.; Vrana, N. E.; McGuinness, G.; Diamond, D. Ionogel-Based Light-Actuated Valves for Controlling Liquid Flow in Micro-Fluidic Manifolds. *Lab Chip* **2010**, *10* (2), 195–201. https://doi.org/10.1039/B914709H.

(54) Chowdhury, S.; Mohan, R. S.; Scott, J. L. Reactivity of Ionic Liquids. *Tetrahedron* **2007**, *63* (11), 2363–2389. https://doi.org/10.1016/j.tet.2006.11.001.

(55) Garcia-Quintana, L.; Jónsson, E.; Yunis, R.; MacFarlane, D. R.; Forsyth, M.; Bond, A. M.; Howlett, P. C.; Pozo-Gonzalo, C. Stabilisation of the Superoxide Anion in Bis(Fluorosulfonyl)Imide (FSI) Ionic Liquid by Small Chain Length Phosphonium Cations: Voltammetric, DFT Modelling and Spectroscopic Perspectives. *Electrochem commun* **2021**, *127*, 107029. https://doi.org/10.1016/j.elecom.2021.107029.

(56) Xue, Z.; Qin, L.; Jiang, J.; Mu, T.; Gao, G. Thermal, Electrochemical and Radiolytic Stabilities of Ionic Liquids. *Physical Chemistry Chemical Physics* **2018**, *20* (13), 8382–8402. https://doi.org/10.1039/C7CP07483B.

(57) De Vos, N.; Maton, C.; Stevens, C. V. Electrochemical Stability of Ionic Liquids: General Influences and Degradation Mechanisms. *ChemElectroChem* **2014**, *1* (8), 1258–1270. https://doi.org/10.1002/celc.201402086.

(58) Crosthwaite, J. M.; Muldoon, M. J.; Dixon, J. K.; Anderson, J. L.; Brennecke, J. F. Phase Transition and Decomposition Temperatures, Heat Capacities and Viscosities of Pyridinium Ionic Liquids. *J Chem Thermodyn* **2005**, *37* (6), 559–568. https://doi.org/10.1016/j.jct.2005.03.013.

(59) Parnham, E. R.; Morris, R. E. Ionothermal Synthesis Using a Hydrophobic Ionic Liquid

as Solvent in the Preparation of a Novel Aluminophosphate Chain Structure. *J Mater Chem* **2006**, *16* (37), 3682. https://doi.org/10.1039/b610774e.

(60) Osada, I.; de Vries, H.; Scrosati, B.; Passerini, S. Polymerelektrolyte Auf Basis Ionischer Flüssigkeiten Für Batterieanwendungen. *Angewandte Chemie* **2016**, *128* (2), 510–523. https://doi.org/10.1002/ange.201504971.

(61) Pan, S.; Yao, M.; Zhang, J.; Li, B.; Xing, C.; Song, X.; Su, P.; Zhang, H. Recognition of Ionic Liquids as High-Voltage Electrolytes for Supercapacitors. *Front Chem* **2020**, *8*. https://doi.org/10.3389/fchem.2020.00261.

(62) Silvester, D. S.; Jamil, R.; Doblinger, S.; Zhang, Y.; Atkin, R.; Li, H. Electrical Double Layer Structure in Ionic Liquids and Its Importance for Supercapacitor, Battery, Sensing, and Lubrication Applications. *The Journal of Physical Chemistry C* **2021**, *125* (25), 13707–13720. https://doi.org/10.1021/acs.jpcc.1c03253.

(63) Mahanta, U.; Choudhury, S.; Venkatesh, R. P.; SarojiniAmma, S.; Ilangovan, S. A.; Banerjee, T. Ionic-Liquid-Based Deep Eutectic Solvents as Novel Electrolytes for Supercapacitors: COSMO-SAC Predictions, Synthesis, and Characterization. *ACS Sustain Chem Eng* **2020**, *8* (1), 372–381. https://doi.org/10.1021/acssuschemeng.9b05596.

(64) Visentin, A. F.; Alimena, S.; Panzer, M. J. Influence of Ionic Liquid Selection on the Properties of Poly(Ethylene Glycol) Diacrylate-Supported Ionogels as Solid Electrolytes. *ChemElectroChem* **2014**, *1* (4), 718–721. https://doi.org/10.1002/celc.201300205.

(65) Zhang, Q.; De Oliveira Vigier, K.; Royer, S.; Jérôme, F. Deep Eutectic Solvents: Syntheses, Properties and Applications. *Chem Soc Rev* **2012**, *41* (21), 7108. https://doi.org/10.1039/c2cs35178a.

(66) Smith, E. L.; Abbott, A. P.; Ryder, K. S. Deep Eutectic Solvents (DESs) and Their

Applications. *Chem Rev* **2014**, *114* (21), 11060–11082. https://doi.org/10.1021/cr300162p.

(67) Florindo, C.; Branco, L. C.; Marrucho, I. M. Quest for Green-Solvent Design: From Hydrophilic to Hydrophobic (Deep) Eutectic Solvents. *ChemSusChem* **2019**, *12* (8), 1549–1559. https://doi.org/10.1002/cssc.201900147.

(68) Paul, N.; Banerjee, T. Study on the Extraction of Acetamiprid and Imidacloprid from an Aqueous Environment Using Menthol-Based Hydrophobic Eutectic Solvents: Quantum Chemical and Molecular Dynamics Insights. *ACS Sustain Chem Eng* **2022**, *10* (13), 4227–4246. https://doi.org/10.1021/acssuschemeng.2c00023.

(69) Verma, R.; Mohan, M.; Goud, V. V.; Banerjee, T. Operational Strategies and Comprehensive Evaluation of Menthol Based Deep Eutectic Solvent for the Extraction of Lower Alcohols from Aqueous Media. *ACS Sustain Chem Eng* **2018**, *6* (12), 16920–16932. https://doi.org/10.1021/acssuschemeng.8b04255.

(70) Verma, R.; Banerjee, T. Palmitic-Acid-Based Hydrophobic Deep Eutectic Solvents for the Extraction of Lower Alcohols from Aqueous Media: Liquid–Liquid Equilibria Measurements, Validation and Process Economics. *Global Challenges* **2019**, *3* (11). https://doi.org/10.1002/gch2.201900024.

(71) Verma, R.; Banerjee, T. Liquid–Liquid Extraction of Lower Alcohols Using Menthol-Based Hydrophobic Deep Eutectic Solvent: Experiments and COSMO-SAC Predictions. *Ind Eng Chem Res* **2018**, *57* (9), 3371–3381. https://doi.org/10.1021/acs.iecr.7b05270.

(72) Verma, R. Liquid-Liquid Extraction and Process Flow Sheeting of Lower Alcohol with Deep Eutectic Solvents, Indian Institute of Technology Guwahati, Guwahati, 2018.

(73) Boisset, A.; Jacquemin, J.; Anouti, M. Physical Properties of a New Deep Eutectic Solvent Based on Lithium Bis[(Trifluoromethyl)Sulfonyl]Imide and N-

Methylacetamide as Superionic Suitable Electrolyte for Lithium Ion Batteries and Electric Double Layer Capacitors. *Electrochim Acta* **2013**, *102*, 120–126. https://doi.org/10.1016/j.electacta.2013.03.150.

(74) Boisset, A.; Menne, S.; Jacquemin, J.; Balducci, A.; Anouti, M. Deep Eutectic Solvents Based on N-Methylacetamide and a Lithium Salt as Suitable Electrolytes for Lithium-Ion Batteries. *Physical Chemistry Chemical Physics* **2013**, *15* (46), 20054. https://doi.org/10.1039/c3cp53406e.

(75) Zaidi, W.; Boisset, A.; Jacquemin, J.; Timperman, L.; Anouti, M. Deep Eutectic Solvents Based on *N* -Methylacetamide and a Lithium Salt as Electrolytes at Elevated Temperature for Activated Carbon-Based Supercapacitors. *The Journal of Physical Chemistry C* **2014**, *118* (8), 4033–4042. https://doi.org/10.1021/jp412552v.

(76) Bae, K.-L.; Kim, K. Flexible Sodium-Ion Supercapacitor Based on Polypyrrole/Carbon Electrode by Use of Harmless Aqueous Electrolyte for Wearable Devices. *Int J Energy Res* **2017**, *41* (9), 1335–1341. https://doi.org/10.1002/er.3716.

(77) Anthony, J. L.; Maginn, E. J.; Brennecke, J. F. Solution Thermodynamics of Imidazolium-Based Ionic Liquids and Water. *J Phys Chem B* **2001**, *105* (44), 10942–10949. https://doi.org/10.1021/jp0112368.

(78) Wong, D. S. H.; Chen, J. P.; Chang, J. M.; Chou, C. H. Phase Equilibria of Water and Ionic Liquids [Emim][PF6] and [Bmim][PF6]. *Fluid Phase Equilib* **2002**, *194–197*, 1089–1095. https://doi.org/10.1016/S0378-3812(01)00790-7.

(79) McFarlane, J.; Ridenour, W. B.; Luo, H.; Hunt, R. D.; DePaoli, D. W.; Ren, R. X. Room Temperature Ionic Liquids for Separating Organics from Produced Water. *Sep Sci Technol* **2005**, *40* (6), 1245–1265. https://doi.org/10.1081/SS-200052807.

(80) Kumaravel, V.; Bartlett, J.; Pillai, S. C. Solid Electrolytes for High-Temperature Stable Batteries and Supercapacitors. *Adv Energy Mater* **2021**, *11* (3).

https://doi.org/10.1002/aenm.202002869.

(81) Guo, Y.; Zhou, X.; Tang, Q.; Bao, H.; Wang, G.; Saha, P. A Self-Healable and Easily Recyclable Supramolecular Hydrogel Electrolyte for Flexible Supercapacitors. *J Mater Chem A Mater* **2016**, *4* (22), 8769–8776. https://doi.org/10.1039/C6TA01441K.

(82) Aswathy, N. R.; Palai, A. K.; Ramadoss, A.; Mohanty, S.; Nayak, S. K. Fabrication of Cellulose Acetate-Chitosan Based Flexible 3D Scaffold-like Porous Membrane for Supercapacitor Applications with PVA Gel Electrolyte. *Cellulose* **2020**, *27* (7), 3871–3887. https://doi.org/10.1007/s10570-020-03030-y.

(83) Na, R.; Wang, X.; Lu, N.; Huo, G.; Lin, H.; Wang, G. Novel Egg White Gel Polymer Electrolyte and a Green Solid-State Supercapacitor Derived from the Egg and Rice Waste. *Electrochim Acta* **2018**, *274*, 316–325. https://doi.org/10.1016/j.electacta.2018.04.127.

(84) Yadav, M.; Kumar, M.; Srivastava, N. Supercapacitive Performance Analysis of Low Cost and Environment Friendly Potato Starch Based Electrolyte System with Anodized Aluminium and Teflon Coated Carbon Cloth as Electrode. *Electrochim Acta* **2018**, *283*, 1551–1559. https://doi.org/10.1016/j.electacta.2018.07.060.

(85) Yadav, M.; Nautiyal, G.; Verma, A.; Kumar, M.; Tiwari, T.; Srivastava, N. Electrochemical Characterization of NaClO4–Mixed Rice Starch as a Cost-Effective and Environment-Friendly Electrolyte. *Ionics (Kiel)* **2019**, *25* (6), 2693–2700. https://doi.org/10.1007/s11581-018-2794-x.

(86) Kim, J.; Scheers, J.; Park, T. J.; Kim, Y. Superior Ion-Conducting Hybrid Solid Electrolyte for All-Solid-State Batteries. *ChemSusChem* **2015**, *8* (4), 636–641. https://doi.org/10.1002/cssc.201402969.

(87) Le Bideau, J.; Viau, L.; Vioux, A. Ionogels, Ionic Liquid Based Hybrid Materials. *Chem. Soc. Rev.* **2011**, *40* (2), 907–925. https://doi.org/10.1039/C0CS00059K.

(88) Joos, B.; Vranken, T.; Marchal, W.; Safari, M.; Van Bael, M. K.; Hardy, A. T. Eutectogels: A New Class of Solid Composite Electrolytes for Li/Li-Ion Batteries. *Chemistry of Materials* **2018**, *30* (3), 655–662. https://doi.org/10.1021/acs.chemmater.7b03736.

(89) Sahrash, R.; Siddiqa, A.; Razzaq, H.; Iqbal, T.; Qaisar, S. PVDF Based Ionogels: Applications towards Electrochemical Devices and Membrane Separation Processes. *Heliyon* **2018**, *4* (11), e00847. https://doi.org/10.1016/j.heliyon.2018.e00847.

(90) Brachet, M.; Brousse, T.; Le Bideau, J. All Solid-State Symmetrical Activated Carbon Electrochemical Double Layer Capacitors Designed with Ionogel Electrolyte. *ECS Electrochemistry Letters* **2014**, *3* (11), A112–A115. https://doi.org/10.1149/2.0051411eel.

(91) Horowitz, A. I.; Panzer, M. J. High-Performance, Mechanically Compliant Silica-Based Ionogels for Electrical Energy Storage Applications. *J Mater Chem* **2012**, *22* (32), 16534. https://doi.org/10.1039/c2jm33496h.

(92) Liu, X.; He, B.; Wang, Z.; Tang, H.; Su, T.; Wang, Q. Tough Nanocomposite Ionogel-Based Actuator Exhibits Robust Performance. *Sci Rep* **2014**, *4* (1), 6673. https://doi.org/10.1038/srep06673.

(93) Andrzejewska, E.; Marcinkowska, A.; Zgrzeba, A. Ionogels – Materials Containing Immobilized Ionic Liquids. *Polimery* **2017**, *62* (05), 344–352. https://doi.org/10.14314/polimery.2017.344.

(94) Kubo, W.; Kambe, S.; Nakade, S.; Kitamura, T.; Hanabusa, K.; Wada, Y.; Yanagida, S. Photocurrent-Determining Processes in Quasi-Solid-State Dye-Sensitized Solar Cells Using Ionic Gel Electrolytes. *J Phys Chem B* **2003**, *107* (18), 4374–4381. https://doi.org/10.1021/jp034248x.

(95) Winterton, N. Solubilization of Polymers by Ionic Liquids. *J Mater Chem* **2006**, *16* (44),

4281. https://doi.org/10.1039/b610143g.

(96) Yan, F.; Yu, S.; Zhang, X.; Qiu, L.; Chu, F.; You, J.; Lu, J. Enhanced Proton Conduction in Polymer Electrolyte Membranes as Synthesized by Polymerization of Protic Ionic Liquid-Based Microemulsions. *Chemistry of Materials* **2009**, *21* (8), 1480–1484. https://doi.org/10.1021/cm900098r.

(97) Wang, P.; Zakeeruddin, S. M.; Grätzel, M. Solidifying Liquid Electrolytes with Fluorine Polymer and Silica Nanoparticles for Quasi-Solid Dye-Sensitized Solar Cells. *J Fluor Chem* **2004**, *125* (8), 1241–1245. https://doi.org/10.1016/j.jfluchem.2004.05.010.

(98) Hench, L. L.; West, J. K. The Sol-Gel Process. *Chem Rev* **1990**, *90* (1), 33–72. https://doi.org/10.1021/cr00099a003.

(99) Wang, J.; Zhang, S.; Ma, Z.; Yan, L. Deep Eutectic Solvents Eutectogels: Progress and Challenges. *Green Chemical Engineering* **2021**, *2* (4), 359–367. https://doi.org/10.1016/j.gce.2021.06.001.

(100) Qin, H.; Panzer, M. J. Chemically Cross-Linked Poly(2-hydroxyethyl Methacrylate)-Supported Deep Eutectic Solvent Gel Electrolytes for Eco-Friendly Supercapacitors. *ChemElectroChem* **2017**, *4* (10), 2556–2562. https://doi.org/10.1002/celc.201700586.

(101) Hong, S.; Yuan, Y.; Liu, C.; Chen, W.; Chen, L.; Lian, H.; Liimatainen, H. A Stretchable and Compressible Ion Gel Based on a Deep Eutectic Solvent Applied as a Strain Sensor and Electrolyte for Supercapacitors. *J Mater Chem C Mater* **2020**, *8* (2), 550–560. https://doi.org/10.1039/C9TC05913J.

(102) Wang, J.; Ma, Z.; Wang, Y.; Shao, J.; Yan, L. Ultra-Stretchable, Self-Healing, Conductive, and Transparent PAA/DES Ionic Gel. *Macromol Rapid Commun* **2021**, *42* (2). https://doi.org/10.1002/marc.202000445.

(103) Mota-Morales, J. D.; Gutiérrez, M. C.; Ferrer, M. L.; Jiménez, R.; Santiago, P.; Sanchez, I. C.; Terrones, M.; Del Monte, F.; Luna-Bárcenas, G. Synthesis of Macroporous

Poly(Acrylic Acid)–Carbon Nanotube Composites by Frontal Polymerization in Deep-Eutectic Solvents. *J Mater Chem A Mater* **2013**, *1* (12), 3970. https://doi.org/10.1039/c3ta01020a.

(104) Isik, M.; Ruiperez, F.; Sardon, H.; Gonzalez, A.; Zulfiqar, S.; Mecerreyes, D. Innovative Poly(Ionic Liquid)s by the Polymerization of Deep Eutectic Monomers. *Macromol Rapid Commun* **2016**, *37* (14), 1135–1142. https://doi.org/10.1002/marc.201600026.

(105) Li, R.; Chen, G.; Fan, T.; Zhang, K.; He, M. Transparent Conductive Elastomers with Excellent Autonomous Self-Healing Capability in Harsh Organic Solvent Environments. *J Mater Chem A Mater* **2020**, *8* (10), 5056–5061. https://doi.org/10.1039/D0TA00050G.

(106) Marullo, S.; Meli, A.; Giannici, F.; D'Anna, F. Supramolecular Eutecto Gels: Fully Natural Soft Materials. *ACS Sustain Chem Eng* **2018**, *6* (10), 12598–12602. https://doi.org/10.1021/acssuschemeng.8b04278.

(107) Florindo, C.; Celia-Silva, L. G.; Martins, L. F. G.; Branco, L. C.; Marrucho, I. M. Supramolecular Hydrogel Based on a Sodium Deep Eutectic Solvent. *Chemical Communications* **2018**, *54* (54), 7527–7530. https://doi.org/10.1039/C8CC03266A.

(108) Ruiz-Olles, J.; Slavik, P.; Whitelaw, N. K.; Smith, D. K. Self-Assembled Gels Formed in Deep Eutectic Solvents: Supramolecular Eutectogels with High Ionic Conductivity. *Angewandte Chemie* **2019**, *131* (13), 4217–4222. https://doi.org/10.1002/ange.201810600.

(109) Gupta, A. K.; Verma, Y. L.; Singh, R. K.; Chandra, S. Studies on an Ionic Liquid Confined in Silica Nanopores: Change in T_g and Evidence of Organic–Inorganic Linkage at the Pore Wall Surface. *The Journal of Physical Chemistry C* **2014**, *118* (3), 1530–1539. https://doi.org/10.1021/jp408142a.

(110) Guyomard-Lack, A.; Delannoy, P.-E.; Dupré, N.; Cerclier, C. V.; Humbert, B.; Le

Bideau, J. Destructuring Ionic Liquids in Ionogels: Enhanced Fragility for Solid Devices. *Phys. Chem. Chem. Phys.* **2014**, *16* (43), 23639–23645. https://doi.org/10.1039/C4CP03187C.

(111) Néouze, M.-A.; Le Bideau, J.; Gaveau, P.; Bellayer, S.; Vioux, A. Ionogels, New Materials Arising from the Confinement of Ionic Liquids within Silica-Derived Networks. *Chemistry of Materials* **2006**, *18* (17), 3931–3936. https://doi.org/10.1021/cm060656c.

(112) Martinelli, A.; Nordstierna, L. An Investigation of the Sol–Gel Process in Ionic Liquid–Silica Gels by Time Resolved Raman and 1H NMR Spectroscopy. *Physical Chemistry Chemical Physics* **2012**, *14* (38), 13216. https://doi.org/10.1039/c2cp41914a.

(113) Schantz Zackrisson, A.; Martinelli, A.; Matic, A.; Bergenholtz, J. Concentration Effects on Irreversible Colloid Cluster Aggregation and Gelation of Silica Dispersions. *J Colloid Interface Sci* **2006**, *301* (1), 137–144. https://doi.org/10.1016/j.jcis.2006.04.066.

(114) Li, X.; Zhang, Z.; Yang, L.; Tachibana, K.; Hirano, S. TiO2-Based Ionogel Electrolytes for Lithium Metal Batteries. *J Power Sources* **2015**, *293*, 831–834. https://doi.org/10.1016/j.jpowsour.2015.06.033.

(115) Wu, F.; Chen, N.; Chen, R.; Zhu, Q.; Qian, J.; Li, L. "Liquid-in-Solid" and "Solid-in-Liquid" Electrolytes with High Rate Capacity and Long Cycling Life for Lithium-Ion Batteries. *Chemistry of Materials* **2016**, *28* (3), 848–856. https://doi.org/10.1021/acs.chemmater.5b04278.

(116) Wu, F.; Chen, N.; Chen, R.; Zhu, Q.; Tan, G.; Li, L. Self-Regulative Nanogelator Solid Electrolyte: A New Option to Improve the Safety of Lithium Battery. *Advanced Science* **2016**, *3* (1). https://doi.org/10.1002/advs.201500306.

(117) Tarkanovskaja, M.; Välbe, R.; Põhako-Esko, K.; Mäeorg, U.; Reedo, V.; Hoop, A.; Saal, K.; Krumme, A.; Kink, I.; Heinmaa, I.; Lõhmus, A. Novel Homogeneous Gel Fibers and

Capillaries from Blend of Titanium Tetrabutoxide and Siloxane Functionalized Ionic Liquid. *Ceram Int* **2014**, *40* (6), 7729–7735. https://doi.org/10.1016/j.ceramint.2013.12.114.

(118) Lee, U.-H.; Kudo, T.; Honma, I. High-Ion Conducting Solidified Hybrid Electrolytes by the Self-Assembly of Ionic Liquids and TiO2. *Chemical Communications* **2009**, No. 21, 3068. https://doi.org/10.1039/b903034d.

(119) Dai, S.; Ju, Y. H.; Gao, H. J.; Lin, J. S.; Pennycook, S. J.; Barnes, C. E. Preparation of Silica Aerogel Using Ionic Liquids as Solvents. *Chemical Communications* **2000**, No. 3, 243–244. https://doi.org/10.1039/a907147d.

(120) Wu, F.; Tan, G.; Chen, R.; Li, L.; Xiang, J.; Zheng, Y. Novel Solid-State Li/LiFePO $_4$ Battery Configuration with a Ternary Nanocomposite Electrolyte for Practical Applications. *Advanced Materials* **2011**, *23* (43), 5081–5085. https://doi.org/10.1002/adma.201103161.

(121) Hsia, B.; Marschewski, J.; Wang, S.; In, J. Bin; Carraro, C.; Poulikakos, D.; Grigoropoulos, C. P.; Maboudian, R. Highly Flexible, All Solid-State Micro-Supercapacitors from Vertically Aligned Carbon Nanotubes. *Nanotechnology* **2014**, *25* (5), 055401. https://doi.org/10.1088/0957-4484/25/5/055401.

(122) Brachet, M.; Gaboriau, D.; Gentile, P.; Fantini, S.; Bidan, G.; Sadki, S.; Brousse, T.; Le Bideau, J. Solder-Reflow Resistant Solid-State Micro-Supercapacitors Based on Ionogels. *J Mater Chem A Mater* **2016**, *4* (30), 11835–11843. https://doi.org/10.1039/C6TA03142K.

(123) Su, Z.; Yang, C.; Xie, B.; Lin, Z.; Zhang, Z.; Liu, J.; Li, B.; Kang, F.; Wong, C. P. Scalable Fabrication of MnO $_2$ Nanostructure Deposited on Free-Standing Ni Nanocone Arrays for Ultrathin, Flexible, High-Performance Micro-Supercapacitor. *Energy Environ. Sci.* **2014**, *7* (8), 2652–2659. https://doi.org/10.1039/C4EE01195C.

(124) Wang, S.; Hsia, B.; Carraro, C.; Maboudian, R. High-Performance All Solid-State Micro-Supercapacitor Based on Patterned Photoresist-Derived Porous Carbon Electrodes and an Ionogel Electrolyte. *J. Mater. Chem. A* **2014**, *2* (21), 7997–8002. https://doi.org/10.1039/C4TA00570H.

(125) Wang, S.; Hsia, B.; Alper, J. P.; Carraro, C.; Wang, Z.; Maboudian, R. Comparative Studies on Electrochemical Cycling Behavior of Two Different Silica-Based Ionogels. *J Power Sources* **2016**, *301*, 299–305. https://doi.org/10.1016/j.jpowsour.2015.09.121.

(126) Noor, S. A. M.; Bayley, P. M.; Forsyth, M.; MacFarlane, D. R. Ionogels Based on Ionic Liquids as Potential Highly Conductive Solid State Electrolytes. *Electrochim Acta* **2013**, *91*, 219–226. https://doi.org/10.1016/j.electacta.2012.11.113.

(127) Yao, M.; Liu, A.; Xing, C.; Li, B.; Pan, S.; Zhang, J.; Su, P.; Zhang, H. Asymmetric Supercapacitor Comprising a Core-Shell TiNb2O7@MoS2/C Anode and a High Voltage Ionogel Electrolyte. *Chemical Engineering Journal* **2020**, *394*, 124883. https://doi.org/10.1016/j.cej.2020.124883.

(128) Zhu, S.; Taberna, P.-L.; Zhao, N.; Simon, P. Salt-Template Synthesis of Mesoporous Carbon Monolith for Ionogel-Based Supercapacitors. *Electrochem commun* **2018**, *96*, 6–10. https://doi.org/10.1016/j.elecom.2018.09.003.

(129) Nègre, L.; Daffos, B.; Taberna, P. L.; Simon, P. Solvent-Free Electrolytes for Electrical Double Layer Capacitors. *J Electrochem Soc* **2015**, *162* (5), A5037–A5040. https://doi.org/10.1149/2.0061505jes.

(130) Negre, L.; Daffos, B.; Turq, V.; Taberna, P. L.; Simon, P. Ionogel-Based Solid-State Supercapacitor Operating over a Wide Range of Temperature. *Electrochim Acta* **2016**, *206*, 490–495. https://doi.org/10.1016/j.electacta.2016.02.013.

(131) Chen, N.; Xing, Y.; Wang, L.; Liu, F.; Li, L.; Chen, R.; Wu, F.; Guo, S. "Tai Chi" Philosophy Driven Rigid-Flexible Hybrid Ionogel Electrolyte for High-Performance

Lithium Battery. *Nano Energy* **2018**, *47*, 35–42. https://doi.org/10.1016/j.nanoen.2018.02.036.

(132) Liu, X.; Wu, B.; Brandon, N.; Wang, Q. Tough Ionogel-in-Mask Hybrid Gel Electrolytes in Supercapacitors with Durable Pressure and Thermal Tolerances. *Energy Technology* **2017**, *5* (2), 220–224. https://doi.org/10.1002/ente.201600251.

(133) Liu, X.; Taiwo, O. O.; Yin, C.; Ouyang, M.; Chowdhury, R.; Wang, B.; Wang, H.; Wu, B.; Brandon, N. P.; Wang, Q.; Cooper, S. J. Aligned Ionogel Electrolytes for High-Temperature Supercapacitors. *Advanced Science* **2019**, *6* (5). https://doi.org/10.1002/advs.201801337.

(134) Pandey, G. P.; Hashmi, S. A. Performance of Solid-State Supercapacitors with Ionic Liquid 1-Ethyl-3-Methylimidazolium Tris(Pentafluoroethyl) Trifluorophosphate Based Gel Polymer Electrolyte and Modified MWCNT Electrodes. *Electrochim Acta* **2013**, *105*, 333–341. https://doi.org/10.1016/j.electacta.2013.05.018.

(135) Visentin, A. F.; Panzer, M. J. Poly(Ethylene Glycol) Diacrylate-Supported Ionogels with Consistent Capacitive Behavior and Tunable Elastic Response. *ACS Appl Mater Interfaces* **2012**, *4* (6), 2836–2839. https://doi.org/10.1021/am300372n.

(136) Xing, C. X.; Zhang, H. T.; Pan, S. S.; Yao, M.; Li, B. S.; Zhang, Y. Q.; Zhang, S. J. Boosting the Safety and Energy Density of Molybdenum Disulfide/Carbon Nanotubes Based Solid-State Sodium-Ion Supercapacitors with an Ionogel Electrolyte. *Mater Today Energy* **2020**, *18*, 100527. https://doi.org/10.1016/j.mtener.2020.100527.

(137) Yang, X.; Zhang, F.; Zhang, L.; Zhang, T.; Huang, Y.; Chen, Y. A High-Performance Graphene Oxide-Doped Ion Gel as Gel Polymer Electrolyte for All-Solid-State Supercapacitor Applications. *Adv Funct Mater* **2013**, *23* (26), 3353–3360. https://doi.org/10.1002/adfm.201203556.

(138) Song, Z.; Li, L.; Zhu, D.; Miao, L.; Duan, H.; Wang, Z.; Xiong, W.; Lv, Y.; Liu, M.;

Gan, L. Synergistic Design of a N, O Co-Doped Honeycomb Carbon Electrode and an Ionogel Electrolyte Enabling All-Solid-State Supercapacitors with an Ultrahigh Energy Density. *J Mater Chem A Mater* **2019**, *7* (2), 816–826. https://doi.org/10.1039/C8TA10406A.

(139) Rana, H. H.; Park, J. H.; Ducrot, E.; Park, H.; Kota, M.; Han, T. H.; Lee, J. Y.; Kim, J.; Kim, J.-H.; Howlett, P.; Forsyth, M.; MacFarlane, D.; Park, H. S. Extreme Properties of Double Networked Ionogel Electrolytes for Flexible and Durable Energy Storage Devices. *Energy Storage Mater* **2019**, *19*, 197–205. https://doi.org/10.1016/j.ensm.2018.11.008.

(140) Zhang, X.; Kar, M.; Mendes, T. C.; Wu, Y.; MacFarlane, D. R. Supported Ionic Liquid Gel Membrane Electrolytes for Flexible Supercapacitors. *Adv Energy Mater* **2018**, *8* (15). https://doi.org/10.1002/aenm.201702702.

(141) Simotwo, S. K.; Chinnam, P. R.; Wunder, S. L.; Kalra, V. Highly Durable, Self-Standing Solid-State Supercapacitor Based on an Ionic Liquid-Rich Ionogel and Porous Carbon Nanofiber Electrodes. *ACS Appl Mater Interfaces* **2017**, *9* (39), 33749–33757. https://doi.org/10.1021/acsami.7b07479.

(142) Mukesh, C.; Gupta, R.; Srivastava, D. N.; Nataraj, S. K.; Prasad, K. Preparation of a Natural Deep Eutectic Solvent Mediated Self Polymerized Highly Flexible Transparent Gel Having Super Capacitive Behaviour. *RSC Adv* **2016**, *6* (34), 28586–28592. https://doi.org/10.1039/C6RA03309A.

(143) Joos, B.; Volders, J.; da Cruz, R. R.; Baeten, E.; Safari, M.; Van Bael, M. K.; Hardy, A. T. Polymeric Backbone Eutectogels as a New Generation of Hybrid Solid-State Electrolytes. *Chemistry of Materials* **2020**, *32* (9), 3783–3793. https://doi.org/10.1021/acs.chemmater.9b05090.

(144) Li, Z.; Zhang, S.; Jiang, Z.; Cai, D.; Gu, C.; Tu, J. Deep Eutectic Solvent-Immobilized

PVDF-HFP Eutectogel as Solid Electrolyte for Safe Lithium Metal Battery. *Mater Chem Phys* **2021**, *267*, 124701. https://doi.org/10.1016/j.matchemphys.2021.124701.

(145) Li, Z.; Xu, X.; Jiang, Z.; Chen, J.; Tu, J.; Wang, X.; Gu, C. A Silk Protein-Based Eutectogel as a Freeze-Resistant and Flexible Electrolyte for Zn-Ion Hybrid Supercapacitors. *ACS Appl Mater Interfaces* **2022**, *14* (39), 44821–44831. https://doi.org/10.1021/acsami.2c12103.

(146) Wu, Y.; Deng, Y.; Zhang, K.; Qiu, J.; Wu, J.; Yan, L. Ultrahigh Conductive and Stretchable Eutectogel Electrolyte for High-Voltage Flexible Antifreeze Quasi-Solid-State Zinc-Ion Hybrid Supercapacitor. *ACS Appl Energy Mater* **2022**, *5* (3), 3013–3021. https://doi.org/10.1021/acsaem.1c03654.

(147) Yang, H.; Zhang, J.; Yao, J.; Zuo, D.; Xu, J.; Zhang, H. A Gel Polymer Electrolyte Based on Ternary Deep Eutectic Solvent for Flexible, Wide-Temperature Tolerant Zinc-Ion Hybrid Supercapacitors. *J Power Sources* **2022**, *548*, 232070. https://doi.org/10.1016/j.jpowsour.2022.232070.

(148) Yan, C.; Li, W.; Liu, Z.; Zheng, S.; Hu, Y.; Zhou, Y.; Guo, J.; Ou, X.; Li, Q.; Yu, J.; Li, L.; Yang, M.; Liu, Q.; Yan, F. Ionogels: Preparation, Properties and Applications. *Adv Funct Mater* **2023**. https://doi.org/10.1002/adfm.202314408.

(149) Zhao, D.; Martinelli, A.; Willfahrt, A.; Fischer, T.; Bernin, D.; Khan, Z. U.; Shahi, M.; Brill, J.; Jonsson, M. P.; Fabiano, S.; Crispin, X. Polymer Gels with Tunable Ionic Seebeck Coefficient for Ultra-Sensitive Printed Thermopiles. *Nat Commun* **2019**, *10* (1), 1093. https://doi.org/10.1038/s41467-019-08930-7.

(150) Fang, Y.; Cheng, H.; He, H.; Wang, S.; Li, J.; Yue, S.; Zhang, L.; Du, Z.; Ouyang, J. Stretchable and Transparent Ionogels with High Thermoelectric Properties. *Adv Funct Mater* **2020**, *30* (51). https://doi.org/10.1002/adfm.202004699.

(151) Liu, Z.; Cheng, H.; He, H.; Li, J.; Ouyang, J. Significant Enhancement in the

Thermoelectric Properties of Ionogels through Solid Network Engineering. *Adv Funct Mater* **2022**, *32* (7). https://doi.org/10.1002/adfm.202109772.

(152) Liu, K.; Lv, J.; Fan, G.; Wang, B.; Mao, Z.; Sui, X.; Feng, X. Flexible and Robust Bacterial Cellulose-Based Ionogels with High Thermoelectric Properties for Low-Grade Heat Harvesting. *Adv Funct Mater* **2022**, *32* (6). https://doi.org/10.1002/adfm.202107105.

(153) Chen, Q.; Cheng, B.; Wang, Z.; Sun, X.; Liu, Y.; Sun, H.; Li, J.; Chen, L.; Zhu, X.; Huang, L.; Ni, Y.; An, M.; Li, J. Rarely Negative-Thermovoltage Cellulose Ionogel with Simultaneously Boosted Mechanical Strength and Ionic Conductivity *via* Ion-Molecular Engineering. *J Mater Chem A Mater* **2023**, *11* (5), 2145–2154. https://doi.org/10.1039/D2TA09068F.

(154) Li, T.; Wang, Y.; Li, S.; Liu, X.; Sun, J. Mechanically Robust, Elastic, and Healable Ionogels for Highly Sensitive Ultra-Durable Ionic Skins. *Advanced Materials* **2020**, *32* (32). https://doi.org/10.1002/adma.202002706.

(155) Hao, S.; Li, T.; Yang, X.; Song, H. Ultrastretchable, Adhesive, Fast Self-Healable, and Three-Dimensional Printable Photoluminescent Ionic Skin Based on Hybrid Network Ionogels. *ACS Appl Mater Interfaces* **2022**, *14* (1), 2029–2037. https://doi.org/10.1021/acsami.1c21325.

(156) Yamada, S.; Toshiyoshi, H. Temperature Sensor with a Water-Dissolvable Ionic Gel for Ionic Skin. *ACS Appl Mater Interfaces* **2020**, *12* (32), 36449–36457. https://doi.org/10.1021/acsami.0c10229.

(157) Syairah, A.; Khanmirzaei, M. H.; Saidi, N. M.; Farhana, N. K.; Ramesh, S.; Ramesh, K.; Ramesh, S. Effect of Different Imidazolium-Based Ionic Liquids on Gel Polymer Electrolytes for Dye-Sensitized Solar Cells. *Ionics (Kiel)* **2019**, *25* (5), 2427–2435. https://doi.org/10.1007/s11581-018-2603-6.

(158) Xi, S.; Tian, F.; Wei, G.; He, X.; Shang, Y.; Ju, Y.; Li, W.; Lu, Q.; Wang, Q. Reversible Dendritic-Crystal-Reinforced Polymer Gel for Bioinspired Adaptable Adhesive. *Advanced Materials* **2021**, *33* (40). https://doi.org/10.1002/adma.202103174.

(159) Yu, Z.; Wu, P. Water-Resistant Ionogel Electrode with Tailorable Mechanical Properties for Aquatic Ambulatory Physiological Signal Monitoring. *Adv Funct Mater* **2021**, *31* (51). https://doi.org/10.1002/adfm.202107226.

(160) Löffelmann, U.; Wang, N.; Mager, D.; Smith, P. J.; Korvink, J. G. Solvent-free Inkjet Printing Process for the Fabrication of Conductive, Transparent, and Flexible Ionic Liquid-polymer Gel Structures. *J Polym Sci B Polym Phys* **2012**, *50* (1), 38–46. https://doi.org/10.1002/polb.22346.

(161) Portillo-Castillo, O. J.; Castro-Ríos, R.; Chávez-Montes, A.; González-Horta, A.; Cavazos-Rocha, N.; Granados-Guzmán, G.; Waksman de Torres, N.; Garza-Tapia, M. Fabrication and Characterization of a Laboratory–Made New Coating Based on 1-Decyl-3-Methylimidazolium Tetrafluoroborate for SPME Fibers, an Exploration to Its Application in Extractions by Direct-Immersion Mode. *J Mex Chem Soc* **2022**, *66* (2). https://doi.org/10.29356/jmcs.v66i2.1693.

(162) Pang, L.; Yang, P.; Pang, R.; Lu, X.; Xiao, J.; Li, S.; Zhang, H.; Zhao, J. Ionogel-Based Ionic Liquid Coating for Solid-Phase Microextraction of Organophosphorus Pesticides from Wine and Juice Samples. *Food Anal Methods* **2018**, *11* (1), 270–281. https://doi.org/10.1007/s12161-017-0997-9.

(163) Pang, L.; Pang, R.; Ge, L.; Zheng, L.; Zhao, J.; Zhang, H. Trace Determination of Organophosphate Esters in Environmental Water Samples with an Ionogel-based Nanoconfined Ionic Liquid Fiber Coating for Solid-phase Microextraction with Gas Chromatography and Flame Photometric Detection. *J Sep Sci* **2016**, *39* (22), 4415–4421. https://doi.org/10.1002/jssc.201600662.

(164) Nabais, A. R.; Neves, L. A.; Tomé, L. C. Mixed-Matrix Ion Gel Membranes for Gas Separation. *ACS Appl Polym Mater* **2022**, *4* (5), 3098–3119. https://doi.org/10.1021/acsapm.1c01737.

(165) Fu, Y.; Chen, L.; Xu, F.; Li, X.; Li, Y.; Sun, J. Spontaneous Self-Healing Ionogels for Efficient and Reliable Carbon Dioxide Separation. *J Mater Chem A Mater* **2022**, *10* (9), 4695–4702. https://doi.org/10.1039/D1TA08915C.

(166) Wang, Y.-M.; Ulrich, V.; Donnelly, G. F.; Lorenzini, F.; Marr, A. C.; Marr, P. C. A Recyclable Acidic Ionic Liquid Gel Catalyst for Dehydration: Comparison with an Analogous SILP Catalyst. *ACS Sustain Chem Eng* **2015**, *3* (5), 792–796. https://doi.org/10.1021/sc5008303.

(167) Gao, Y.; Zhang, W.; Li, L.; Wang, Z.; Shu, Y.; Wang, J. Ionic Liquid-Based Gels for Biomedical Applications. *Chemical Engineering Journal* **2023**, *452*, 139248. https://doi.org/10.1016/j.cej.2022.139248.

(168) Rizzo, C.; Arrigo, R.; Dintcheva, N. Tz.; Gallo, G.; Giannici, F.; Noto, R.; Sutera, A.; Vitale, P.; D'Anna, F. Supramolecular Hydro- and Ionogels: A Study of Their Properties and Antibacterial Activity. *Chemistry – A European Journal* **2017**, *23* (64), 16297–16311. https://doi.org/10.1002/chem.201702937.

(169) Viau, L.; Tourné-Péteilh, C.; Devoisselle, J.-M.; Vioux, A. Ionogels as Drug Delivery System: One-Step Sol–Gel Synthesis Using Imidazolium Ibuprofenate Ionic Liquid. *Chem. Commun.* **2010**, *46* (2), 228–230. https://doi.org/10.1039/B913879J.

(170) Trewyn, B. G.; Whitman, C. M.; Lin, V. S.-Y. Morphological Control of Room-Temperature Ionic Liquid Templated Mesoporous Silica Nanoparticles for Controlled Release of Antibacterial Agents. *Nano Lett* **2004**, *4* (11), 2139–2143. https://doi.org/10.1021/nl048774r.

(171) Moniruzzaman, M.; Tahara, Y.; Tamura, M.; Kamiya, N.; Goto, M. Ionic Liquid-

Assisted Transdermal Delivery of Sparingly Soluble Drugs. *Chemical Communications* **2010**, *46* (9), 1452. https://doi.org/10.1039/b907462g.

(172) Vijayaraghavan, R.; Thompson, B. C.; MacFarlane, D. R.; Kumar, R.; Surianarayanan, M.; Aishwarya, S.; Sehgal, P. K. Biocompatibility of Choline Salts as Crosslinking Agents for Collagen Based Biomaterials. *Chem. Commun.* **2010**, *46* (2), 294–296. https://doi.org/10.1039/B910601D.

(173) Silva, J. M.; Reis, R. L.; Paiva, A.; Duarte, A. R. C. Design of Functional Therapeutic Deep Eutectic Solvents Based on Choline Chloride and Ascorbic Acid. *ACS Sustain Chem Eng* **2018**, *6* (8), 10355–10363. https://doi.org/10.1021/acssuschemeng.8b01687.

(174) Marullo, S.; Meli, A.; Dintcheva, Nadka. Tz.; Infurna, G.; Rizzo, C.; D'Anna, F. Environmentally Friendly Eutectogels Comprising <scp>l-a</Scp> Mino Acids and Deep Eutectic Solvents: Efficient Materials for Wastewater Treatment. *Chempluschem* **2020**, *85* (2), 301–311. https://doi.org/10.1002/cplu.202000017.

(175) Ren'ai, L.; Zhang, K.; Chen, G.; Su, B.; Tian, J.; He, M.; Lu, F. Green Polymerizable Deep Eutectic Solvent (PDES) Type Conductive Paper for Origami 3D Circuits. *Chemical Communications* **2018**, *54* (18), 2304–2307. https://doi.org/10.1039/C7CC09209A.

(176) Wang, M.; Li, R.; Chen, G.; Zhou, S.; Feng, X.; Chen, Y.; He, M.; Liu, D.; Song, T.; Qi, H. Highly Stretchable, Transparent, and Conductive Wood Fabricated by in situ Photopolymerization with Polymerizable Deep Eutectic Solvents. *ACS Appl Mater Interfaces* **2019**, *11* (15), 14313–14321. https://doi.org/10.1021/acsami.9b00728.

Chapter 2

Materials and Methods

CHAPTER 2

Materials and Methods

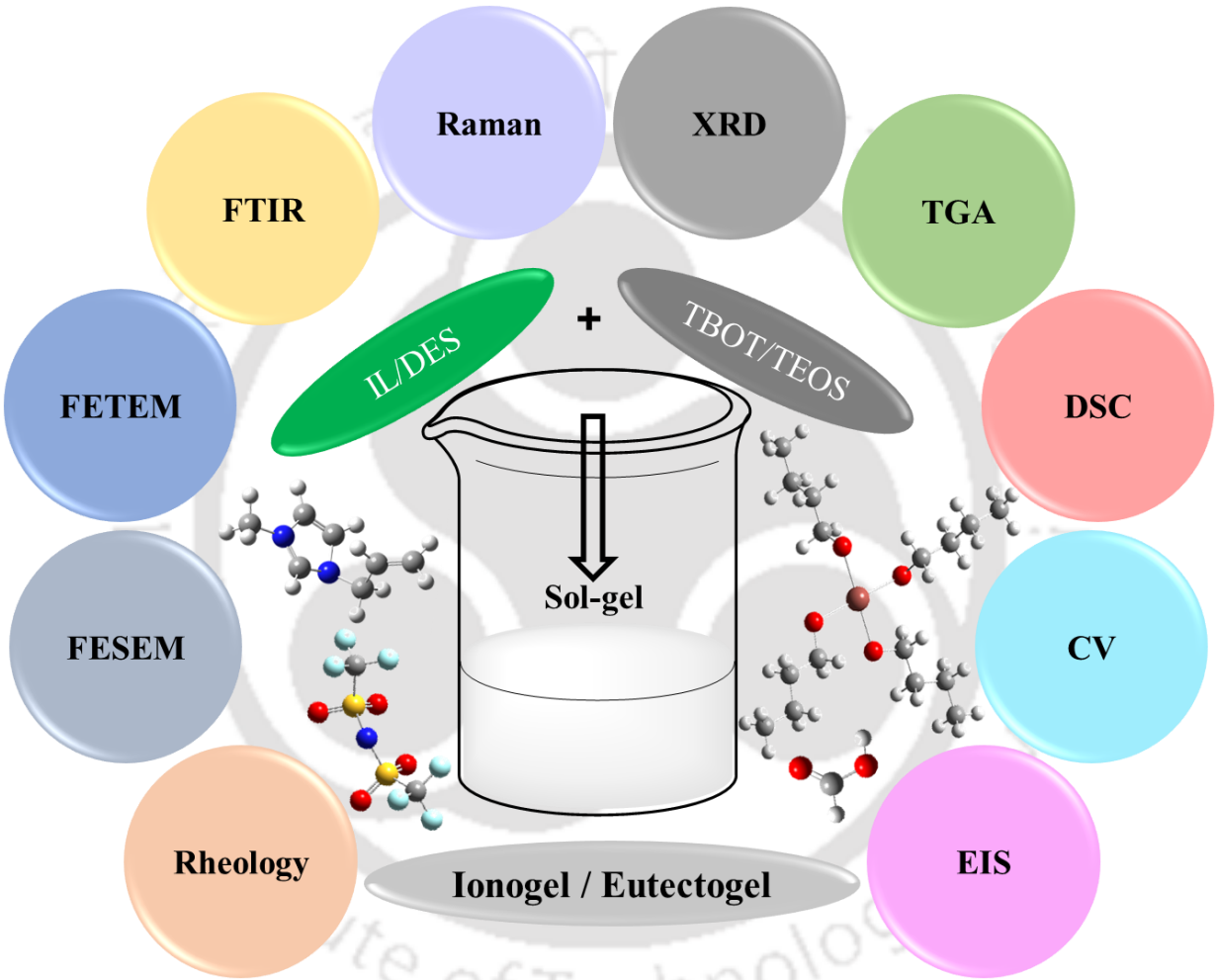

2.1. Introduction

This chapter outlines pivotal information pertaining to the materials employed in the experimental investigations, coupled with their corresponding sources. It furnishes an intricate exposition of the synthesis methodologies deployed for the ionogels, DESs, and eutectogels. Moreover, the chapter elucidates diverse techniques for characterization, accompanied by a delineation of the associated instrumentation and the prescribed procedures for sample preparation. Additionally, it provides insight into the experimental protocols employed for the assessment of various properties inherent to the DESs and gels.

2.2. Materials

2.2.1. Chemicals Used for Electrolyte Preparation and Characterization

The ILs trihexyl(tetradecyl)phosphonium bis(trifluoromethylsulfonyl)imide ([P_{66614}][TFSI]), trihexyl(tetradecyl)phosphonium dicyanamide ([P_{66614}][DCA]), 1-hexyl-3-methylimidazolium tetrafluoroborate ([HMIM][BF_4]), 1-allyl-3-methylimidazolium bis(trifluoromethylsulfonyl)imide ([AMIM][TFSI]), 1-ethyl-3-methylimidazolium trifluorotris(pentafluoroethyl)phosphate ([EMIM][FAP]), 1-propyl-3-methylimidazolium bis(trifluoromethylsulfonyl)imide ([PMIM][TFSI]), and butyl(trimethyl)ammonium bis(trifluoromethylsulfonyl)imide ([BTMA][TFSI]), were considered for the preparation of ionogels. The NADESs were synthesized using DL-Menthol ($C_{10}H_{20}O$) as the HBA and the four carboxylic acids, *viz.* decanoic acid ($C_{10}H_{20}O_2$), lauric acid ($C_{12}H_{24}O_2$), myristic acid ($C_{14}H_{28}O_2$), and palmitic acid ($C_{16}H_{32}O_2$) as the corresponding HBDs. On the other hand, 1-butyl-3-methylimidazolium methanesulfonate ([BMIM][$MeSO_3$]) and *N*-methylacetamide (NMAc) were respectively chosen as HBA and HBD for the IL-based DES. Titanium(IV) butoxide (TBOT) and tetraethyl orthosilicate (TEOS) were used as crosslinking precursors for the formation of TiO_2 and SiO_2 inorganic solid matrices. Formic acid (FA) was taken as the

catalyst in the synthesis of ionogels and eutectogels. The IL 1-butyl-3-methylimidazolium tetrafluoroborate ([BMIM][BF_4]) was used to prepare hybrid gels with the NADES-based eutectogels. Dry methanol (CH_3OH) was used as the base solvent in Karl Fischer titration of DES samples. Furthermore, nuclear magnetic resonance (NMR) spectroscopy was performed on the DESs wherein deuterated dimethyl sulfoxide-d6 (DMSO-d_6) was utilized as the solvent. Finally, ethanol (C_2H_5OH) was utilized to prepare ionogel and eutectogel samples for field emission transmission electron microscopy (FETEM) analysis. Acetone (C_3H_6O) was used to dry-clean glassware and components of the copper coin cell used for electrochemical experiments. Details of the chemicals purchased from different suppliers have been tabulated in **Table 2.1**. All chemicals were used as received.

Table 2.1. Details of purchased reagents and solvents used in experiments

Sl. No.	Name of the material	Formula / Abbreviation	Supplier	Purity (≥ %)
1	Trihexyl(tetradecyl)phosphonium bis(trifluoromethylsulfonyl)imide	[P_{66614}][TFSI]	Sigma-Aldrich	95
2	Trihexyl(tetradecyl)phosphonium dicyanamide	[P_{66614}][DCA]	TCI	93
3	1-Hexyl-3-methylimidazolium tetrafluoroborate	[HMIM][BF_4]	TCI	97
4	1-Allyl-3-methylimidazolium bis(trifluoromethylsulfonyl)imide	[AMIM][TFSI]	TCI	98
5	1-Ethyl-3-methylimidazolium trifluorotris(pentafluoroethyl)phosphate	[EMIM][FAP]	Sigma-Aldrich	High purity
6	1-Propyl-3-methylimidazolium bis(trifluoromethylsulfonyl)imide	[PMIM][TFSI]	Sigma-Aldrich	98

Table 2.1 continues

Sl. No.	Name of the material	Formula / Abbreviation	Supplier	Purity (≥ %)
7	Butyltrimethylammonium bis(trifluoromethylsulfonyl)imide	[BTMA][TFSI]	TCI	98
8	Decanoic acid	$C_{10}H_{20}O_2$	Sigma-Aldrich	98
9	Lauric acid	$C_{12}H_{24}O_2$	Sigma-Aldrich	97
10	Myristic acid	$C_{14}H_{28}O_2$	Sigma-Aldrich	98
11	Palmitic acid	$C_{16}H_{32}O_2$	Sigma-Aldrich	99
12	DL-Menthol	$C_{10}H_{20}O$	Sigma-Aldrich	98
13	1-Butyl-3-methylimidazolium methanesulfonate	[BMIM][$MeSO_3$]	Sigma-Aldrich	95
14	*N*-Methylacetamide	NMAc	Sigma-Aldrich	99
15	Titanium(IV) butoxide	TBOT	Sigma-Aldrich	97
16	Tetraethyl orthosilicate	TEOS	Alfa Aesar	98
17	Formic acid	HCOOH / FA	Sigma-Aldrich	98
18	1-Butyl-3-methylimidazolium tetrafluoroborate	[BMIM][BF_4]	IoLiTec	99
19	Methanol	CH_3OH	Sigma-Aldrich	99
20	Dimethyl sulfoxide-d6	DMSO-d_6	Sigma-Aldrich	99.8
21	Ethanol	C_2H_5OH	Sigma-Aldrich	99
22	Acetone	C_3H_6O	Sigma-Aldrich	99

2.2.2. Electrode Material

All electrochemical investigations were conducted employing a symmetrical two-electrode configuration. This specific arrangement necessitates the utilization of two electrodes composed of identical materials, serving as the working electrode (WE) and the counter

electrode (CE). Exfoliated carbon, specifically reduced graphene oxide (rGO), was employed to assess the ionic conductivities and characterize the electrochemical properties of the ionogel and eutectogel electrolytes (**Figure 2.1**). The porous exfoliated carbon sheet electrodes, which incorporated a butyl rubber binder, were procured from Vikram Sarabhai Space Center, Thiruvanthapuram, India. The Brunauer-Emmett-Teller (BET) surface area of these electrodes was determined to be 635 m^2 g^{-1} in the presence of the binder, along with an average pore size of 2.6 nm as measured using Quantachrome (Autosorb-IQ MP) surface area and pore size analysis.

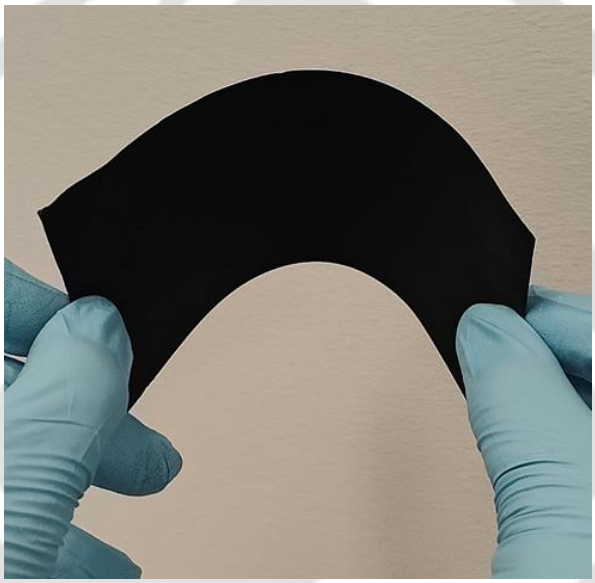

Figure 2.1. Photograph of a piece of the exfoliated reduced graphene oxide (rGO) sheet utilized as electrode in this research.

2.3. Preparation of Ionogels, DESs, and Eutectogels

This section outlines the details pertaining to the preparation of ionogels, DESs, and eutectogels for this research. The materials were synthesized, as and when required, with and in facilities available at the Department of Chemical Engineering at the Indian Institute of Technology (IIT) Guwahati or the School of Molecular and Life Sciences at Curtin University, Australia.

2.3.1. Preparation of Ionogels

Gelation of the ILs was obtained through a simple nonaqueous sol−gel process.[1,2] The precursor solution contained the IL, the crosslinker TBOT, and FA catalyst in a 1:1:7.8 molar ratio. The structures of the precursors have been represented in **Figure 2.2**, while their stoichiometric details and nomenclature of the corresponding ionogels have been tabulated in **Table 2.2**. To obtain a homogeneous quasi-solid phase of the confined IL, a unit molar ratio of the IL and TBOT was employed for the synthesis process.[1,2] **Figure 2.3** illustrates the experimental setup and synthesis route of the ionogels using the aforementioned precursors. Initially, a calculated amount of IL was poured into a beaker (**Figure 2.3**: step A). To that, the required volume of TBOT was added with the help of a micropipette (**Figure 2.3**: step B) and thoroughly stirred using a magnetic stirrer (TARSONS SPINOT, India) for about 15 min until a homogeneous mixture was formed (**Figure 2.3**: step C). Thereafter, the designated volume of FA was added dropwise into the mixture (**Figure 2.3**: step D) and stirred for another 5 min (**Figure 2.3**: step E). The appearance of turbidity immediately indicated the occurrence of hydrolysis of TBOT. The sol phase, thus formed (**Figure 2.3**: step F), was left to age at room temperature for about 48 h (**Figure 2.3**: step G). Finally, complete gelation was obtained by drying it at ~70 °C in vacuum for about 24 h so as to completely remove unreacted FA and other volatile byproducts (**Figure 2.3**: step H). The gels manifested a quasi-solid characteristic. Post acquisition, the gels were properly sealed with parafilm to avoid the contact of moisture and stored away from sunlight.

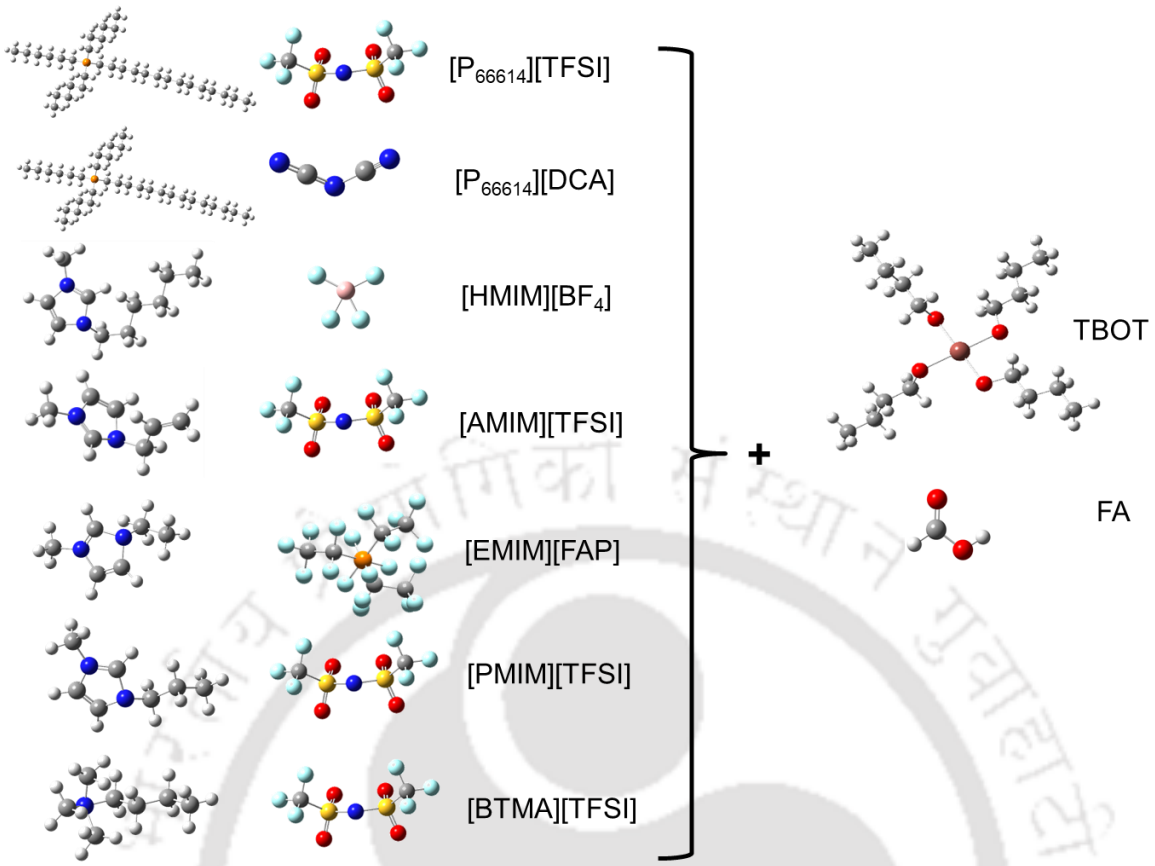

Figure 2.2. Structures of the precursors used for the preparation of the seven inorganic ionogels. These include the ILs $[P_{66614}][TFSI]$, $[P_{66614}][DCA]$, $[HMIM][BF_4]$, [AMIM][TFSI], [EMIM][FAP], [PMIM][TFSI], and [BTMA][TFSI]; the crosslinker TBOT; and the catalyst FA. (boron: pink, carbon: black, fluorine: green, hydrogen: white, nitrogen: blue, oxygen: red, phosphorus: golden, sulfur: yellow, and titanium: brown)

Table 2.2. Nomenclature and composition details used for preparation of ionogels

IL	Precursor	Mole	Quantity	Matrix	Ionogel
1	$[P_{66614}][TFSI]$	1	4.3 g		
	TBOT	1	1.9 mL	TiO_2	TIGel1
	FA	7.8	1.6 mL		
2	$[P_{66614}][DCA]$	1	3.6 g		
	TBOT	1	2.2 mL	TiO_2	TIGel2
	FA	7.8	1.9 mL		
3	$[HMIM][BF_4]$	1	4.6 g		
	TBOT	1	6.2 mL	TiO_2	TIGel3
	FA	7.8	5.3 mL		
4	[AMIM][TFSI]	1	6.0 g		
	TBOT	1	5.1 mL	TiO_2	TIGel4
	FA	7.8	4.4 mL		
5	[EMIM][FAP]	1	6.8 g		
	TBOT	1	4.2 mL	TiO_2	TIGel5
	FA	7.8	3.6 mL		
6	[PMIM][TFSI]	1	5.8 g		
	TBOT	1	4.9 mL	TiO_2	TIGel6
	FA	7.8	4.2 mL		
7	[BTMA][TFSI]	1	5.6 g		
	TBOT	1	4.8 mL	TiO_2	TIGel7
	FA	7.8	4.1 mL		

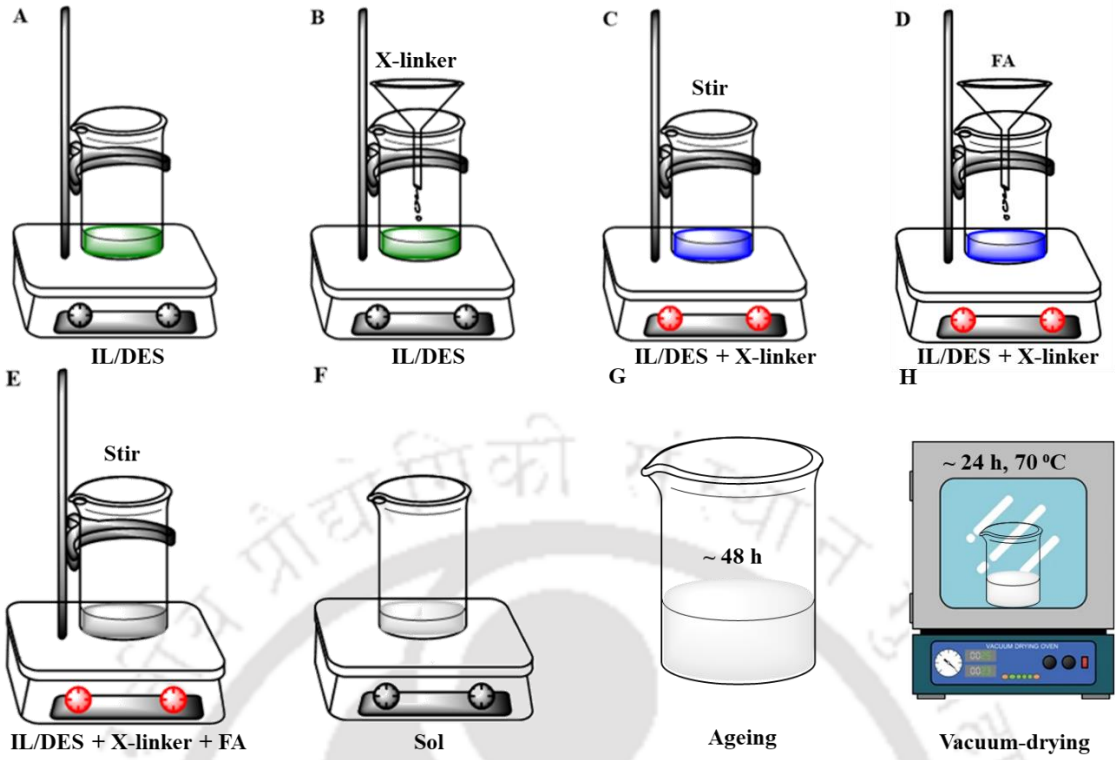

Figure 2.3. Schematic illustration of the step-by-step experimental procedure (A through H) for the gelation of ILs and DESs using TBOT or TEOS and FA with a magnetic stirrer at room temperature, followed by ageing and vacuum-drying.

The reaction scheme is illustrated in **Figure 2.4**. A total of five steps of chemical reactions are involved in the process. The reaction is initiated by the carboxylation of TBOT and FA on the Ti atom, which generates butanol molecules and formate derivatives (**equation 2.1**). **Equation 2.2** represents the nonhydrolytic hydroxylation, which is followed by an esterification reaction (**equation 2.3**) that delivers water for subsequent hydrolysis of the carboxylized product (**equation 2.4**). Finally, condensation takes place with the formation of TiO_2 through dehydration of the Ti−OH group (**equation 2.5**a and b). The IL acts as a solvent and does not take part in the sol−gel reactions.[2]

Carboxylation: $Ti(OBu)_4 + 4HCOOH \rightarrow Ti(OOCH)_4 + 4BuOH$ **(2.1)**

Hydroxylation: $Ti(OOCH)_4 + 4BuOH \rightarrow Ti(OH)_4 + 4BuOOCH$ **(2.2)**

Esterification: $HCOOH + BuOH \rightarrow H_2O + BuOOCH$ **(2.3)**

Hydrolysis: $Ti(OOCH)_4 + 4H_2O \rightarrow Ti(OH)_4 + 4HCOOH$ **(2.4)**

Condensation: $Ti(OH)_4 + Ti(OOCH)_4 \rightarrow 2TiO_2 + 4HCOOH$ **(2.5a)**

$2Ti(OH)_4 \rightarrow 2TiO_2 + 4H_2O$ **(2.5b)**

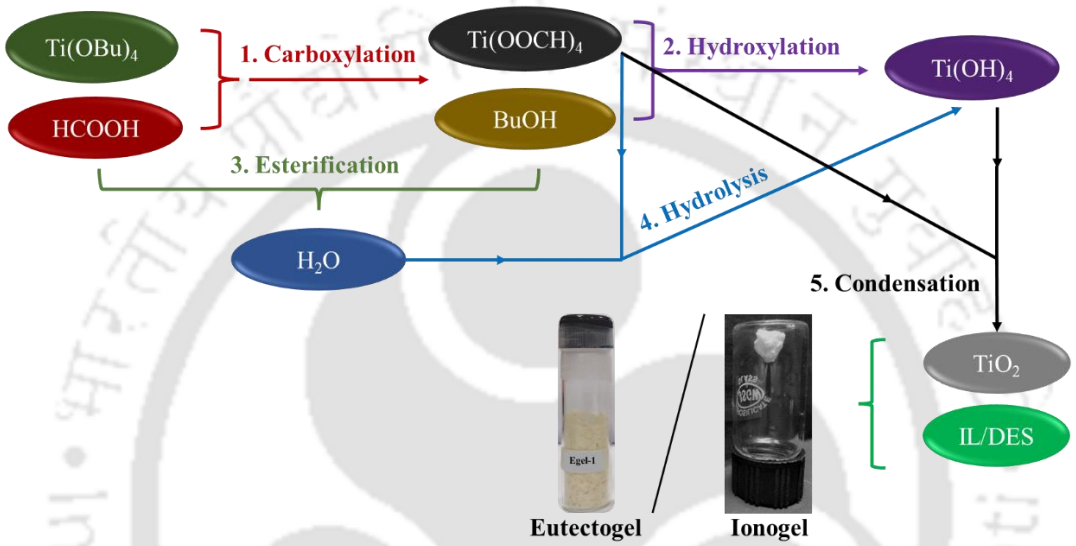

Figure 2.4. Schematic representation of the five steps of chemical reactions involved in the sol-gel synthesis of TiO_2-based inorganic ionogels and eutectogels.

2.3.2. Preparation of DESs

2.3.2.1. Preparation of NADESs

Four NADESs (DESs 1–4) were prepared as per the methods reported in previous works. To prepare the hydrophobic DESs, in each case, the carboxylic acid (HBD) and DL-Menthol (HBA) were first mixed in a 100 mL flat-bottom flask in a specific molar ratio as tabulated in **Table 2.3**.[3–6] The mixture was then placed on a magnetic hot plate (TARSONS SPINOT-magnetic stirrer and hot plate-DIGITAL, MC02, India) and allowed to heat at a temperature of 50 °C while being continuously stirred for approximately 2 h at 1 atm pressure until the

acquisition of a homogeneous colorless clear liquid. Thereafter, the as-obtained DESs were kept under vacuum at a lowered pressure of 600 mmHg and a temperature of 60 °C for 48 h to remove any potential water content and unwanted volatile impurities.

2.3.2.2. Preparation of IL-based DES

The synthesis process of the IL-based DES (DES5) followed the steps as outlined by Mahanta et al.[7] [BMIM][$MeSO_3$] (HBA) and NMAc (HBD) underwent vacuum drying for 10−12 hours at 80 °C to eliminate volatile impurities. The preparation of the DES involved initially combining the HBA and the HBD in a molar ratio of 2:1, as detailed in **Table 2.3**. Subsequently, the mixture was transferred to a 100 mL flat-bottom flask and positioned on a magnetic hot plate (TARSONS SPINOT-magnetic stirrer and hot plate-DIGITAL, MC02, India). A eutectic solvent was then obtained by continuously stirring the mixture at 70 °C until the acquisition of a clear liquid.

Table 2.3. Nomenclature and composition details used for preparation of DESs

DES	Precursor	Role	Mole	Mass (g)
1	Decanoic acid	HBD	1	47.0
	DL-Menthol	HBA	1	42.6
2	Lauric acid	HBD	1	32.5
	DL-Menthol	HBA	2	50.7
3	Myristic acid	HBD	1	18.7
	DL-Menthol	HBA	4	51.1
4	Palmitic acid	HBD	1	6.5
	DL-Menthol	HBA	12	47.7
5	NMAc	HBD	2	20.0
	[BMIM][$MeSO_3$]	HBA	1	32.0

2.3.3. Preparation of Eutectogels

Similar to ILs, the gelation of the DESs was also procured through a simple non-aqueous sol-gel process.[8] Each DES was confined into two different solid matrices, *viz.* TiO_2 and SiO_2, yielding a total of ten novel inorganic eutectogels from the five DESs mentioned in **Table 2.3**. The precursor solutions consisted of the DES, the crosslinker TBOT or TEOS, and FA as the catalyst in a specified molar ratio as shown in **Table 2.4**. The structures of the precursors have been represented in **Figure 2.5**, while their stoichiometric details and nomenclature of the corresponding eutectogels have been tabulated in **Table 2.4**. First, the required quantities of DES and TBOT or TEOS were mixed in a beaker (**Figure 2.3**: steps A and B) and stirred thoroughly using a magnetic stirrer (TARSONS SPINOT, India) until the formation of a homogeneous mixture (**Figure 2.3**: step C). After that, a calculated volume of FA was added dropwise to the mixture with a micropipette (**Figure 2.3**: step D) and allowed to stir until the obvious occurrence of gelation (**Figure 2.3**: step E). The DESs immobilized with SiO_2 took a longer period of time (> 1 h) to gellify as compared to the ones with TiO_2 (< 5 min), which is consistent with observations reported previously.[1] The sol formed (**Figure 2.3**: step F) was then left undisturbed for about 48 h at ambient conditions (**Figure 2.3**: step G). Subsequently, complete gelation was obtained by drying it at ~75 °C in vacuum for about 12–24 h so as to completely remove excess FA and other volatile side products (**Figure 2.3**: step H). The gel was then sealed properly with parafilm to avert contamination with moisture and meticulously stored away from sunlight. The gels were obtained in a pulverised solid (powder grains) form.

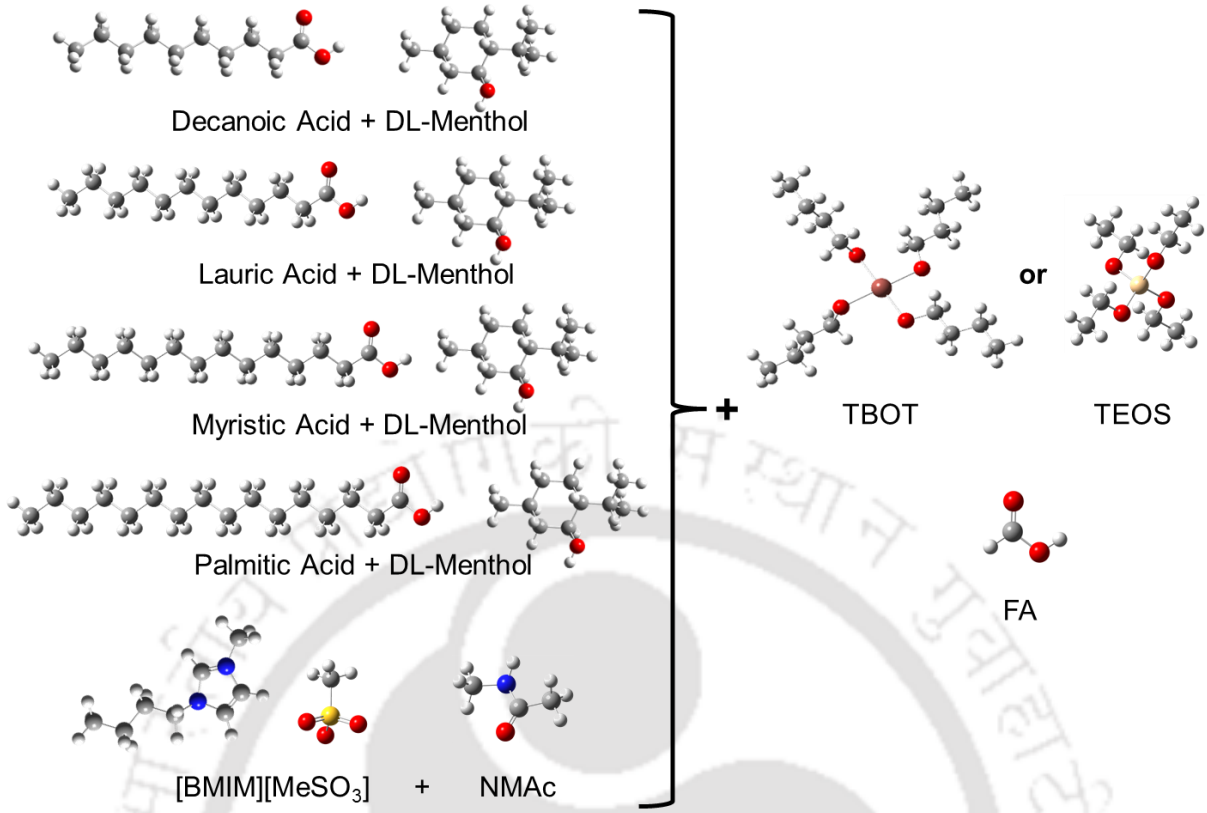

Figure 2.5. Structures of the precursors used for the preparation of the eight NADES-based inorganic eutectogels and the two IL-based inorganic eutectogels. These include DESs 1–5, the crosslinkers TBOT and TEOS, and the catalyst FA. (carbon: black, hydrogen: white, nitrogen: blue, oxygen: red, silicon: yellow, sulfur: golden, and titanium: brown)

Table 2.4. Nomenclature and composition details used for preparation of eutectogels

Precursor	Mole	Quantity	Matrix	Ionogel
DES1	1	5 g		
TBOT	2	20.7 mL	TiO_2	TEGel1
FA	7.8	8.9 mL		
DES1	1	5 g		
TEOS	2	13.6 mL	SiO_2	SEGel1
FA	7.8	8.9 mL		

Table 2.4 continues

Precursor	Mole	Quantity	Matrix	Ionogel
DES2	1	5 g		
TBOT	2	19.9 mL	TiO_2	TEGel2
FA	7.8	8.6 mL		
DES2	1	5 g		
TEOS	2	13.1 mL	SiO_2	SEGel2
FA	7.8	8.6 mL		
DES3	1	5 g		
TBOT	2	19.9 mL	TiO_2	TEGel3
FA	7.8	8.6 mL		
DES3	1	5 g		
TEOS	2	13.1 mL	SiO_2	SEGel3
FA	7.8	8.6 mL		
DES4	1	5 g		
TBOT	2	20.8 mL	TiO_2	TEGel4
FA	7.8	8.9 mL		
DES4	1	5 g		
TEOS	2	13.6 mL	SiO_2	SEGel4
FA	7.8	8.9 mL		
DES5	1	5 g		
TBOT	1	13.4 mL	TiO_2	TIEGel
FA	7.8	11.6 mL		
DES5	1	5 g		
TEOS	1	8.8 mL	SiO_2	SIEGel
FA	7.8	11.6 mL		

The reaction scheme for sol-gel-derived inorganic eutectogels follows the same steps as those of inorganic ionogels obtained through a sol-gel approach. The process involving the formation of TiO_2-based gels has already been illustrated in **Figure 2.4** and detailed in **equations 2.1** through **2.5**. For nonaqueous sol-gel immobilization of DESs into SiO_2 the reaction is initiated by the carboxylation of TEOS and FA on the Si atom, which generates ethanol molecules and formate derivatives (**equation 2.6**).[9] **Equation 2.7** represents the nonhydrolytic hydroxylation, which is followed by an esterification reaction (**equation 2.8**) that delivers water for subsequent hydrolysis of the carboxylized product (**equation 2.9**). Finally, condensation takes place with the formation of SiO_2 through dehydration of the Si−OH group (**equation 2.10**). The overall reaction leading to the formation of the SiO_2 matrix is represented by **equation 2.11**. The DES acts as a solvent and does not take part in the sol−gel reactions. The reaction scheme is depicted in **Figure 2.6.**

Carboxylation: $\equiv Si–OEt + HCOOH \rightarrow EtOH + SiCOOH$ **(2.6)**

Hydroxylation: $SiCOOH + EtOH \rightarrow SiOH + EtCOOH$ **(2.7)**

Esterification: $HCOOH + EtOH \rightarrow EtCOOH + H_2O$ **(2.8)**

Hydrolysis: $SiCOOH + H_2O \rightarrow SiOH + HCOOH$ **(2.9)**

Condensation: $SiOH + SiCOOH \rightarrow Si–O–Si + HCOOH$ **(2.10)**

Overall: $2HC(O)OH + (C_2H_5O)_4Si \rightarrow SiO_2 + 2C_2H_5OH + 2HC(O)OC_2H_5$ **(2.11)**

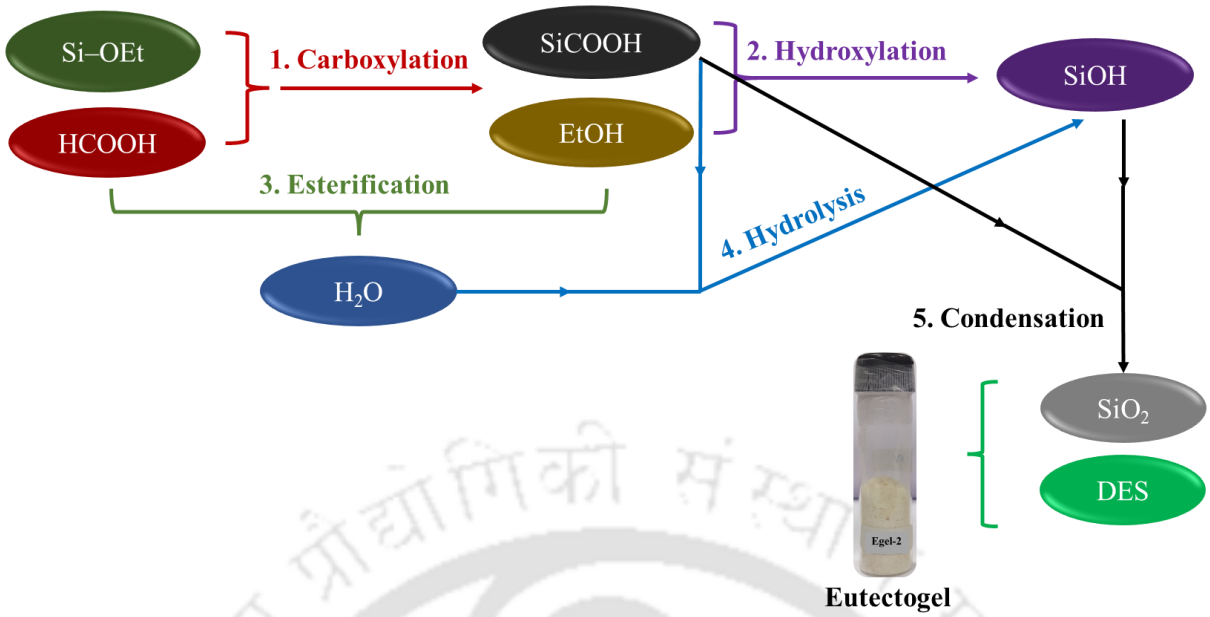

Figure 2.6. Schematic representation of the five steps of chemical reactions involved in the sol-gel synthesis of SiO_2-based inorganic eutectogels.

2.4. Materials Characterization

This section details the different characterization techniques deployed to study the physical, morphological, structural, and thermal properties of the DESs and the gels. The analyses were carried out with facilities available at the Central Instruments Facility of IIT Guwahati; Analytical Laboratory at the Department of Chemical Engineering, IIT Guwahati; Centre for the Environment, IIT Guwahati; or the Spectroscopy and Analytical Test Facility at the Indian Institute of Science (IISc), Bangalore.

2.4.1. Karl Fischer Titration

The electrochemical stability of electrolytes is influenced by the presence of water in the solvents, and hence the corresponding gels. Consequently, assessing the moisture content in the DESs prepared in the laboratory was imperative. The moisture content was determined through Karl Fischer titration using a 787 KF Titrino apparatus (Make: Metrohm, Switzerland). The method involves a reagent-based titration wherein the reagent reacts with water, converting

it into a non-conductive chemical. Dry methanol served as the base solvent in this process. The Karl Fischer reagent (526 KFR) utilized in this study was obtained from Thermo Fisher Scientific India Pvt. Ltd.

2.4.2. Nuclear Magnetic Resonance Spectroscopy

NMR spectroscopy serves as a principal method for elucidating detailed and quantitative insights into the molecular structure, functional groups, topology, and dynamics of molecules in both solution and the solid state.[10] In this technique, the sample is positioned within a high-power magnetic field and subjected to radio waves. Subsequent processing of the received signals enables the extraction of information regarding the composition of atomic groups within the molecule. In this work, the NMR technique was used to examine the purity of the laboratory-prepared DES samples. ^{1}H NMR spectroscopy was performed on a 600 MHz NMR instrument (Bruker, Germany) operated with 16 scans at room temperature. The samples were prepared on 5 mm NMR tubes by mixing ~30 mg of DES with 0.5 mL of DMSO-d_6. The homogeneity of the samples was ensured with vortex mixing. The samples were washed repeatedly four times to check their hydrophobicity.

2.4.3. Contact Angle Goniometry

Contact angle goniometry is a standard and one of the most popular tensiometric methods to determine the wettability of substances with respect to a particular surface. [11] In this process, the angle subtended by the contact point on both the left and right sides of a back-lit drop (silhouette) is optically imaged. This angle is then determined either manually using an optical goniometer or through computerized image analysis. Ideally, an angle over 90° is considered poorly wettable or highly hydrophobic by the scientific community.[12,13] Here, goniometry was used to estimate the hydrophobicity of the four NADESs used in the preparation of TEGels and SEGels. The contact angle of the sample was determined at room temperature (relative

humidity 70 %) using a goniometer (Model: HO-IAD-CAM-01B, Make: Holmarc Opto-Mechatronics) against a water droplet volume of 2 µL.

2.4.4. Rheology

Viscosity, as a diffusional property of an analyte, can significantly impact the capacitive performance of supercapacitors. In this study, viscosity investigations of pure DESs and quasi-solid ionogels were conducted at room temperature using an interfacial rheometer (Model: Physica MCR 301; Make: Anton Paar, Austria). The relative uncertainty of the dynamic viscosity was ± 0.35 %. The rheometer functions by measuring the viscosity of a liquid or gel, which is positioned on a stationary plate, while shear stress is applied through a rotating plate. For the DESs, the cone plate method (CP25-2/S) with 1° angle and 0.1 mm gap was employed and approximately 1 mL of the sample was utilized for viscosity measurements along the shear rate range of 1 to 1000 s^{-1}. The instrument enables various experiments, such as viscosity vs. temperature, shear stress vs. shear strain, constant shear stress or strain method, amplitude sweep test, frequency sweep test, among others. Additionally, the instrument offers the capability of parallel plate configuration for rheological studies.

Rheological analyses of the quasi-solid ionogels were performed using the same interfacial rheometer with a parallel plate (50 mm diameter) geometry and a gap of 1.1 mm between the plates. The flow behavior of the ionogel was measured by varying the shear rate range from 0.01 to 1000 s^{-1}. To determine the linear viscoelastic (LVE) region, an amplitude sweep test was performed over a strain range of 0.1−1000 % with a constant frequency of 1 Hz. Finally, a frequency sweep test was carried out by varying the frequency from 0.1 to 100 Hz at a constant strain (obtained from LVE analysis). The experimental data obtained from the flow behavior test were fitted and analyzed by the power law model, given in **equation 2.12**.

$$\eta = m(\gamma)^{n-1} \quad \textbf{(2.12)}$$

where, η is the apparent viscosity, m is the consistency index, γ is the shear rate, and n is the power law index.

2.4.5. Field Emission Scanning Electron Microscopy

Field emission scanning electron microscopy (FESEM) serves as a primary tool for the analysis of surface morphology including homogeneity and porosity,[14] which reveals vital information concerning the specimen's feasibility as electrolyte. Differing from an optical microscope, the scanning electron microscope utilizes electron beams for imaging instead of light. Due to the smaller wavelength of electron beams compared to light, FESEM achieves higher magnification, resolution, and a larger depth of focus. In the process, when a current passes through the metallic filament, electrons generated at the cathode are accelerated toward the anode by a high voltage. Following collimation by apertures at the anode, the electron beam is directed onto the surface of the sample through the column. Upon interaction with the sample surface, the electron beam gives rise to secondary electrons and backscattered electrons. The secondary electrons are then detected and converted into an electronic signal. The position of this electron signal is determined by systematically "scanning" the sample with the electron beam. Consequently, secondary electrons effectively reflect the morphology of the sample's surface. On the other hand, backscattered electrons are those incident electrons that bounce off the sample, revealing variations in absorption by elements. This distinction makes it easier to identify areas with different mean atomic numbers. Samples of ionogels and eutectogels were prepared for FESEM by affixing them to a stub using carbon tape, following which the stub underwent sputter coating with double layers of gold. The morphological characteristics of the samples were then observed using a Zeiss, Sigma 300 FESEM.

2.4.6. Field Emission Transmission Electron Microscopy

Similar to FESEM, FETEM imaging relies on the interaction between a high-energy electron beam (typically 80 keV or more) and a solid specimen.[15] The electron beam, generated through an appropriate illumination system, is focused by electromagnetic lenses onto the sample and passed through it. However, in contrast to FESEM, the electrons in FETEM are transmitted through the sample and further passed through additional lenses to form an image of the specimen. This capability enables the investigation of sample morphology and structure at the nanometric scale. The morphology of selected ionogels and eutectogels were further studied by visualizing their samples under a 200 keV FETEM (Model: 2100F, Make: JEOL). To prepare the samples, in each case, ~8 mg of gel was mixed with ~10 mL of ethanol and subjected to ultrasonication at room temperature for a duration of 20 min. Following this, the sample was drop-cast onto an ultrathin carbon-coated 300 mesh copper grid (Merck, India) and subsequently allowed to air-dry overnight.

2.4.7. Fourier Transform Infrared Spectroscopy

Fourier transform infrared (FTIR) spectroscopy offers a method for examining the structural details of specimens with high spatial and temporal resolution.[16] Vibrational frequencies associated with specific chemical groups are anticipated in distinct regions, contingent upon the types of atoms involved and the nature of chemical bonds. FTIR spectroscopy reveals the presence of functional groups by detecting characteristic infrared absorption bands that correspond to the fundamental vibrations of these groups. Here, the effect of the inorganic matrix (TiO_2 or SiO_2) on the structural properties of the immobilized IL or DES was analyzed through FTIR spectroscopy. One drop of IL or DES, or pelleted form of ~2 mg gel was used to obtain transmission spectra of the solvents and their corresponding gels using an FTIR instrument (Model: IRAFFINITY – 1; Make: Shimadzu, Japan).

2.4.8. Raman Spectroscopy

Another technique to identify structures is Raman spectroscopy which relies on the Raman scattering phenomenon of electromagnetic radiation by molecules. When materials are exposed to electromagnetic radiation of a single frequency, the light undergoes both elastic and inelastic scattering by the molecules. In case of the latter, known as Raman scattering, the scattered light exhibits a different frequency compared to the incident radiation. A typical Raman spectrum captures the frequency changes resulting from Stokes scattering by molecules. This alteration in frequency is referred to as the Raman shift in the spectrum and ideally falls within the same range as the infrared absorption spectrum.[14] In this study, Raman was performed on selected DESs and eutectogels to validate the observations from FTIR. Raman spectra for the samples were obtained on a Horiba LabRAM HR-800 microscope Raman system (Horiba Jobin Vyon) with an Ar-green laser beam excitation source of 532 nm. Prior to analysis, the samples were placed in a cuvette (for DESs) or on a blank glass slide (for eutectogels), and spectroscopy was subsequently conducted and analyzed. The excitation laser light was concentrated with a 100× objective lens, resulting in a typical spot size of 1 μm, and the laser power was maintained at 1.5 mW to prevent sample overheating. Signal detection was carried out using a cooled charge-coupled device (CCD) through a multimode fiber grating with 1800 grooves mm^{-1}.

2.4.9. X-Ray Diffraction Spectroscopy

X-ray diffraction (XRD) stands as a widely utilized analytical technique for the phase identification of crystallized materials.[17]

According to Bragg's law (**equation 2.13**):

$$n\lambda = 2d \times sin\theta \ (n = 1, 2, 3, \dots) \quad \textbf{(2.13)}$$

In the presence of a crystalline sample, the incident X-ray beam undergoes scattering at different planes within the crystal. The optical path length of the diffracted X-rays varies depending on the interplanar crystal spacing (*d*), incident angle (θ), and X-ray wavelength (*λ*). In a typical XRD measurement, monochromatic X-rays are directed towards the sample, scattering off its crystal planes. Detectors selectively capture constructive interference signals at specific angles, resulting in the appearance of peaks in the XRD pattern. Since the wavelength of monochromatic X-rays is constant, the angles are continuously recorded along with the corresponding X-ray intensity. The outcome of the measurement is represented by the XRD pattern, a plot of X-ray intensity on the y-axis versus the angle between the incident and diffracted beams (2θ) on the x-axis. The presence of crystallinity is characterized by diffraction peaks which correspond to specific crystal planes. The presence/absence of crystallinity in the solid matrices of the gels was discerned through XRD measurements performed on a Rigaku Micromax-007HF XRD system using a Cu X-ray source and an R-AXIS IV++ X-ray detector (wavelength, λ = 1.54184 Å) with a scanning angle range from 5 to 80°. The sample preparation involved placing ~1 g of sample on a glass slide followed by roll-spreading it to a thin and uniform layer.

2.4.10. Thermogravimetric Analysis

One of the important deterministic factors for the usability of an electrolyte in electrochemical devices is its critical safety requirement, which can be assessed from its thermal stability.[2] Thermogravimetric analysis (TGA) is a basic technique to observe mass loss of a compound with increase in temperature. Besides thermal stability of the sample, it also gives information about its change in composition and chemical reaction's kinetic parameters.[18] To study the alteration in properties, if any, thermal analyses of the ILs, DESs and their corresponding gels were carried out on a TG 209 F1 Libra (Make: M/s Netzsch, Germany) or a TGA Q500 V20.13 Build 39, as per accessibility. About 9 mg of each sample was taken in an aluminum crucible

and heated in a nitrogen atmosphere between temperatures 20 and 600 °C at a rate of 5 or 10 °C min^{-1} with a nitrogen flow rate of 40 mL min^{-1}. It may be noted here that the exposure time plays an important role in the examination of degradation kinetics and thermal degradation.[19] Therefore, isothermal TGA was also conducted on selected gels for 12 h to study their mass-loss patterns at constant temperatures of 80 and 90 °C under a nitrogen atmosphere at a heating rate of 20 °C min^{-1}. For all measurements, the uncertainty in temperature was ± 0.5 K.

2.4.11. Differential Scanning Calorimetry

Differential scanning calorimetry (DSC) is another widely employed thermal analysis technique that investigates thermal events in a sample through controlled heating or cooling, without any mass exchange with its surroundings. The key thermal events examined by DSC encompass solid-phase transformations, glass transitions, crystallization, and melting. The term "differential" highlights that the analysis is centered on the distinctions between the sample material and a reference material where the analyzed thermal events do not take place.[14] In this study, DSC was performed on samples of selected ionogels and eutectogels to substantiate the findings of TGA. The experiments were conducted on a DSC 1 instrument (M/s Mettler Toledo, Switzerland) by heating ~9 mg of sample placed in a crimped aluminum pan in a nitrogen atmosphere between the temperature window of -100 and 600 °C (as per requirement) at a rate of 10 °C min^{-1} with a nitrogen flow rate of 40 mL min^{-1}.

2.5. Electrochemical Characterization

This section specifies the details pertaining to the characterization and analyses of the electrochemical properties of the inorganic ionogels and eutectogels. The analyses were carried out with facilities available at the Centre for Nanotechnology, IIT Guwahati or the School of Molecular and Life Sciences at Curtin University, Australia.

2.5.1. Types of Electrochemical Experimental Setup

In electrochemical experiments, various setups can be employed, including two-electrode, three-electrode, or four-electrode configurations.[20] These configurations offer varying degrees of control and are selected based on the specific requirements and complexity of the electrochemical system under investigation. Each configuration serves specific purposes, and a brief introduction to each is provided below.

2.5.1.1. Two-Electrode Configuration

A two-electrode experiment is the simplest configuration, where the current-carrying electrodes are also utilized for voltage measurement. In this set-up, the electrodes are designated as working and working sense, short-circuited to form one (working) electrode, while reference and counter are connected to a second electrode. Two-electrode setups are predominantly employed for whole cell voltage measurements and low current or short time-scale systems. The former is suitable in cases where the measurement of the entire cell voltage is significant, such as in electrochemical energy devices. On the other hand, the latter is used for systems where the counter-electrode potential is not expected to drift significantly during the experiment or the counter-electrode potential stability can be assumed, typically in systems with very low currents or relatively short time scales. In the majority of conductivity and impedance material measurements, electrode polarization or contact effects are minimally pronounced. In such instances, the standard configuration, wherein the sample material is positioned between two parallel electrodes, proves to be most advantageous, allowing reproducible and flexible sample preparation. As such, this configuration is favored in practical and commercial levels for its simplicity and reliability in obtaining accurate measurements without significant interference from electrode-related phenomena.

2.5.1.2. Three-Electrode Configuration

In three-electrode configuration, the reference lead is isolated from the counter electrode and connected to a third electrode. This additional electrode is typically positioned in close proximity to the working electrode. Although more complex than their two-electrode counterparts, three-electrode setups offer the capability to exclusively measure one half of the cell. Specifically, the potential changes at the working electrode are measured independently, irrespective of changes that may occur at the counter electrode. This isolation allows for a more accurate study of specific reactions. For this reason, the three-electrode configuration is the most commonly employed setup in conventional electrochemical experimentations with higher currents and/or higher concentrations of analyte.

2.5.1.3. Four-Electrode Configuration

In a four-electrode configuration, the working sense lead is detached from the working electrode, leaving the reference and counter electrodes as the other two components. In this mode, the potentials associated with any electrochemical reactions taking place at the working (and counter) electrodes are not directly measured. Instead, the focus is laid on assessing the impact of an applied current on the solution itself or on a barrier within that solution. It may be worth noting that this approach is not a common practice in electrochemistry, as the primary emphasis in electrochemical studies typically involves measuring the potential changes at the working electrode.

2.5.2. Electrochemical Experiments

2.5.2.1. Preparation of Electrolyte Samples and Experimental Setup

To assess the practical viability of the gel electrolytes with supercapacitors, a device-level symmetric two-electrode coin-cell assembly with porous rGO as the working and counter electrodes was employed (**Figure 2.7**). The electrochemical performance of the gels was

evaluated at room temperature and atmospheric pressure via cyclic voltammetry (CV) and electrochemical impedance spectroscopy (EIS) on a CH Instruments, 600 C potentiostat (Gamry) or a PGSTAT101 Autolab potentiostat (Eco, Chemie, The Netherlands), as per availability. The potentiostats were interfaced to a PC-compatible Gamry software and Nova 1.11.2 or Nova 2.1 software, respectively. The cell assembly was positioned within an aluminum Faraday cage to safeguard against external perturbations. Electrochemical characteristics of the ionogel and the eutectogel performing the best at room temperature were also studied at controlled temperatures of 25, 50, 80, and 100 °C and atmospheric pressure via CV and EIS using a second coin cell identical to the one used for the previous experiments. To materialize the same, the electrolyte-laden coin cell was placed inside an oven (Model: VT 6060 M, Make: Thermo Fisher Scientific) and the device was held for ~1 h at each temperature.[21] At the onset of electrochemical measurements, the open circuit potential (OCP) was observed to assess the stability of the system. Experiments were duplicated, conducting each procedure at least twice, to ensure and verify reproducibility.

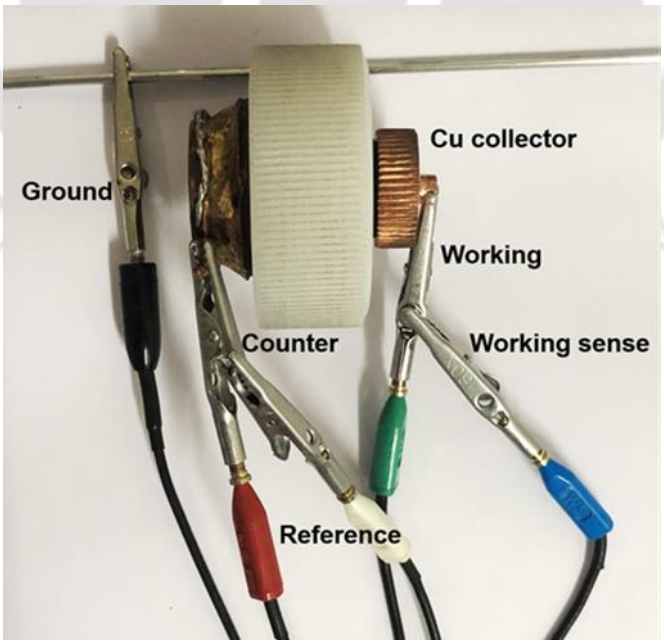

Figure 2.7. Photograph of the two-electrode coin-cell system as connected to the potentiostat. The rGO electrodes and the gel electrolytes are encapsulated inside the assembly.

2.5.2.1.1. Preparation of Ionogel Samples

Two pieces of rGO sheets were first cut to the required circular size (diameter ~1.9 cm, mass ~0.069 g) and placed inside the cleaned coin-cell assembly shown in **Figure 2.8**. A small amount of the freshly-prepared quasi-solid ionogel was lifted off the storing vessel with a clean spatula and meticulously applied on either side of each electrode sheet. The sheets were then isolated from each other using a piece of filter paper separator (Whatman, Cat no. 1001-110) of similar size placed between them so as to eliminate potential risks of short-circuiting due to the two electrodes coming in contact with each other. The assembly was then mantled and connected to the potentiostat through the copper current collectors on either side of the cell using connector cables. The components of the coin cell were rinsed with distilled water and dry-cleaned with acetone every time before loading a new sample. Fresh pieces of electrodes and separator, arranged in the aforementioned fashion were used for each ionogel.

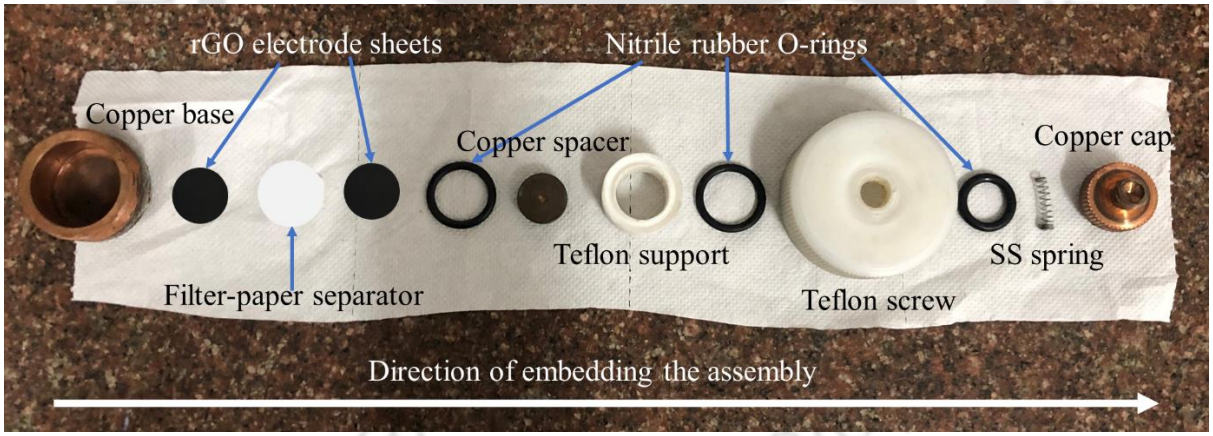

Figure 2.8. Photograph of the dismantled coin-cell assembly showing its different components along with the rGO electrodes and the filter-paper separator.

2.5.2.1.2. Preparation of Eutectogel Samples

Two sheets of rGO were first cut into the desired circular size (~1–2 cm diameter). Accordingly, fresh eutectogel samples were pressed into pellets of ~0.15 g each with a

thickness of ~0.1–0.2 cm using a Specac Activon 15T hydraulic press. A pellet of the eutectogel was meticulously positioned between the two electrode sheets. The solid gel pellet served both as the electrolyte and the separator at the same time. The system was then assembled and connected to the potentiostat with the help of connecting cables through the copper current collectors on either side of the cleaned copper cell. To observe the effect of the presence of an IL, ~0.15 g of each NADES-based eutectogel sample was mixed with 100 µL of the IL [BMIM][BF_4]. 5 µL of each sample was then dropped on each side of two fresh electrode sheets and placed inside the coin cell. The assembly was then connected to the potentiostat in the same fashion as stated above to conduct electrochemical characterization on the IL-modified systems. [BMIM][BF_4] was chosen for the purpose owing to its good wettability and high thermal stability, besides possessing superior electrochemical characteristics and bearing less cost as compared to other ubiquitous ILs.[22,23] The components of the coin cell were rinsed with distilled water and dry-cleaned with acetone every time before loading a new sample. Fresh pieces of electrodes arranged in the aforementioned manner were used for each eutectogel.

2.5.2.2. Cyclic Voltammetry

CV is a robust and widely employed characterization technique in electrochemistry for the assessment of electrolyte oxidation (anodic) and reduction (cathodic) processes[24] or double-layer behavior at the electrode/electrolyte interface.[7] As the name implies, it depicts the forward and reverse current versus potential profiles of an electrochemical cell. CV is a direct current (DC) electrochemical technique, capturing the variation in current as a potential scan is applied to the working electrode at a specific scan rate in both forward and reverse directions. CV scans can be conducted as single or multiple cycles. In processes involving Faradaic reactions, cyclic voltammograms reveal the oxidation and reduction of the redox species. Notably, the CV profile with discernible oxidation and reduction peaks is a characteristic feature of

pseudocapacitors.[25] On the other hand, for EDLCs, wherein the storage mechanism involves pure physical adsorption-desorption, the CV plot displays a uniform change in current with respect to potential. The CV profile of an EDLC tends to be more rectangular in shape, with an increase in capacitance observed.[25] Besides determining the redox behavior of an analyte, CV is a critical tool for the estimation of its electrochemical stability and OPW, along with the specific capacitance, energy, and power of the associated electrochemical device. **Figures 2.9** represents typical cyclic voltammograms corresponding to EDLCs utilizing a two-electrode arrangement. For CV scanned only to a positive potential window, the OPW corresponds to the entire window swept by the voltammogram (**Figure 2.9**a). However, for CVs on two-electrode EDLCs extended to a negative potential, only the positive portion of the window is considered to be the OPW,[26] as, in this case, the cell is allowed to charge twice in opposite polarities (**Figure 2.9**b).

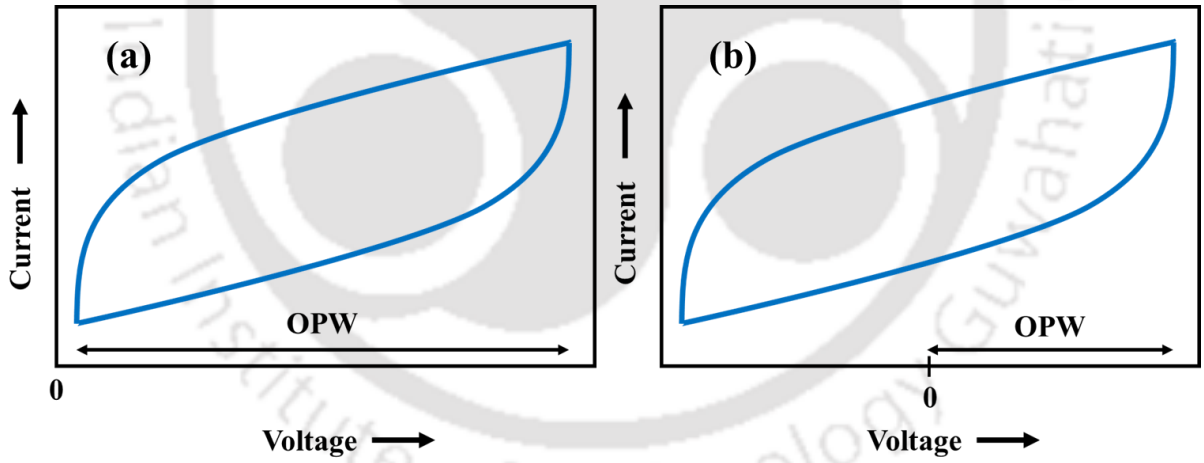

Figure 2.9. Schematic representation of typical cyclic voltammograms and OPW for EDLCs based on a two-electrode configuration obtained from CV (a) scanned to a positive potential window, and (b) extended to a negative potential window.

For this work, CV experiments were performed on the ionogel and eutectogel electrolytes in the potential window of −4 to +4 V at a set of different scan rates ranging from 1 to 100 mV s^{-1} with a step potential of 10 mV, so as to unfold the electrochemical stability or

redox nature of the systems within the said potential window. The area under the voltammogram represents the total amount of charge stored (Q). Therefore, specific capacitance (C_{sp}) of the EDLCs was calculated from CV using **equations 2.14**a or **2.14**b.[27] Thereafter, specific energy (E_{sp}) of the systems was determined from **equation 1.1**.

$$C_{sp}\ (\text{gravimetric}) = \frac{\int_{V_a}^{V_b} I(V)dV}{2mv(V_b - V_a)} \qquad \textbf{(2.14a)}$$

$$C_{sp}\ (\text{areal}) = \frac{\int_{V_a}^{V_b} I(V)dV}{2Av(V_b - V_a)} \qquad \textbf{(2.14b)}$$

Here, I is the current, V is the voltage, m is the mass of the electrode or active area, v is the scan rate, ($V_b - V_a$) is the potential window swept by the voltammogram, and A is the cross-sectional area of the active surface.

2.5.2.3. Electrochemical Impedance Spectroscopy

EIS has been acknowledged as a reliable tool for characterizing electrochemical energy storage devices, including supercapacitors, batteries, and fuel cells.[28] This non-destructive process enables the assessment of the electrical response of chemical systems, providing insights into small-scale chemical mechanisms at the electrode/electrolyte interface and within the electrolyte solution. EIS is highly sensitive compared to other electrochemical techniques, and various DC or AC methods have been reported in the literature for EIS measurements, as indicated in reference.[29] Among these methods, the frequency response analyzer (FRA) has emerged as a prominent technique for measuring impedance. FRA involves applying a low-amplitude sinusoidal perturbation (typically 5-15 mV) from the working electrode through the electrolyte to the counter electrode, with the corresponding AC current measurement. The output is obtained in the form of the impedance (Z) of the electrochemical cell as a function of frequency, combining both the real (Z') and imaginary (Z'') parts.

The Nyquist plot, a plot of -*Z*″ against *Z*′, illustrates different types of resistive and capacitive behavior in the system. A typical Nyquist plot is depicted in **Figure 2.10**a. **Figure 2.10**b represents its corresponding electrical equivalent circuit.[30] The first part of the plot indicating the insertion of the curve on the x-axis represents the solution resistance (R_s), while the semicircle's diameter represents the charge-transfer resistance (R_{ct}). The second part shows a straight line with a slope of 45º, representing Warburg impedance (Z_w).[31] Due to the typically smaller value of Z_w, ESR is often considered as a combined effect of R_s and R_{ct}, calculated by simple algebraic addition of the two values.[32] The electrochemical capacitor manifests with an impedance line with a slope of around 45º, followed by a nearly vertical tail at lower frequencies indicating pure capacitive behavior. Correspondingly, C_c and C_d in **Figure 2.10**b represent contact capacitance and double-layer capacitance, respectively.

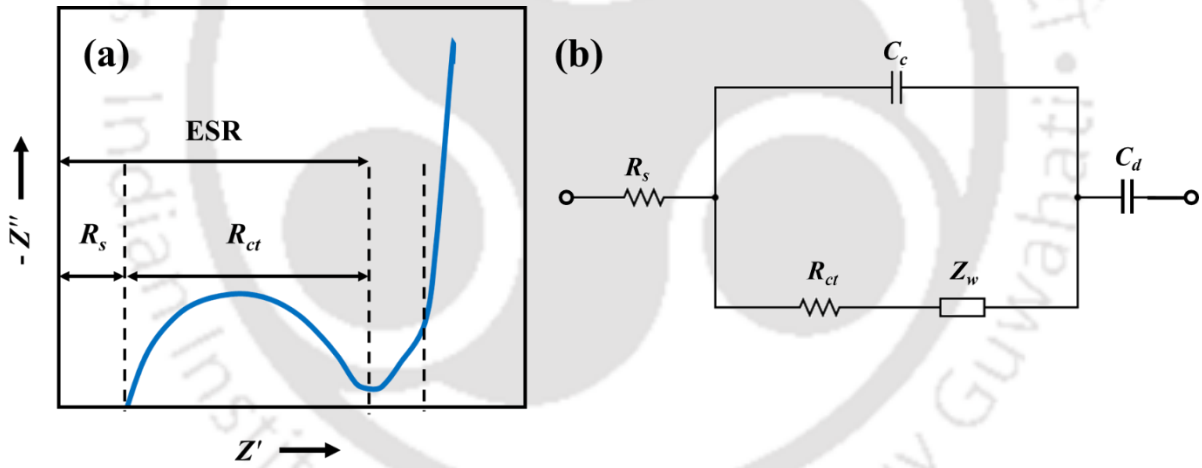

Figure 2.10. Schematic representation of (a) a typical Nyquist plot, and (b) its corresponding electrical equivalent circuit for an EDLC.

In order to study the resistive and capacitive responses of the gel-based systems, EIS was performed at the OCP by applying a small AC voltage of 5 mV amplitude over a frequency ranging between 0.01 Hz and 100 kHz.[21,33] ZSimpWin software was used to iterate the impedance data further by fitting the electrical equivalent circuit. Thereafter, the ionic

conductivity (σ) of the gels and the specific power of the corresponding systems were calculated using **equations 2.15** and **1.2**, respectively.

$$\sigma = \frac{t}{R_S A} \quad \textbf{(2.15)}$$

Here, *t* is the thickness of the electrolyte layer/pellet and *A* is the cross-sectional area of the active portion.

References

(1) Wu, F.; Chen, N.; Chen, R.; Zhu, Q.; Tan, G.; Li, L. Self-Regulative Nanogelator Solid Electrolyte: A New Option to Improve the Safety of Lithium Battery. *Advanced Science* **2016**, *3* (1). https://doi.org/10.1002/advs.201500306.

(2) Wu, F.; Chen, N.; Chen, R.; Zhu, Q.; Qian, J.; Li, L. "Liquid-in-Solid" and "Solid-in-Liquid" Electrolytes with High Rate Capacity and Long Cycling Life for Lithium-Ion Batteries. *Chemistry of Materials* **2016**, *28* (3), 848–856. https://doi.org/10.1021/acs.chemmater.5b04278.

(3) Verma, R. Liquid-Liquid Extraction and Process Flow Sheeting of Lower Alcohol with Deep Eutectic Solvents, Indian Institute of Technology Guwahati, Guwahati, 2018.

(4) Verma, R.; Banerjee, T. Liquid–Liquid Extraction of Lower Alcohols Using Menthol-Based Hydrophobic Deep Eutectic Solvent: Experiments and COSMO-SAC Predictions. *Ind Eng Chem Res* **2018**, *57* (9), 3371–3381. https://doi.org/10.1021/acs.iecr.7b05270.

(5) Verma, R.; Banerjee, T. Palmitic-Acid-Based Hydrophobic Deep Eutectic Solvents for the Extraction of Lower Alcohols from Aqueous Media: Liquid–Liquid Equilibria Measurements, Validation and Process Economics. *Global Challenges* **2019**, *3* (11). https://doi.org/10.1002/gch2.201900024.

(6) Verma, R.; Mohan, M.; Goud, V. V.; Banerjee, T. Operational Strategies and Comprehensive Evaluation of Menthol Based Deep Eutectic Solvent for the Extraction of Lower Alcohols from Aqueous Media. *ACS Sustain Chem Eng* **2018**, *6* (12), 16920–16932. https://doi.org/10.1021/acssuschemeng.8b04255.

(7) Mahanta, U.; Choudhury, S.; Venkatesh, R. P.; SarojiniAmma, S.; Ilangovan, S. A.; Banerjee, T. Ionic-Liquid-Based Deep Eutectic Solvents as Novel Electrolytes for Supercapacitors: COSMO-SAC Predictions, Synthesis, and Characterization. *ACS Sustain Chem Eng* **2020**, *8* (1), 372–381. https://doi.org/10.1021/acssuschemeng.9b05596.

(8) Joos, B.; Vranken, T.; Marchal, W.; Safari, M.; Van Bael, M. K.; Hardy, A. T. Eutectogels: A New Class of Solid Composite Electrolytes for Li/Li-Ion Batteries. *Chemistry of Materials* **2018**, *30* (3), 655–662. https://doi.org/10.1021/acs.chemmater.7b03736.

(9) Gupta, A. K.; Singh, M. P.; Singh, R. K.; Chandra, S. Low Density Ionogels Obtained by Rapid Gellification of Tetraethyl Orthosilane Assisted by Ionic Liquids. *Dalton Transactions* **2012**, *41* (20), 6263. https://doi.org/10.1039/c2dt30318c.

(10) Diehl, B. Principles in NMR Spectroscopy. In *NMR Spectroscopy in Pharmaceutical Analysis*; Elsevier, 2008; pp 1–41. https://doi.org/10.1016/B978-0-444-53173-5.00001-9.

(11) Krishnan, A.; Liu, Y.-H.; Cha, P.; Woodward, R.; Allara, D.; Vogler, E. A. An Evaluation of Methods for Contact Angle Measurement. *Colloids Surf B Biointerfaces* **2005**, *43* (2), 95–98. https://doi.org/10.1016/j.colsurfb.2005.04.003.

(12) Law, K.-Y. Definitions for Hydrophilicity, Hydrophobicity, and Superhydrophobicity: Getting the Basics Right. *J Phys Chem Lett* **2014**, *5* (4), 686–688. https://doi.org/10.1021/jz402762h.

(13) Jose, A. J.; Alagar, M. Preparation and Characterization of Polysulfone-Based Nanocomposites. In *Manufacturing of Nanocomposites with Engineering Plastics*; Elsevier, 2015; pp 31–59. https://doi.org/10.1016/B978-1-78242-308-9.00003-3.

(14) Leng, Y. *Materials Characterization: Introduction to Microscopic and Spectroscopic Methods*, 2nd ed.; John Wiley & Sons, 2013.

(15) Dorfs, D.; Krahne, R.; Falqui, A.; Manna, L.; Giannini, C.; Zanchet, D. Quantum Dots: Synthesis and Characterization. In *Comprehensive Nanoscience and Technology*; Elsevier, 2011; pp 219–270. https://doi.org/10.1016/B978-0-12-374396-1.00028-3.

(16) Berthomieu, C.; Hienerwadel, R. Fourier Transform Infrared (FTIR) Spectroscopy. *Photosynth Res* **2009**, *101* (2–3), 157–170. https://doi.org/10.1007/s11120-009-9439-x.

(17) Khan, H.; Yerramilli, A. S.; D'Oliveira, A.; Alford, T. L.; Boffito, D. C.; Patience, G. S. Experimental Methods in Chemical Engineering: X-ray Diffraction Spectroscopy—<scp>XRD</Scp>. *Can J Chem Eng* **2020**, *98* (6), 1255–1266. https://doi.org/10.1002/cjce.23747.

(18) Mahanta, U. Ionic Liquids and Deep Eutectic Solvents as Electrolytes for Energy Efficient Electrical Double Layer Capacitor, Indian Institute of Technology Guwahati, Guwahati, 2021.

(19) Baranyai, K. J.; Deacon, G. B.; MacFarlane, D. R.; Pringle, J. M.; Scott, J. L. Thermal Degradation of Ionic Liquids at Elevated Temperatures. *Aust J Chem* **2004**, *57* (2), 145. https://doi.org/10.1071/CH03221.

(20) Gamry Instruments. *Two, Three and Four Electrode Experiments*. Gamry Instruments.

(21) Liu, X.; Wu, B.; Brandon, N.; Wang, Q. Tough Ionogel-in-Mask Hybrid Gel Electrolytes in Supercapacitors with Durable Pressure and Thermal Tolerances. *Energy Technology* **2017**, *5* (2), 220–224. https://doi.org/10.1002/ente.201600251.

(22) Liu, X.; Taiwo, O. O.; Yin, C.; Ouyang, M.; Chowdhury, R.; Wang, B.; Wang, H.; Wu, B.; Brandon, N. P.; Wang, Q.; Cooper, S. J. Aligned Ionogel Electrolytes for High-Temperature Supercapacitors. *Advanced Science* **2019**, *6* (5). https://doi.org/10.1002/advs.201801337.

(23) Polat, H. M.; Kavak, S.; Kulak, H.; Uzun, A.; Keskin, S. CO2 Separation from Flue Gas Mixture Using [BMIM][BF4]/MOF Composites: Linking High-Throughput Computational Screening with Experiments. *Chemical Engineering Journal* **2020**, *394*, 124916. https://doi.org/10.1016/j.cej.2020.124916.

(24) Elgrishi, N.; Rountree, K. J.; McCarthy, B. D.; Rountree, E. S.; Eisenhart, T. T.; Dempsey, J. L. A Practical Beginner's Guide to Cyclic Voltammetry. *J Chem Educ* **2018**, *95* (2), 197–206. https://doi.org/10.1021/acs.jchemed.7b00361.

(25) Eftekhari, A. Supercapacitors Utilising Ionic Liquids. *Energy Storage Mater* **2017**, *9*, 47–69. https://doi.org/10.1016/j.ensm.2017.06.009.

(26) Shabeeba, P.; Thasneema, K. K.; Thayyil, M. S.; Pillai, M. P.; Niveditha, C. V. A Graphene-Based Flexible Supercapacitor Using Trihexyl(Tetradecyl)Phosphonium Bis(Trifluoromethanesulfonyl)Imide Ionic Liquid Electrolyte. *Mater Res Express* **2017**, *4* (8), 085501. https://doi.org/10.1088/2053-1591/aa7b14.

(27) Kim, M.; Oh, I.; Kim, J. Effects of Different Electrolytes on the Electrochemical and Dynamic Behavior of Electric Double Layer Capacitors Based on a Porous Silicon Carbide Electrode. *Physical Chemistry Chemical Physics* **2015**, *17* (25), 16367–16374. https://doi.org/10.1039/C5CP01728A.

(28) Mei, B.-A.; Munteshari, O.; Lau, J.; Dunn, B.; Pilon, L. Physical Interpretations of Nyquist Plots for EDLC Electrodes and Devices. *The Journal of Physical Chemistry C* **2018**, *122* (1), 194–206. https://doi.org/10.1021/acs.jpcc.7b10582.

(29) Chang, B.-Y.; Park, S.-M. Electrochemical Impedance Spectroscopy. *Annual Review of Analytical Chemistry* **2010**, *3* (1), 207–229. https://doi.org/10.1146/annurev.anchem.012809.102211.

(30) PANDEY, G. P.; HASHMI, S. A. Studies on Electrical Double Layer Capacitor with a Low-Viscosity Ionic Liquid 1-Ethyl-3-Methylimidazolium Tetracyanoborate as Electrolyte. *Bulletin of Materials Science* **2013**, *36* (4), 729–733. https://doi.org/10.1007/s12034-013-0511-y.

(31) Lei, C.; Markoulidis, F.; Ashitaka, Z.; Lekakou, C. Reduction of Porous Carbon/Al Contact Resistance for an Electric Double-Layer Capacitor (EDLC). *Electrochim Acta* **2013**, *92*, 183–187. https://doi.org/10.1016/j.electacta.2012.12.092.

(32) Kötz, R.; Carlen, M. Principles and Applications of Electrochemical Capacitors. *Electrochim Acta* **2000**, *45* (15–16), 2483–2498. https://doi.org/10.1016/S0013-4686(00)00354-6.

(33) Mahanta, U.; Kundu, D.; Venkatesh, R. P.; Sujatha, S.; Ilangovan, S. A.; Banerjee, T. Electrochemical Performance and Molecular Structure of Diluted 1-Alkyl-3-Methylimidazolium Tetrafluoroborate Ionic Liquids and Their Mixture as Electrolytes for Double-Layer Capacitors: An Integrated Approach by Electrochemical Characterization and Molecular Dynamics Simulation. *Ind Eng Chem Res* **2019**, *58* (51), 22741–22753. https://doi.org/10.1021/acs.iecr.9b04350.

Chapter 3

TiO_2-Mediated Ionic-Liquid-Based Inorganic Ionogels

CHAPTER 3

TiO_2-Mediated Ionic-Liquid-Based Inorganic Ionogels

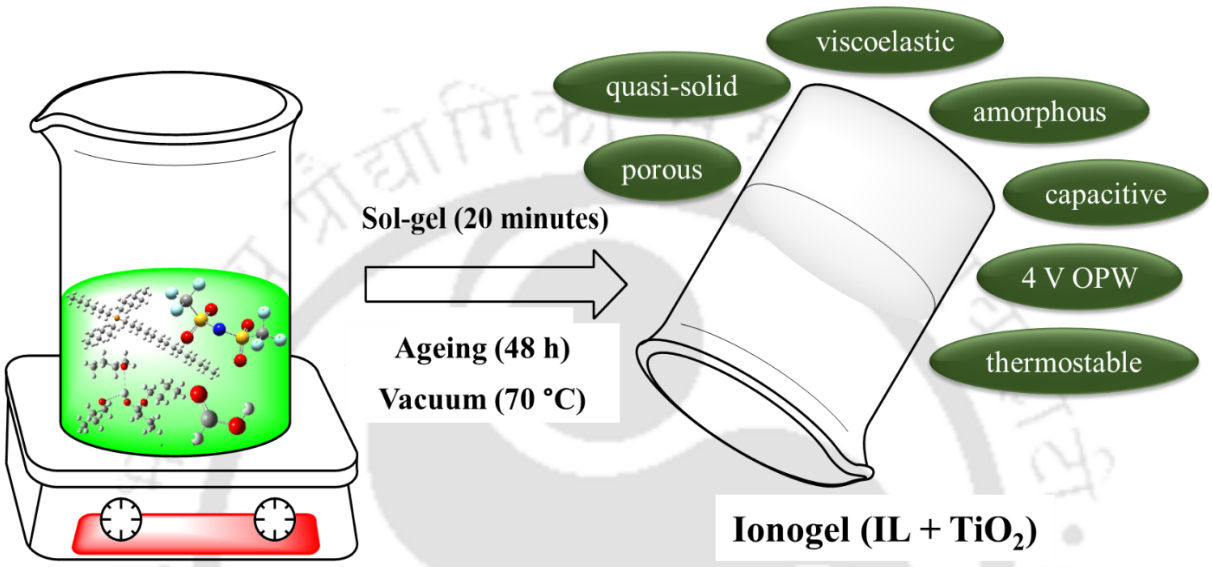

List of publications from Chapter 3:

(1) **Dutta, A.**; Mishra, D. K.; Kundu, D.; Mahanta, U.; Jiang, S. P.; Silvester, D. S.; Banerjee, T. Examining the Electrochemical Nature of an Ionogel Based on the Ionic Liquid $[P_{66614}][TFSI]$ and TiO_2: Synthesis, Characterization, and Quantum Chemical Calculations. *Ind. Eng. Chem. Res.* **2022**, *61* (25), 8763–8774. https://doi.org/10.1021/acs.iecr.2c00550.

(2) **Dutta, A.**; Mahanta, J.; Millar, W.; Silvester, D. S.; Banerjee, T. Titania-Confined Novel Ionogels with a Wide Operating Potential Window as Propitious Solid-State Electrolytes for Electrochemical Supercapacitors. *(In line for submission)*

3.1. Introduction

This chapter discusses the morphological, structural, thermal, and electrochemical properties of seven novel inorganic ionogels (TIGels 1–7) derived by immobilizing each of the ILs, *viz.* IL1: $[P_{66614}][TFSI]$, IL2: $[P_{66614}][DCA]$, IL3: $[HMIM][BF_4]$, IL4: [AMIM][TFSI], IL5: [EMIM][FAP], IL6: [PMIM][TFSI], and IL7: [BTMA][TFSI] into an inorganic matrix of TiO_2 derived from a TBOT precursor through the sol-gel strategy of synthesis as detailed in Chapter 2 of this thesis. The process employed was fast and simple and did not involve any additional sample-preparation steps. The ionogels, thus obtained were characterized using FESEM, FETEM, rheology, FTIR spectroscopy, XRD, TGA, and DSC. Furthermore, to verify their practicality as electrolytes in supercapacitor-based applications, electrochemical tests were also performed on the ionogels through CV and EIS. As a proof of concept, synthesis and characterization was first conducted on TIGel1. Thereafter, TIGels 2–7 were synthesized and their properties thoroughly analyzed. Electrochemical characteristics of the ionogel performing the best at room temperature were also studied at controlled temperatures of 25, 50, and 100 °C via CV and EIS. To the best of our knowledge, the sol-gel-derived TiO_2-based ionogels reported herein are the first of their kind.

3.2. Results and Discussion on TIGel1

3.2.1. Morphological Analysis

FESEM studies confirmed that the inorganic gel matrix possesses a porous structure (**Figure 3.1**a−c). The IL is confined as an interconnected liquid film layered on the surface of the TiO_2 particles, thus rendering a quasi-solid nature to the ionogel. Furthermore, the formation of 3D interconnected nanostructures indicates that the IL is completely assimilated into the TiO_2 matrix through in-situ gelation on the nanometer scale. The TiO_2 particles are seen to join

together in a worm-like structure (**Figure 3.1**c), developing a potentially convenient pathway for the transport of ions.[1]

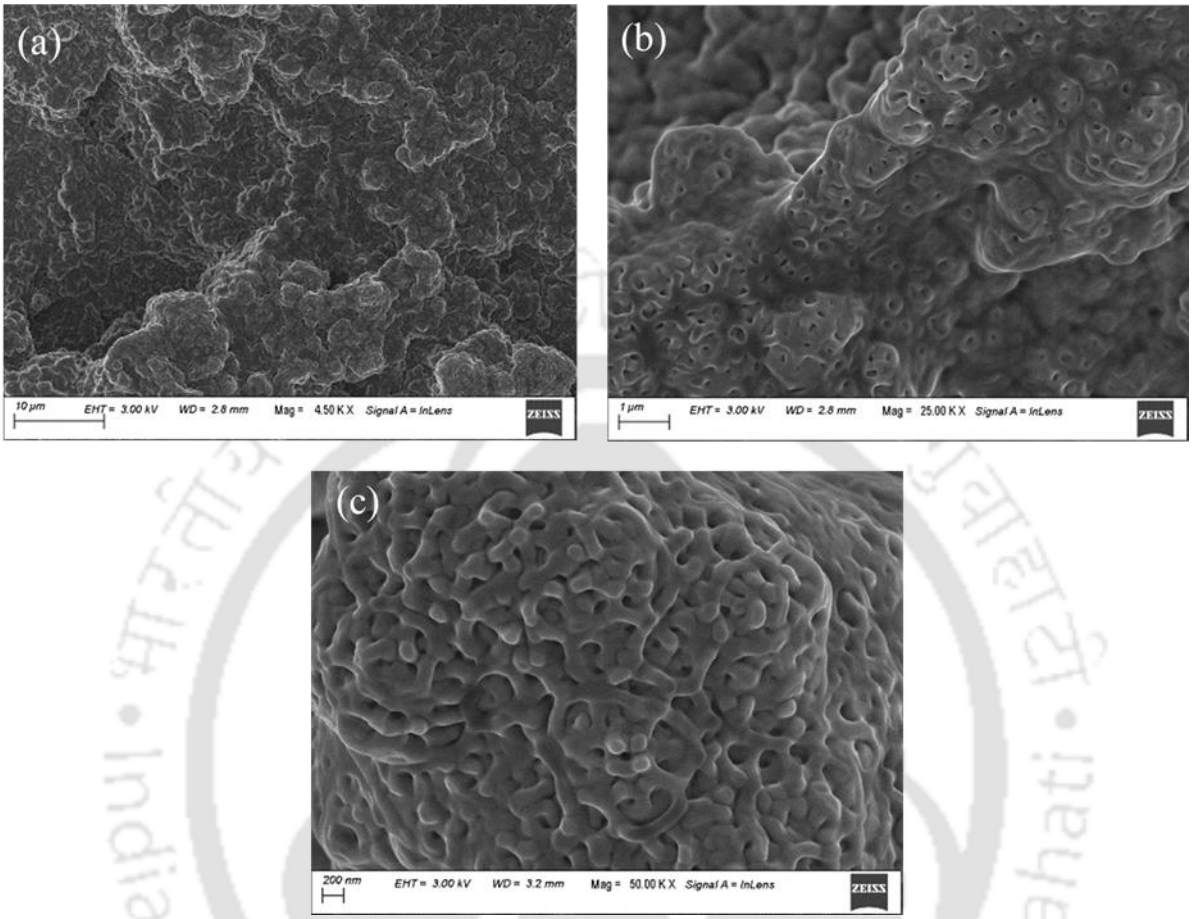

Figure 3.1. FESEM images of the ionogel matrix at (a) 10 µm, (b) 1 µm, and (c) 200 nm scales.

3.2.2. Rheological Analysis

The variation of viscosity of the ionogel with shear rate as an average across three different experimental runs is depicted by the inclusion of error bars in **Figure 3.2**a. It can be observed that with an increase in shear rate, the viscosity of the ionogel decreases, which indicates that the ionogel behaves as a shear-thinning fluid. This may be attributed to the loosening of physical crosslinking between the IL and the TiO_2 matrix or, in other words, waning of the non-bonded intermolecular interactions between the IL molecules and the titanium moieties. Fitting the obtained data with the power law model yields an R^2 (square of the correlation

coefficient) value of 0.9844, which is a good indication that the power law model fitted well to the experimental data obtained. IL1 is quite hydrophobic in nature and is known to exhibit an immiscible phase with moisture at room temperature. In addition, the water uptake of the IL is also relatively low in atmospheric conditions. Nevertheless, all conventional ILs are known to be impacted by moisture at different levels, even at low humidities.[2,3] Because increased water content lowers viscosity, a reduced viscosity over time may be expected due to the absorption of moisture into the IL and the ionogel, leading to an increased diffusion coefficient of dissolved species such as analytes and/or impurities.[4] Additionally, viscosity is sensitive to variation in temperature. Increasing the temperature is typically expected to result in a decreased viscosity.

An oscillatory shear test was performed to study the viscoelastic nature of the ionogel. Initially, an amplitude sweep test was conducted to determine the LVE region over the strain range from 0.1 to 1000 %. From **Figure 3.2**b, it can be observed that until ~1 % strain the storage modulus ($G^{/}$) of the ionogel is constant, which shows that the structure of the sample remains undisturbed. However, beyond a strain of 1 %, a decrease in $G^{/}$ can be seen, possibly due to the weakening of the physical interactions between the precursors. Hence, the LVE region for the ionogel is taken between 0.5 to 1 % of strain. Furthermore, the dominance of storage moduli over loss moduli is observed for the ionogel in the LVE region, indicating its viscoelastic solid-like behavior.

A frequency sweep test was performed by varying the frequency from 0.1 to 100 Hz at a constant strain obtained from the corresponding LVE region. **Figure 3.2**c depicts the viscoelastic nature of the ionogel. It is noted that the $G^{/}$ of the ionogel is higher than the corresponding loss moduli ($G^{//}$) at all points within the given frequency range. Furthermore, the $G^{/}$ is observed to increase constantly, indicating that the ionogel possesses much solid-like

behavior. In addition, there is no observation of any cross-over point in the given frequency range, which suggests that the ionogel has a dominant elastic nature.

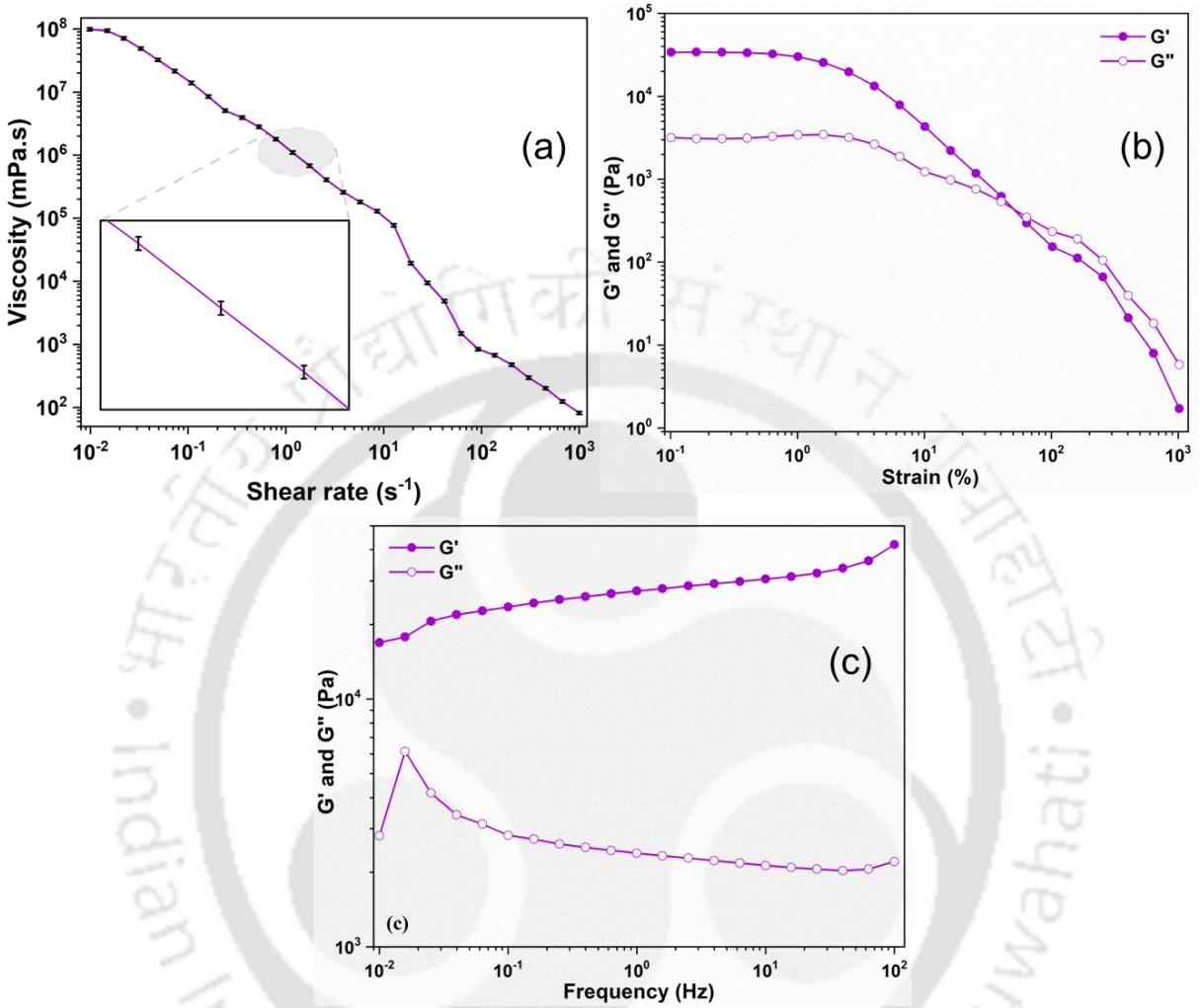

Figure 3.2. Plots depicting the rheological properties of TIGel1: (a) viscosity versus shear rate as an average across three experimental runs. The inset shows a magnified version of a small section of the graph with error bars, (b) storage and loss moduli versus strain amplitude sweep, and (c) storage and loss moduli versus frequency sweep. The ionogel exhibits shear-thinning, viscoelastic solid-like characteristics with dominant elasticity.

3.2.3. Structural Analysis

To determine the effect of confinement of the IL within a porous matrix on the structure of the IL, FTIR spectroscopy was performed on both the IL and the ionogel. As seen from **Figure**

3.3, the FTIR spectra of the IL and the ionogel are very similar, except for an additional peak for the ionogel at 1557 cm^{-1} corresponding to a ν_sH−O−H stretching.[5] This indicates that TBOT and IL1 did not undergo direct chemical bonding. Hence, it can be deduced that the physical confinement within the crosslinking matrix did not alter the integrity of the IL. Additionally, it provides evidence of the complete interconnection of IL1 within the ionogel.[5] However, marginal shifts are seen in the vibrational bands of the ionogel as compared to those of the IL. This suggests the presence of non-bonded interactions of the IL molecules with the pore wall surfaces of the TiO_2 moieties.[1] The presence of such non-bonded interactions result in potential alteration in the thermal properties of the confined IL.[6]

Table 3.1 represents some of the noticeable shifts in the vibrational bands of the IL and the ionogel corresponding to their assignments. A characteristic band at 1557 cm^{-1} of the ionogel pertaining to the symmetric stretching of H−O−H is found to be absent in the unconfined IL. The vibrational band at 1412 cm^{-1} of the IL corresponding to asymmetric C−H scissoring is found to shift by 2 cm^{-1} to 1410 cm^{-1} for the ionogel. The interaction of the IL anion with TiO_2 is confirmed by the change in the vibrational band related to symmetric S=O stretching from 1331 to 1333 cm^{-1}. The peak related to symmetric O=S=O stretching of the IL corresponding to the frequency 1182 cm^{-1} is seen to shift to 1184 cm^{-1} for the ionogel. The peak for the vibrational band concerning the symmetric S–N stretching of the IL is observed at 762 cm^{-1}. However, this is changed to 760 cm^{-1} upon confinement. A 2 cm^{-1} shift in frequency is also observed for symmetric S–N–S stretching; 654 cm^{-1} for the unconfined IL, whereas the same for the ionogel was achieved at 652 cm^{-1}. Finally, the band peaks corresponding to 538, 511, and 430 cm^{-1} of the IL owing to C−H bending are shifted to 540, 509, and 428 cm^{-1} respectively, after confinement into TiO_2. Limited content of titania in the ionogel, resulted in a domination of vibrations corresponding to the IL.

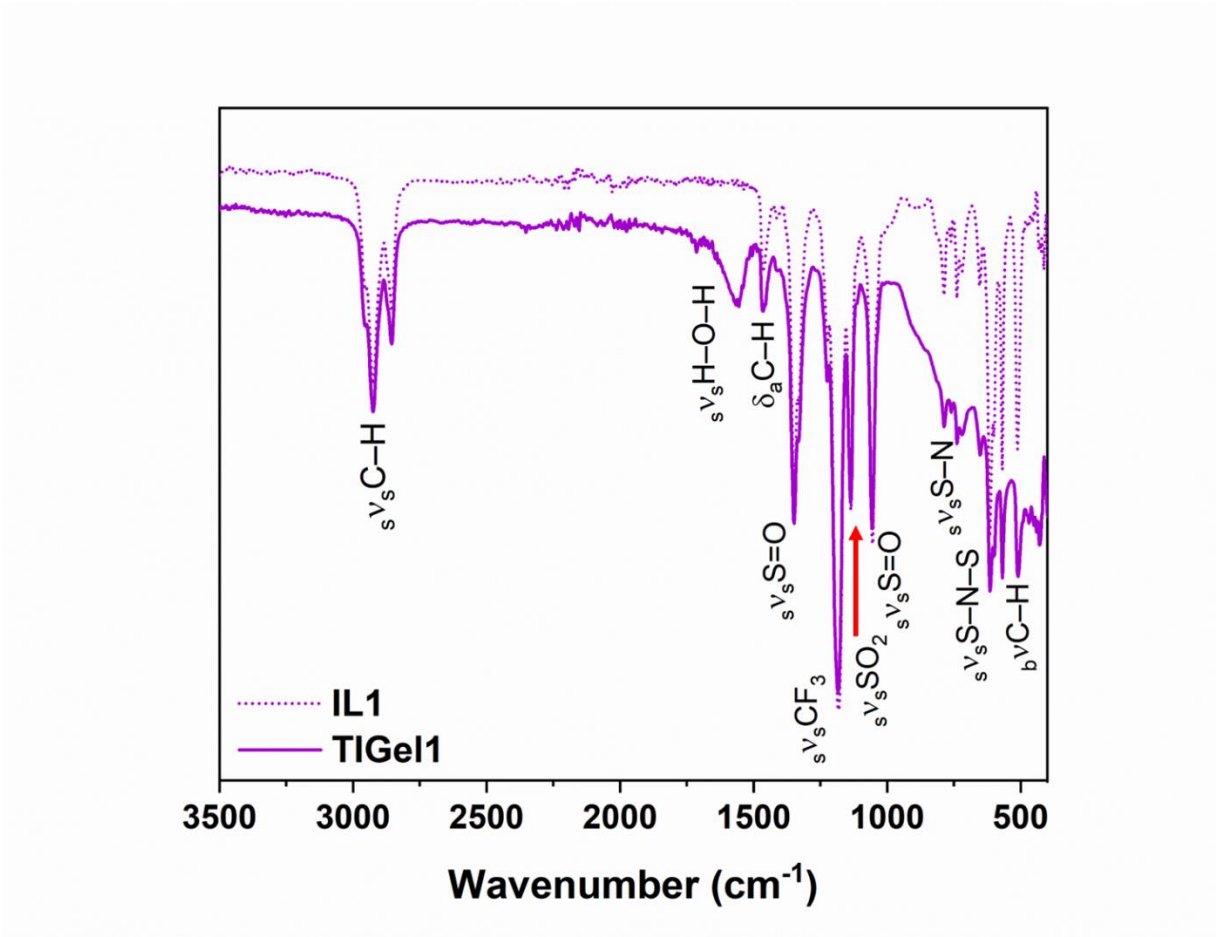

Figure 3.3. FTIR spectra of IL1 and TIGel1. The results provide evidence of complete non-bonded interconnection of the TiO_2 and the IL network within the ionogel.

Table 3.1. Vibrational bands of IL1 and TIGel1 along with their corresponding assignments

Assignment	Vibrational band (cm^{-1})	
	IL1	**TIGel1**
${}_s\nu_s$H−O−H	−	1557
δ_aC−H	1412	1410
${}_s\nu_s$S=O	1331	1333
${}_s\nu_s$$SO_2$	1182	1184
${}_s\nu_s$S−N	762	760
${}_s\nu_s$S−N−S	654	652
${}_b\nu$C−H	538	540
${}_b\nu$C−H	511	509
${}_b\nu$C−H	430	428

${}_s\nu_s$: symmetric stretching, δ_a: asymmetric scissoring, ${}_b\nu$: bending

XRD measurements were performed on the ionogel to discern the degree of crystallinity of the sample. Conforming to findings reported previously,[5–8] the inorganic ionogel presented herein also demonstrates the presence of a typical amorphous TiO_2 matrix in co-existence with the IL. The XRD pattern of the ionogel depicted in **Figure 3.4** is observed to consist of frail and broad peaks, revealing the amorphous or low crystalline nature of the sample within the given range of 2θ. The introduction of IL interferes with the consistent arrangement of the TiO_2 matrix, and leads to an increase in the amorphous area.

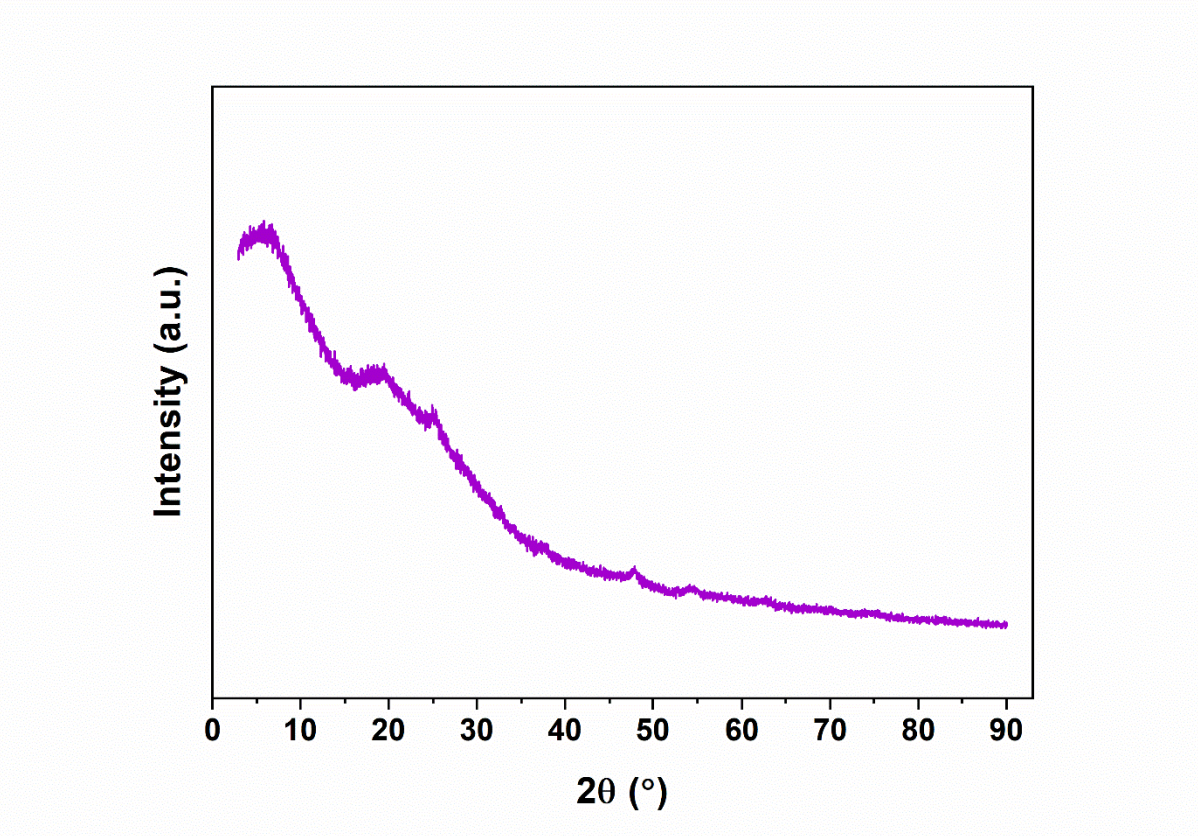

Figure 3.4. XRD spectrum of TIGel1.

3.2.4. Thermal Analysis

TGA was conducted on IL1 and TIGel1 using a TGA Q500 V20.13 Build 39 and a TG 209 F1 Libra (Make: M/s Netzsch, Germany), respectively. Both experiments were carried out in a nitrogen atmosphere, for which the samples were heated from 30 to 600 °C at a rate of 10 °C min^{-1} under nitrogen flow at 40 mL min^{-1}. DSC was conducted on TIGel1 under the same conditions between -100 and 200 °C. **Figure 3.5** shows the TGA profiles of IL1 and TIGel1.

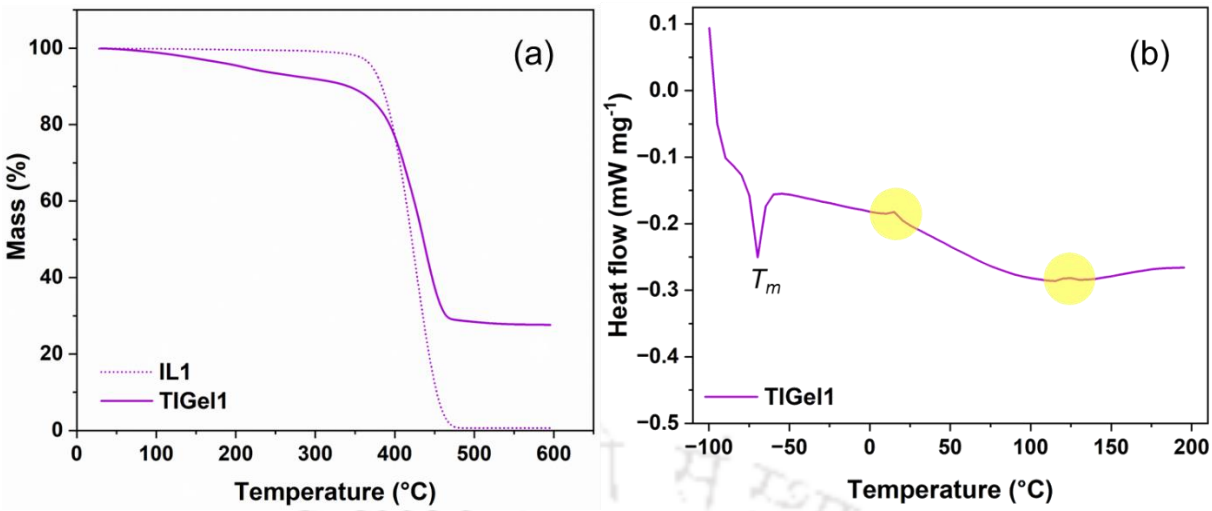

Figure 3.5. (a) TGA profiles of IL1 and TIGel1. The overall thermal stability of the IL is reduced upon confinement into the inorganic matrix of TiO_2; (b) DSC profile of TIGel1.

It is observed that the decomposition of the IL begins at an onset temperature of ~330 °C. On the other hand, there is insignificant mass loss (< 1 %) of the ionogel up to a temperature of ~93 °C, which can be considered as its onset degradation temperature. This small mass loss is associated with the removal of water at this temperature range.[9,10] This proves that the thermal stability of the IL is reduced upon its confinement into the TiO_2 matrix. However, this also indicates that the ionogel can still be conveniently utilized in specific high-temperature applications.[11] The IL demonstrates a single-step decomposition, whereas the decomposition of the ionogel can be divided into three distinct phases. A small amount of mass loss of 5% at low temperatures is attributed to the dehydration of entrapped moisture and evaporation of potential organic impurities.[2,9,12] This is the threshold temperature ($T_{5\%}$) of the ionogel after which it loses its thermal stability progressively. Here, $T_{5\%}$ for the ionogel is 210.5 °C. The second mass loss in the curve corresponds to the decomposition of the $[TFSI]^-$ and $[P_{66614}]^+$ ions[9,13] which is seen to occur at a temperature of ~320 °C. Finally, the straight line in the thermogram indicates the complete degradation of the organic composition, leaving behind only the inorganic component.[9] The mass fraction of the inorganic TiO_2 component is about

28 wt%. Overall, it can be concluded that the confinement of IL1 into an inorganic matrix of TiO_2 results in a reduction of its thermal stability potentially due to the presence of non-bonded interactions between the IL molecules and the TiO_2 pore wall surface.[6] The findings of TGA are in good agreement with that of DSC performed on the ionogel (**Figure 3.5**b). The gel shows good stability with no major occurrences of endothermic or exothermic reactions beyond room temperature up to a temperature of 200 °C.[5] The gradual drop with small distinct exothermic peaks at ~15 and ~120 °C may be attributed to the loss of volatile impurities and/or moisture.[6] The endothermic melting point (T_m) of the ionogel stands at -69.7 °C.[5]

3.2.5. Electrochemical Performance

Figure 3.6 shows cyclic voltammograms of TIGel1 with the rGO-based two-electrode system obtained on a Gamry-interfaced CH Instruments, 600 C potentiostat (Gamry) at scan rates of 1, 5, and 10 mV s^{-1} at room temperature. The quasi-rectangular CV profiles at all three scan rates indicate a capacitive behavior of the system.[14,15] The absence of any redox peaks at each scan rate further indicates that the charge-storage mechanism of the ionogel-based cell is non-Faradaic or double-layer in nature within the potential window.[11,14,15] The double-layer capacitive characteristic becomes more prominent at reduced scan rates owing to the absence of the electrolyte starvation effect. At higher scan rates with shorter time, the charged species fail to undergo complete adsorption at the electrode/electrolyte interface, which results in poorer rate performance of the electrode.[11,16,17] Although the existence of functional groups at the surface of the electrode and/or the presence of dissolved impurities may impart some pseudocapacitance, the linearity of the measured current suggests that the system is predominantly non-Faradaic within this potential range.[18] However, a relatively narrow current is obtained over the given potential window. This could be due to the presence of the bulky P_{66614} molecule resulting in charge-shielding and resistance to ionic mobility,[19] and the absence of an ideally polarizable reference electrode.[20] It may also be worth noting here that the self-

diffusivity of cations and anions in immobilized ILs may remain low on account of surface forces arising from the interactions between absorbed ions and matrix surface, leading to restricted kinetics.[1]

Nevertheless, the cell is consistently observed to deliver a double-layer capacitive behavior within a wide potential window of about 4 V (- 4 V to + 4 V) with the porous rGO electrodes at all three scan rates of 1, 5, and 10 mV s^{-1}. Interestingly, the same IL has also been proven to achieve a potential window of 4 V with graphene electrodes when tested with a two-electrode cell system.[18] Therefore, immobilization of the IL into TiO_2 did not affect the OPW of the IL. In other words, the same potential window could be retained with the quasi-solid viscoelastic form of the electrolyte as was obtained with the liquid IL. The OPW was found to be the widest when compared with those of ionogels obtained with the immobilization of ILs into a matrix of TiO_2 in similar works (**Table 3.2**).

The slight reductions in the potential window at the lower scan rates may be attributed to the fact that increasing the scan rates can improve the chemical reversibility and increase the electrochemical stability of the system.[21] Nevertheless, the potential window can also be subject to variation depending on the type of electrode material, the electrode configuration, and the properties of the electrolyte, in addition to the ambient conditions and the method of measurement.[22,23] Using a porous carbon electrode narrows the anodic and cathodic stabilities of the electrolyte.[11] Consequently, the potential window of the system is expected to reduce when measured with a porous electrode compared to that measured with inert working electrodes such as gold and platinum. Similarly, the potential window is tapered at high temperatures.[1]

Even commercial ILs obtained with the highest level of purity contain certain impurities.[4] Nonetheless, the purity of an electrolyte has a significant effect on its

electrochemical stability,[4,11,24] and hence on the operating potential of the system. It is noted here that the sample of IL1 used in this work was not at its highest purity grade (≥ 95 %) (**Table 2.1**) and the constituent chemicals were used as received, without having undergone any additional purification steps. The presence of synthetic impurities can narrow the potential window, which may be further aggravated by the existence of water.[4] The reduction of the potential window takes place at both the anodic and cathodic limits. This may be attributed to the electrolysis of the water present.[3] The redox peaks associated with dissolved impurities intrinsic to the IL gain prominence with an increase in the water content.[4] As such, a smoother voltammogram with a broader potential window for the ionogel may be expected by conducting the test with purer chemicals. This suggests that the ionogel reported in this work has an excellent potential to be utilized as a stable electrolyte in open-air electrochemical storage applications, especially in EDLCs as well as in other pertinent realms of electrochemistry.

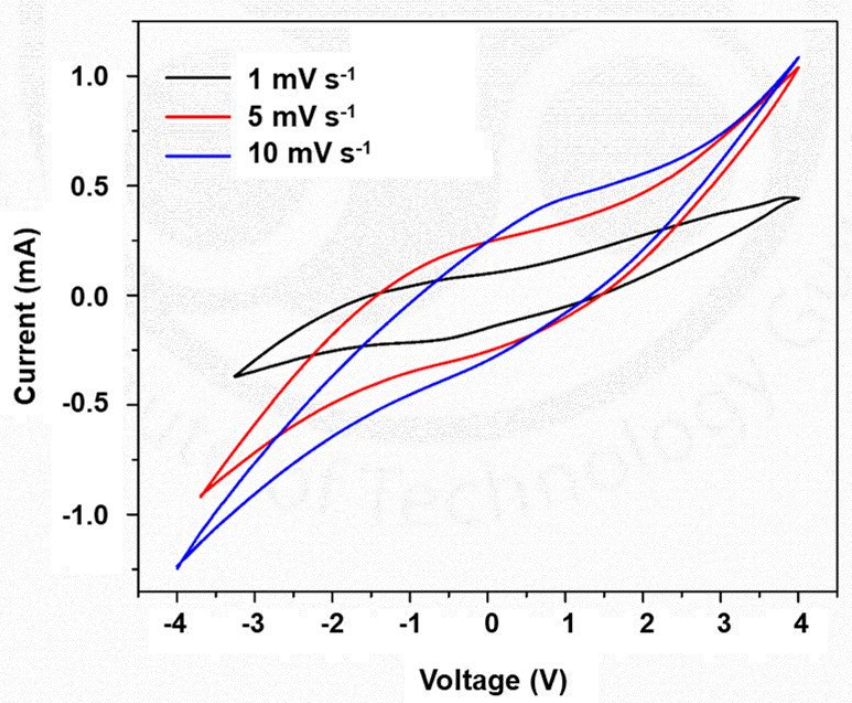

Figure 3.6. Cyclic voltammograms of the system performed at room temperature on a two-electrode coin-cell assembly with rGO electrodes and TIGel1 electrolyte at scan rates of 1, 5, and 10 mV s^{-1}.

Table 3.2. Comparison of the OPW of TIGels 1–7 and that of ionogels reported in similar works

Ionogel	Working electrode	Scan rate ($mV\ s^{-1}$)	Temperature (^oC)	Potential window (V)
$[P_{66614}][TFSI]$ + TiO_2 (TIGel1)	rGO	10	~25	4
$[P_{66614}][DCA]$ + TiO_2 (TIGel2)	rGO	5, 10, 25, 50, 100	~25	4
[HMIM][TFSI] + TiO_2 (TIGel3)	rGO	5, 10, 25, 50, 100	~25	4
[AMIM][TFSI] + TiO_2 (TIGel4)	rGO	5, 10, 25, 50, 100	~25	4
[EMIM][FAP] + TiO_2 (TIGel5)	rGO	5, 10, 25, 50, 100	25, 50	4
[PMIM][TFSI] + TiO_2 (TIGel6)	rGO	5, 10, 25, 50, 100	~25	4
[BTMA][TFSI] + TiO_2 (TIGel7)	rGO	5, 10, 25, 50, 100	~25	4
$[BMIM][BF_4]$ + DMAA + TiO_2[25]	carbon nanocage	–	25, 80, 100, 200	~3
$[BMIM][PF_6]$ + PEGMA + PEGDA + TiO_2[26]	carbon nanocage	25	~25	3
$[BMIM][BF_4]$ + DMAA + MBAA + TiO_2[27]	AC	–	25, 60, 100, 150, 200	~3
$[BMIM][BF_4]$ + HEMA + TiO_2[8]	Au-Ti-coated AC	5, 10, 50, 100	~25	~3

3.3. Results and Discussion on TIGels 2–7

3.3.1. Morphological Analysis

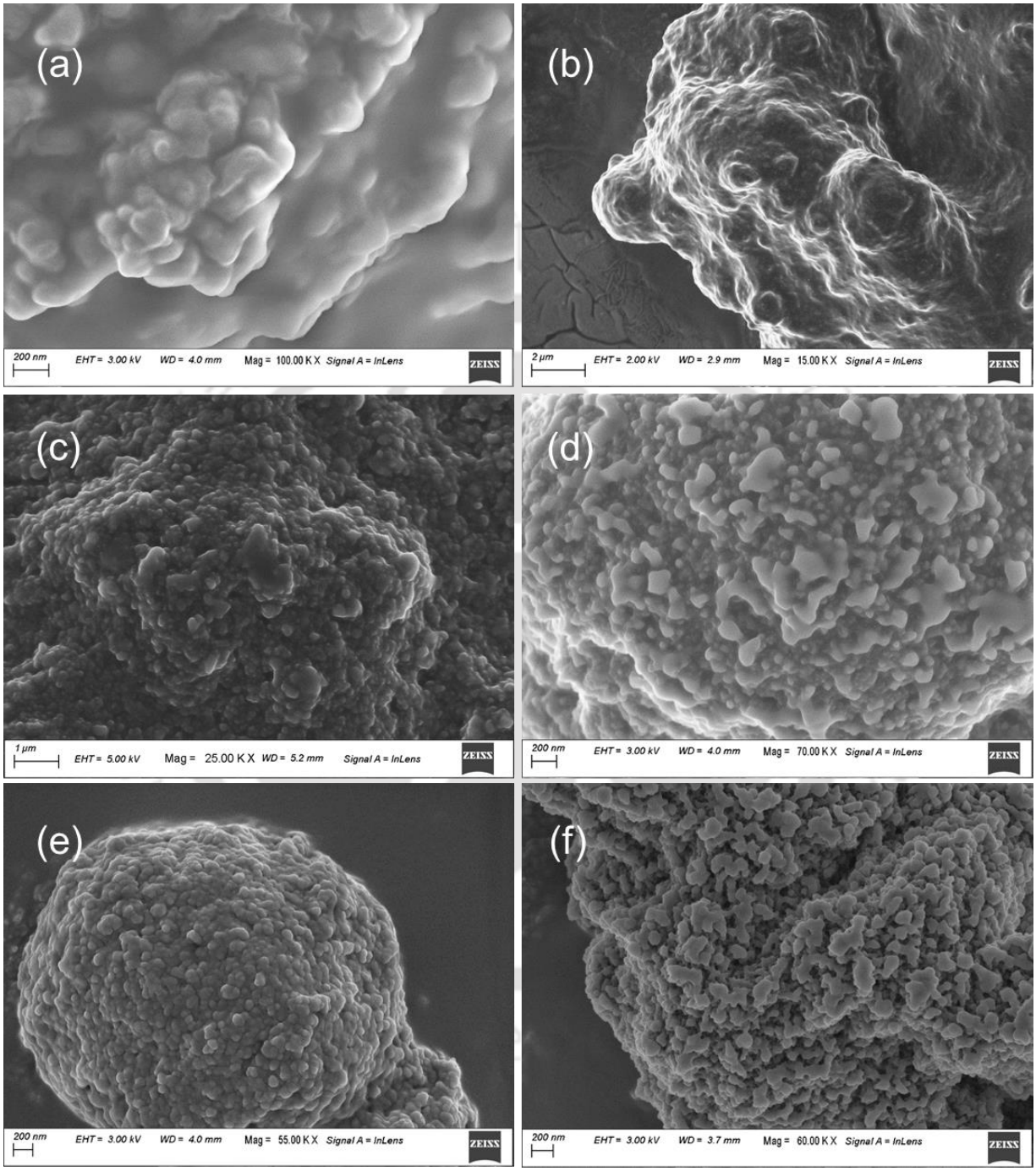

Figure 3.7. FESEM images of (a) TIGel2, (b) TIGel3, (c) TIGel4, (d) TIGel5, (e) TIGel6, and (f) TIGel7.

The FESEM images of the ionogels provided confirmation that TiO_2 particles were uniformly crosslinked with the IL frameworks (**Figure 3.7**a−f). Further FESEM studies suggested the possible existence of porosity within the inorganic gel matrices. Similar to TIGel1, ILs 2–7 were observed to be confined as interconnected liquid films layered within TiO_2, imparting a quasi-solid nature to the ionogels. The inorganic gel samples exhibited a cluster-like assembly of small agglomerated titania moieties incrusted on the surface of the ILs through a self-assembly mechanism. Moreover, the formation of 3D interconnected nanostructures indicated that the ILs were fully assimilated into the TiO_2 matrix through in-situ gelation on the nanometer scale. The interconnected structures of the TiO_2 particles generated continuous channels, serving as potentially convenient pathways for ion transport.[1]

FETEM was conducted on TIGels 3, 5, and 7. The FETEM micrographs (**Figure 3.8**a–c) validated the presence of interconnected aggregates of inorganic TiO_2 particles, resulting in porous structures within the ionogels.[28] As mentioned earlier, these aggregates create 3D nanostructured continuous channels, facilitating ion transport. The observed continuous channels suggest that the ILs are embedded within them through the sol-gel gelation process.

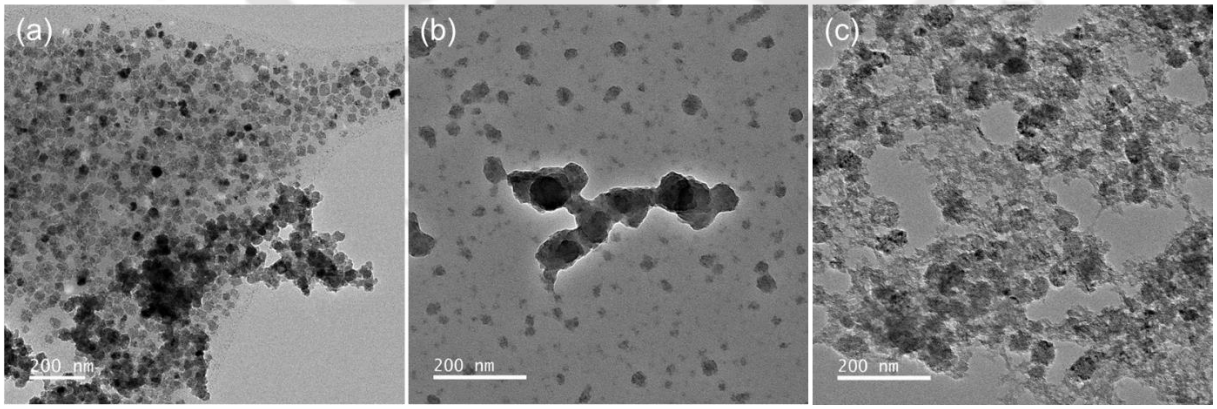

Figure 3.8. FETEM images of (a) TIGel3, (b) TIGel5, and (c) TIGel7.

3.3.2. Rheological Analysis

Figure 3.9a illustrates the relationship between shear rate and viscosity fluctuation of the ionogels. It is evident that when the shear rate increases, the viscosity of the ionogels decreases. This suggests that TIGels 2–7, just like TIGel1, also exhibit shear-thinning behavior. This can be related to the weakening of the physical crosslinking between the ILs and the TiO_2 matrix, or more simply, the decrease in the non-bonded interactions between the IL molecules and the titania moieties. In addition, when the acquired data is fitted with the power law model, the values of *n* for all ionogels are found to be smaller than unity, providing further evidence of their shear-thinning nature. Furthermore, the ionogels have a value of R^2 greater than 0.98, indicating a strong match of the power law model to the experimental data. Moisture affects all conventional ILs to varying degrees, including at low levels of humidity.[2,3] The absorption of moisture into the IL and ionogel can lead to a decrease in viscosity over time, since higher water content is known to reduce viscosity. Consequently, this can result in an increased diffusion coefficient of dissolved species, such as analytes and/or contaminants.[4] Moreover, viscosity exhibits a high degree of sensitivity to changes in temperature. Raising the temperature often leads to a reduction in viscosity.

An oscillatory shear test was conducted to examine the viscoelastic properties of the ionogels. First, an amplitude sweep test was performed to identify the LVE region within a strain range of 0.1 to 1000 %. **Figure 3.9**b demonstrates that G' of all ionogels remain unchanged until a strain of about 1 %, indicating that the structures of the samples remain intact. However, when the strain exceeds 1 %, there is a noticeable reduction in G' which may be attributed to the deterioration of the physical crosslinking between the precursors. Therefore, the LVE region for the ionogels may be defined within the strain range of 0.5 to 1 %. Moreover, the ionogels in the LVE region exhibit a prevalence of storage moduli over loss moduli, suggesting their viscoelastic solid-like characteristics, which are comparable to that of TIGel1.

A frequency sweep test was conducted by systematically changing the frequency within the range of 0.1 to 100 Hz, while maintaining a consistent strain level acquired from the associated LVE region. **Figure 3.9**c illustrates the viscoelastic properties of the ionogels. The $G^{/}$ values of the ionogels are consistently greater than that of $G^{//}$ across the entire frequency range. In addition, the $G^{/}$ consistently increases, showing that the ionogels exhibit significant solid-like characteristics. Furthermore, no occurrence of a cross-over point is seen within the specified frequency range, indicating that the ionogels possess a predominant elastic characteristic, similar to that of TIGel1.

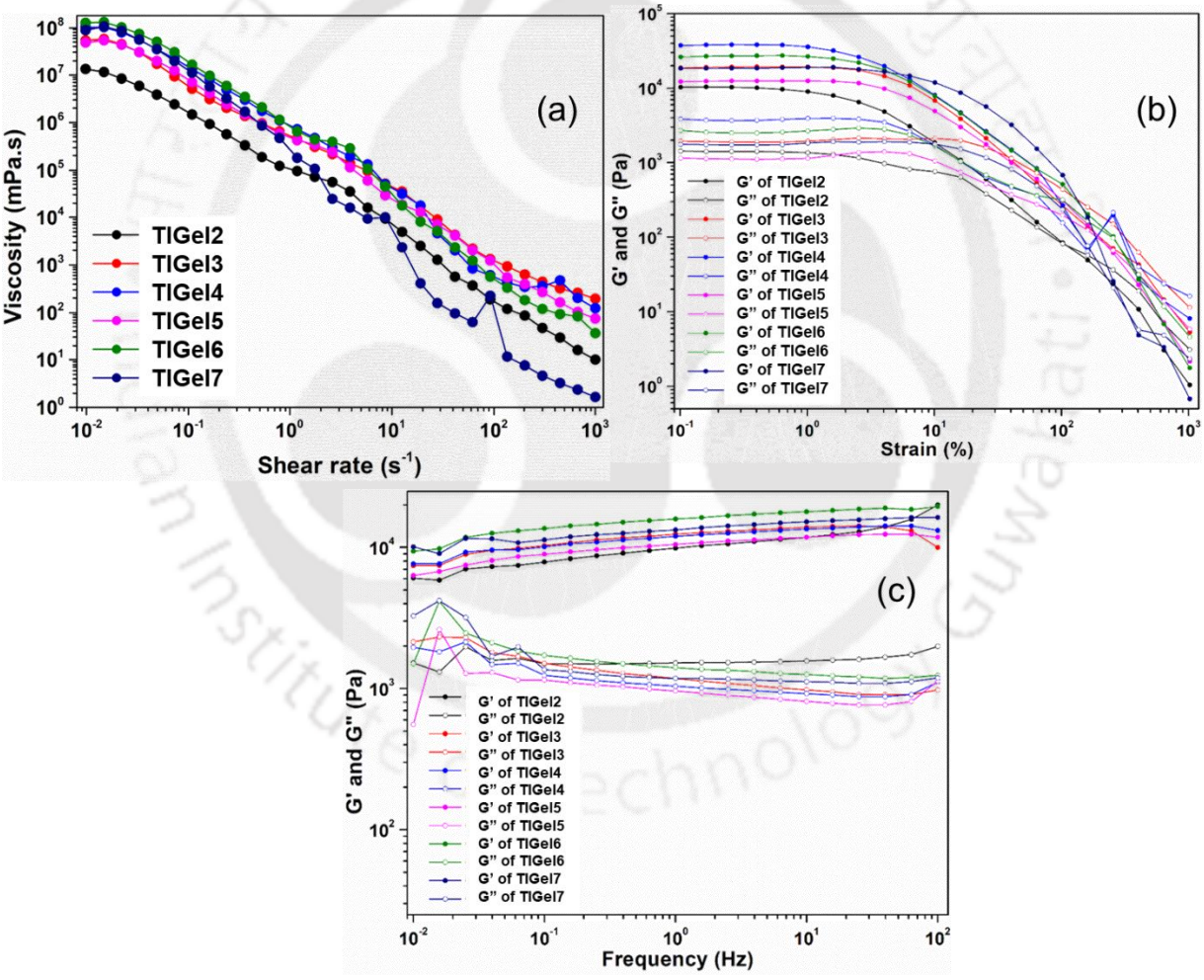

Figure 3.9. Plots depicting the rheological properties of TIGels 2–7: (a) viscosity versus shear rate, (b) storage and loss moduli versus strain amplitude, and (c) storage and loss moduli versus frequency.

3.3.3. Structural Analysis

To confirm the formation of the ionogels through physical confinement of ILs into TiO_2 matrix, FTIR spectroscopy was performed on all the ILs and their corresponding ionogels. **Figure 3.10**a–f reveals that the FTIR spectra of ILs 2–7 and the respective ionogels are highly similar, with the exception of an extra peak observed in each ionogel, which corresponds to a stretching of ν_sH−O−H.[5] It can thus be inferred that TBOT and the ILs did not form a direct chemical bond. It may further be inferred that the physical confinement within the crosslinking matrix did not affect the integrity of the ILs. Furthermore, it offers proof of the comprehensive interconnectedness of the ILs within the ionogels.[5] Nevertheless, there are slight shifts in the vibrational bands of the ionogels in comparison to those of the ILs, as was observed in case of IL1 and TIGel1. This indicates that there are non-bonded interactions between the IL molecules and the pore wall surfaces of the TiO_2 moieties.[1] The existence of these non-bonded interactions leads to potential changes in the thermal characteristics of the confined IL.[6] **Table A1** in Appendix A of this thesis displays some of the noticeable changes in the vibrational bands of the ILs after confinement, corresponding to their respective assignments.

The vibrational bands around 1500 cm^{-1} represent asymmetric C−H scissoring. C−N stretching is represented by peaks at ~1300 and ~900 cm^{-1} of the spectra. Meanwhile, the bands between 700 and 500 cm^{-1} are characteristic of C−H bending. For IL2, the vibrational bands at 1307, 900, 719, and 663 cm^{-1} correspond to P−CH_2−R deformation, symmetric C−N stretching, P−C vibration, and asymmetric N−C≡N stretching, respectively. The peaks at 1469 and 1168 cm^{-1} of the spectrum for IL3 represent the in-plane C−C and C−N bands of the imidazolium ring, while the one at 1033 cm^{-1} is due to B−F stretching in the anion. ILs 4, 6, and 7 exhibit peaks at similar positions owing to the presence of the common TFSI anion. The vibrations associated with symmetric SO_2 stretching in these ILs are represented around 1348, 1142, and 611 cm^{-1}. The bands about 1178 and 740 cm^{-1} may be attributed to CF_3 stretching and bending,

respectively. A peak at ~1051 cm^{-1} is observed for symmetric S–N–S stretching while the one at 788 cm^{-1} characterizes symmetric C–S stretching. In IL5, the C−F stretching of the anion is indicated by the presence of peaks between 1300 and 900 cm^{-1} while PF_3 bending and asymmetric P−F stretching are confirmed from the bands at 495 and 430 cm^{-1}, respectively. The bands at 818 and 717 of the spectrum of the same IL represent ring H−C=C−H asymmetric and symmetric out-of-plane bending. An out-of-plane ring deformation of the cation is characterized by a vibrational band at 615 cm^{-1}.[5,29–35] Again, limited content of titania in the ionogels, resulted in a domination of vibrations corresponding to the IL.

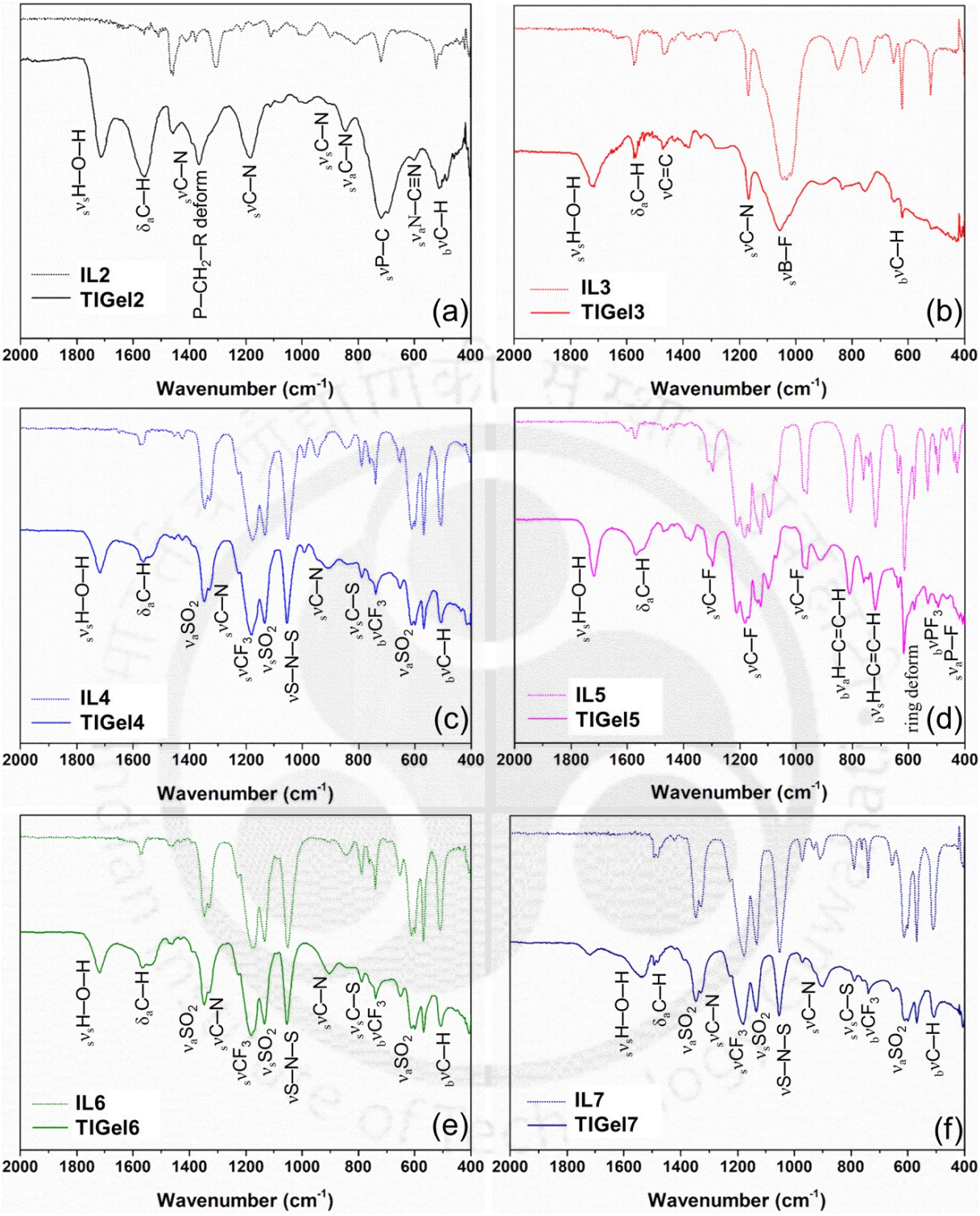

Figure 3.10. FTIR spectra of (a) IL2 and TIGel2, (b) IL3 and TIGel3, (c) IL4 and TIGel4, (d) IL5 and TIGel5, (e) IL6 and TIGel6, and (f) IL7 and TIGel7.

XRD studies were conducted on the ionogels to assess the degree of crystallinity of the samples. Consistent with the findings from TIGel1 and other relevant works reported previously,[5–8], all the ionogels described in this study also exhibit the existence of a characteristic amorphous TiO_2 matrix alongside the ILs. The XRD patterns of the ionogels shown in **Figure 3.11** consist predominantly of weak and broad peaks, indicating the amorphous or low-crystalline structure of the samples within the specified window of 2θ. The introduction of IL disrupts the uniform structure of the TiO_2 matrix, resulting in an expansion of the amorphous region.

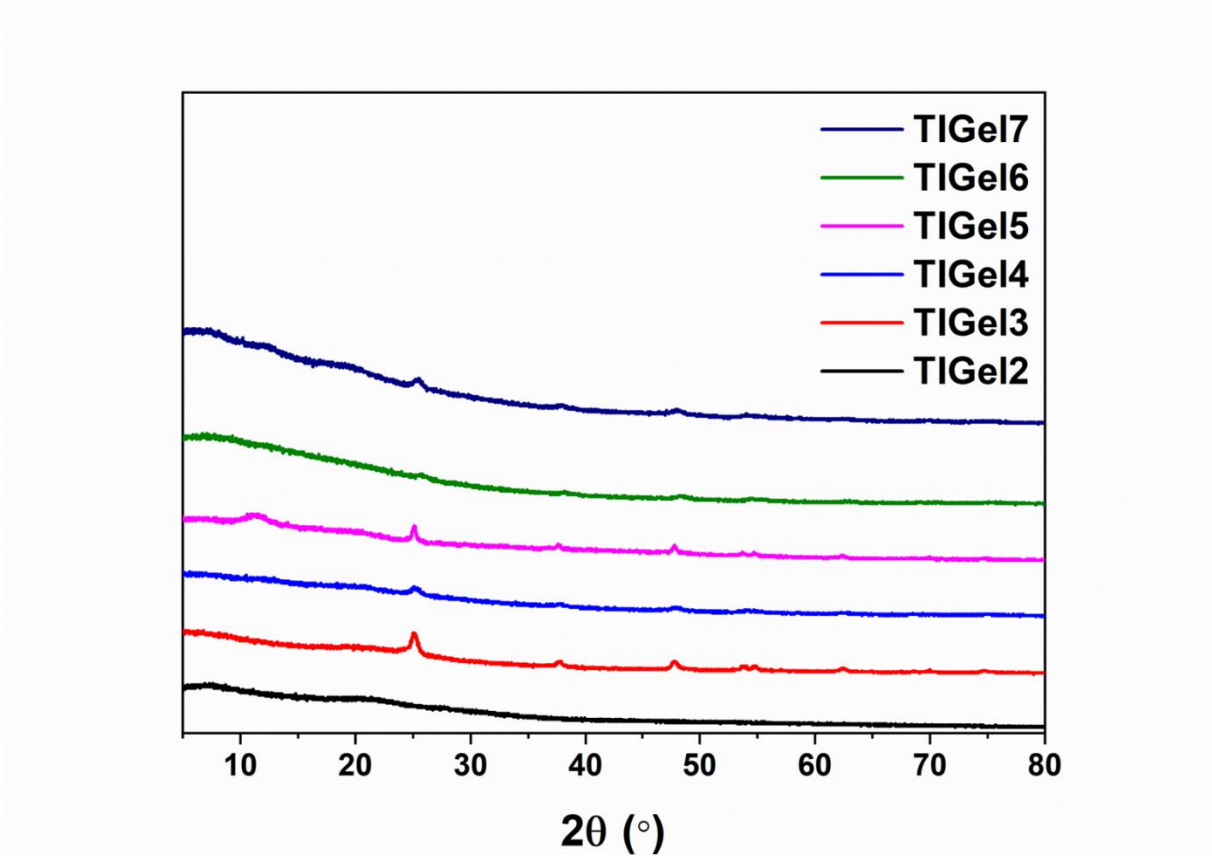

Figure 3.11. XRD spectra of TIGels 2–7.

3.3.4. Thermal Analysis

Thermal stabilities of the ILs and the ionogels were studied via TGA performed on a TG 209 F1 Libra (Make: M/s Netzsch, Germany). The experiments were carried out in a nitrogen atmosphere, for which the samples were heated from 20 to 600 °C at a rate of 5 °C min^{-1} under nitrogen flow at 40 mL min^{-1}. **Figure 3.12**a–f shows the TGA profiles of the ILs and their corresponding ionogels. All the ILs, except IL5 undergo decomposition in a single step. IL5, however, exhibits a two-step decomposition route.[36] It is seen that all six ILs are impeccably stable up to ~300 °C. However, their thermal stability is reduced with multiple decomposition upon confinement into the TiO_2, as previously observed in case of TIGel1. The sol-gel strategy usually introduces certain volatile byproducts during hydrolysis which are sometimes difficult to remove completely post synthesis. This lowers the onset degradation temperature of the solvent.[1] Furthermore, thermal stability decreases with increasing hydrophilicity.[37] The anion plays a significant role in determining the thermal stability of an IL,[38] and hence its corresponding ionogel.

DCA is predominantly a hydrophilic anion,[39] leading to the potential absorption and/or adsorption of substantial amount of moisture along with volatile impurities. It may also be worth mentioning that the sample of IL2 used here was not at its highest grade of purity (≥ 93 %) (**Table 2.1**) with the possible presence of inherent water and/or impurities. This possibly explains the initial steep loss of mass in the TGA profile of TIGel2 at 20 and ~150 °C.[6] The degradation step starting at ~220 °C corresponds to the decomposition of the IL components. This fact was substantiated by DSC on the same ionogel (-100–200 °C, 10 °C min^{-1}), wherein the gel is seen to exhibit a gradual descend up to about 150 °C, followed by a broad endothermic peak which could be attributed to the commencement of the decomposition of the IL (inset of **Figure 3.12**a). The loss of volatile impurities and moisture can be seen distinctly in the form of peaks at ~15 and ~110 °C. T_m for TIGel2 is -69.5 °C. It is also seen that TIGel5 experiences

an abrupt degradation at ~211 °C following the degradation of adsorbed or absorbed volatile substances between 20 and ~73 °C revealing its lower thermal stability. This is corroborated by findings of other researchers where they have noticed a lower thermal stability for FAP-based ILs, especially when compared to TFSI-based ones.[40] However, interactions between the TiO_2 matrix and the IL seem to have further reduced the thermal stability of the latter. The hump at ~320 °C on the thermogram of the ionogel corresponds to the second decomposition peak at ~340 °C of the IL. For TIGels 3, 4, 6, and 7, the first two steps of decomposition in the temperature windows of ~20–80 °C and ~210–300 °C are associated with mass loss due to the vaporization of physically or chemically absorbed water and/or organic residues.[6] This is followed by the decomposition of the ILs. The relatively better thermal stability of the said ionogels are in agreement with the fact that imidazolium ILs containing [BF_4] and [TFSI] anions and ammonium ILs with [TFSI] anions are intrinsically highly stable.[38,39] The straight lines towards the end of the thermograms of all ionogels indicate complete degradation of the organic compounds, leaving behind only the inorganic components.[9] Thus, confining the ILs into an inorganic matrix of TiO_2 resulted in a reduction of their thermal stability potentially due to the presence of volatile impurities and non-bonded interactions between the IL molecules and the TiO_2 pore wall surfaces.[6] However, the temperature window of stability for all the ionogels is still wide enough for their application in electrochemical devices.[11]

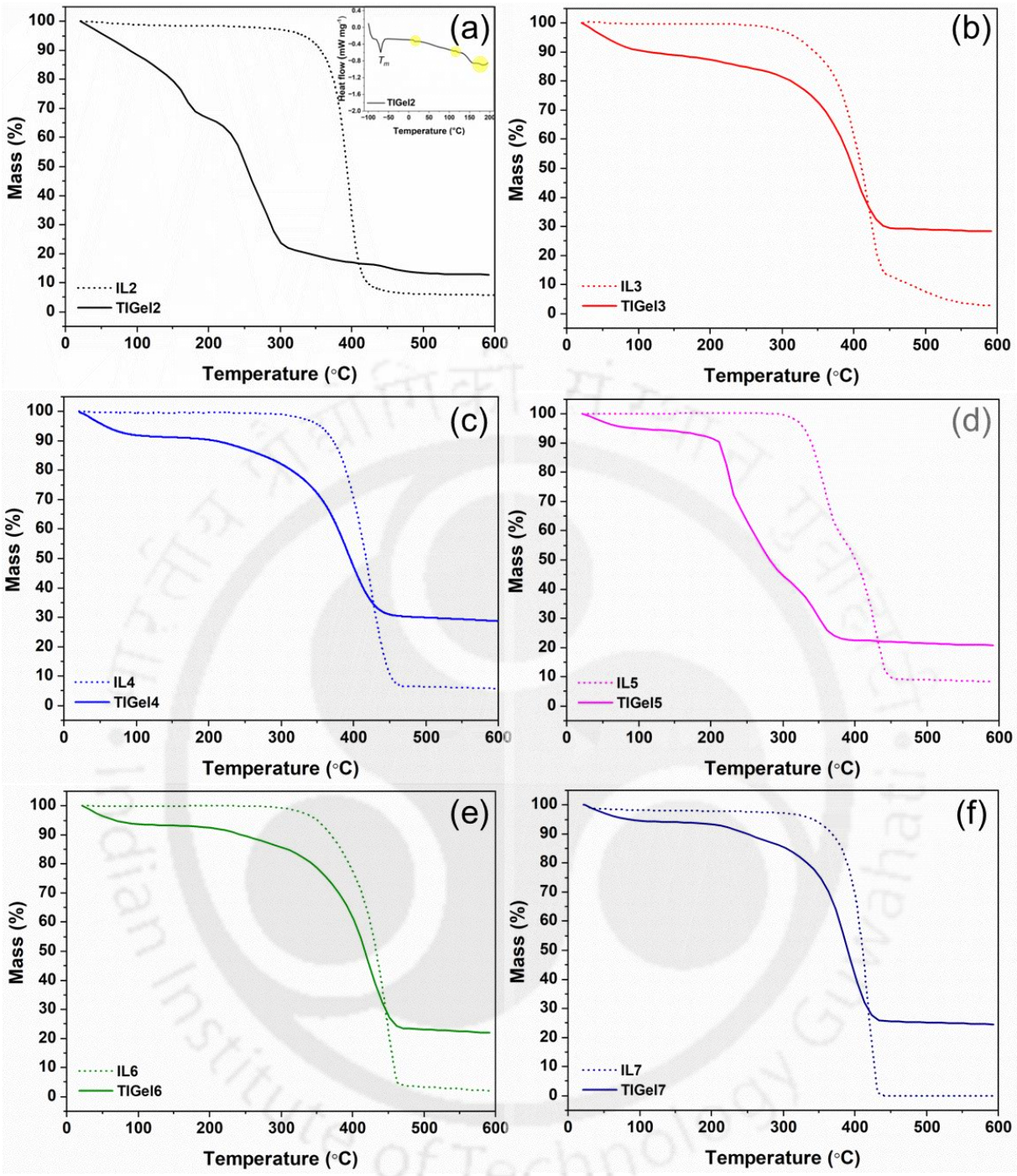

Figure 3.12. TGA profiles of (a) IL2 and TIGel2 (inset: DSC profile of TIGel2), (b) IL3 and TIGel3, (c) IL4 and TIGel4, (d) IL5 and TIGel5, (e) IL6 and TIGel6, and (f) IL7 and TIGel7.

3.3.5. Electrochemical Performance

3.3.5.1. Cyclic Voltammetry

Figure 3.13a–f shows the cyclic voltammograms of TIGels 2–7 obtained at room temperature with the rGO-based two-electrode cell on a Gamry-interfaced CH Instruments, 600 C potentiostat (Gamry) at scan rates of 5, 10, 25, 50, and 100 mV s^{-1}. The quasi-rectangular CV profiles at all five scan rates indicate a capacitive behavior of the systems.[14,15] The absence of any redox peaks at each scan rate further indicates that the charge-storage mechanism is non-Faradaic or double-layer in nature within the potential window.[11,14,15] The presence of dissolved impurities and/or functional groups on the electrode surface may impart some pseudocapacitance. However, the linearity of the current indicates that the systems are predominantly non-Faradaic within the potential range.[18] TIGels 2 and 4 exhibit a relatively low current with the latter indicating the presence of very high intrinsic resistance over the given potential window. This could be due to the presence of the bulky P_{66614} molecule in TIGel2 resulting in charge-shielding and resistance to ionic mobility,[19] potentially the same reason behind the low current response of TIGel1. In case of TIGel4, the unsaturated –$CH=CH_2$ group in the cation possibly inhibits easy and fast dissociation of ions. The absence of an ideally polarizable reference electrode may also be responsible for the poor current response.[20] It may be noted that self-diffusivity of cations and anions in immobilized ILs may remain low on account of surface forces arising from the interaction between absorbed ions and matrix surface, leading to restricted kinetics.[1]

Nonetheless, the ionogels are observed to consistently deliver a double-layer capacitive behavior within a wide potential window of 4 V (-4 V to +4 V) against the porous rGO electrodes at all five scan rates of 5, 10, 25, 50, and 100 mV s^{-1}. This can be attributed to several factors.[19,38,41,42] Phosphonium-based ILs are known to possess wide ESPW because of their

increased chain-length, which, in turn, increases the cathodic and anodic limits. This explains the broad OPW of TIGel2. On the other hand, the presence of imidazolium and/or TFSI ions in an IL enhances the electrochemical stability through charge-delocalization effect, weakening ion-ion interactions. This attribute favored TIGels 3–7, offering them a wide potential window. Additionally, high hydrophobicity of [EMIM][[FAP] eliminated possibilities of a shrunken voltage window in TIGel5 due to the intervention of water. Moreover, the electrochemical stability of ILs containing ammonium cations is high due to the latter's superior resistance towards reduction, which further corroborates the wide OPW of TIGel7. On comparing the OPW with that of ionogels obtained with the immobilization of ILs into a matrix of TiO_2 in similar works reported previously, the widest window of 4 V could be found in this work (**Table 3.2**).

It is noteworthy to reiterate that the potential window can vary based on several factors, including the electrode material, electrode configuration, properties of the electrolyte, ambient conditions, and the measurement method.[22,23] The use of a porous carbon electrode, for instance, can limit the anodic and cathodic stabilities of the electrolyte, resulting in a reduced potential window compared to inert electrodes such as gold and platinum.[11] Similarly, the potential window may taper at high temperatures.[1]

Even commercial ILs obtained with the highest level of purity may contain certain impurities.[4] The purity of an electrolyte significantly affects its electrochemical stability,[4,11,24] and thus the OPW of the system. Here, the constituent chemicals were used as received, without undergoing additional purification steps. The presence of synthetic impurities can narrow the potential window, an effect that may be exacerbated by the presence of water.[4] A reduction in the potential window occurs at both the anodic and cathodic limits and can be attributed to the electrolysis of water, especially as the water content increases.[3] The redox peaks associated

with dissolved impurities intrinsic to the IL become more prominent with an increase in water content.[4]

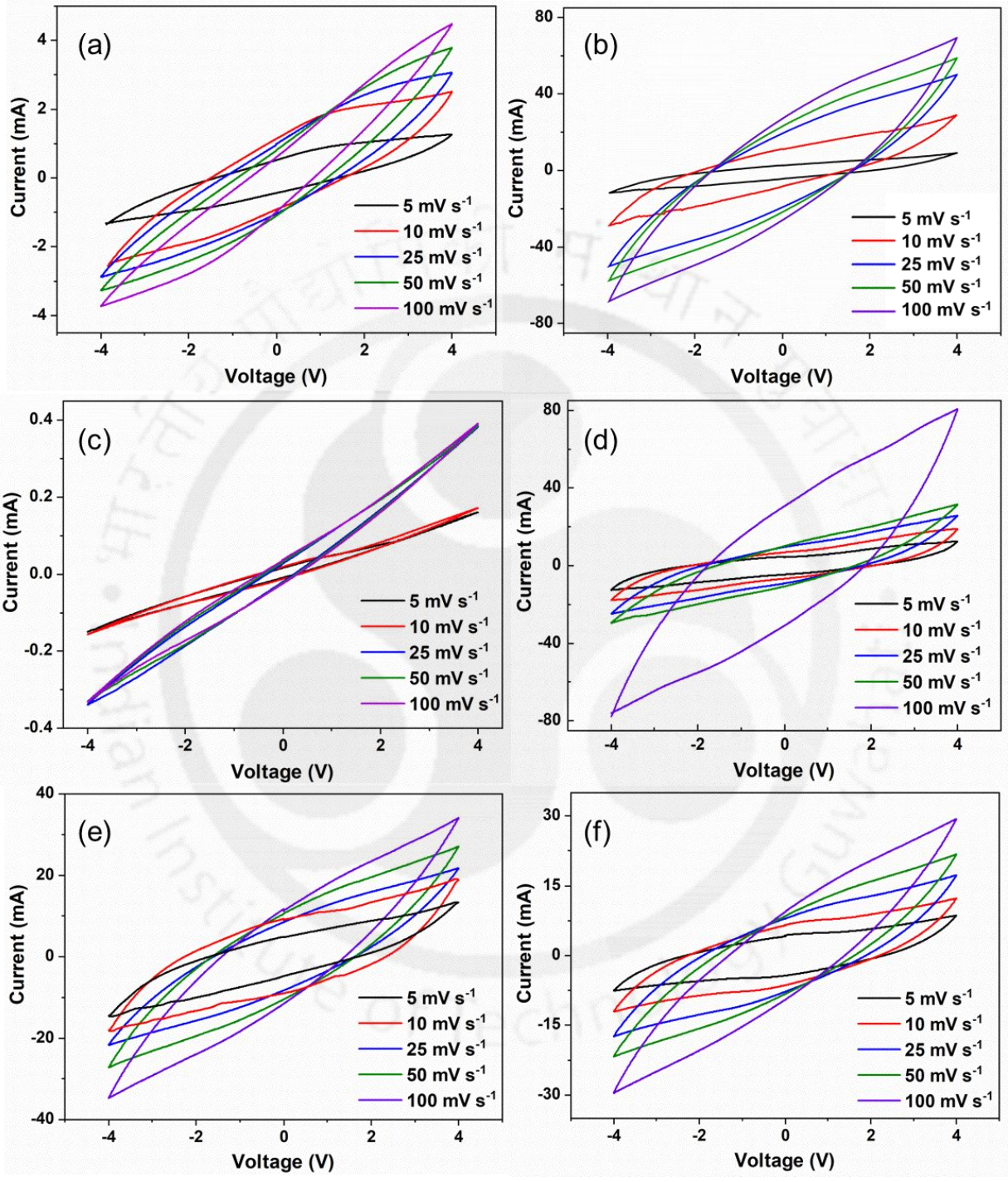

Figure 3.13. Cyclic voltammograms obtained at room temperature from CV conducted on the two-electrode coin-cell assembly with rGO electrodes at scan rates of 5, 10, 25, 50, and 100 mV s^{-1} for (a) TIGel2, (b) TIGel3, (c) TIGel4, (d) TIGel5, (e) TIGel6, and (f) TIGel7.

The maximum values of specific capacitance and specific energy for all the ionogels were obtained at the scan rate of 5 mV s^{-1} (**Table 3.3**). TIGel5 showed the highest values for specific capacitance (11.5 F g^{-1} or 277.7 mF cm^{-2}) and specific energy (25.4 W h kg^{-1}). This is most likely due to the comparably low room-temperature viscosity (60.5 mPa s) of IL5, in addition to an increased charge distribution due to delocalization of the cation.[19,43] Specific capacitance, and hence energy are significantly influenced by the characteristics of the electrode material, primarily its surface area and nature of porosity. Furthermore, the specific capacitance of a supercapacitor is also affected by mass loading of the electrolyte, along with the latter's diffusive properties and internal resistance.[11] TIGel5 delivered specific capacitances of 8.3 (202.3), 4.0 (98.1), 3.3 (78.9), and 2.2 (52.2) F g^{-1} (mF cm^{-2}) with specific energy of 18.5, 8.9, 7.2, and 4.8 W h kg^{-1} at scan rates of 10, 25, 50, and 100 mV s^{-1}, respectively (**Table 3.4**). The values of specific capacitance obtained here closely agree with those reported previously with substantial mass loading for similar electrolytes.[44] Also, due to the wide OPW of the ionogels, the energy contained herein is higher than that obtained with polymeric ionogels and rGO electrodes.[45] The variation in specific capacitance (gravimetric and areal) and specific energy with scan rate for TIGel5 is represented in **Figure 3.14**a–c. The profiles clearly reveal the effect of electrolyte starvation in the system, leading to a reduced specific capacitance and specific energy at higher scan rates. The system retained ~73 % and ~19 % of its initial capacitance (and energy) at 10 mV s^{-1} and 100 mV s^{-1}, respectively.

Table 3.3. Specific capacitance and specific energy of TIGels 2–7 at room temperature and 5 mV s^{-1}

TIGel	$C_{sp\text{-}5\ mV\ s^{-1}}$ (F g^{-1})	$C_{sp\text{-}5\ mV\ s^{-1}}$ (mF cm^{-2})	$E_{sp\text{-}5\ mV\ s^{-1}}$ (W h kg^{-1})
2	0.99	23.99	2.19
3	10.54	255.77	23.43
4	0.02	0.47	0.04
5	11.45	277.72	25.44
6	10.15	246.15	22.55
7	8.55	207.48	19.01

Table 3.4. Specific capacitance and specific energy of TIGel5 at room temperature and scan rates of 5, 10, 25, 50, and 100 mV s^{-1}

Scan rate (mV s^{-1})	C_{sp} (F g^{-1})	C_{sp} (mF cm^{-2})	E_{sp} (W h kg^{-1})
5	11.45	277.72	25.44
10	8.34	202.31	18.53
25	4.04	98.08	8.98
50	3.25	78.87	4.78
100	2.15	52.20	7.23

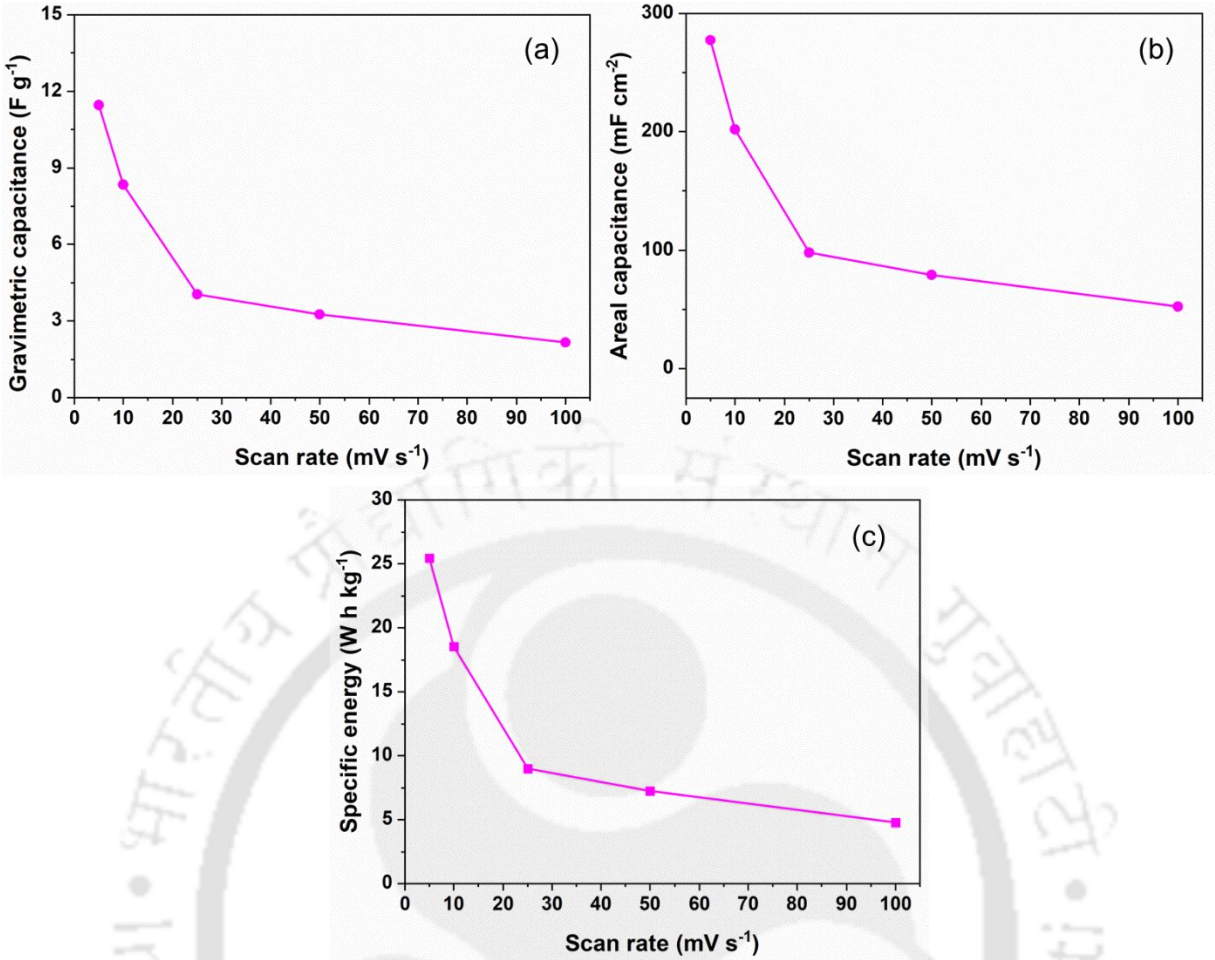

Figure 3.14. (a) Gravimetric capacitance, (b) areal capacitance, and (c) specific energy of TIGel5 as a function of scan rate at room temperature.

CV was also performed on TIGel5 at controlled temperatures of 25, 50, and 100 °C in the same potential range (-4 V to +4 V) using a second coin cell identical to the one used in previous experiments. The experiments were conducted for the same five scan rates on a PGSTAT101 Autolab potentiostat (Eco, Chemie, The Netherlands) interfaced to a Nova 2.1 software. The double-layer capacitive behavior and the 4 V OPW of the ionogel were seen to remain unaltered with no trace of electrolyte degradation at 25 and 50 °C for all five scan rates, revealing a stable performance of the system (**Figure 3.15**a,b). However, the appearance of distorted voltammograms at 100 °C hinted towards potential constriction of the electrochemical stability and/or degradation of the electrolyte at that temperature (**Figure A1**).

The latter, in particular, could possibly be attributed to the lower thermal stability of TIGel5, which might have been aggravated by prolonged use at higher temperatures. The higher current response at higher temperatures indicates faster kinetics, which is expected for such devices.[44] Elevated temperatures lead to better ionic mobility and dissociation of more ions into the electrode pores. This, in turn, increases the effective area at the electrode/electrolyte interface, resulting in higher specific capacitance.[46] The values of maximum specific capacitance and specific energy obtained at 5 mV s^{-1} and 25 °C were 15.4 F g^{-1} (373.2 mF cm^{-2}) and 34.2 W h kg^{-1}, respectively (**Table 3.5**). However, at 50 °C, the values for the same parameters increased by a factor of 1.6 and stood at 24.4 F g^{-1} (591.5 mF cm^{-2}) and 54.2 W h kg^{-1}, respectively.

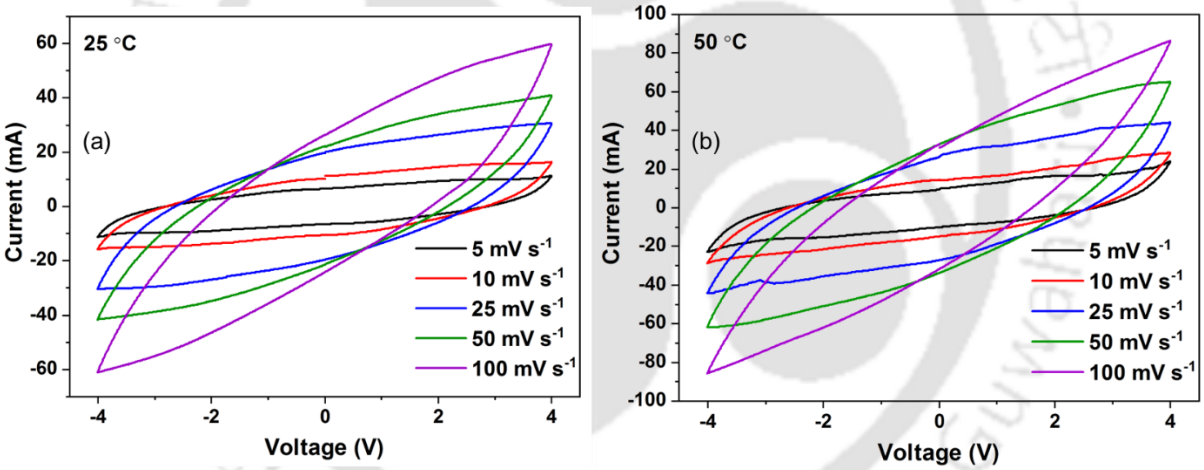

Figure 3.15. Cyclic voltammograms of the TIGel5-based system obtained from CV conducted using the two-electrode coin-cell assembly with rGO electrodes at scan rates of 5, 10, 25, 50, and 100 mV s^{-1} at controlled temperatures of (a) 25 °C and (b) 50 °C.

Table 3.5. Specific capacitance and specific energy of TIGel5 at scan rates of 5, 10, 25, 50, and 100 mV s^{-1} and controlled temperatures of 25 and 50 °C

Temperature (°C)	Scan rate (mV s^{-1})	C_{sp} (F g^{-1})	C_{sp} (mF cm^{-2})	E_{sp} (W h kg^{-1})
25	5	15.39	373.19	34.19
	10	11.99	291.06	26.67
	25	8.54	207.23	18.99
	50	4.73	114.63	10.50
	100	2.82	68.49	6.28
50	5	24.39	591.54	54.19
	10	16.82	408.08	37.39
	25	11.35	275.27	25.22
	50	7.24	175.53	16.08
	100	3.38	81.98	7.51

At 25 °C, the ionogel delivered specific capacitances of 11.9 (291.1), 8.5 (207.2), 4.7 (114.6), and 2.8 (68.5) F g^{-1} (mF cm^{-2}) with specific energy of 26.7, 18.9, 10.5, and 6.3 W h kg^{-1} at scan rates of 10, 25, 50, and 100 mV s^{-1}, respectively. On the other hand, at 50 °C, it acquired capacitance values of 16.8 (408.1), 11.3 (275.3), 7.2 (175.5), and 3.4 (81.9) F g^{-1} (mF cm^{-2}) with specific energy of 37.4, 25.2. 16.1, and 7.5 W h kg^{-1} for the same respective scan rates. A difference in values of capacitance (by ~4 F g^{-1} or ~95 mF cm^{-2} at 5 mV s^{-1}) was observed for the same ionogel when conducted at room temperature and at a controlled temperature of 25 °C. This may primarily be attributed to the possible differences in temperatures, mass of sample loaded, and the utilization of two different coin cells. The variation in specific capacitance (gravimetric and areal) and specific energy with scan rate for 25 and 50 °C is represented in **Figure 3.16**a–c. The profiles again show the existence of

electrolyte starvation effect in the system at each temperature, leading to a reduced specific capacitance and specific energy at higher scan rates. At 25 °C, the device was able to retain ~78 % and ~18 % of its initial capacitance (and energy) at 10 mV s^{-1} and 100 mV s^{-1}, respectively. However, it exhibited a capacity (and energy) retention of ~69 % and ~14 % at the same respective scan rates and 50 °C. The faster decay of capacitance at higher temperature for ionogel-supported supercapacitor is in agreement with findings reported previously,[47] and may be attributed to the faster kinetics of the system.

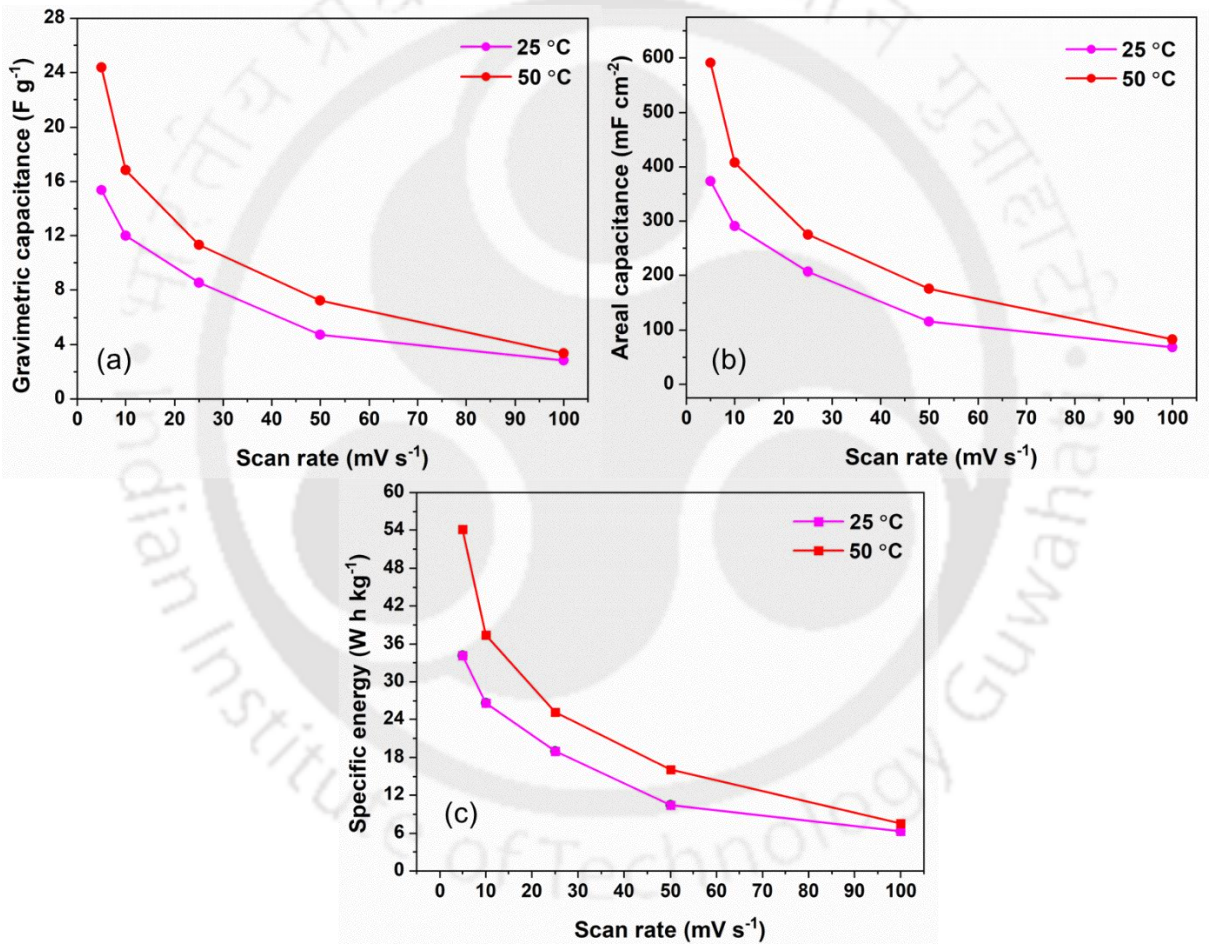

Figure 3.16. (a) Gravimetric capacitance, (b) areal capacitance, and (c) specific energy of TIGel5 as a function of scan rate at controlled temperatures of 25 and 50 °C.

3.3.5.2. Electrochemical Impedance Spectroscopy

EIS was performed on TIGels 2–7 at the OCP by applying an AC voltage of 5 mV in the frequency range of 0.01 Hz to 100 kHz. The experiments were conducted at room temperature using the rGO-based two-electrode coin-cell system on a Gamry-interfaced CH Instruments, 600 C potentiostat (Gamry). **Figure 3.17**a–f shows the Nyquist plots obtained with the ionogel samples. Confirming the findings from CV, all the ionogels are seen to exhibit typical EDLC characteristics. The presence of a Warburg element in the plots is a result of the frequency dependence of ion diffusion/transport in the ionogels sandwiched between the porous rGO electrodes.[44] R_s, R_{ct}, and ESR of each ionogel sample were determined from its corresponding Nyquist plot. Thereafter, the ionic conductivity (σ) of the sample and power (P) delivered by the device were calculated using **equations 2.15** (t ~ 0.07 cm) and **1.2**, respectively. The data have been tabulated in **Table 3.6**.

Table 3.6. Solution resistance, charge-transfer resistance, equivalent series resistance, ionic conductivity, and power associated with TIGels 2–7 at room temperature

TIGel	R_s (Ω)	R_{ct} (Ω)	ESR (Ω)	σ (mS cm^{-1})	P (kW kg^{-1})
2	823.25	119.05	948.67	0.030	0.25
3	56.68	51.50	109.86	0.436	2.12
4	23637.61	304.07	23941.68	0.001	0.01
5	18.43	16.70	36.16	1.341	6.44
6	60.48	23.65	84.13	0.409	2.77
7	119.62	37.00	157.67	0.207	1.48

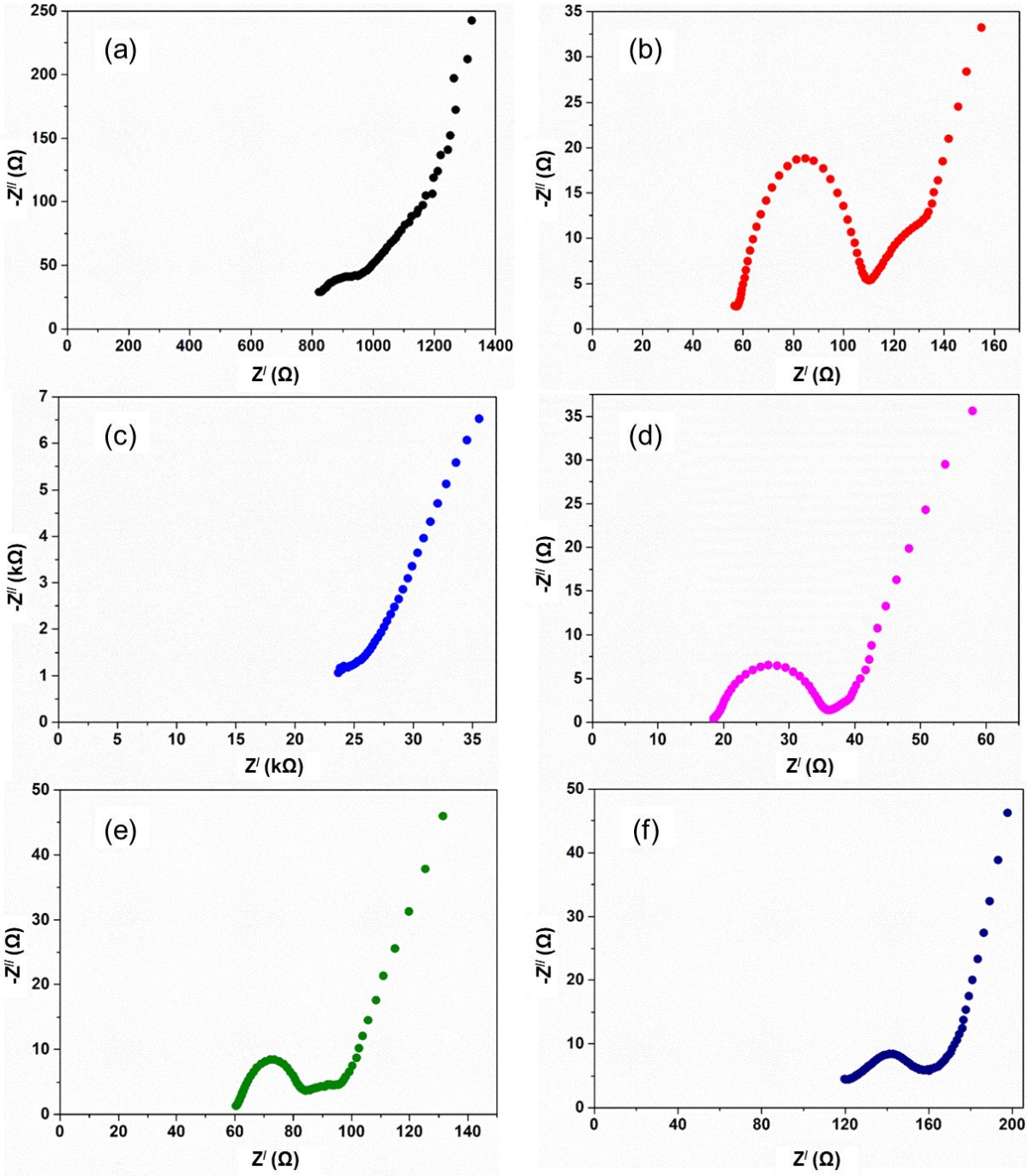

Figure 3.17. Nyquist plots of the systems obtained from EIS conducted on the rGO-based two-electrode coin cell with (a) TIGel2, (b) TIGel3, (c) TIGel4, (d) TIGel5, (e) TIGel6, and (f) TIGel7 electrolytes at room temperature.

Evidence of restricted kinetics could be seen in the ionogels in the form of intrinsic resistance possibly due to interactions between absorbed ions and matrix surface, resulting in low self-diffusivity.[1] TIGel2 exhibited a low ionic conductivity of 0.03 mS cm^{-1} at room

temperature, which is in agreement with observations presented in previous reports.[19] As mentioned earlier, the cationic charge of phosphonium-based ILs is largely alkyl-shielded by the bulky cation molecules. On the contrary, the cationic charge of imidazolium ILs is mostly delocalized due to the extensive π-bonding of the heterocycle, resulting in weaker ionic interactions and enhanced ionic conductivity.[19] Thus, TIGels 3, 5, and 6 showed relatively higher values for conductivity. Nevertheless, TIGel4 showed high ESR with poor ionic conductivity (0.001 mS cm^{-1}) potentially because of the presence of the unsaturated –$CH=CH_2$ group in the cation, which results in the inhibition of easy and fast dissociation of ions. Between TIGels 3 and 6, the former possesses a slightly higher conductivity (0.436 mS cm^{-1} against 0.409 mS cm^{-1}) owing to the presence of the smaller-sized BF_4 anion. The ionic conductivity of TIGel7 (0.207 mS cm^{-1}) is lower than that of its fairly performing imidazolium-based counterparts because of its higher intrinsic resistance possibly generated from the relatively low ionic conductivity of IL7.[48,49] However, the room-temperature ionic conductivity of TIGel5 (1.341 mS cm^{-1}) is found to be the highest corresponding to an ESR of 36.2 Ω, the lowest among all. This is again most likely due to the comparably low room-temperature viscosity of the IL, in addition to the increased charge distribution.[19] The value obtained is in agreement with those reported for other sol-gel-derived inorganic ionogels.[9,50] Owing to the low ESR, the cell loaded with TIGel5, also delivered the highest power (6.4 kW kg^{-1}) at room temperature. These findings are consistent with the results obtained from cyclic voltammetry. Although the conductivities of the ionogels with porous rGO electrodes are not appealing, they demonstrate good compatibility with the latter with a wide OPW, resulting in high performance EDLCs.

EIS was further conducted on TIGel5 at the controlled temperatures of 25, 50, and 100 °C using a different coin cell, the one used to perform CV on the same ionogel at the said temperatures. The experiments were conducted on a PGSTAT101 Autolab potentiostat (Eco,

Chemie, The Netherlands) interfaced to a Nova 2.1 software. The Nyquist plots at 25 and 50 °C confirm that the system was able to maintain its EDLC nature at each temperature (**Figure 3.18**). However, evidence of potential degradation was again observed at 100 °C (**Figure A2**). Also, EIS at 50 °C yielded a less distorted profile with lower solution and charge-transfer resistances and a capacitive tail with a greater slope than that at 25 °C, thus reconfirming the occurrence of faster kinetics at higher temperatures. High temperature facilitates the formation of self-assembled ionic channels, thus reducing resistance and enhancing faster transfer of charges.[44,51]

The calculated resistances, along with the ionic conductivity and power of the system at each temperature are shown in **Table 3.7**. Reduced R_s and R_{ct} at 50 °C confirms faster charge transfer. The ionic conductivity at 25 °C (~0.3 mS cm^{-1}) is increased by a factor of 5.9 at 50 °C (1.7 mS cm^{-1}). It is noteworthy that the ESR of the ionogel at 25 °C (126 Ω) is, however, reduced just by a factor of 3.3 at 50 °C (~38 Ω). This indicates that the cell resistance is predominantly governed by the diffusion of ions in the electrode pores.[44] Consequently, the specific power is seen to increase from 1.8 kW kg^{-1} at 25 °C to 6.2 kW kg^{-1} at 50 °C. Possible differences in temperatures and mass of sample loaded, along with the use of two different coin cells may again be largely accounted for the variation in values of resistances and ionic conductivity of the same ionogel conducted at room temperature and at a controlled temperature of 25 °C.

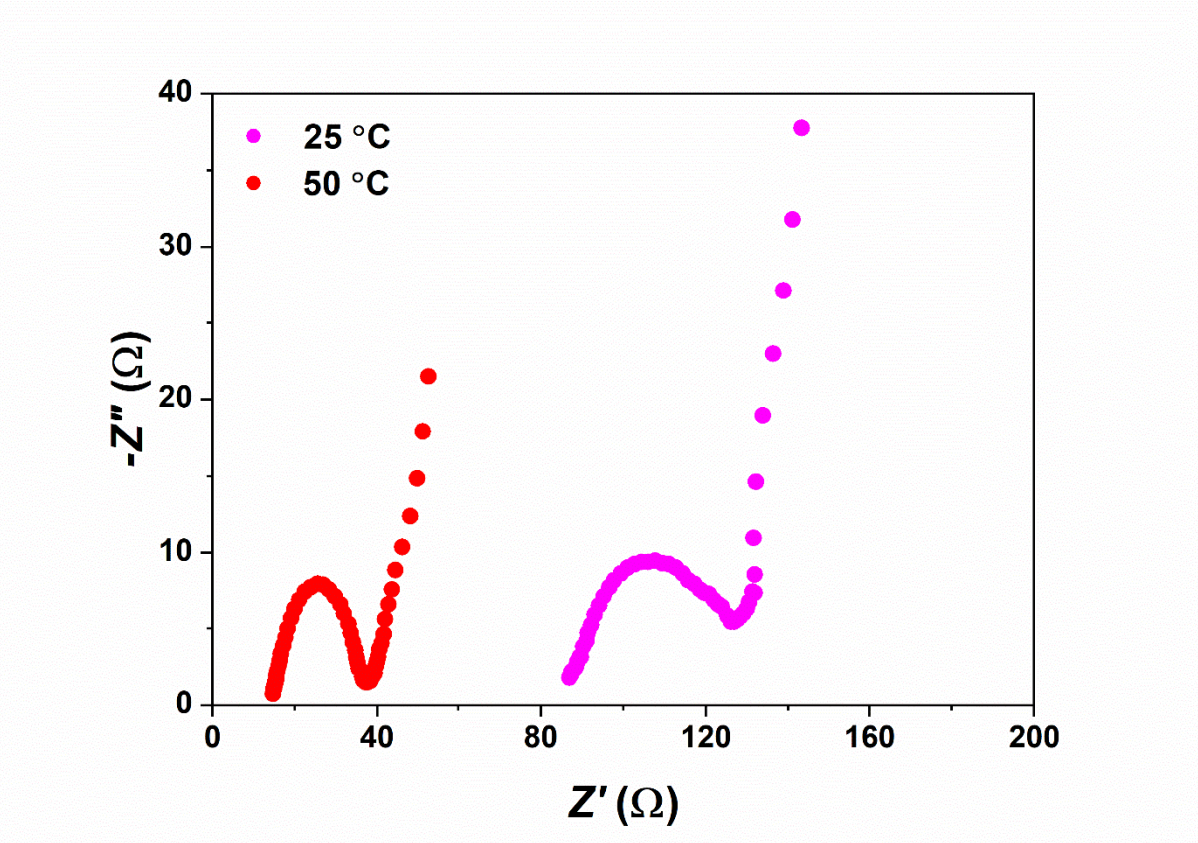

Figure 3.18. Nyquist plots of the system obtained from EIS conducted on the rGO-based two-electrode coin cell with TIGel5 electrolyte at 25 and 50 °C.

Table 3.7. Solution resistance, charge-transfer resistance, equivalent series resistance, ionic conductivity, and power associated with TIGel5 at 25 and 50 °C

Temperature (^{0}C)	R_s (Ω)	R_{ct} (Ω)	ESR (Ω)	σ (mS cm^{-1})	P (kW kg^{-1})
25	86.96	39.11	126.07	0.28	1.85
50	14.78	22.81	37.59	1.67	6.19

3.4. Conclusions

The sol-gel confinement of the seven ILs into TBOT-derived TiO_2 yielded seven quasi-solid inorganic ionogels with porous structures and 3D nanostructured continuous channels, as confirmed from FESEM and FETEM. The synthesis process for each ionogel utilized a minimal number of precursors without the need for any additional sample-preparation steps, making it fast, simple, and cost-effective. Rheology studies showed that the ionogels behave as shear-thinning, viscoelastic fluids with dominant elasticity. FTIR analyses indicated that the structural integrity of the ILs was not affected by their confinement into TiO_2, thus confirming gelation through a physical crosslinking. However, marginal shifts in vibrational frequencies of the ionogels were noticed owing to non-bonded interactions between the pore wall surfaces of the TiO_2 moieties and IL molecules. XRD suggested the co-existence of the ILs and the TiO_2 matrix in amorphous state. It was observed from TGA studies that the thermal stability of the ILs is compromised after immobilization, which may be attributed to interactions between the ILs and TiO_2. The TFSI-based ionogels were found to be more stable thermally. Nevertheless, the stability windows of all ionogels are sufficient for potential moderate- to high-temperature applications.

From the electrochemical point of view, all seven ionogels manifest a double-layer capacitive behavior within a wide potential window of 4 V owing to the good electrochemical stability and hydrophobic qualities of the host ILs. This highlights their good compatibility with rGO electrodes and excellent stability in applications with EDLCs. Consequently, the ionogels are able to achieve specific energy comparable to rGO and AC-based polymeric ionogels reported previously. However, decent values for specific capacitance and specific power have been reported due to restricted kinetics and higher intrinsic resistance, especially in TIGels 4, 2, and 7. Although thermally less stable, TIGel5 performs the best electrochemically, delivering the highest specific capacitance (11.5 F g^{-1} or 277.7 mF cm^{-2}),

lowest ESR (36.2 Ω), and highest ionic conductivity (1.3 mS cm^{-1}) because of the high hydrophobicity and low room-temperature viscosity of IL5, combined with increased charge distribution facilitated by cation delocalization. The corresponding values of specific energy and power delivered by the device stand at 25.4 W h kg^{-1} and 6.4 kW kg^{-1}. The same ionogel is also able to maintain its OPW and EDLC characteristics at controlled temperatures of 25 and 50 °C while showing an increase in its specific capacitance and ionic conductivity by factors of 1.6 and 5.9 respectively, at the latter temperature. It may, thus be concluded that the ionogels have the potential to be utilized as stable electrolytes in electrochemical storage applications, especially in EDLCs as well as other pertinent realms of electrochemistry. Additionally, the promising characteristics of these ionogels, especially those of TIGel5, may provide an appealing route for researchers to undertake further research on the integration of other materials for higher-temperature electrochemical applications.

References

(1) Chen, N.; Zhang, H.; Li, L.; Chen, R.; Guo, S. Ionogel Electrolytes for High-Performance Lithium Batteries: A Review. *Advanced Energy Materials*. Wiley-VCH Verlag April 25, 2018. https://doi.org/10.1002/aenm.201702675.

(2) Schröder, U.; Wadhawan, J. D.; Compton, R. G.; Marken, F.; Suarez, P. A. Z.; Consorti, C. S.; de Souza, R. F.; Dupont, J. Water-Induced Accelerated Ion Diffusion: Voltammetric Studies in 1-Methyl-3-[2,6-(S)-Dimethylocten-2-Yl]Imidazolium Tetrafluoroborate, 1-Butyl-3-Methylimidazolium Tetrafluoroborate and Hexafluorophosphate Ionic Liquids. *New Journal of Chemistry* **2000**, *24* (12), 1009–1015. https://doi.org/10.1039/b007172m.

(3) O'Mahony, A. M.; Silvester, D. S.; Aldous, L.; Hardacre, C.; Compton, R. G. Effect of Water on the Electrochemical Window and Potential Limits of Room-Temperature Ionic

Liquids. *J Chem Eng Data* **2008**, *53* (12), 2884–2891. https://doi.org/10.1021/je800678e.

(4) Doblinger, S.; Donati, T. J.; Silvester, D. S. Effect of Humidity and Impurities on the Electrochemical Window of Ionic Liquids and Its Implications for Electroanalysis. *The Journal of Physical Chemistry C* **2020**, *124* (37), 20309–20319. https://doi.org/10.1021/acs.jpcc.0c07012.

(5) Wu, F.; Chen, N.; Chen, R.; Zhu, Q.; Tan, G.; Li, L. Self-Regulative Nanogelator Solid Electrolyte: A New Option to Improve the Safety of Lithium Battery. *Advanced Science* **2016**, *3* (1). https://doi.org/10.1002/advs.201500306.

(6) Verma, Y. L.; Tripathi, A. K.; Shalu; Singh, V. K.; Balo, L.; Gupta, H.; Singh, S. K.; Singh, R. K. Preparation and Properties of Titania Based Ionogels Synthesized Using Ionic Liquid 1-Ethyl-3-Methyl Imidazolium Thiocyanate. *Materials Science and Engineering: B* **2017**, *220*, 37–43. https://doi.org/10.1016/j.mseb.2017.03.010.

(7) Hudiono, Y. C.; Carlisle, T. K.; Bara, J. E.; Zhang, Y.; Gin, D. L.; Noble, R. D. A Three-Component Mixed-Matrix Membrane with Enhanced CO2 Separation Properties Based on Zeolites and Ionic Liquid Materials. *J Memb Sci* **2010**, *350* (1–2), 117–123. https://doi.org/10.1016/j.memsci.2009.12.018.

(8) Liu, X.; He, B.; Wang, Z.; Tang, H.; Su, T.; Wang, Q. Tough Nanocomposite Ionogel-Based Actuator Exhibits Robust Performance. *Sci Rep* **2014**, *4* (1), 6673. https://doi.org/10.1038/srep06673.

(9) Wu, F.; Chen, N.; Chen, R.; Zhu, Q.; Qian, J.; Li, L. "Liquid-in-Solid" and "Solid-in-Liquid" Electrolytes with High Rate Capacity and Long Cycling Life for Lithium-Ion Batteries. *Chemistry of Materials* **2016**, *28* (3), 848–856. https://doi.org/10.1021/acs.chemmater.5b04278.

(10) Verma, Y. L.; Singh, M. P.; Singh, R. K. Ionic Liquid Assisted Synthesis of Nano-Porous TiO2 and Studies on Confined Ionic Liquid. *Mater Lett* **2012**, *86*, 73–76. https://doi.org/10.1016/j.matlet.2012.07.025.

(11) Mahanta, U.; Choudhury, S.; Venkatesh, R. P.; SarojiniAmma, S.; Ilangovan, S. A.; Banerjee, T. Ionic-Liquid-Based Deep Eutectic Solvents as Novel Electrolytes for Supercapacitors: COSMO-SAC Predictions, Synthesis, and Characterization. *ACS Sustain Chem Eng* **2020**, *8* (1), 372–381. https://doi.org/10.1021/acssuschemeng.9b05596.

(12) Liu, Y.; Li, J.; Wang, M.; Li, Z.; Liu, H.; He, P.; Yang, X.; Li, J. Preparation and Properties of Nanostructure Anatase TiO $_2$ Monoliths Using 1-Butyl-3-Methylimidazolium Tetrafluoroborate Room-Temperature Ionic Liquids as Template Solvents. *Cryst Growth Des* **2005**, *5* (4), 1643–1649. https://doi.org/10.1021/cg050017z.

(13) Fernández, A.; Torrecilla, J. S.; García, J.; Rodríguez, F. Thermophysical Properties of 1-Ethyl-3-Methylimidazolium Ethylsulfate and 1-Butyl-3-Methylimidazolium Methylsulfate Ionic Liquids. *J Chem Eng Data* **2007**, *52* (5), 1979–1983. https://doi.org/10.1021/je7002786.

(14) Pilathottathil, S.; Thasneema, K. K.; Shahin Thayyil, M.; Pillai, M. P.; Niveditha, C. V. A High Voltage Supercapacitor Based on Ionic Liquid with an Activated Carbon Electrode. *Mater Res Express* **2017**, *4* (7), 075503. https://doi.org/10.1088/2053-1591/aa7116.

(15) Hamsan, M. H.; Aziz, S. B.; Kadir, M. F. Z.; Brza, M. A.; Karim, W. O. The Study of EDLC Device Fabricated from Plasticized Magnesium Ion Conducting Chitosan Based

Polymer Electrolyte. *Polym Test* **2020**, *90*, 106714. https://doi.org/10.1016/j.polymertesting.2020.106714.

(16) Chong, M. Y.; Numan, A.; Liew, C.-W.; Ng, H. M.; Ramesh, K.; Ramesh, S. Enhancing the Performance of Green Solid-State Electric Double-Layer Capacitor Incorporated with Fumed Silica Nanoparticles. *Journal of Physics and Chemistry of Solids* **2018**, *117*, 194–203. https://doi.org/10.1016/j.jpcs.2018.02.030.

(17) Miao, L.; Song, Z.; Zhu, D.; Li, L.; Gan, L.; Liu, M. Ionic Liquids for Supercapacitive Energy Storage: A Mini-Review. *Energy & Fuels* **2021**, *35* (10), 8443–8455. https://doi.org/10.1021/acs.energyfuels.1c00321.

(18) Shabeeba, P.; Thasneema, K. K.; Thayyil, M. S.; Pillai, M. P.; Niveditha, C. V. A Graphene-Based Flexible Supercapacitor Using Trihexyl(Tetradecyl)Phosphonium Bis(Trifluoromethanesulfonyl)Imide Ionic Liquid Electrolyte. *Mater Res Express* **2017**, *4* (8), 085501. https://doi.org/10.1088/2053-1591/aa7b14.

(19) Kavanagh, A.; Copperwhite, R.; Oubaha, M.; Owens, J.; McDonagh, C.; Diamond, D.; Byrne, R. Photo-Patternable Hybrid Ionogels for Electrochromic Applications. *J Mater Chem* **2011**, *21* (24), 8687. https://doi.org/10.1039/c1jm10704f.

(20) López Zavala, M. Á.; González Peña, O. I.; Cabral Ruelas, H.; Delgado Mena, C.; Guizani, M. Use of Cyclic Voltammetry to Describe the Electrochemical Behavior of a Dual-Chamber Microbial Fuel Cell. *Energies (Basel)* **2019**, *12* (18), 3532. https://doi.org/10.3390/en12183532.

(21) Espinoza, E. M.; Clark, J. A.; Soliman, J.; Derr, J. B.; Morales, M.; Vullev, V. I. Practical Aspects of Cyclic Voltammetry: How to Estimate Reduction Potentials When Irreversibility Prevails. *J Electrochem Soc* **2019**, *166* (5), H3175–H3187. https://doi.org/10.1149/2.0241905jes.

(22) Khomenko, V.; Raymundo-Piñero, E.; Béguin, F. A New Type of High Energy Asymmetric Capacitor with Nanoporous Carbon Electrodes in Aqueous Electrolyte. *J Power Sources* **2010**, *195* (13), 4234–4241. https://doi.org/10.1016/j.jpowsour.2010.01.006.

(23) Stoller, M. D.; Ruoff, R. S. Best Practice Methods for Determining an Electrode Material's Performance for Ultracapacitors. *Energy Environ Sci* **2010**, *3* (9), 1294. https://doi.org/10.1039/c0ee00074d.

(24) Pan, S.; Yao, M.; Zhang, J.; Li, B.; Xing, C.; Song, X.; Su, P.; Zhang, H. Recognition of Ionic Liquids as High-Voltage Electrolytes for Supercapacitors. *Front Chem* **2020**, *8*. https://doi.org/10.3389/fchem.2020.00261.

(25) Liu, X.; Taiwo, O. O.; Yin, C.; Ouyang, M.; Chowdhury, R.; Wang, B.; Wang, H.; Wu, B.; Brandon, N. P.; Wang, Q.; Cooper, S. J. Aligned Ionogel Electrolytes for High-Temperature Supercapacitors. *Advanced Science* **2019**, *6* (5). https://doi.org/10.1002/advs.201801337.

(26) Liu, X.; Wang, B.; Jin, Z.; Wang, H.; Wang, Q. Elastic Ionogels with Freeze-Aligned Pores Exhibit Enhanced Electrochemical Performances as Anisotropic Electrolytes of All-Solid-State Supercapacitors. *J Mater Chem A Mater* **2015**, *3* (30), 15408–15412. https://doi.org/10.1039/C5TA03184B.

(27) Liu, X.; Wu, B.; Brandon, N.; Wang, Q. Tough Ionogel-in-Mask Hybrid Gel Electrolytes in Supercapacitors with Durable Pressure and Thermal Tolerances. *Energy Technology* **2017**, *5* (2), 220–224. https://doi.org/10.1002/ente.201600251.

(28) Joos, B.; Vranken, T.; Marchal, W.; Safari, M.; Van Bael, M. K.; Hardy, A. T. Eutectogels: A New Class of Solid Composite Electrolytes for Li/Li-Ion Batteries.

Chemistry of Materials **2018**, *30* (3), 655–662. https://doi.org/10.1021/acs.chemmater.7b03736.

(29) Ren, J.; Li, J.; Lv, L.; Wang, J. Regeneration of [Bmim]BF4 Ionic Liquid by Ozonation: Hydrogen Bond Roles, Synergistic Effect, and DFT Calculation. *Environmental Science and Pollution Research* **2021**, *28* (10), 12909–12917. https://doi.org/10.1007/s11356-020-11298-7.

(30) Andrew, C.; Murugesan, C.; Jayakumar, M. Electrochemical Behavior of Sm(III) and Electrodeposition of Samarium from 1-Butyl-1-Methylpyrrolidinium Dicyanamide Ionic Liquid. *J Electrochem Soc* **2022**, *169* (2), 022503. https://doi.org/10.1149/1945-7111/ac4f76.

(31) González, R.; Battez, A. H.; Viesca, J. L.; Higuera-Garrido, A.; Fernández-González, A. Lubrication of DLC Coatings with Two Tris(Pentafluoroethyl)Trifluorophosphate Anion-Based Ionic Liquids. *Tribology Transactions* **2013**, *56* (5), 887–895. https://doi.org/10.1080/10402004.2013.810319.

(32) Markiewicz, R.; Klimaszyk, A.; Jarek, M.; Taube, M.; Florczak, P.; Kempka, M.; Fojud, Z.; Jurga, S. Influence of Alkyl Chain Length on Thermal Properties, Structure, and Self-Diffusion Coefficients of Alkyltriethylammonium-Based Ionic Liquids. *Int J Mol Sci* **2021**, *22* (11), 5935. https://doi.org/10.3390/ijms22115935.

(33) Kim, D.; Kannan, P. K.; Chung, C. High-Performance Flexible Supercapacitors Based on Ionogel Electrolyte with an Enhanced Ionic Conductivity. *ChemistrySelect* **2018**, *3* (7), 2190–2195. https://doi.org/10.1002/slct.201702711.

(34) Mao, J. X.; Damodaran, K. Spectroscopic and Computational Analysis of the Molecular Interactions in the Ionic Liquid [Emim]+[FAP]−. *Ionics (Kiel)* **2015**, *21* (6), 1605–1613. https://doi.org/10.1007/s11581-014-1341-7.

(35) Ullah, Z.; azmi Bustam, M.; Sada Khan, A.; Azmi Bustam, M.; Man, Z. Phosphonium-Based Ionic Liquids and Their Application in Separation of Dye from Aqueous Solution. **2016**, *11* (3).

(36) King, A. W. T.; Parviainen, A.; Karhunen, P.; Matikainen, J.; Hauru, L. K. J.; Sixta, H.; Kilpeläinen, I. Relative and Inherent Reactivities of Imidazolium-Based Ionic Liquids: The Implications for Lignocellulose Processing Applications. *RSC Adv* **2012**, *2* (21), 8020. https://doi.org/10.1039/c2ra21287k.

(37) Cao, Y.; Mu, T. Comprehensive Investigation on the Thermal Stability of 66 Ionic Liquids by Thermogravimetric Analysis. *Ind Eng Chem Res* **2014**, *53* (20), 8651–8664. https://doi.org/10.1021/ie5009597.

(38) Xue, Z.; Qin, L.; Jiang, J.; Mu, T.; Gao, G. Thermal, Electrochemical and Radiolytic Stabilities of Ionic Liquids. *Physical Chemistry Chemical Physics* **2018**, *20* (13), 8382–8402. https://doi.org/10.1039/C7CP07483B.

(39) Agafonov, A. V.; Kudryakova, N. O.; Ramenskaya, L. M.; Grishina, E. P. The Confinement and Anion Type Effect on the Physicochemical Properties of Ionic Liquid/Halloysite Nanoclay Ionogels. *Arabian Journal of Chemistry* **2020**, *13* (12), 9090–9104. https://doi.org/10.1016/j.arabjc.2020.10.033.

(40) Salgado, J.; Parajó, J. J.; Fernández, J.; Villanueva, M. Long-Term Thermal Stability of Some 1-Butyl-1-Methylpyrrolidinium Ionic Liquids. *J Chem Thermodyn* **2014**, *74*, 51–57. https://doi.org/10.1016/j.jct.2014.03.030.

(41) Visentin, A. F.; Alimena, S.; Panzer, M. J. Influence of Ionic Liquid Selection on the Properties of Poly(Ethylene Glycol) Diacrylate-Supported Ionogels as Solid Electrolytes. *ChemElectroChem* **2014**, *1* (4), 718–721. https://doi.org/10.1002/celc.201300205.

(42) Silvester, D. S.; Jamil, R.; Doblinger, S.; Zhang, Y.; Atkin, R.; Li, H. Electrical Double Layer Structure in Ionic Liquids and Its Importance for Supercapacitor, Battery, Sensing, and Lubrication Applications. *The Journal of Physical Chemistry C* **2021**, *125* (25), 13707–13720. https://doi.org/10.1021/acs.jpcc.1c03253.

(43) Nazet, A.; Sokolov, S.; Sonnleitner, T.; Makino, T.; Kanakubo, M.; Buchner, R. Densities, Viscosities, and Conductivities of the Imidazolium Ionic Liquids [Emim][Ac], [Emim][FAP], [Bmim][BETI], [Bmim][FSI], [Hmim][TFSI], and [Omim][TFSI]. *J Chem Eng Data* **2015**, *60* (8), 2400–2411. https://doi.org/10.1021/acs.jced.5b00285.

(44) Asbani, B.; Douard, C.; Brousse, T.; Le Bideau, J. High Temperature Solid-State Supercapacitor Designed with Ionogel Electrolyte. *Energy Storage Mater* **2019**, *21*, 439–445. https://doi.org/10.1016/j.ensm.2019.06.004.

(45) Rana, H. H.; Park, J. H.; Ducrot, E.; Park, H.; Kota, M.; Han, T. H.; Lee, J. Y.; Kim, J.; Kim, J.-H.; Howlett, P.; Forsyth, M.; MacFarlane, D.; Park, H. S. Extreme Properties of Double Networked Ionogel Electrolytes for Flexible and Durable Energy Storage Devices. *Energy Storage Mater* **2019**, *19*, 197–205. https://doi.org/10.1016/j.ensm.2018.11.008.

(46) Xiong, G.; Kundu, A.; Fisher, T. S. Influence of Temperature on Supercapacitor Performance; 2015; pp 71–114. https://doi.org/10.1007/978-3-319-20242-6_4.

(47) Ortega, P. F. R.; Trigueiro, J. P. C.; Silva, G. G.; Lavall, R. L. Improving Supercapacitor Capacitance by Using a Novel Gel Nanocomposite Polymer Electrolyte Based on Nanostructured SiO2, PVDF and Imidazolium Ionic Liquid. *Electrochim Acta* **2016**, *188*, 809–817. https://doi.org/10.1016/j.electacta.2015.12.056.

(48) Egashira, M.; Okada, S.; Yamaki, J.; Dri, D. A.; Bonadies, F.; Scrosati, B. The Preparation of Quaternary Ammonium-Based Ionic Liquid Containing a Cyano Group and Its Properties in a Lithium Battery Electrolyte. *J Power Sources* **2004**, *138* (1–2), 240–244. https://doi.org/10.1016/j.jpowsour.2004.06.022.

(49) Egashira, M.; Okada, S.; Yamaki, J.; Yoshimoto, N.; Morita, M. Effect of Small Cation Addition on the Conductivity of Quaternary Ammonium Ionic Liquids. *Electrochim Acta* **2005**, *50* (18), 3708–3712. https://doi.org/10.1016/j.electacta.2005.01.016.

(50) Brachet, M.; Brousse, T.; Le Bideau, J. All Solid-State Symmetrical Activated Carbon Electrochemical Double Layer Capacitors Designed with Ionogel Electrolyte. *ECS Electrochemistry Letters* **2014**, *3* (11), A112–A115. https://doi.org/10.1149/2.0051411eel.

(51) Wu, Y.; Deng, Y.; Zhang, K.; Qiu, J.; Wu, J.; Yan, L. Ultrahigh Conductive and Stretchable Eutectogel Electrolyte for High-Voltage Flexible Antifreeze Quasi-Solid-State Zinc-Ion Hybrid Supercapacitor. *ACS Appl Energy Mater* **2022**, *5* (3), 3013–3021. https://doi.org/10.1021/acsaem.1c03654.

Chapter 4

TiO_2- and SiO_2-Mediated Natural-Deep-Eutectic-Solvent-Based Inorganic Eutectogels

CHAPTER 4

TiO_2- and SiO_2-Mediated Natural-Deep-Eutectic-Solvent-Based Inorganic Eutectogels

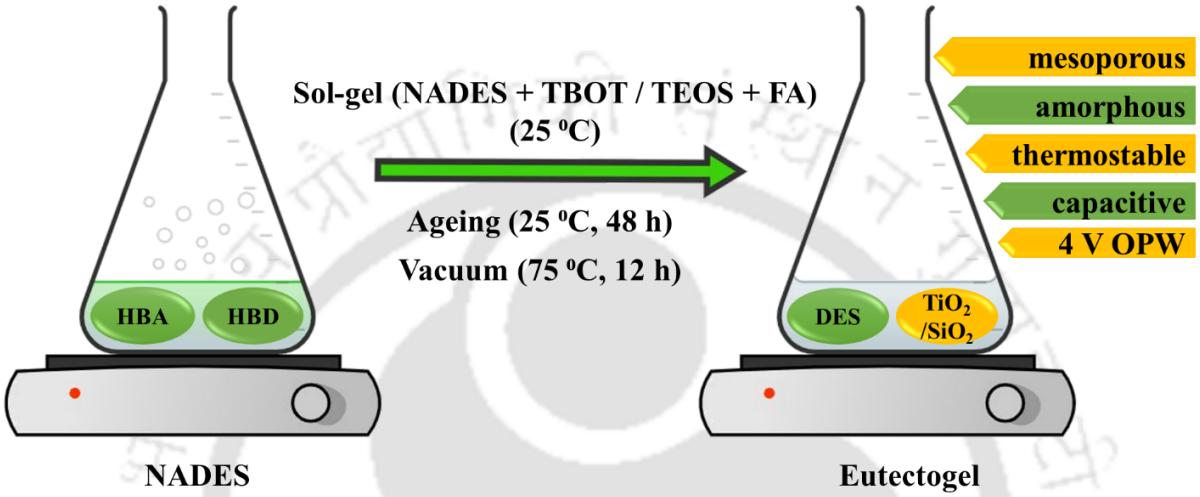

List of publications from Chapter 4:

(1) **Dutta, A.**; Kundu, D.; Sharma, S.; Paul, N.; Naik, P. K.; Silvester, D. S.; Banerjee, T. Physically Cross-Linked Titania-Supported Novel Eutectogels as Solid-State Electrolytes: An Experimental and Quantum Chemical Investigation. *ACS Sustain Chem Eng* **2023**, *12* (1), 248–262. https://doi.org/10.1021/acssuschemeng.3c05551

(2) **Dutta, A.**; Kundu, D.; Naik, P. K.; Silvester, D. S.; Banerjee, T. Synthesis and Properties of Physically Cross-Linked Silica-Mediated Novel Eutectogels Developed from Carboxylic-Acid-Based Natural Deep Eutectic Solvents. (*Communicated*)

(3) **Dutta A.**; Kundu D.; Sharma S.; Silvester D. S.; Banerjee T. Investigating the Electrochemical Properties of Ionic-Liquid-Mediated Inorganic Eutectogels Derived from Carboxylic-Acid-Based Hydrophobic Deep Eutectic Solvents. (*Communicated*)

4.1. Introduction

The seven TiO_2-confined inorganic ionogel electrolytes discussed in Chapter 3 of this thesis showed properties that may be decently favorable for applications in supercapacitors and the broader electrochemical domain. Nevertheless, the production and extensive use of ILs can be complex and cost-intensive,[1] thrusting researchers to navigate alternative options that tame the potential to provide the best trade-off between cost and performance. In this context, this chapter focuses primarily on the morphological, structural, thermal, and electrochemical properties of eight novel inorganic eutectogels derived by confining each of the four benign NADESs, *viz.* DES1: decanoic acid + DL-Menthol, DES2: lauric acid + DL-Menthol, DES3: myristic acid + DL-Menthol, and DES4: palmitic acid + DL-Menthol into an inorganic matrix of TiO_2 (TEGels 1–4) or SiO_2 (SEGels 1–4). The matrices were obtained respectively from a TBOT or TEOS precursor through the sol-gel approach of synthesis as detailed in Chapter 2 of this thesis. The processes employed in the preparation of both the DESs and the eutectogels were fast and simple. The eutectogels, thus obtained were characterized using FESEM, FETEM, FTIR spectroscopy, Raman spectroscopy, XRD, TGA, and DSC. Furthermore, to verify their practicality as electrolytes in supercapacitor-based applications, electrochemical tests were also performed on the as-obtained eutectogels through CV and EIS. To the best of our knowledge, the sol-gel-derived TiO_2- and SiO_2-tethered NADES gels reported herein are the first of their kind.

4.2. Results and Discussion on TEGels

4.2.1. Morphological Analysis

Morphological studies were conducted on the TEGels 1–4 using FESEM and FETEM. The images of the eutectogels obtained from FESEM confirmed that the TiO_2 particles were uniformly crosslinked with the DES frameworks (**Figure 4.1**a−d). The inorganic gel samples

exhibited the presence of cluster-like assembly of small agglomerated titania moieties incrusted on the surface of the DESs via a self-assembly mechanism through in-situ gelation, rendering a solid characteristic to the immobilized DESs.

FETEM image of TEGel4 (**Figure 4.1**e) revealed interconnected aggregates of inorganic TiO_2 particles, leading to a porous structure of the gel.[2] These aggregates provide 3D, nanostructured, continuous channels, enabling transportation of ions. The continuous channels evince that the DES is enfolded into them through gelation. Given that all four DESs belong to the same long-chain carboxylic fatty acid group and share similar inherent characteristics, it can be anticipated that TEGels 1–3 possess comparable porosity and 3D nanostructured channels. The similar nature of the DESs suggests that their corresponding eutectogels would exhibit analogous morphological features and structural characteristics.

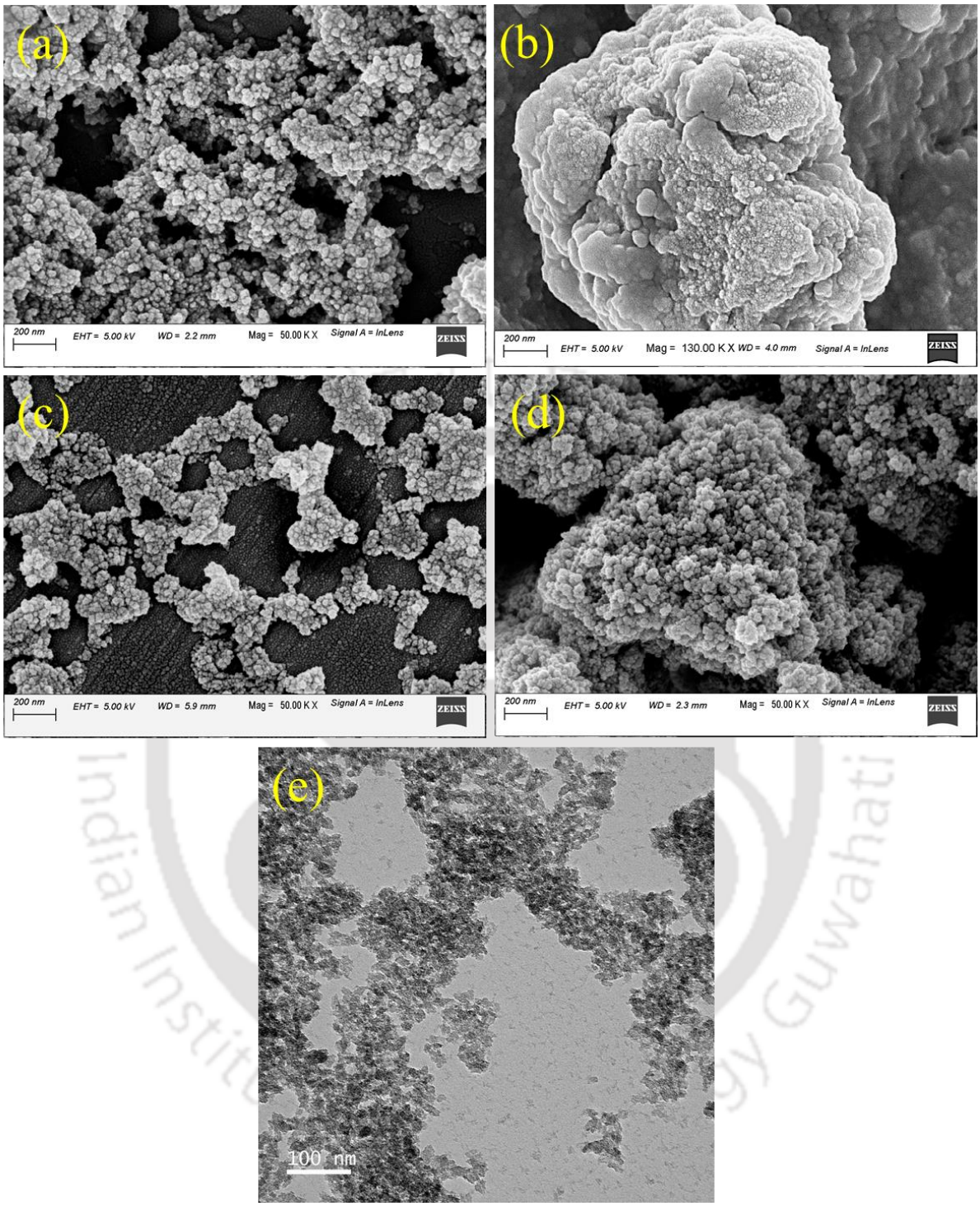

Figure 4.1. FESEM images of (a) TEGel1, (b) TEGel2, (c) TEGel3, (d) TEGel4, and (e) FETEM image of TEGel4.

4.2.2. Structural Analysis

The impact of immobilization of the DESs into a porous matrix on their structure was observed by performing FTIR on DESs 1–4 and TEGels 1–4. As it is seen from **Figure 4.2**a−d, the FTIR spectra of the DESs are very similar to those of their corresponding eutectogels. The peaks at ~2920 cm^{-1} for the DESs or ~2925 cm^{-1} for the eutectogels indicate the presence of O−H stretching. This is represented by a distinct characteristic band at about 2920 or 2925 cm^{-1} with shoulders around 2936, 2862, and 2852 cm^{-1}. The vibrational bands at ~1711 or ~1727 cm^{-1}, ~1456 or ~1490 cm^{-1}, ~1369 or ~1361 cm^{-1}, and ~1180 or ~1179 cm^{-1} of the DES or eutectogel spectra respectively, represent C=O stretching, C−H bending, O–H bending, and C−O stretching, respectively. The broad band at ~3350 cm^{-1} in the standalone DESs may be assigned to the potential stretching vibration of moisture adsorbed by the systems during storage and handling.[2] The distinct strong bands at 1539 cm^{-1} on the spectra of the eutectogels are associated to the stretching vibrations of Ti−O−Ti.[3] However, the titania content in the eutectogels is limited, resulting in a domination of the DES vibrations. Nonetheless, the absorption bands between 1800 and 1100 cm^{-1} of the eutectogels are stronger in intensity than those of the pure DESs owing to the superposition with the strongly absorbing vibrations of the TiO_2 framework within this region of the spectra.[2]

No new absorption peaks otherwise are present in the spectra of the eutectogels. This indicates towards the fact that TiO_2 and the DESs are not bonded chemically. Thus, it can be inferred that the immobilization of the DES into the crosslinking matrix does not affect the characteristics of the DES substantially. In other words, the components of the DESs primarily behave as a template for the development of the titania matrix. In addition, the similarity in the two spectra indicate that the DESs are completely interconnected within the TiO_2 framework.[4] Nonetheless, the vibrational bands of the eutectogels have been observed to shift marginally from their original positions in the spectrum of the corresponding DES (**Table 4.1**). This proves

the potential existence of weak non-bonded interaction between the DES molecules and the titanium moieties. The existence of such non-bonded interactions can lead to possible changes in the thermal characteristics of the immobilized solvent.[5]

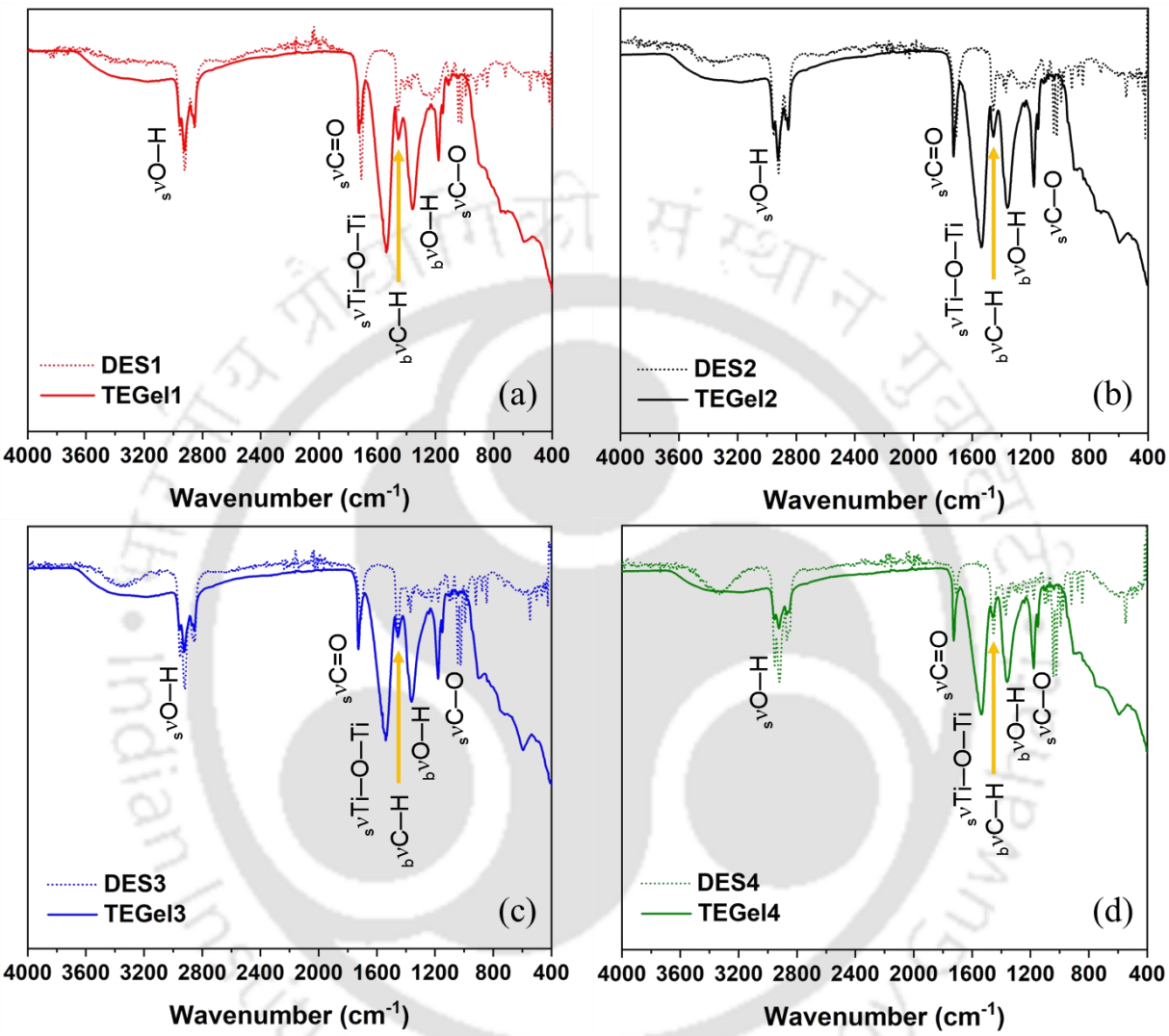

Figure 4.2. FTIR graphs of (a) DES1 and TEGel1, (b) DES2 and TEGel2, (c) DES3 and TEGel3, and (d) DES4 and TEGel4.

Table 4.1. Vibrational bands of DESs 1−4 and TEGels 1−4 with their respective assignments

Assignment	System							
	Vibrational band (cm^{-1})							
	DES1	**TEGel1**	**DES2**	**TEGel2**	**DES3**	**TEGel3**	**DES4**	**TEGel4**
$_s\nu$O−H	2920	2924	2920	2925	2920	2925	2922	2925
$_s\nu$C=O	1709	1727	1711	1727	1711	1727	1711	1726
$_s\nu$Ti−O−Ti	–	1539	–	1539	–	1539	–	1539
$_b\nu$C−H	1456	1456	1456	1495	1456	1493	1454	1490
$_b\nu$O−H	1369	1361	1369	1361	1369	1362	1369	1365
$_s\nu$C−O	1180	1180	1180	1179	1180	1179	1179	1178

$_s\nu$: stretching, $_b\nu$: bending

XRD measurements were performed on TEGels 1–4 to assess the degree of crystallinity of the samples. Conforming to findings reported previously,[4–7] the inorganic eutectogels also demonstrated the presence of a typical amorphous TiO_2 matrix in co-existence with the DESs. The XRD patterns of the eutectogels depicted in **Figure 4.3** is observed to consist of frail and broad peaks, revealing the amorphous or low crystalline nature of the samples within the given range of 2θ. The introduction of DES interferes with the consistent arrangement of the TiO_2 matrix and leads to an increase in the amorphous area.

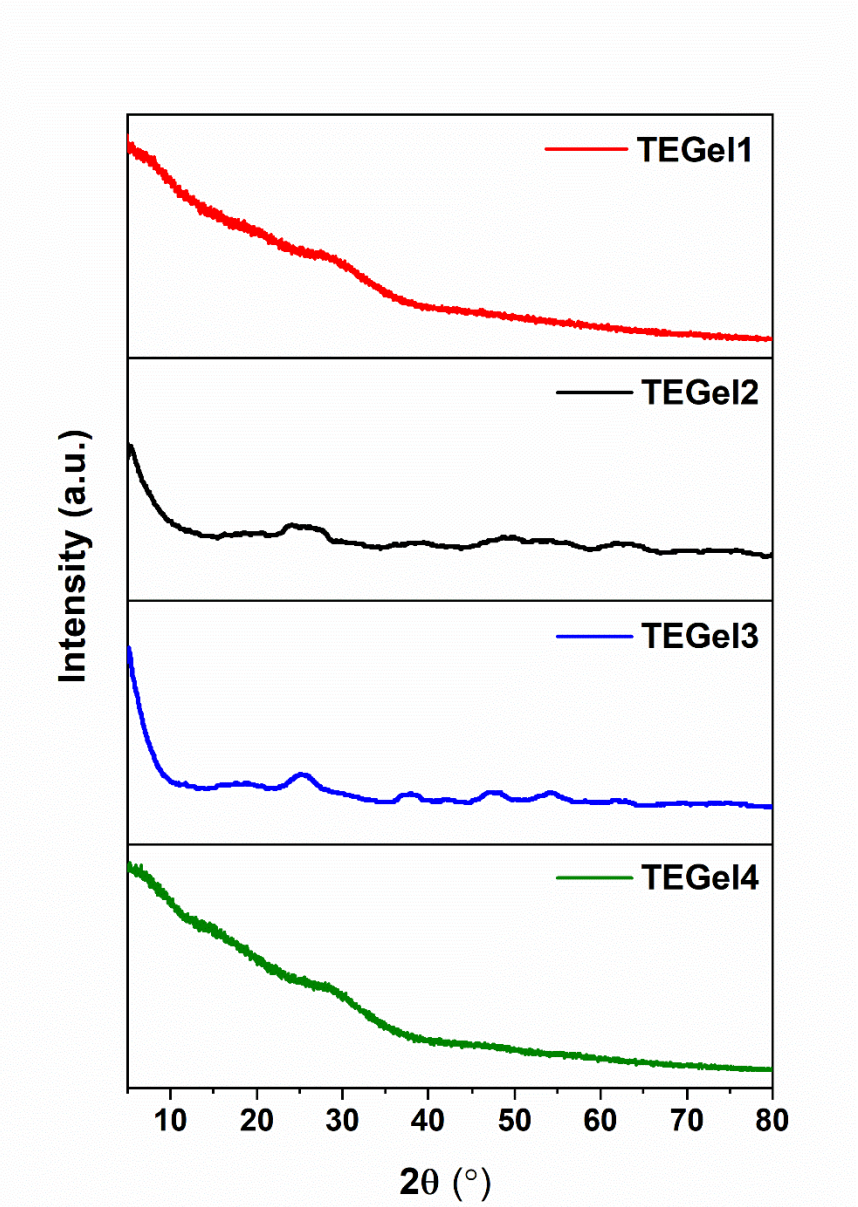

Figure 4.3. XRD patterns of TEGels 1–4.

4.2.3. Thermal Analysis

Thermal analyses of the DESs and TEGels were carried out on a TG 209 F1 Libra (Make: M/s Netzsch, Germany) under a nitrogen atmosphere between temperatures 25 and 600 °C at a rate of 10 °C min^{-1} with a nitrogen flow of 40 mL min^{-1}. **Figure 4.4**a shows the TGA thermograms of DESs 1–4 and the TEGels 1–4. **Table 4.2** shows that the temperature ($T_{5\%}$) at which the eutectogel loses less than 5 % of its initial mass is lower than that of its parent DES.

Nonetheless, exposure time plays an important role in the examination of degradation kinetics and thermal degradation. For instance, isothermal TGA conducted on TEGel4 (**Figure 4.4**b) at 80 and 90 °C for 12 h (heating rate 20 °C min^{-1}) shows rapid degradation up to about 60 min and 35 min, respectively. The mass loss attains constancy after ~1.5 h. Approximately, 32 % and 39 % of mass is lost in the form of volatile products at 80 °C and 90 °C, respectively.[8] Similarly, the remaining three TEGels (1–3) are also expected to exhibit a similar pattern of decomposition under isothermal conditions. The isothermal TGA was conducted under nitrogen atmosphere.

Evidently, there are three primary stages of mass loss in the TGA profiles of the eutectogels, which may be attributed to the evaporation or degradation of three distinct substances.[9] The first platform of mass loss between 25 and 154 °C should be on account of the evaporation of residual impurities and/or water adsorbed physically.[5] The second steep decline in mass between 191 and 263 °C occurs potentially due to the decomposition of DL-Menthol from the DESs. The third one starting from ~321 °C for TEGels 1–3 and from ~388 °C for TEGel4 up to ~468 °C may be attributed to the degradation of the HBDs. Lastly, the straight lines at the end of the thermograms suggest the complete decomposition of the organic components, with only the inorganic parts remaining (35.6–40 wt%). The DSC thermograms of the four eutectogels (inset of **Figure 4.4**a) are characterized by an endothermic peak followed by an exothermic peak at ~240 °C and a sharp endothermic peak at ~440 °C, both coinciding respectively with the decomposition temperatures of DL-Menthol and the acids as per TGA. The small bump at ~38 °C of each profile may represent the glass-transition temperature (T_g) of the gel, while the broad exothermic peak around 105 °C may be due to the loss of moisture and/or volatile impurities.[5,10] On the other hand, TGA profiles of the DESs evince two distinct steps of decomposition which results from the degradation of DL-Menthol and the acids respectively, with a small amount of mass lost below ~100 °C due to the

vaporization of adsorbed moisture, before degrading off completely. Introduction of the inorganic TiO_2 results in a decrease in the content of volatile phase of the DESs.

Interestingly, the organic components of the eutectogels undergo complete degradation at temperatures (T_{cd}) that are higher than the temperatures (T_{cd}) at which their corresponding DESs decompose completely (**Table 4.2**). This suggests strong confinement of the DESs within the titania framework.[2] The decomposition temperatures of the individual components of the DESs are tabulated in **Table 4.3**. From **Figure 4.4**a it is observed that the degradation temperature of the DES differs from that of its individual components. This is on account of inter-molecular interactions between the two components of the DES. The decomposition pattern of the DES is further altered, and the degradation temperatures shifted on its confinement into TiO_2.[11–14] This, again, indicates the existence of weak non-bonded interactions between the DES molecules and the titanium moieties.[5]

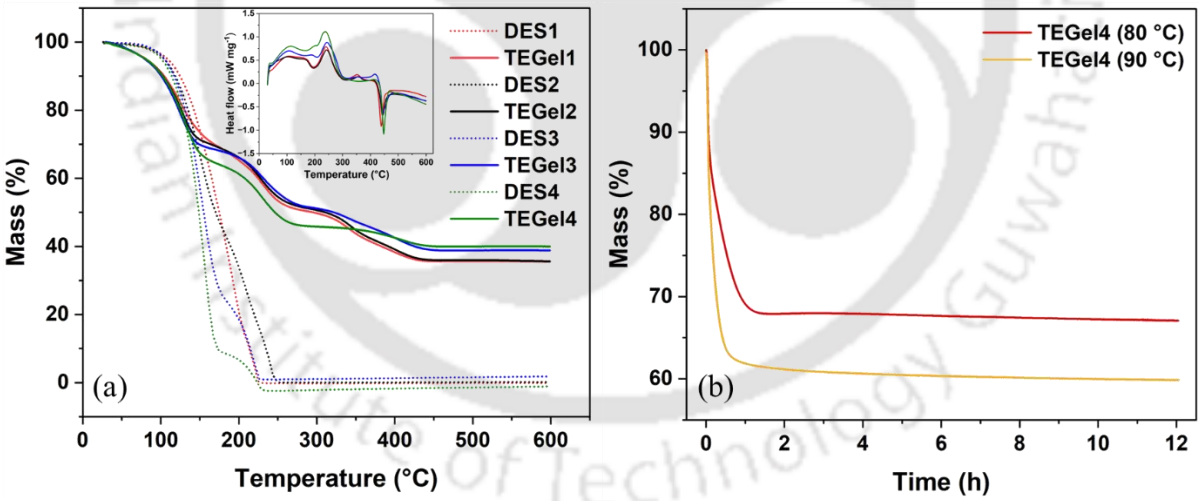

Figure 4.4. (a) TGA thermograms of DESs 1–4 and TEGels 1–4 (inset: DSC profiles of TEGels 1–4), and (b) Isothermal TGA thermograms of TEGel4 at 80 °C and 90 °C.

Table 4.2. $T_{5\%}$ and T_{cd} of DESs 1–4 and TEGels 1–4

DES / TEGel	$T_{5\%}$ (°C)	T_{cd} (°C)
DES1	111	231
TEGel1	81.3	458
DES2	105	249.9
TEGel2	80.3	458
DES3	106	232.4
TEGel3	79.8	468.7
DES4	101.2	227.2
TEGel4	80.8	467.7

Table 4.3. Decomposition temperatures of the individual components of DESs 1–4

Component	Decomposition temperature (°C)
DL-Menthol	168.95[15]
Decanoic acid	230[16]
Lauric acid	292.34[15]
Myristic acid	236[17]
Palmitic acid	257[18]

4.2.4. Electrochemical Performance

4.2.4.1. Cyclic Voltammetry

Figure 4.5a–d represents the cyclic voltammograms of TEGels 1–4 obtained at room temperature with the rGO-based two-electrode cell on a Nova 1.11.2-interfaced PGSTAT101 Autolab potentiostat (Eco, Chemie, Netherlands) at a scan rate of 10 mV s^{-1}. At higher scan rates, the ions of the electrolyte are deprived of adequate time to be able to penetrate deeper into the inner side of the electrode material which results in lower charge accumulation

(electrolyte starvation effect). The CV profiles demonstrate a quasi-rectangular shape which hints towards a capacitive behavior of the systems.[19,20] Furthermore, the absence of any redox peaks suggests that the TEGel-based systems store charge through the non-Faradaic route or by the formation of an electric double layer at the electrolyte/electrode interface.[19–21]

A fairly narrow current density is obtained for each system over the voltage window it is tested for. This could possibly be due to low self-diffusivity on account of DES/TiO_2 interactions[22] and the absence of an ideal polarizable reference electrode.[23] The relatively narrow area under the curves suggests that the eutectogels have a low specific capacitance and that the systems are intrinsically resistive in nature. The reason behind this could be attributed to the fact that the gelated systems are apparently more viscous and the NADESs involved in the synthesis of the eutectogels do not exhibit polar behavior, thus inhibiting the possession of excellent electrochemical characteristics as compared to those of ILs. Particularly in case of TEGels 3 and 4, the existence of bulkier groups in the DESs induce steric hindrance which act as a resistance to charge transfer and ionic movement. The higher room-temperature viscosities of the respective DESs (**Figure B1**, **Table B1**) substantiate the same. Consequently, the systems involving TEGels 1 and 2 are seen to manifest a comparatively higher area under their voltammetry curves (**Figure 4.5**e) because of the absence of relative bulky molecular groups and high viscosity of their corresponding DESs (**Figure B1**, **Table B1**). This supposition was confirmed from the low values of specific capacitance delivered by the eutectogels (**Table 4.4**). While the systems based on TEGels 3 and 4 exhibited specific capacitance of 2.7 μF g^{-1} (0.4 μF cm^{-2}) and 2.1 μF g^{-1} (0.4 μF cm^{-2}) at 10 mV s^{-1}, the ones with TEGels 1 and 2 showed slightly higher values of 15 μF g^{-1} (2.9 μF cm^{-2}) and 18.7 μF g^{-1} (3.6 μF cm^{-2}), respectively.

However, all four eutectogels have an exceptional OPW of about 4 V, which is comparable to that of ILs[24] and the ionogels discussed in Chapter 3 of this thesis, and higher than that of the IL-based DESs composed of NMAc and EG as HBDs and the IL

[BMIM][$MeSO_3$] as the HBA, reported previously.[21] Moreover, on comparing the OPW with that of eutectogels reported in pertinent works, the TEGels presented herein showed the highest potential window among all (**Table 4.5**). Water plays a vital role in the determination of the electrochemical stability of a DES in a way where a higher water content results in a narrower potential window.[21] The wide OPW in the TEGels 1–4 may be attributed to the hydrophobic characteristic of the components of their parent DESs. This was confirmed by the low water content (< 1 wt%) in the DESs, as obtained from Karl Fischer titration (**Table B1**). Furthermore, ^{1}H NMR spectra of the DES samples (**Figure B2**a–d) indicate the absence of water, even after repeated washing. Also, the contact angle of DES3 measured against water yielded an angle of 95.7° (**Figure B3**), further validating the hydrophobic nature of this particular class of DESs.[25,26] Based on their specific capacitance and OPW, the device supported by TEGels 1–4 was able to store energy up to 33.4, 41.6, 6.0, and 4.8 μW h kg^{-1}, respectively.

Interestingly, with the incorporation of the IL [BMIM][BF_4], not only is the EDLC characteristic maintained in the window 4 V, but the area under the curves is also dramatically increased (**Figure 4.6**), leading to values of specific capacitance as high as 47.7 F g^{-1} (2087 mF cm^{-2}) (TEGel2), as tabulated in **Table 4.4**. TEGels 1, 3, and 4 followed suit with specific capacitance values of 35.9 (1569.9), 16.4 (718), and 16.2 F g^{-1} (710.1 mF cm^{-2}). Because of the exceptional potential window and decent specific capacitances, all the four hybrid gels are seen to deliver values of specific energy (79.8, 106, 36.5, and 36.1 W h kg^{-1}) that are comparable to those of other stand-alone eutectogels,[27–31] room-temperature ILs, and ionogels,[32] and higher than those of aqueous electrolytes.[33] Additionally, the current density is seen to have surged up for each system indicating considerable abatement of its internal resistance. This could be attributed to the fact that the presence of the polar IL in the systems enhances the process of

charge transfer and ion mobility by creating a conducting pathway, thus rendering the systems relatively more "ionic".

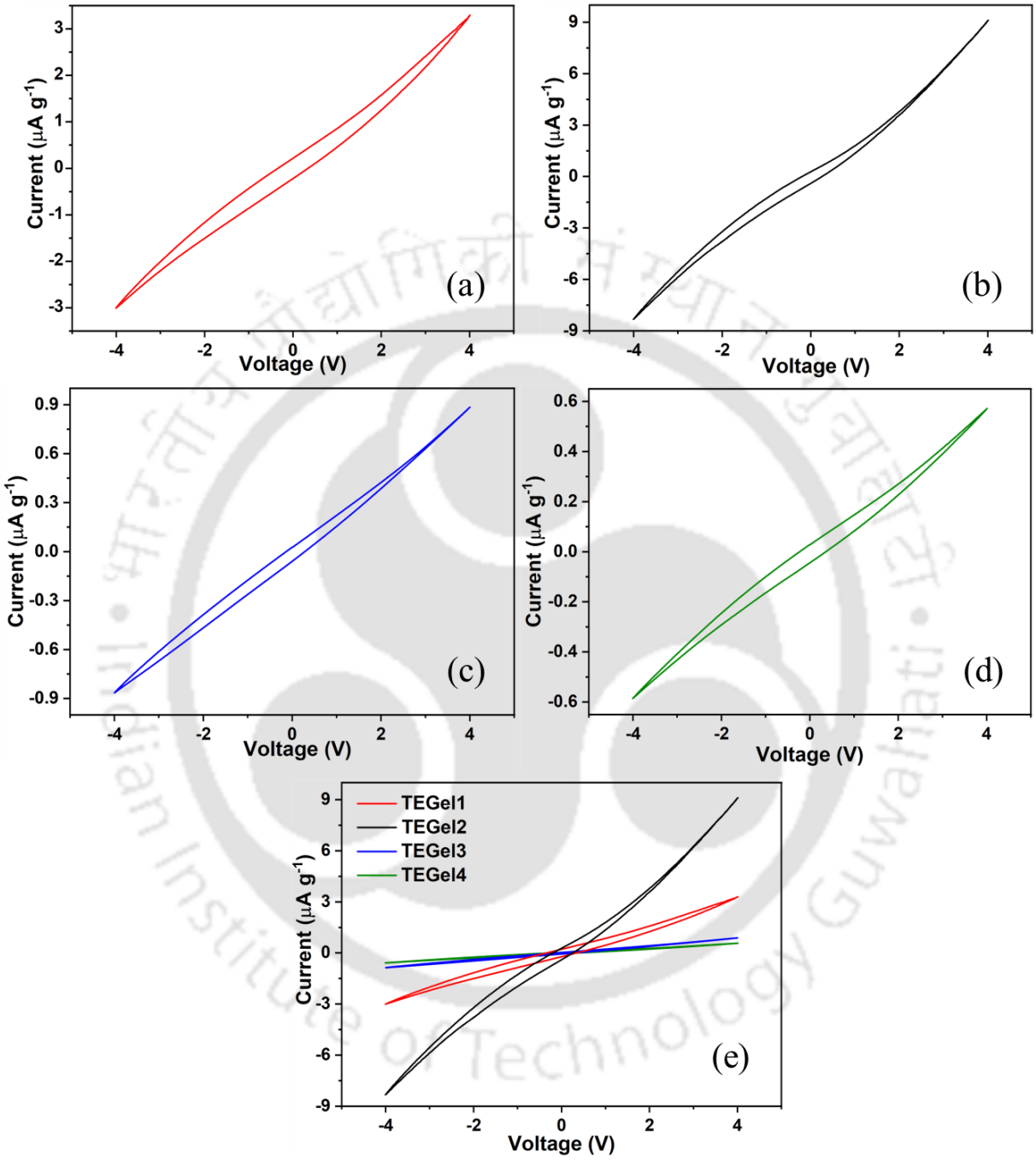

Figure 4.5. Cyclic voltammetry profiles of the systems conducted on the two-electrode coin-cell with rGO electrodes and (a) TEGel1, (b) TEGel2, (c) TEGel3, and (d) TEGel4 electrolytes at a scan rate of 10 mV s^{-1}. (e) Comparison of the voltammograms of all four systems on a single plot.

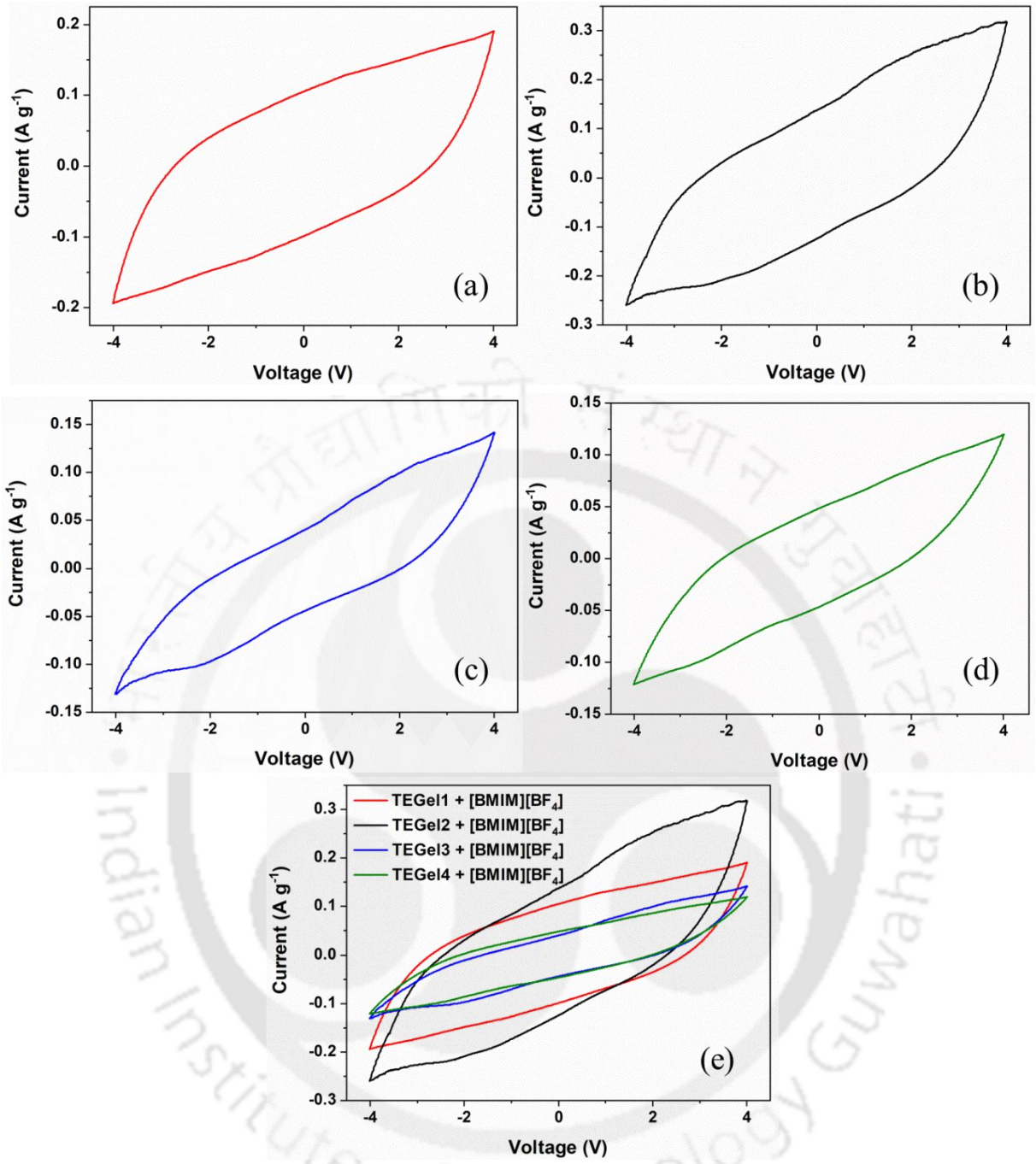

Figure 4.6. Cyclic voltammetry profiles of the systems at a scan rate of 10 mV s^{-1} conducted on the two-electrode coin-cell with rGO electrodes and (a) TEGel1, (b) TEGel2, (c) TEGel3, and (d) TEGel4 electrolytes after incorporation of the IL [BMIM][BF_4]. (e) Comparison of the voltammograms of all four systems on a single plot.

Table 4.4. Specific capacitance and specific energy of TEGels 2–7 (with and without [BMIM][BF_4]) at 10 mV s^{-1}

System	$C_{sp\text{-}10\ mV\ s^{-1}}$ (F g^{-1})	$C_{sp\text{-}10\ mV\ s^{-1}}$ (mF cm^{-2})	$E_{sp\text{-}10\ mV\ s^{-1}}$ (W h kg^{-1})
TEGel1	1.50×10^{-5}	2.87×10^{-3}	3.34×10^{-5}
TEGel2	1.87×10^{-5}	3.58×10^{-3}	4.16×10^{-5}
TEGel3	2.71×10^{-6}	5.17×10^{-4}	6.01×10^{-6}
TEGel4	2.15×10^{-6}	4.09×10^{-4}	4.77×10^{-6}
TEGel1 + [BMIM][BF_4]	35.89	1569.91	79.77
TEGel2 + [BMIM][BF_4]	47.72	2087.05	106.04
TEGel3 + [BMIM][BF_4]	16.42	718.04	36.48
TEGel4 + [BMIM][BF_4]	16.24	710.06	36.08

Table 4.5. OPW of TEGels 1–4 (with and without [BMIM][BF_4]) and SEGels 1–4 compared with that of eutectogels reported in similar works

Eutectogel components	Electrodes	Scan rate (mV s^{-1})	Temperature (^oC)	OPW (V)
Decanoic acid + DL-Menthol + TiO_2 / SiO_2 (TEGel1 / SEGel1)	rGO | rGO	10	~25	4
Lauric acid + DL-Menthol + TiO_2 / SiO_2 (TEGel2 / SEGel2)	rGO | rGO	10	~25	4
Myristic acid + DL-Menthol + TiO_2 / SiO_2 (TEGel3 / SEGel3)	rGO | rGO	10	~25	4
Palmitic acid + DL-Menthol + TiO_2 / SiO_2 (TEGel4 / SEGel4)	rGO | rGO	10	~25	4
TEGel1 + [BMIM][BF_4]	rGO | rGO	10	~25	4
TEGel2 + [BMIM][BF_4]	rGO | rGO	10	~25	4

Table 4.5 continues

Eutectogel components	Electrodes	Scan rate ($mV\ s^{-1}$)	Temperature (^oC)	OPW (V)
TEGel3 + $[BMIM][BF_4]$	rGO | rGO	10	~25	4
TEGel4 + $[BMIM][BF_4]$	rGO | rGO	10	~25	4
ChCl + EG + HEMA + PEGDA[27]	Indium Tin Oxide (ITO) | ITO	1	~25	1.5
ChCl + urea + glycerol + cellulose + PAAM[28]	AC | AC	5, 10, 20, 50, 100	~25	2
EG + urea + ChCl +$ZnCl_2$ + silk fiber[31]	Zn | AC	1, 10, 20, 50	~25	1.4
$Zn(ClO_4)_2$ + AM + H_2O[29]	Zn | N-rGO	5, 10, 20, 30, 50, 100	~25	2.2
EG + $Zn(ClO_4)_2$ + H_2O +SPEEK + PAAM[30]	Zn | AC	5, 10, 20, 50, 100	~25	1.7

4.2.4.2. Electrochemical Impedance Spectroscopy

EIS was performed on TEGels 1–4 in the frequency window of 0.1 Hz to 100 kHz to assess the resistive and/or capacitive behavior of the systems. The experiments were conducted in the rGO-based two-electrode coin cell at room temperature on a Nova 1.11.2-interfaced PGSTAT101 Autolab potentiostat (Eco, Chemie, Netherlands). **Figure 4.7** shows the Nyquist plots for the eutectogel samples. R_s, R_{ct}, and ESR of each eutectogel sample were determined from its corresponding Nyquist plot (**Table 4.6**). The ionic conductivities of the samples were calculated using **equation 2.15** (t ~ 0.2 cm, A ~ 0.78 cm^2) while power delivered by the device was computed using **equation 1.2** (**Table 4.6**).

Table 4.6. Solution resistance, charge-transfer resistance, equivalent series resistance, ionic conductivity, and power associated with TEGels 1–4 (with and without [BMIM][BF_4])

System	R_s (Ω)	R_{ct} (Ω)	ESR (Ω)	σ (mS cm^{-1})	P (kW kg^{-1})
TEGel1	1.44×10^4	1.2×10^7	1.2×10^7	1.77×10^{-2}	8.67×10^{-6}
TEGel2	8.18×10^3	1.6×10^6	1.6×10^6	3.11×10^{-2}	6.54×10^{-5}
TEGel3	2.34×10^4	1.8×10^7	1.8×10^7	1.09×10^{-2}	6.08×10^{-6}
TEGel4	3.02×10^4	2.7×10^7	2.7×10^7	8.43×10^{-3}	3.93×10^{-6}
TEGel1 + [BMIM][BF_4]	16.05	61.92	85.97	15.87	2.71
TEGel2 + [BMIM][BF_4]	15.64	51.35	66.99	16.28	3.48
TEGel3 + [BMIM][BF_4]	17.47	107.47	124.94	14.58	1.86
TEGel4 + [BMIM][BF_4]	17.52	118.4	135.92	14.53	1.71

From **Figure 4.7**a−d, it is observed that all four eutectogel systems are highly resistive in nature with TEGel2 being the least (ESR 1.6 MΩ) and TEGel4 being the most (ESR 27.2 MΩ) resistive, respectively (**Figure 4.7**e). In corroboration, ionic conductivities of the same two gels are found to be the highest (0.031 mS cm^{-1}) and the lowest (0.008 mS cm^{-1}), respectively (**Table 4.6**). The conductivities of TEGels 1 and 3 were found to be 0.031 mS cm^{-1} (ESR 12.3 MΩ) and 0.011 mS cm^{-1} (17.6 MΩ). This is in agreement with the differences in viscosities of the base DESs (**Table B1**). While DESs 1 and 2 exhibit low viscosity (< 0.03 Pa s), DESs 3 and 4 possess viscosities in the higher range at room temperature. The resistive behavior of the eutectogels is also in agreement with the fact that carboxylic acid-based DESs with low water content (< 2 wt%) typically possess very low conductivities at room temperature.[34,35] Consequently, the device based on TEGels 1−4 demonstrate low specific power of 8.7, 65.4, 6.0, and 3.9 mW kg^{-1}. Additionally, the systems are seen to deviate from the double-layer capacitive nature. This is probably because of apparent higher viscosity of the

gelated DESs, and the lack of polarity and a suitable conducting pathway for the movement of ions in the solution, resulting in low ionic conductivity. Again, the highly resistive nature, especially of TEGels 3 and 4 is potentially a result of low self-diffusivity on account of DES/TiO_2 interactions[22] and the presence of bulkier molecular groups in the corresponding DESs inducing steric-hindered resistance to charge transfer. The high values of R_{ct} indicate substantial electrolyte ionic resistance inside the electrode pores, resulting in higher ESR.

However, the [BMIM][BF_4]-supported eutectogel systems show a tremendous diminution in their intrinsic resistance (ESR 66.9–135.9 Ω) and increase in ionic conductivity (**Table 4.6**). TEGels 2 and 4 showed the highest (16.3 mS cm^{-1}) and the lowest (14.5 mS cm^{-1}) conductivities, respectively, which are even higher than the room-temperature ionic conductivity of the IL (3–5 mS cm^{-1})[36] The conductivities of TEGels 1 and 3 were increased to 15.9 and 14.6 mS cm^{-1}. The introduction of the IL potentially forms a hybrid network, instilling its superior ionic properties into the same. The interaction of the IL molecules with the TiO_2 particles may form an interconnected network providing a continuous channel for ion transport, hence ensuring better mobility of the ions.[722] Moreover, [BMIM][BF_4] is known for its good wettability.[36] Elevated water content augments the diffusive characteristics of ions, consequently leading to an overall increased ionic conductivity, attributed to the attenuation of ionic interactions.[21] Decent values of specific power (2.71, 3.48, 1.86, and 1.71 kW kg^{-1}) are obtained due to the fairly high ESR. Obviously, TEGels 3 and 4 possess values of R_{ct} much higher than those of their two counterparts, rendering them higher intrinsic resistance and lower specific power than those of the latter. Nevertheless, the delivered power is still comparable to those of ionogels[37,38] and eutectogels[27–31] reported by other researchers. All these findings are consistent with the observations from CV.

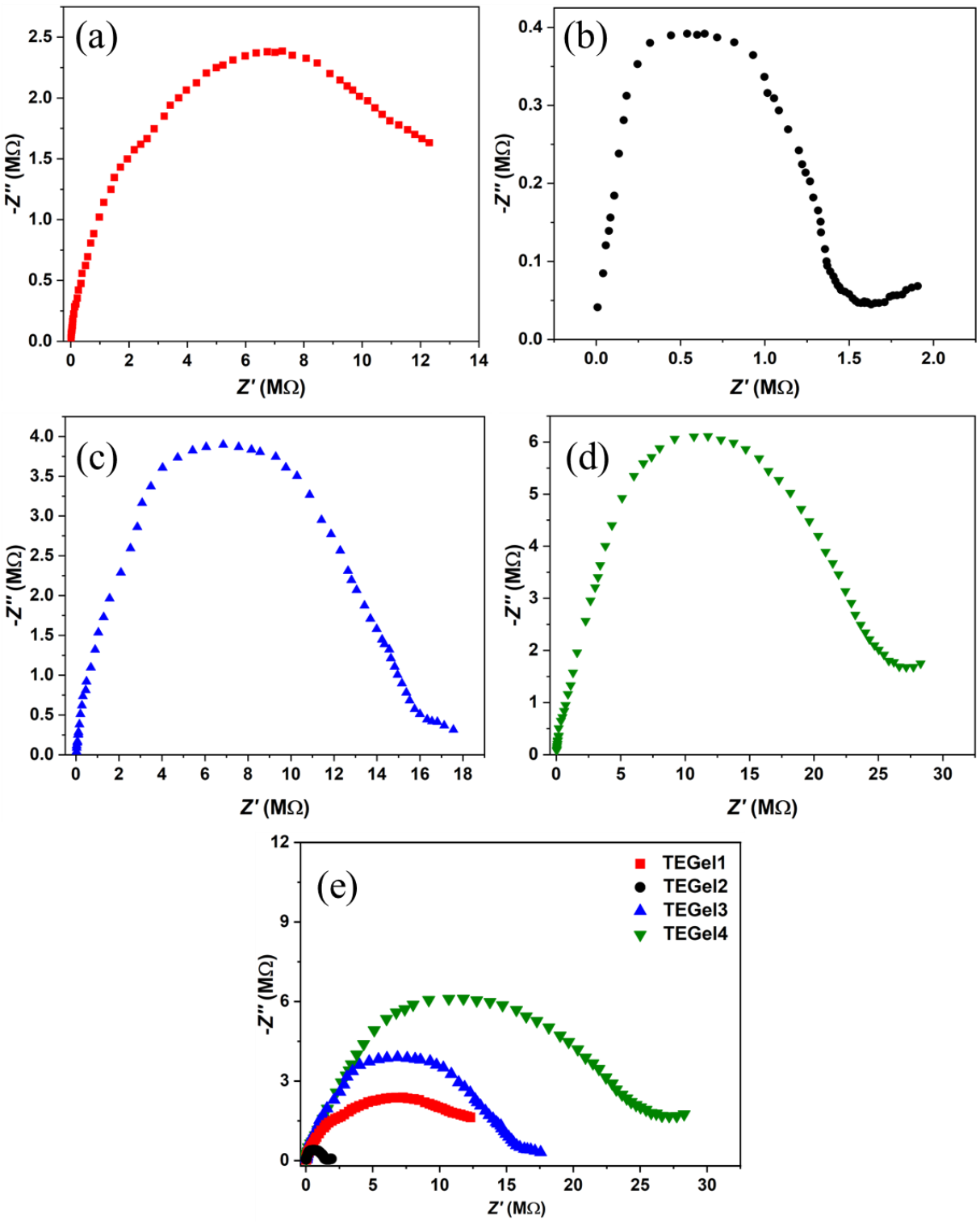

Figure 4.7. Nyquist plots obtained from EIS conducted on the two-electrode coin-cell with rGO electrodes and (a) TEGel1, (b) TEGel2, (c) TEGel3, and (d) TEGel4 electrolytes. (e) Comparison of the spectra of all four TEGels on a single plot.

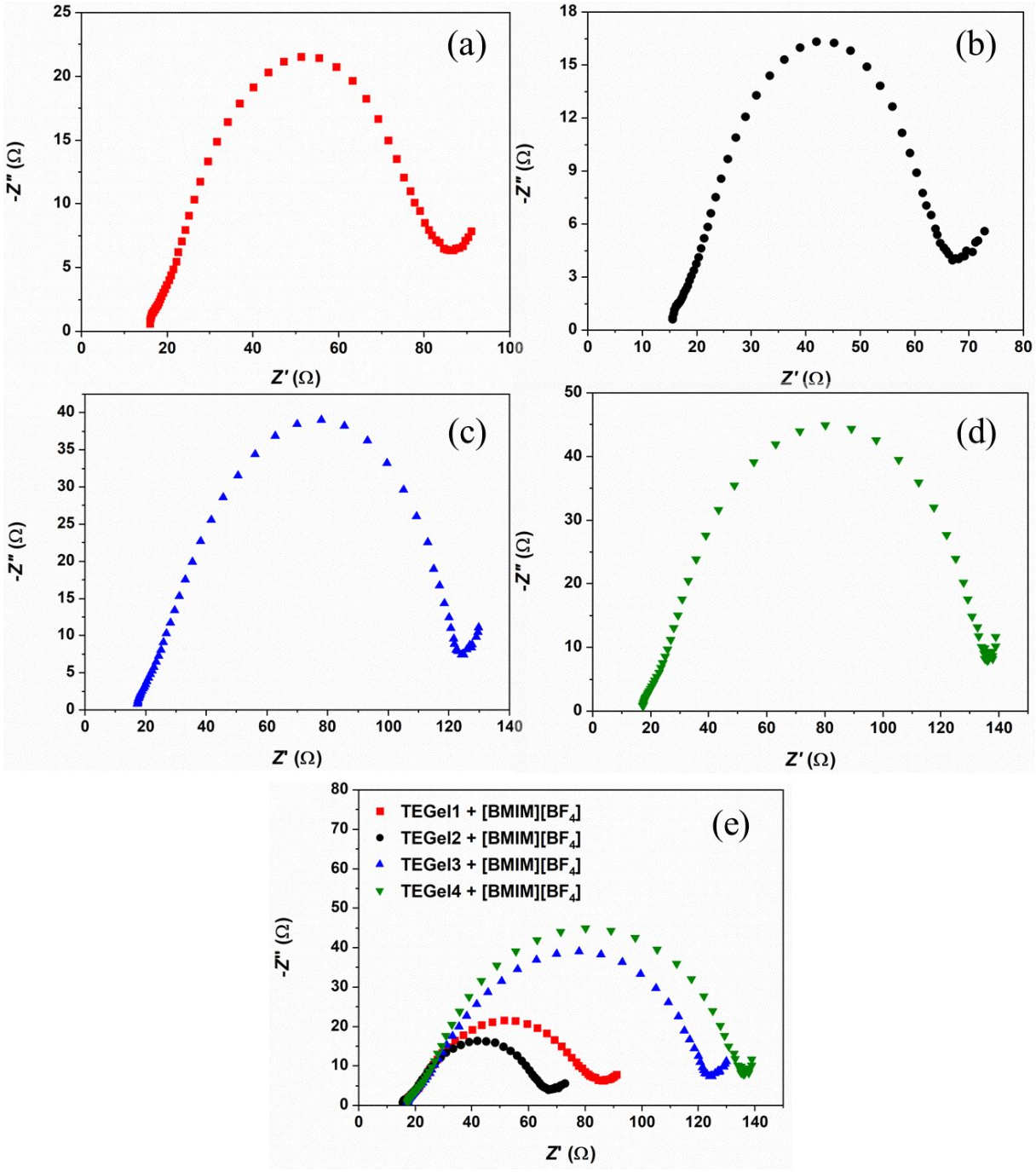

Figure 4.8. Nyquist plots obtained from EIS conducted on the two-electrode coin-cell with rGO electrodes and (a) TEGel1, (b) TEGel2, (c) TEGel3, and (d) TEGel4 electrolytes after incorporation of the IL [BMIM][BF_4]. (e) Comparison of the spectra of all four TEGels on a single plot.

4.3. Results and Discussion on SEGels

4.3.1. Morphological Analysis

Morphological studies were conducted on SEGels 1–4 using FESEM and FETEM. The FESEM images of the eutectogels confirmed the uniform crosslinking of SiO_2 particles with the DES frameworks (**Figure 4.9**a−d). The inorganic gel samples exhibited a cluster-like assembly of small, agglomerated silica moieties, forming crevices incrusted on the surface of the DESs through a self-assembly mechanism during in-situ gelation. This process imparted a solid characteristic to the immobilized DESs.

The FETEM image of SEGel2 (**Figure 4.9**e) revealed interconnected aggregates of inorganic SiO_2 particles, resulting in a porous gel structure.[2] These aggregates create 3D nanostructured continuous channels, facilitating ion transport. The observed continuous channels suggest that the DES is embedded within them through obvious gelation. Since all four DESs belong to the same long-chain carboxylic fatty acid group with similar inherent characteristics, SEGels 1, 3, and 4 are expected to possess similar porosity and 3D nanostructured channels. The similar nature of the DESs implies that their corresponding eutectogels are likely to display similar morphological features and structural characteristics.

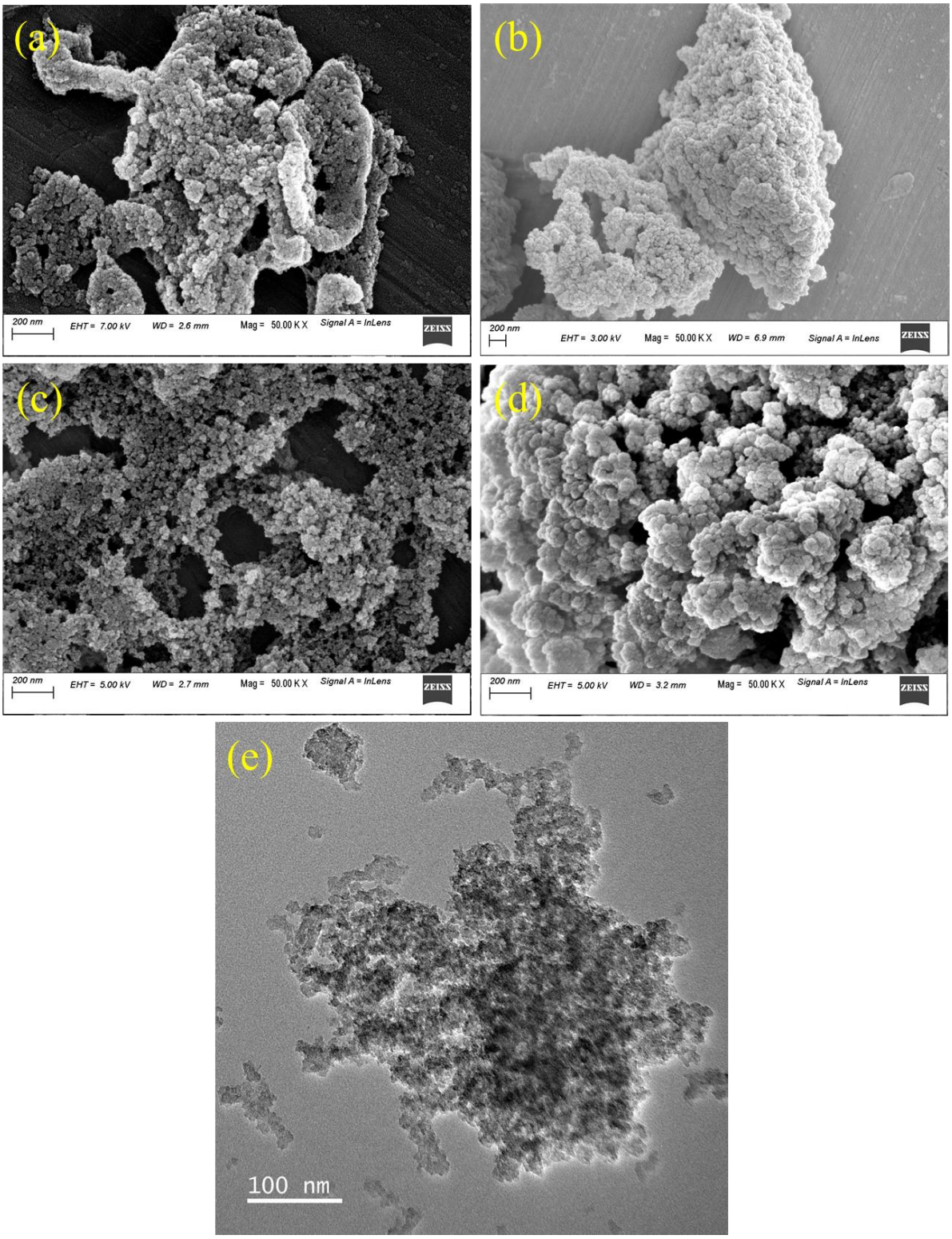

Figure 4.9. FESEM images of (a) SEGel1, (b) SEGel2, (c) SEGel3, (d) SEGel4, and (e) FETEM image of SEGel2.

4.3.2. Structural Analysis

The impact of immobilization of the DESs into a porous matrix on their structure was observed by performing FTIR on SEGels 1–4 and comparing the spectra with those of their parent DESs. As it is seen from **Figure 4.10**a−d, the FTIR spectra of SEGels are very similar to those of their corresponding DESs and TEGels. The peaks at ~2920 cm^{-1} indicate the presence of O−H stretching. This is represented by a distinct characteristic band at about 2920 cm^{-1} with shoulders around 2953 and 2852 cm^{-1}. The vibrational bands at ~1700 and ~1180 cm^{-1} represent C=O and C−O stretching, respectively. The bands of O–H bending are depicted by peaks between 1500 and 1300 cm^{-1} in the spectra. On the other hand, the existence of C−H bending is represented by the bands in the windows of 1500−1400 cm^{-1} and 1000−700 cm^{-1}. The broad band at ~3350 cm^{-1} in the standalone DESs may be assigned to the potential stretching vibration of moisture adsorbed by the systems during storage and handling.[2] The distinct strong bands at 1060 cm^{-1} on the spectra of the SEGels, otherwise absent on that of the TEGels, could possibly be associated to the stretching vibrations of Si−O−Si.[39] However, the silica content in the eutectogels is limited, resulting in the domination of the DES vibrations. Nevertheless, the absorption bands between 1600 and 1000 cm^{-1} in the eutectogels are more intense than those of the pure DESs due to the superposition with the strongly absorbing vibrations of the SiO_2 framework within this spectral region.[2] Conversely, the bands around 500 cm^{-1} in the fingerprint region of the SEGel spectra are less intense, as robust SiO_2 vibrations are absent.[2]

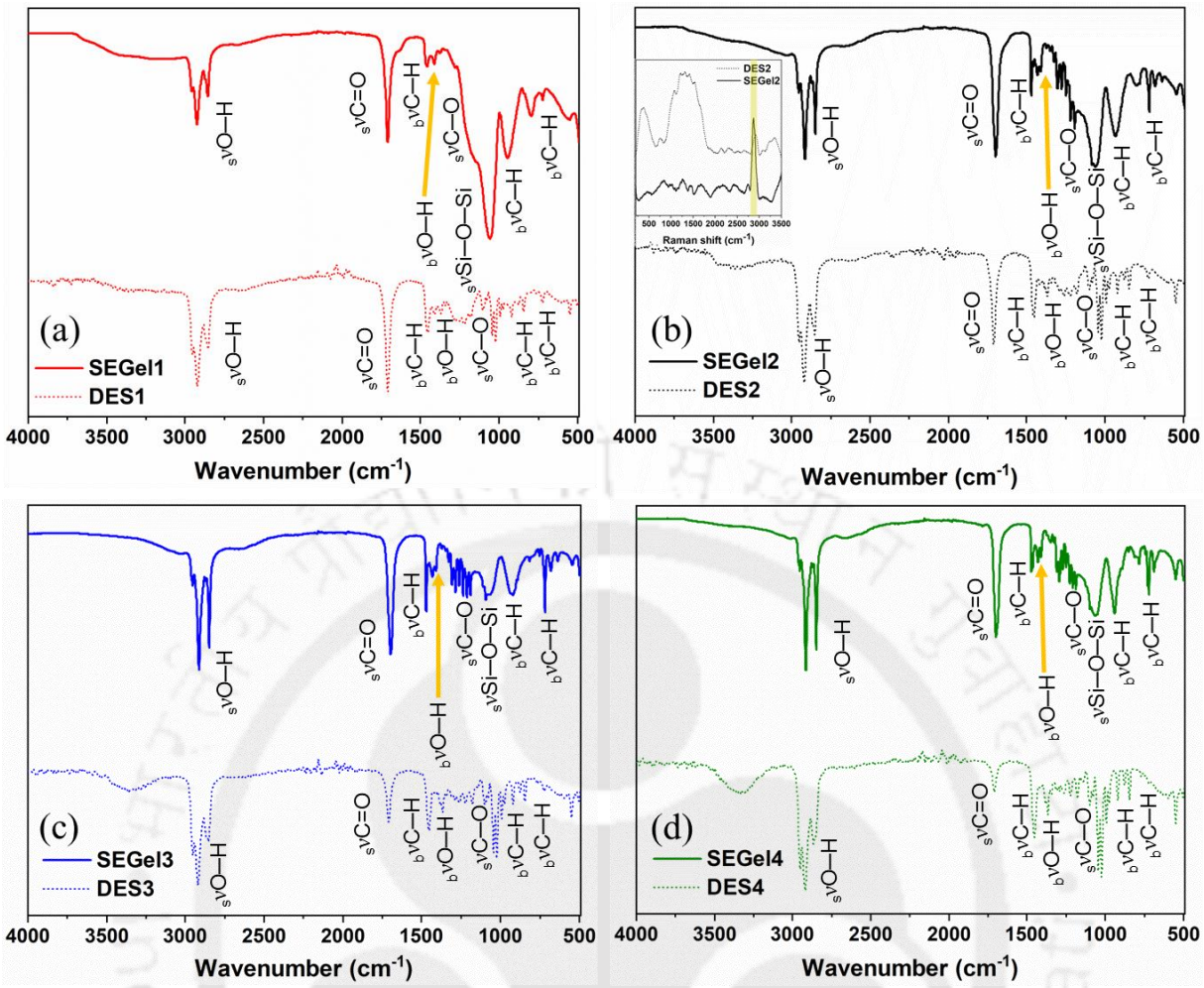

Figure 4.10. FTIR graphs of (a) DES1 and SEGel1, (b) DES2 and SEGel2 (inset: Raman spectra of DES2 and SEGel2), (c) DES3 and SEGel3, and (d) DES4 and SEGel4.

No new absorption peaks are present in the eutectogel spectra, indicating that SiO_2 and the DESs are not chemically bonded. Therefore, it can be inferred that the immobilization of the DES into the crosslinking matrix does not substantially alter the characteristics of the DES. In other words, the components of the DESs primarily act as a template for the formation of the silica matrix. Additionally, the similarity in the two spectra suggests that the DESs are fully interconnected within the SiO_2 framework.[4] Nonetheless, the vibrational bands of the DESs have been observed to shift marginally from their original positions in the spectrum of the corresponding eutectogel (**Table 4.7**). This was substantiated by the Raman spectra of DES2 and SEGel2 (inset of **Figure 4.10**b), where although quite similar, the peaks in the two spectra

exhibit visible differences in their intensities and positions. Distinctly evident is the shift of the peak corresponding to O−H stretching from 2921 cm^{-1} in the spectrum of DES2 to 2872 cm^{-1} in that of the gel. This again indicates the potential existence of weak non-bonded interactions between the DES molecules and the silica moieties. The presence of such non-bonded interactions can potentially lead to changes in the thermal characteristics of the immobilized solvent.[5] The slight variations in the new positions of the FTIR peaks between SEGels and corresponding TEGels indicate a difference in the nature of interaction of their respective matrices with the DESs.

Table 4.7. Vibrational bands of DESs 1−4 and SEGels 1−4 with their respective assignments

Assignment	System							
	Vibrational band (cm^{-1})							
	DES1	SEGel1	DES2	SEGel2	DES3	SEGel3	DES4	SEGel4
$_s\nu$O−H	2920	2923	2920	2916	2920	2913	2922	2916
$_s\nu$C=O	1709	1708	1711	1698	1711	1697	1711	1698
$_b\nu$C−H	1456	1457	1456	1471	1456	1471	1454	1472
$_b\nu$O−H	1369	1379	1369	1410	1369	1407	1369	1406
$_s\nu$C−O	1180	1132	1180	1193	1180	1190	1179	1187
$_s\nu$Si−O−Si	–	1059	–	1060	–	1060	–	1060
$_b\nu$C−H	920	943	920	932	920	919	920	939
$_b\nu$C−H	723	721	723	717	719	716	719	720

$_s\nu$: stretching, $_b\nu$: bending

XRD measurements were conducted on SEGels 1–4 to evaluate the degree of crystallinity of the samples. In accordance with previous findings,[4–7] the XRD analysis of the inorganic eutectogels revealed the presence of a typical amorphous SiO_2 matrix coexisting with the DESs, similar to their TEGel counterparts. The XRD patterns of the eutectogels shown in **Figure 4.11** exhibit weak and broad peaks, indicative of the amorphous or low-crystalline

nature of the samples within the given range of 2θ. The introduction of DES disrupts the regular arrangement of the SiO_2 matrix, resulting in an increase in the amorphous portion of the material.

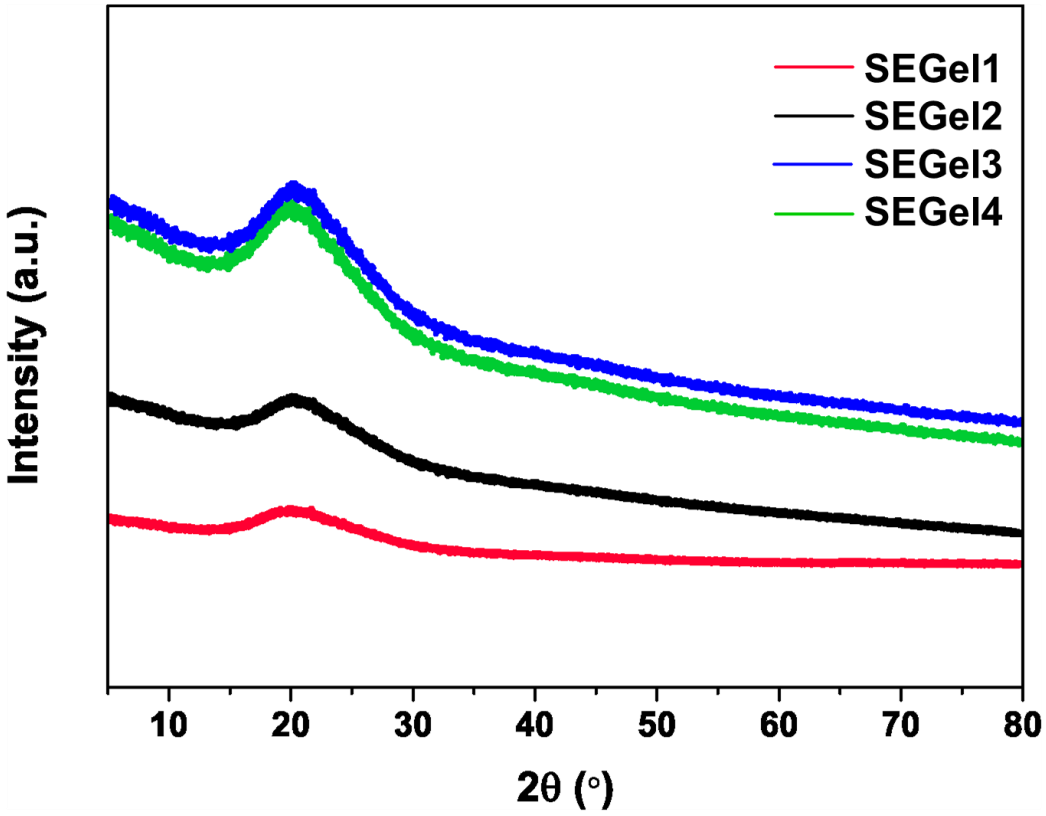

Figure 4.11. XRD patterns of SEGels 1–4.

4.3.3. Thermal Analysis

Thermal analyses of the DESs and SEGels were carried out on a TG 209 F1 Libra (Make: M/s Netzsch, Germany) in a nitrogen atmosphere between temperatures 25 and 600 °C at a rate of 10 °C min^{-1} with a nitrogen flow of 40 mL min^{-1}. **Figure 4.12** shows the TGA thermograms of the DESs 1–4 and SEGels 1–4. **Table 4.8** shows that, unlike in case of TEGels, $T_{5\%}$ of SEGels are comparable to those of their parent DESs, indicating negligible effect of the pore structure of SiO_2 on the onset degradation temperature.[22] The mass loss below ~150 °C on the

TGA profiles of the SEGels should predominantly be on account of the evaporation of moisture and/or volatile impurities.[5] The decline in mass between ~120 and ~235 °C occurs potentially due to the decomposition of DL-Menthol from the DESs. Subsequently, the one starting around 389 °C may be attributed to the degradation of the acids. Lastly, the straight lines observed at the end of the thermograms beyond ~500 °C indicate complete decomposition of the organic components, leaving only the inorganic parts behind (approximately 35–46 wt%). The DSC thermograms of the four SEGels (inset of **Figure 4.12**) are characterized by an exothermic peak at about 250 °C and another exothermic peak at ~485 °C between two endothermic ones, both in close agreement with the decomposition temperatures of DL-Menthol and the acids as per TGA. The small bumps around 35 °C of the profiles most likely represent T_g of the gels, while the exothermic peaks between 45 and 100 °C may have resulted due to the loss of water and/or organic impurities.[5,10] In contrast, the DESs undergo two distinct decomposition steps resulting from the degradation of DL-Menthol and the acids, with a small mass loss occurring below ~100 °C due to the vaporization of adsorbed moisture before complete degradation. The incorporation of inorganic SiO_2 leads to a reduction in the volatile phase content of the DESs.

As noted earlier, the degradation temperature of each DES differs from that of its individual components (**Table 4.3**) because of inter-molecular interactions between the components. The decomposition pattern of the DES is further altered and the degradation temperatures shifted on its confinement into SiO_2.[11–14] This confirms the existence of weak non-bonded interactions between the DES molecules and the silica moieties.[5] T_{cd} of SEGel is higher than that of its corresponding DES (**Table 4.8**) and TEGel (**Table 4.2**). This indicates strong confinement of the DESs within the silica framework.[2] Variations in the decomposition temperature windows of the DES components were also observed between SEGels and TEGels, further suggesting that silica interacts differently with the DESs than titania.

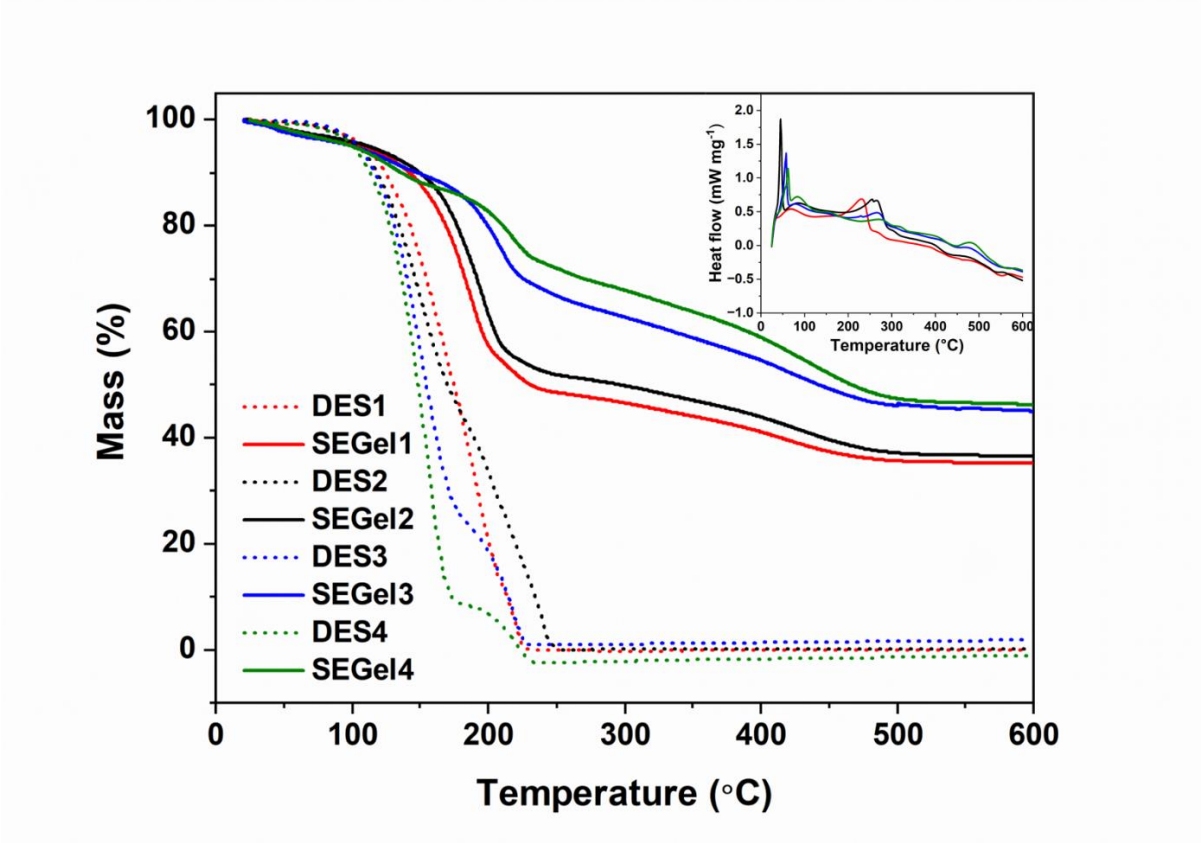

Figure 4.12. TGA thermograms of DESs 1–4 and SEGels 1–4 (inset: DSC profiles of SEGels 1–4).

Table 4.8. $T_{5\%}$ and T_{cd} of DESs 1–4 and SEGels 1–4

DES / SEGel	$T_{5\%}$ (°C)	T_{cd} (°C)
DES1	111	231
SEGel1	108.8	482.2
DES2	105	249.9
SEGel2	111.8	505.2
DES3	106	232.4
SEGel3	99.8	513.7
DES4	101.2	227.2
SEGel4	99.8	511.7

4.3.4. Electrochemical Performance

Figure 4.13a–d depicts the cyclic voltammograms of SEGels 1–4 acquired at room temperature with the rGO-based two-electrode cell on a Gamry-interfaced CH Instruments, 600 C potentiostat (Gamry) at a scan rate of 10 mV s^{-1}. At higher scan rates, the ions within the electrolyte may not have sufficient time to penetrate deeper into the electrode material, resulting in reduced charge accumulation (electrolyte starvation effect). The voltammograms evince a quasi-rectangular profile which hints towards a capacitive behavior of the systems.[19,20] Furthermore, the absence of any distinct redox peaks in them suggests that the SEGel-based systems store charge non-Faradaically or by the establishment of an electric double layer at the electrolyte/electrode interface.[19–21]

Again, a narrow current density is observed for each system within the tested voltage window. This phenomenon may be attributed to the potential influence of low self-diffusivity, arising from DES/SiO_2 interactions[22], along with the absence of an ideal polarizable reference electrode.[23] Again, the constricted areas under the curves indicate that the eutectogels possess a low specific capacitance and inherently exhibit resistive characteristics, just like their titania-based counterparts. This behavior could be attributed to the apparent higher viscosity of the gelated systems. Additionally, the NADESs involved in the synthesis of the eutectogels lack ideal polar behavior, thus hindering the attainment of excellent electrochemical characteristics comparable to those of ILs. Specifically, in the case of SEGels 3 and 4, the presence of bulkier groups in the host DESs induces steric hindrance, acting as resistance to charge transfer and ionic movement. The higher room-temperature viscosities of the respective DESs support this explanation (**Figure B1, Table B1**). However, the systems involving SEGels 1 and 2 exhibit a comparatively higher area under their voltammetry curves (**Figure 4.13e**), attributed to the absence of relatively bulky molecular groups and the lower viscosity of their corresponding DESs (**Figure B1, Table B1**). This hypothesis is further supported by the low values of specific

capacitance delivered by the eutectogels (**Table 4.9**). While systems based on SEGels 3 and 4 demonstrated specific capacitance values of 78.2 µF g^{-1} (6.8 µF cm^{-2}) and 30.1 µF g^{-1} (2.6 µF cm^{-2}) at 10 mV s^{-1}, those with SEGels 1 and 2 showed slightly higher values of 637.5 µF g^{-1} (55.8 µF cm^{-2}) and 991.9 µF g^{-1} (86.8 µF cm^{-2}), respectively.

Nevertheless, all four eutectogels exhibit an outstanding OPW of 4 V, which is on par with that of ILs[24] and the ionogels discussed in Chapter 3 of this thesis, and surpasses that of IL-based DESs.[21] Furthermore, when compared with the OPW of eutectogels reported in relevant literature, the SEGels presented in this study demonstrate the highest potential window among all (**Table 4.5**). It is noteworthy that water content significantly influences the electrochemical stability of a DES, with higher water content resulting in a narrower potential window.[21] The wide OPW in the SEGels 1–4 may be attributed to the hydrophobic characteristic of the components of their parent DESs, as confirmed by Karl Fischer Titration (**Table B1**) and ^{1}H NMR spectroscopy (**Figure B2**a–d). Also, the high contact angle of DES3 against water (95.7°) (**Figure B3**), further validated the hydrophobic nature of this particular class of DESs.[25,26] Based on their specific capacitance and OPW, the device supported by SEGels 1–4 was able to store energy up to 1416.6, 2204.3, 173.7, and 66.8 µW h kg^{-1}, respectively. In comparison with TEGels, the silica-mediated eutectogels investigated in this study exhibited slightly higher values of specific capacitance (and energy). This could possibly be attributed to the large surface area of SiO_2, facilitating long-range weak dipole interactions between the matrix and the NADESs with weak polarity. This also indicates that silica interacts differently with the DESs than titania. However, it is noteworthy that the specific capacitance still remains low, clearly indicating the retention of high intrinsic resistance in the systems. Therefore, further analysis was not pursued for the SEGels.

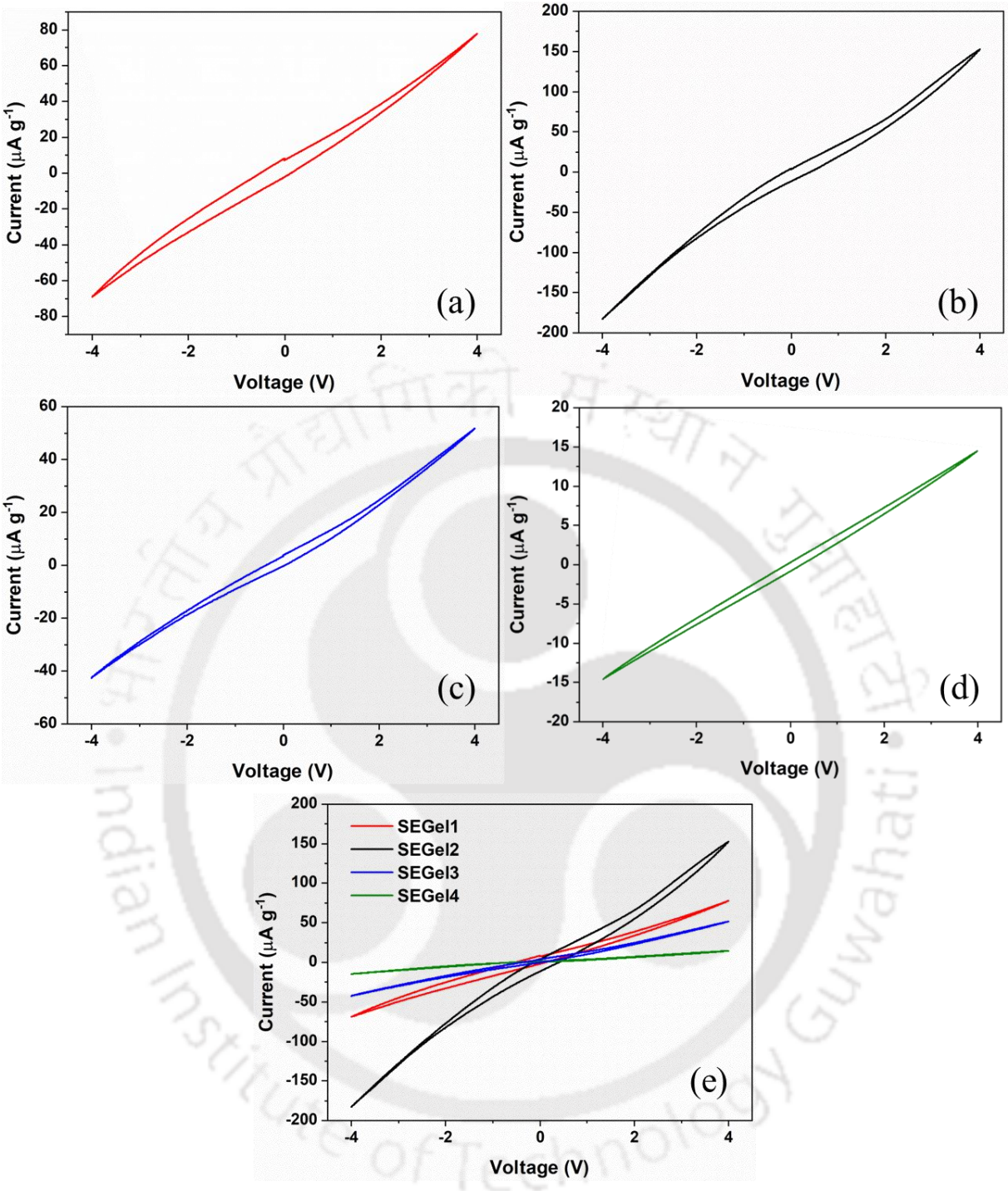

Figure 4.13. Cyclic voltammetry profiles of the systems conducted on the two-electrode coin-cell with rGO electrodes and (a) SEGel1, (b) SEGel2, (c) SEGel3, and (d) SEGel4 electrolytes at a scan rate of 10 mV s^{-1}. (e) Comparison of the voltammograms of all four systems on a single plot.

Table 4.9. Specific capacitance and specific energy of SEGels 1–4 at 10 mV s^{-1}

System	$C_{sp\text{-}10\ mV\ s^{-1}}$ (F g^{-1})	$C_{sp\text{-}10\ mV\ s^{-1}}$ (mF cm^{-2})	$E_{sp\text{-}10\ mV\ s^{-1}}$ (W h kg^{-1})
SEGel1	6.37×10^{-4}	5.58×10^{-2}	1.42×10^{-3}
SEGel2	9.92×10^{-4}	8.68×10^{-2}	2.20×10^{-3}
SEGel3	7.82×10^{-5}	6.83×10^{-3}	1.74×10^{-4}
SEGel4	3.01×10^{-5}	2.63×10^{-3}	6.68×10^{-5}

4.4. Conclusions

The eight hydrophobic eutectogels were prepared through a facile sol−gel method by the physical confinement of four NADESs into TiO_2 or SiO_2 derived respectively from TBOT or TEOS. The eutectogels were obtained in amorphous solid form with apparent porosity and interconnected aggregates of titania or silica particles, as confirmed from XRD, FESEM, and FETEM. FTIR analyses indicated that the structural properties of the DESs were not altered by their immobilization into the solid matrices. However, marginal shifts in the vibrational frequencies of the DESs were observed due to non-bonded interactions between the DES molecules and the TiO_2 or SiO_2 moieties. Furthermore, TGA analyses showed that the thermal stabilities of the DESs tend to alter after gelation, which is potentially again because of such interactions. The difference in the interactive nature of the two matrices with the DESs was marked by the variation in the IR vibrational shifts and decomposition temperatures of the confined DESs in the two cases. In each case, a reprieve in the degradation of the DES components was observed which indicated strong confinement of the DESs within the matrix frameworks.

From voltammetry studies, it was observed that all eight eutectogels manifest a double-layer capacitive behavior within an impressively wide operating voltage window of 4 V owing

to high hydrophobicity of the DES components. This highlights their good compatibility with rGO electrodes and excellent stability in applications with EDLCs. However, the small area under the curves and a low peak current density in each case suggested the presence of high intrinsic resistance, procuring values of specific capacitance and specific energy only as high as 0.9 mF g^{-1} (86.8 µF cm^{-2}) and 2.2 mW h kg^{-1} (SEGel2). Between the two categories, SEGels deliver slightly higher specific capacitance (and energy) due to the large surface area of SiO_2, which facilitates long-range weak dipole interactions between the matrix and the weakly polar NADESs, further confirming the difference in the manner the two matrices interact with the DESs. EIS studies on TEGels confirmed the existence of high ESR in the systems resulting in low ionic conductivity and specific power, the respective maximum values obtained being only 0.031 mS cm^{-1} and 65.4 mW kg^{-1} (TEGel2). The TEGels when modified with the IL [BMIM][BF_4], however, not only retained their EDLC characteristic within the 4 V window, but also showed tremendous reduction in internal resistance leading to specific capacitance and ionic conductivity as high as 47.7 F g^{-1} (2087 mF cm^{-2}) and 16.3 mS cm^{-1} (TEGel2). This was a result of the potential formation of a hybrid network of interconnected "ionic" channels with the introduction of the IL along with good wettability of the latter. Thus, the absence of an ionic or polar component combined with the presence of steric hindrance provided by the bulky molecules in the DESs inhibit the ability of the resulting eutectogels to possess appealing electrochemical properties like those of ionogels, as presented in Chapter 3.

The findings suggest that on the basis of certain properties, the NADES-based eutectogels hold promise as cost-effective, solid-state electrolytes. Nevertheless, there is room for enhancement in the capacitance and conductivity of these gels. Given the tunability and ease of synthesis of DESs, it is conceivable to produce eutectogels with elevated capacitance and ionic conductivity. A possible approach could be the replacement of non-ionic and long-chained DES-forming components with ionic and less bulkier ones. Such advancements could

position them as a novel and competitive category of solid-state electrolytes for high-performance supercapacitors.

References

(1) Zhong, C.; Deng, Y.; Hu, W.; Qiao, J.; Zhang, L.; Zhang, J. A Review of Electrolyte Materials and Compositions for Electrochemical Supercapacitors. *Chem Soc Rev* **2015**, *44* (21), 7484–7539. https://doi.org/10.1039/C5CS00303B.

(2) Joos, B.; Vranken, T.; Marchal, W.; Safari, M.; Van Bael, M. K.; Hardy, A. T. Eutectogels: A New Class of Solid Composite Electrolytes for Li/Li-Ion Batteries. *Chemistry of Materials* **2018**, *30* (3), 655–662. https://doi.org/10.1021/acs.chemmater.7b03736.

(3) Vetrivel, V.; Rajendran, K.; Kalaiselvi, V. Synthesis and Characterization of Pure Titanium Dioxide Nanoparticles by Sol- Gel Method. *Int J Chemtech Res* **2015**, *7* (3), 1090–1097.

(4) Wu, F.; Chen, N.; Chen, R.; Zhu, Q.; Tan, G.; Li, L. Self-Regulative Nanogelator Solid Electrolyte: A New Option to Improve the Safety of Lithium Battery. *Advanced Science* **2016**, *3* (1), 1500306. https://doi.org/10.1002/advs.201500306.

(5) Verma, Y. L.; Tripathi, A. K.; Shalu; Singh, V. K.; Balo, L.; Gupta, H.; Singh, S. K.; Singh, R. K. Preparation and Properties of Titania Based Ionogels Synthesized Using Ionic Liquid 1-Ethyl-3-Methyl Imidazolium Thiocyanate. *Materials Science and Engineering: B* **2017**, *220*, 37–43. https://doi.org/10.1016/j.mseb.2017.03.010.

(6) Li, Z.; Zhang, S.; Jiang, Z.; Cai, D.; Gu, C.; Tu, J. Deep Eutectic Solvent-Immobilized PVDF-HFP Eutectogel as Solid Electrolyte for Safe Lithium Metal Battery. *Mater Chem Phys* **2021**, *267*, 124701. https://doi.org/10.1016/j.matchemphys.2021.124701.

(7) Li, X.; Zhang, Z.; Yang, L.; Tachibana, K.; Hirano, S. TiO2-Based Ionogel Electrolytes for Lithium Metal Batteries. *J Power Sources* **2015**, *293*, 831–834. https://doi.org/10.1016/j.jpowsour.2015.06.033.

(8) Baranyai, K. J.; Deacon, G. B.; MacFarlane, D. R.; Pringle, J. M.; Scott, J. L. Thermal Degradation of Ionic Liquids at Elevated Temperatures. *Aust J Chem* **2004**, *57* (2), 145–147. https://doi.org/10.1071/CH03221.

(9) Ma, Z.; Wang, J.; Deng, Y.; Wang, Y.; Yan, L. Synthesis of Highly Ion-Conductive Lignin Eutectogels in a Ternary Deep Eutectic Solvent and Nitrogen-Doped 3D Hierarchical Porous Carbons for Supercapacitors. *Biomacromolecules* **2021**, *22* (10), 4181–4190. https://doi.org/10.1021/acs.biomac.1c00706.

(10) Seera, S. D. K.; Kundu, D.; Gami, P.; Naik, P. K.; Banerjee, T. Synthesis and Characterization of Xylan-Gelatin Cross-Linked Reusable Hydrogel for the Adsorption of Methylene Blue. *Carbohydr Polym* **2021**, *256*, 117520. https://doi.org/10.1016/j.carbpol.2020.117520.

(11) Verma, R.; Mohan, M.; Goud, V. V; Banerjee, T. Operational Strategies and Comprehensive Evaluation of Menthol Based Deep Eutectic Solvent for the Extraction of Lower Alcohols from Aqueous Media. *ACS Sustain Chem Eng* **2018**, *6* (12), 16920–16932. https://doi.org/10.1021/acssuschemeng.8b04255.

(12) Verma, R.; Banerjee, T. Palmitic-Acid-Based Hydrophobic Deep Eutectic Solvents for the Extraction of Lower Alcohols from Aqueous Media: Liquid–Liquid Equilibria Measurements, Validation and Process Economics. *Global Challenges* **2019**, *3* (11), 1900024. https://doi.org/10.1002/gch2.201900024.

(13) Verma, R.; Banerjee, T. Liquid–Liquid Extraction of Lower Alcohols Using Menthol-Based Hydrophobic Deep Eutectic Solvent: Experiments and COSMO-SAC

Predictions. *Ind Eng Chem Res* **2018**, *57* (9), 3371–3381. https://doi.org/10.1021/acs.iecr.7b05270.

(14) Verma, R. Liquid-Liquid Extraction and Process Flow Sheeting of Lower Alcohol with Deep Eutectic Solvents, Indian Institute of Technology Guwahati, Guwahati, 2018.

(15) Ribeiro, B. D.; Florindo, C.; Iff, L. C.; Coelho, M. A. Z.; Marrucho, I. M. Menthol-Based Eutectic Mixtures: Hydrophobic Low Viscosity Solvents. *ACS Sustain Chem Eng* **2015**, *3* (10), 2469–2477. https://doi.org/10.1021/acssuschemeng.5b00532.

(16) Liu, P.; Gu, X.; Bian, L.; Cheng, X.; Peng, L.; He, H. Thermal Properties and Enhanced Thermal Conductivity of Capric Acid/Diatomite/Carbon Nanotube Composites as Form-Stable Phase Change Materials for Thermal Energy Storage. *ACS Omega* **2019**, *4* (2), 2964–2972. https://doi.org/10.1021/acsomega.8b03130.

(17) Subramanian, A.; Appukuttan, S. Sol-Gel Synthesis and Characterization of Microencapsulated Strontium Titanate-Myristic Acid Phase Change Material for Thermal Energy Storage. *J Solgel Sci Technol* **2020**, *94* (3), 573–581. https://doi.org/10.1007/s10971-019-05084-2.

(18) Wan, Y.; Chen, Y.; Cui, Z.; Ding, H.; Gao, S.; Han, Z.; Gao, J. A Promising Form-Stable Phase Change Material Prepared Using Cost Effective Pinecone Biochar as the Matrix of Palmitic Acid for Thermal Energy Storage. *Sci Rep* **2019**, *9* (1), 11535. https://doi.org/10.1038/s41598-019-47877-z.

(19) Pilathottathil, S.; Thasneema, K. K.; Shahin Thayyil, M.; Pillai, M. P.; Niveditha, C. V. A High Voltage Supercapacitor Based on Ionic Liquid with an Activated Carbon Electrode. *Mater Res Express* **2017**, *4* (7), 75503. https://doi.org/10.1088/2053-1591/aa7116.

(20) Hamsan, M. H.; Aziz, S. B.; Kadir, M. F. Z.; Brza, M. A.; Karim, W. O. The Study of EDLC Device Fabricated from Plasticized Magnesium Ion Conducting Chitosan Based Polymer Electrolyte. *Polym Test* **2020**, *90*, 106714. https://doi.org/10.1016/j.polymertesting.2020.106714.

(21) Mahanta, U.; Choudhury, S.; Venkatesh, R. P.; SarojiniAmma, S.; Ilangovan, S. A.; Banerjee, T. Ionic-Liquid-Based Deep Eutectic Solvents as Novel Electrolytes for Supercapacitors: COSMO-SAC Predictions, Synthesis, and Characterization. *ACS Sustain Chem Eng* **2020**, *8* (1), 372–381. https://doi.org/10.1021/acssuschemeng.9b05596.

(22) Chen, N.; Zhang, H.; Li, L.; Chen, R.; Guo, S. Ionogel Electrolytes for High-Performance Lithium Batteries: A Review. *Advanced Energy Materials*. Wiley-VCH Verlag April 25, 2018. https://doi.org/10.1002/aenm.201702675.

(23) López Zavala, M. Á.; González Peña, O. I.; Cabral Ruelas, H.; Delgado Mena, C.; Guizani, M. Use of Cyclic Voltammetry to Describe the Electrochemical Behavior of a Dual-Chamber Microbial Fuel Cell. *Energies*. 2019. https://doi.org/10.3390/en12183532.

(24) Shabeeba, P.; Thasneema, K. K.; Thayyil, M. S.; Pillai, M. P.; Niveditha, C. V. A Graphene-Based Flexible Supercapacitor Using Trihexyl(Tetradecyl)Phosphonium Bis(Trifluoromethanesulfonyl)Imide Ionic Liquid Electrolyte. *Mater Res Express* **2017**, *4* (8), 085501. https://doi.org/10.1088/2053-1591/aa7b14.

(25) Jose, A. J.; Alagar, M. Preparation and Characterization of Polysulfone-Based Nanocomposites. In *Manufacturing of Nanocomposites with Engineering Plastics*; Elsevier, 2015; pp 31–59. https://doi.org/10.1016/B978-1-78242-308-9.00003-3.

(26) Law, K.-Y. Definitions for Hydrophilicity, Hydrophobicity, and Superhydrophobicity: Getting the Basics Right. *J Phys Chem Lett* **2014**, *5* (4), 686–688. https://doi.org/10.1021/jz402762h.

(27) Qin, H.; Panzer, M. J. Chemically Cross-Linked Poly(2-hydroxyethyl Methacrylate)-Supported Deep Eutectic Solvent Gel Electrolytes for Eco-Friendly Supercapacitors. *ChemElectroChem* **2017**, *4* (10), 2556–2562. https://doi.org/10.1002/celc.201700586.

(28) Hong, S.; Yuan, Y.; Liu, C.; Chen, W.; Chen, L.; Lian, H.; Liimatainen, H. A Stretchable and Compressible Ion Gel Based on a Deep Eutectic Solvent Applied as a Strain Sensor and Electrolyte for Supercapacitors. *J Mater Chem C Mater* **2020**, *8* (2), 550–560. https://doi.org/10.1039/C9TC05913J.

(29) Wu, Y.; Deng, Y.; Zhang, K.; Qiu, J.; Wu, J.; Yan, L. Ultrahigh Conductive and Stretchable Eutectogel Electrolyte for High-Voltage Flexible Antifreeze Quasi-Solid-State Zinc-Ion Hybrid Supercapacitor. *ACS Appl Energy Mater* **2022**, *5* (3), 3013–3021. https://doi.org/10.1021/acsaem.1c03654.

(30) Yang, H.; Zhang, J.; Yao, J.; Zuo, D.; Xu, J.; Zhang, H. A Gel Polymer Electrolyte Based on Ternary Deep Eutectic Solvent for Flexible, Wide-Temperature Tolerant Zinc-Ion Hybrid Supercapacitors. *J Power Sources* **2022**, *548*, 232070. https://doi.org/10.1016/j.jpowsour.2022.232070.

(31) Li, Z.; Xu, X.; Jiang, Z.; Chen, J.; Tu, J.; Wang, X.; Gu, C. A Silk Protein-Based Eutectogel as a Freeze-Resistant and Flexible Electrolyte for Zn-Ion Hybrid Supercapacitors. *ACS Appl Mater Interfaces* **2022**, *14* (39), 44821–44831. https://doi.org/10.1021/acsami.2c12103.

(32) Eftekhari, A. Supercapacitors Utilising Ionic Liquids. *Energy Storage Mater* **2017**, *9*, 47–69. https://doi.org/10.1016/j.ensm.2017.06.009.

(33) Shi, M.; Kou, S.; Yan, X. Engineering the Electrochemical Capacitive Properties of Graphene Sheets in Ionic-Liquid Electrolytes by Correct Selection of Anions. *ChemSusChem* **2014**, *7* (11), 3053–3062. https://doi.org/10.1002/cssc.201402275.

(34) Lin, Z.; Zhang, Y.; Zhao, Q.; Chen, A.; Jiao, B. Ultrasound-Assisted Dispersive Liquid-Phase Microextraction by Solidifying L-Menthol-Decanoic Acid Hydrophobic Deep Eutectic Solvents for Detection of Five Fungicides in Fruit Juices and Tea Drinks. *J Sep Sci* **2021**, *44* (20), 3870–3882. https://doi.org/10.1002/jssc.202100590.

(35) Ruggeri, S.; Poletti, F.; Zanardi, C.; Pigani, L.; Zanfrognini, B.; Corsi, E.; Dossi, N.; Kivel, H.; Salom, M. Electrochimica Acta Chemical and Electrochemical Properties of a Hydrophobic Deep Eutectic Solvent. **2019**, *295*, 124–129. https://doi.org/10.1016/j.electacta.2018.10.086.

(36) Liu, X.; Taiwo, O. O.; Yin, C.; Ouyang, M.; Chowdhury, R.; Wang, B.; Wang, H.; Wu, B.; Brandon, N. P.; Wang, Q.; Cooper, S. J. Aligned Ionogel Electrolytes for High-Temperature Supercapacitors. *Advanced Science* **2019**, *6* (5). https://doi.org/10.1002/advs.201801337.

(37) Xing, C. X.; Zhang, H. T.; Pan, S. S.; Yao, M.; Li, B. S.; Zhang, Y. Q.; Zhang, S. J. Boosting the Safety and Energy Density of Molybdenum Disulfide/Carbon Nanotubes Based Solid-State Sodium-Ion Supercapacitors with an Ionogel Electrolyte. *Mater Today Energy* **2020**, *18*, 100527. https://doi.org/10.1016/j.mtener.2020.100527.

(38) Simotwo, S. K.; Chinnam, P. R.; Wunder, S. L.; Kalra, V. Highly Durable, Self-Standing Solid-State Supercapacitor Based on an Ionic Liquid-Rich Ionogel and Porous Carbon Nanofiber Electrodes. *ACS Appl Mater Interfaces* **2017**, *9* (39), 33749–33757. https://doi.org/10.1021/acsami.7b07479.

(39) Saravanan, S.; Dubey, R. S. Synthesis of SiO2 Nanoparticles by Sol-Gel Method and Their Optical and Structural Properties. *Romanian Journal of Information Science and Technology* **2020**, *23* (1), 105–112.

Chapter 5

TiO_2- and SiO_2-Mediated Inorganic Eutectogels Developed from an Ionic-Liquid-Based Deep Eutectic Solvent

CHAPTER 5

TiO_2- and SiO_2-Mediated Inorganic Eutectogels Developed from an Ionic-Liquid-Based Deep Eutectic Solvent

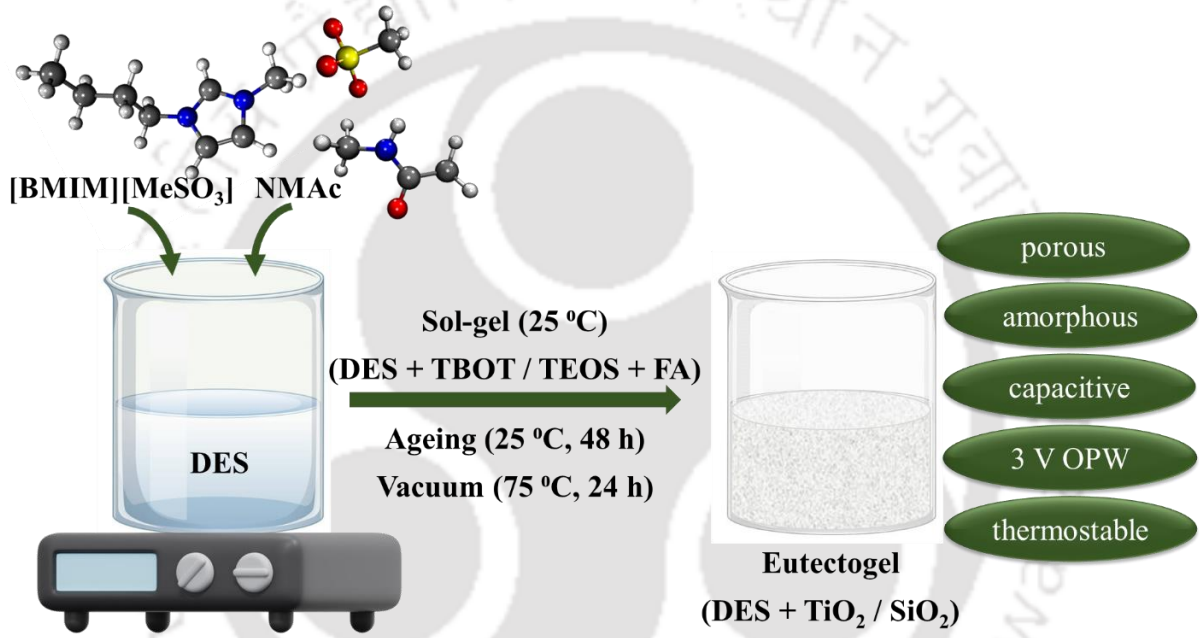

List of publication from Chapter 5:

(1) **Dutta, A.**; Millar, W.; Silvester, D. S.; Banerjee, T. Novel Eutectogels Derived from an Ionic-Liquid-Based Deep Eutectic Solvent as Electrolytes for Supercapacitors: Synthesis and Characterization. *(In line for submission)*

5.1. Introduction

Most of the IL-based inorganic ionogels discussed in Chapter 3 of this thesis exhibit reasonable electrochemical characteristics within a wide voltage window, favoring their potential utilization in supercapacitors. On the other hand, although more cost-effective and electrochemically stable, the carboxylic-acid-based inorganic eutectogels presented in Chapter 4 demonstrate high intrinsic resistance primarily because of the absence of an appropriate ionic medium. The same eutectogels, however, show a dramatic reduction in their internal resistance with improved specific capacitance and ionic conductivity after the incorporation of an IL. Therefore, to benefit from the desirable electrochemical characteristics of ILs while limiting the cost of synthesis, this chapter explores two eutectogels derived from the hybrid DES (DES5) composed of the IL [BMIM][$MeSO_3$] as HBA and NMAc as HBD. The same DES has previously been reported as an "effective electrolyte for supercapacitors".[1] The chapter discusses the morphological, structural, thermal, and electrochemical properties of the two eutectogels obtained by confining the DES into an inorganic matrix of TiO_2 (TIEGel) or SiO_2 (SIEGel). The matrices were derived from a TBOT or TEOS precursor using the sol-gel synthesis method outlined in Chapter 2 of this thesis. The procedures involved in the synthesis of both the DES and the eutectogels were facile. The eutectogels were characterized using FESEM, FETEM, FTIR spectroscopy, Raman spectroscopy, XRD, and TGA. Moreover, to assess their viability as electrolytes in supercapacitor applications, their electrochemical performance was analyzed using CV and EIS. The electrochemical properties of the eutectogel exhibiting the best performance at room temperature were further studied under controlled temperatures of 25, 50, and 80 °C. To the best of our knowledge, the sol-gel-derived TiO_2- and SiO_2-supported IL-based DES gels reported herein are the first of their kind.

5.2. Results and Discussion on TIEGel and SIEGel

5.2.1. Morphological Analysis

Morphological studies were conducted on TIEGel and SIEGel using FESEM and FETEM. The FESEM micrographs confirmed the uniform crosslinking of TiO_2 or SiO_2 moieties with the DES frameworks in the eutectogels. (**Figure 5.1**a,b). The inorganic eutectogel samples displayed a cluster-like arrangement of small, agglomerated titania or silica particles embedded on the surface of the DES through a self-assembly mechanism during in-situ gelation. This process imparted a solid characteristic to the immobilized DES in either case.

FETEM images of the two eutectogels (**Figure 5.1**c,d) depicted interconnected aggregates of inorganic TiO_2 or SiO_2 particles, resulting in a porous structure within the gels.[2] These aggregates create 3D, nanostructured, continuous channels that facilitate the transportation of ions. The continuous channels indicate that the DES is integrated into them through gelation.

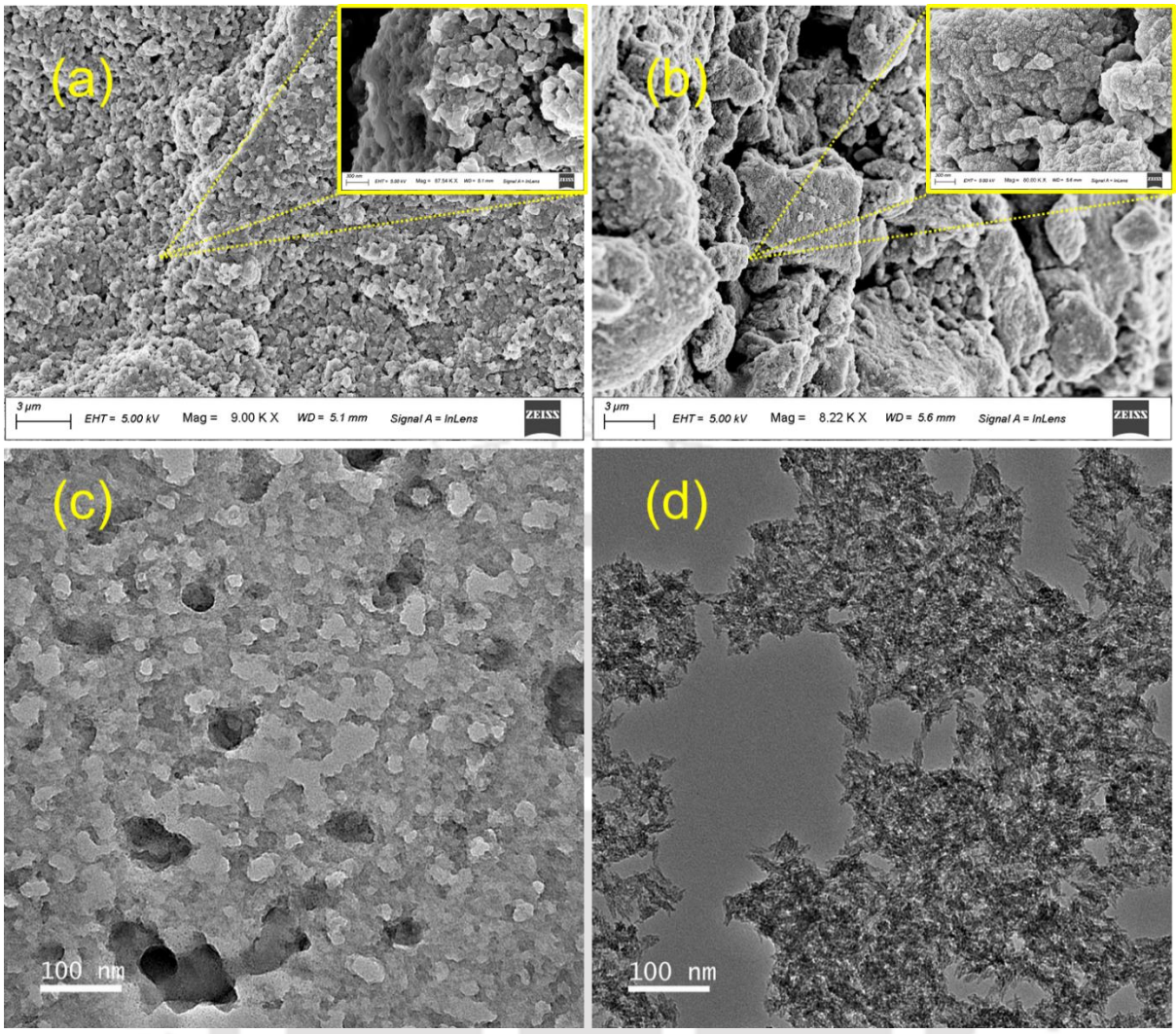

Figure 5.1. FESEM images of (a) TIEGel at 3 µm (inset: TIEGel at 300 nm) and (b) SIEGel at 3 µm (inset: SIEGel at 300 nm); FETEM images of (c) TIEGel at 100 nm and (d) SIEGel at 100 nm.

5.2.2. Structural Analysis

The impact of immobilization of the DES into a porous matrix on its structure was observed by performing FTIR on TIEGel and SIEGel and comparing the spectra with that of the DES. As seen from **Figure 5.2**a, the FTIR spectra of the eutectogels are very similar to that of the DES. The distinct strong bands at 1552 cm^{-1} in the spectrum of TIEGel and at 1042 cm^{-1} in that of SIEGel, could possibly be associated to the stretching vibrations of Ti−O−Ti[3] and Si−O−Si,[4] respectively. However, the content of titania or silica in the eutectogels is limited,

resulting in the domination of the DES vibrations. No additional absorption peaks otherwise are detected in the spectra of the eutectogels, indicating that the DES is not chemically bonded with TiO_2 or SiO_2. Thus, it can be concluded that the immobilization of the DES into the crosslinking matrix does not significantly alter the characteristics of the DES. Essentially, the components of the DES serve as a template for the matrix formation. Moreover, the similarity between the two spectra suggests that the DES is fully integrated within the matrix framework.[5] However, marginal shifts are observed in the vibrational bands of the eutectogels as compared to those of the DES. **Table 5.1** illustrates several such significant shifts in the vibrational bands of the DES and the eutectogels, along with their corresponding assignments.

The broad bands between 3500 and 3000 cm^{-1} in the spectra indicate the presence of traces of moisture that may have been adsorbed or absorbed by the systems during storage and handling.[2] The vibrational band at 2957 cm^{-1} of the DES corresponding to symmetric C−H stretching[6] is found to shift to 2960 and 2941 cm^{-1} for TIEGel and SIEGel, respectively. The interaction of the DES with the matrices is also confirmed by the change in the vibrational bands related to C=O stretching[6–8] from 1652 and 1560 cm^{-1} to 1717 and 1619 cm^{-1} in case of TIEGel, and 1710 and 1616 cm^{-1} in that of SIEGel. The peak related to C−N stretching[8] of the DES corresponding to the frequency 1361 cm^{-1} is seen to shift to 1368 and 1378 cm^{-1} for the two eutectogels, respectively. The peak for the vibrational band concerning the symmetric and asymmetric SO_3 stretching of the DES are observed at 1182 and 1039 cm^{-1}.[9] However, these are changed to 1167 and 1040 cm^{-1}, and 1153 and 956 cm^{-1} upon confinement into TiO_2 and SiO_2. The band peaks corresponding to 1456 and 768 cm^{-1} of the DES due to C−H bending[7,8] are shifted to 1460 and 899 cm^{-1}, and 1465 and 778 cm^{-1} after confinement into TiO_2 and SiO_2. A shift in frequency is also observed for N–H vibration; 525 cm^{-1} for the unconfined DES,[6] whereas the same for the titania- and silica-based eutectogels were obtained at 596 and 552 cm^{-}

[1]. The slight deviations in the new positions of the peaks seen in TIEGel and SIEGel suggest a distinction in the way the two matrices interact with the DES.

These observations are further supported by the Raman spectra of the three systems under consideration (**Figure 5.2**b), which, although similar, clearly differ in intensities and positions of their corresponding peaks. Distinctly evident are the shifts of the peaks corresponding to symmetric C−H stretching; C=O stretching; C−H bending; and SO_3 stretching from 2935; 1652; 1418, 875, and 770; and 1040 cm^{-1} in the spectrum of DES5 to 2940; 1703; 1420, 881, and 771; and 1051 cm^{-1} in that of TIEGel and 2941; 1720; 1419, 885, and 778; and 1047 cm^{-1} in that of SIEGel. These observations suggest the possible presence of weak non-bonded interactions between the DES molecules and the titania or silica moieties. These non-bonded interactions may have implications for the thermal characteristics of the immobilized solvent.[10]

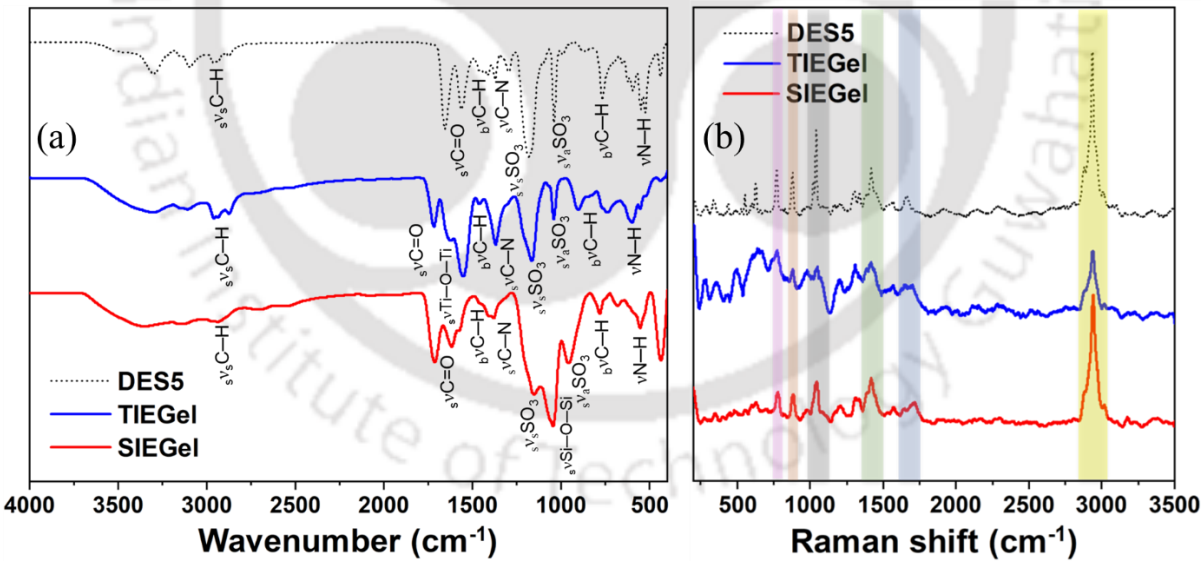

Figure 5.2. FTIR (a) and Raman (b) spectra of DES5, TIEGel, and SIEGel.

Table 5.1. Vibrational bands of DES5, TIEGel, and SIEGel with their respective assignments as observed from FTIR

Assignment	System		
	Vibrational band (cm^{-1})		
	DES5	TIEGel	SIEGel
${}_s\nu_s$C−H	2957	2960	2941
${}_s\nu$C=O	1652	1717	1710
${}_s\nu$C=O	1560	1619	1616
${}_s\nu$Ti−O−Ti	–	1552	–
${}_b\nu$C−H	1456	1460	1465
${}_s\nu$C−N	1361	1368	1378
${}_s\nu_s SO_3$	1182	1167	1153
${}_s\nu$Si−O−Si	–	–	1042
${}_s\nu_a SO_3$	1039	1040	956
${}_b\nu$C−H	768	899	778
νN−H	525	596	552

${}_s\nu_s$: symmetric stretching, ${}_s\nu$: stretching, ${}_b\nu$: bending, ${}_s\nu_a$: asymmetric stretching

XRD measurements were carried out on TIEGel and SIEGel to determine the degree of crystallinity of the samples. Consistent with previous research findings,[5,10–12] the XRD analysis of the inorganic eutectogels demonstrated the coexistence of a typical amorphous TiO_2 or SiO_2 matrix with the DES. The XRD patterns of the eutectogels depicted in **Figure 5.3** reveal weak and broad peaks, indicating the dominant amorphous or low-crystalline nature of the samples within the specified range of 2θ. The incorporation of DES disrupts the regular arrangement of the solid matrix, leading to an increase in the amorphous fraction of the material.

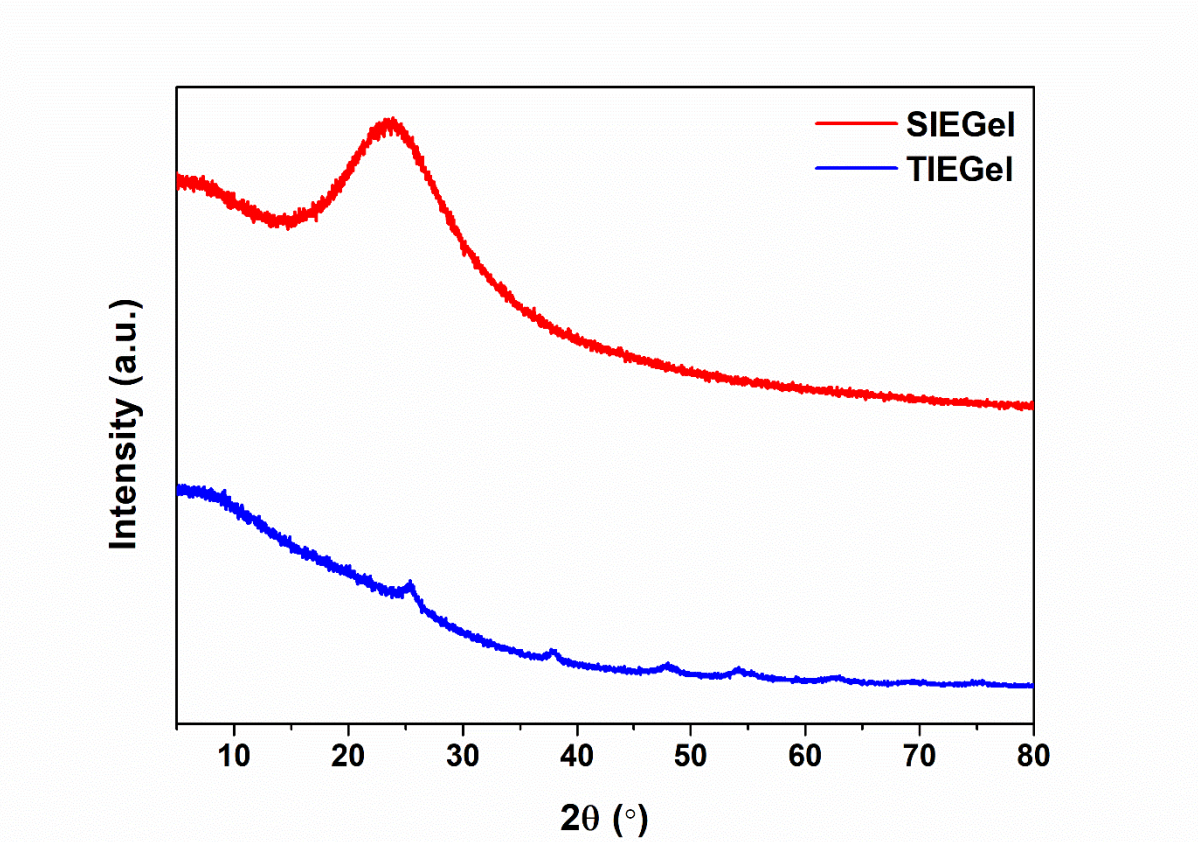

Figure 5.3. XRD patterns of TIEGel and SIEGel.

5.2.3. Thermal Analysis

Thermal analyses of DES5, TIEGel, and SIEGel were carried out via TGA on a TG 209 F1 Libra (Make: M/s Netzsch, Germany) under a nitrogen atmosphere between temperatures 30 and 400 °C[1] at a rate of 10 °C min^{-1} with a nitrogen flow of 40 mL min^{-1}. **Figure 5.4** shows the TGA thermograms of the DES and the eutectogels, wherein all three profiles are seen to undergo decomposition through a multi-step route. The DES exhibits insignificant loss in mass until a temperature of about 86 °C, which may be attributed to the elimination of moisture or impurities from the system.[1] Thereafter, the DES starts losing mass in the form of NMAc at ~89.9 °C, which may be considered as its onset degradation temperature. The eutectogels show a similar pattern of mass loss within the examined temperature window, however with relatively lower onset degradation temperatures. Both the IL [BMIM][$MeSO_3$][13] and NMAc[14]

are predominantly hydrophilic in nature, leading to the potential absorption and/or adsorption of substantial amount of moisture along with volatile impurities during storage and handling of the physically-crosslinked eutectogels. Moreover, the sample of the IL used here was not at its highest grade of purity (≥ 95 %) (**Table 2.1**) with the possible presence of inherent water and/or impurities. These possibly explain the initial loss of mass in the TGA profiles. The onset degradation temperatures of TIEGel and SIEGel stand at about 80.1 and 67 °C, respectively. The mass loss below this temperature for each system is possibly due to the release of organic residues.[10] On the other hand, the degradation step between the onset degradation temperatures and ~185 °C corresponds to the decomposition of NMAc. The samples show slow decomposition beyond 185 °C, indicating their good thermal stability.[15] The initiation of the second substantial mass loss for the DES appears at ~327 °C, which confirms the commencement of decomposition of the IL. The corresponding temperatures for TIEGel and SIEGel are ~340 and ~347 °C respectively, beyond which only the inorganic components remain (~35 and ~27 wt%). The incorporation of inorganic matrices leads to a reduction in the volatile phase content of the DES. The decomposition pattern of the DES is altered and the degradation temperatures of the components shifted on its confinement into the matrices. This confirms the existence of weak non-bonded interactions between the DES molecules and the titania or silica particles.[10] Variations in the degradation temperature windows of the DES components were also observed between TIEGel and SIEGel, further suggesting that titania interacts differently with the DES than silica.

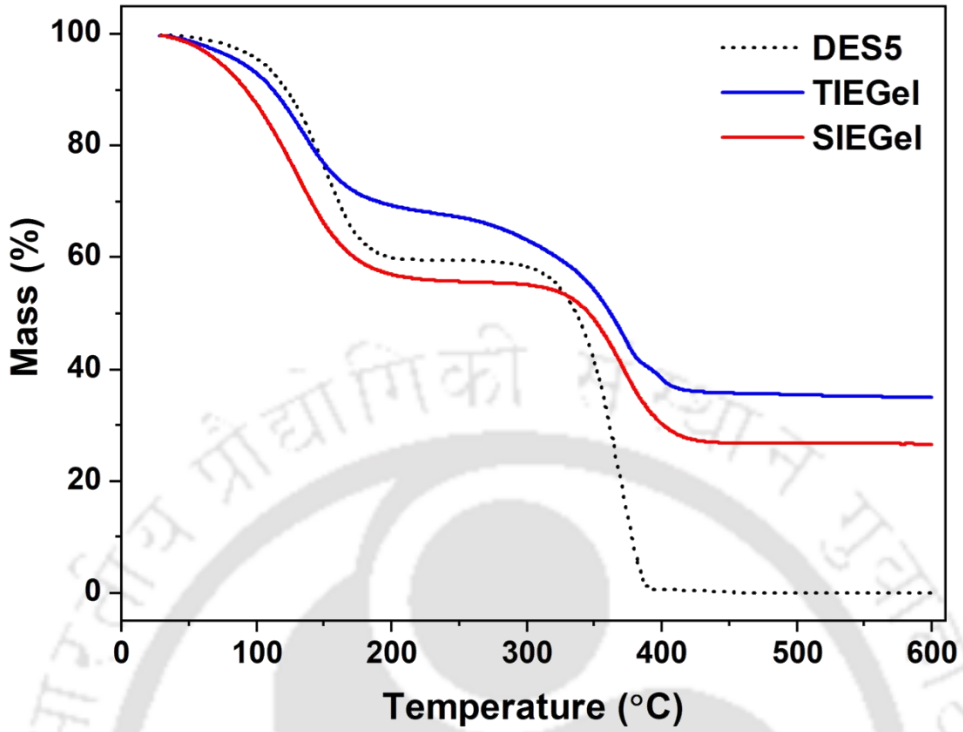

Figure 5.4. TGA thermograms of DES5, TIEGel, and SIEGel.

5.2.4. Electrochemical Performance

5.2.4.1. Cyclic Voltammetry

Figure 5.5a,b shows the cyclic voltammograms of TIEGel and SIEGel obtained at room temperature with the rGO-based two-electrode cell on a Gamry-interfaced CH Instruments, 600 C potentiostat (Gamry) at scan rates of 5, 10, 25, 50, and 100 mV s^{-1}. The quasi-rectangular CV profiles at all five scan rates indicate a capacitive behavior of the systems.[16,17] The absence of any redox peaks at each scan rate further indicates that the charge-storage mechanism is non-Faradaic or double-layer in nature within the potential window.[1,16,17] The presence of dissolved impurities and/or functional groups on the electrode surface may impart some pseudocapacitance. However, the linearity of the current indicates that the systems are predominantly non-Faradaic within the potential range.[18] SIEGel exhibits a relatively lower

peak current as compared to that of TIEGel. It may be noted that self-diffusivity of cations and anions in immobilized ILs may remain low on account of surface forces arising from the interaction between absorbed ions and matrix surface, leading to restricted kinetics.[19] The absence of an ideally polarizable reference electrode may also result in a poor current response.[20]

Nevertheless, both eutectogels are observed to consistently deliver double-layer capacitive behavior within a wide potential window of 3 V (-3 V to +3 V) against the porous rGO electrodes at all five scan rates of 5, 10, 25, 50, and 100 mV s^{-1}. Interestingly, the same DES is also able to deliver a potential window of 3 V with rGO electrodes when tested with a three-electrode cell.[1] Therefore, immobilization of the DES into TiO_2 or SiO_2 did not affect its OPW. The presence of the imidazolium-based IL in the DES may be acclaimed for the retention of the OPW of the DES after gelation by enhancing the electrochemical stability and weakening ionic interactions in the latter through cationic charge-delocalization.[21] Water content is also known to significantly influence the electrochemical stability of a solvent, with higher content of water resulting in a narrower potential window.[22] Therefore, the relatively low water content (~0.3 wt%) of the vacuum-dried DES, as evinced by Karl Fischer titration and ^{1}H NMR spectroscopy (**Figure C1**) may also be credited for the good OPW of TIEGel and SIEGel. The OPW obtained here is comparable to that of pertinent ionogels[23–31] and higher than that of eutectogels[32–36] reported in similar works (**Table 5.2**).

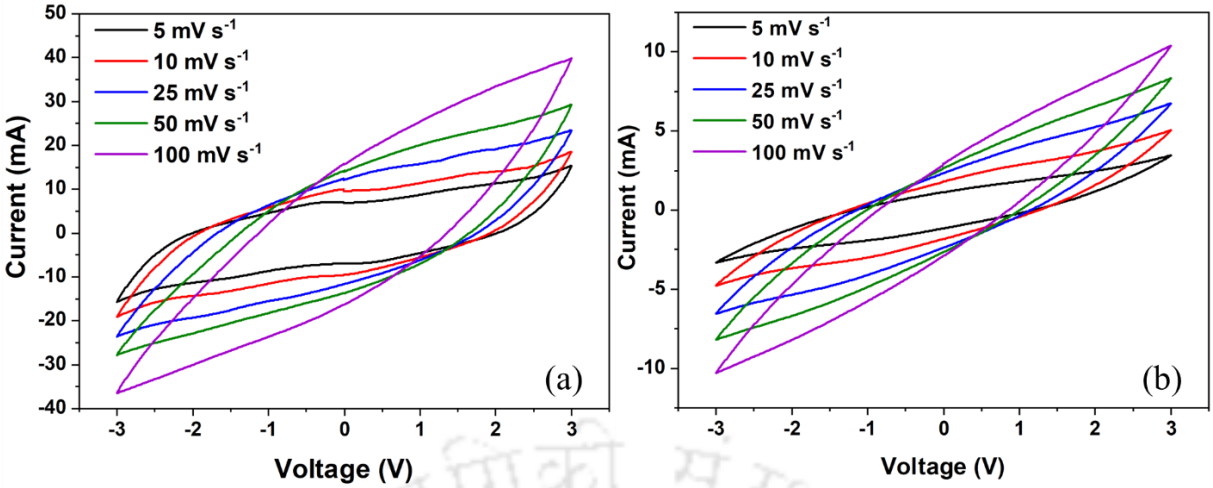

Figure 5.5. Cyclic voltammograms obtained at room temperature from CV conducted on the two-electrode coin-cell assembly with rGO electrodes at scan rates of 5, 10, 25, 50, and 100 mV s^{-1} for (a) TIEGel and (b) SIEGel.

Table 5.2. Comparison of the OPW of TIEGel and SIEGel with that of pertinent ionogels and eutectogels reported in similar works

System	Electrodes / Working electrode	Scan rate (mV s^{-1})	Temperature (°C)	OPW (V)
[BMIM][$MeSO_3$] + NMAc + TiO_2 (TIEGel)	rGO | rGO	5, 10, 25, 50, 100	25, 50, 80	3
[BMIM][$MeSO_3$] + NMAc + SiO_2 (SIEGel)	rGO | rGO	5, 10, 25, 50, 100	~25	3
[BMIM][BF_4] + DMAA + TiO_2[31]	carbon nanocage	–	25, 80, 100, 200	~3
[BMIM][PF_6] + PEGMA + PEGDA + TiO_2[29]	carbon nanocage	25	~25	3
[BMIM][BF_4] + DMAA + MBAA + TiO_2[28]	AC	–	25, 60, 100, 150, 200	~3
[BMIM][BF_4] + HEMA + TiO_2[30]	Au-Ti-coated AC	5, 10, 50, 100	~25	~3

Table 5.2 continues

System	Electrodes / Working electrode	Scan rate ($mV\ s^{-1}$)	Temperature (^oC)	OPW (V)
[EMIM][TFSI] + SiO_2[23]	glassy carbon	1000, 1600, 2500, 5000, 10000	~22	2.5
[EMIM][TFSI] + SiO_2[24]	VACNT	100, 1000, 10000, 100000, 500000	~25	3
[EMIM][TFSI] + SiO_2[26]	AC	2, 5, 10	~20–25	2.5
[EMIM][TFSI] + SiO_2[27]	carbon monolith	20	~25	2.5
[EMIM][TFSI] + DMDMS + SiO_2[25]	Si nanowires	50, 100, 200, 500, 1000, 2000, 5000, 10000	~25	2.5
ChCl + EG + HEMA + PEGDA[32]	ITO | ITO	1	~25	1.5
ChCl + urea + glycerol + cellulose + PAAM[33]	AC | AC	5, 10, 20, 50, 100	~25	2
EG + urea + ChCl +$ZnCl_2$ + silk fiber[34]	Zn | AC	1, 10, 20, 50	~25	1.4
$Zn(ClO_4)_2$ + AM + H_2O[35]	Zn | N-rGO	5, 10, 20, 30, 50, 100	~25	2.2
EG + $Zn(ClO_4)_2$ + H_2O +SPEEK + PAAM[36]	Zn | AC	5, 10, 20, 50, 100	~25	1.7

It is noteworthy that the potential window can vary based on several factors, including the electrode material, electrode configuration, properties of the electrolyte, ambient conditions, and the measurement method.[37,38] The use of a porous carbon electrode, for instance, can limit the anodic and cathodic stabilities of the electrolyte, resulting in a reduced potential window compared to inert electrodes such as gold and platinum.[1] Similarly, the potential window may shrink at high temperatures.[19]

Even commercial ILs obtained with the highest level of purity may contain certain impurities.[39] The purity of an electrolyte significantly affects its electrochemical stability,[1,39,40] and thus the OPW of the system. It may again be worth noting that the sample of [BMIM][$MeSO_3$] used in this work was not at its highest level of purity (≥ 95 %) (**Table 2.1**) and the constituent chemicals were utilized as received, without having undergone any additional purification steps. The presence of synthetic impurities can narrow the potential window, an impact that may be intensified by the presence of water.[39] A reduction in the potential window occurs at both the anodic and cathodic limits and can be attributed to the electrolysis of water, especially as the water content increases.[41] The redox peaks associated with dissolved impurities intrinsic to the IL become more prominent with an increase in water content.[39]

Table 5.3 tabulates the specific capacitance and specific energy delivered by the TIEGel- and SIEGel-based systems at the five scan rates. The maximum values of specific capacitance and specific energy for TIEGel and SIEGel were obtained at the scan rate of 5 mV s^{-1}. TIEGel delivered specific capacitances of 16.3 (395.8), 10.1 (245.4), 4.9 (121.0), 2.8 (67.3), and 1.6 (38.1) F g^{-1} (mF cm^{-2}) with specific energies of 20.4, 12.6, 6.2, 3.5, and 1.9 W h kg^{-1} at scan rates of 5, 10, 25, 50, and 100 mV s^{-1}, respectively. On the other hand, SIEGel procured specific capacitance values of 2.2 (54.5), 1.8 (44.4), 0.9 (23.4), 0.5 (12.9), and 0.3 (6.9) F g^{-1} (mF cm^{-2}) along with specific energies of 2.8, 2.3, 1.2, 0.7, and 0.4 W h kg^{-1} at the respective scan rates. Specific capacitance, and hence energy are significantly influenced by the characteristics of the electrode material, primarily its surface area and nature of porosity. Furthermore, the specific capacitance of a supercapacitor is also affected by mass loading of the electrolyte, along with the latter's diffusive properties and internal resistance.[1] TIEGel showed higher values for specific capacitance and specific energy. Because of the presence of the highly polar IL and the higher dielectric constant of TiO_2, the polarizing effect can be

stronger for TIEGel, promoting a higher degree of ionic dissociation than that of SIEGel, and hence increasing the charge density accumulated at the electrode/electrolyte interface. This resulted in an increased double-layer capacitance in the case of TIEGel.[42] Additionally, due to its wide OPW and decent capacitance, the energy contained by the same system is higher than that obtained with polymeric ionogels and rGO electrodes.[43] Moreover, the values for specific capacitance and energy are comparable to those of the ionogels discussed in Chapter 3 and much higher than those of the NADES-based eutectogels explored in Chapter 4 of this thesis, clearly indicating the advantages of the presence of the IL. The variation in specific capacitance (gravimetric and areal) and specific energy with scan rate for TIEGel and SIEGel is represented in **Figure 5.6**a–c. The profiles clearly reveal the effect of electrolyte starvation in the systems, leading to a reduced specific capacitance and specific energy at higher scan rates. The TIEGel-based system retained 62 % and ~10 % of its initial capacitance (and energy) at 10 mV s^{-1} and 100 mV s^{-1}, respectively. The SIEGel-supported device, however, was able to retain ~81 % and ~13 % of its initial capacitance (and energy) at the same two corresponding scan rates.

Table 5.3. Specific capacitance and specific energy of TIEGel and SIEGel at room temperature and scan rates of 5, 10, 25, 50, and 100 mV s^{-1}

System	Scan rate (mV s^{-1})	C_{sp} (F g^{-1})	C_{sp} (mF cm^{-2})	E_{sp} (W h kg^{-1})
TIEGel	5	16.32	395.78	20.39
	10	10.12	245.41	12.65
	25	4.99	121.05	6.24
	50	2.77	67.30	3.45
	100	1.57	38.09	1.96

Table 5.3 continues

System	Scan rate (mV s^{-1})	C_{sp} (F g^{-1})	C_{sp} (mF cm^{-2})	E_{sp} (W h kg^{-1})
SIEGel	5	2.25	54.53	2.81
	10	1.83	44.37	2.29
	25	0.96	23.39	1.21
	50	0.53	12.99	0.67
	100	0.29	6.97	0.36

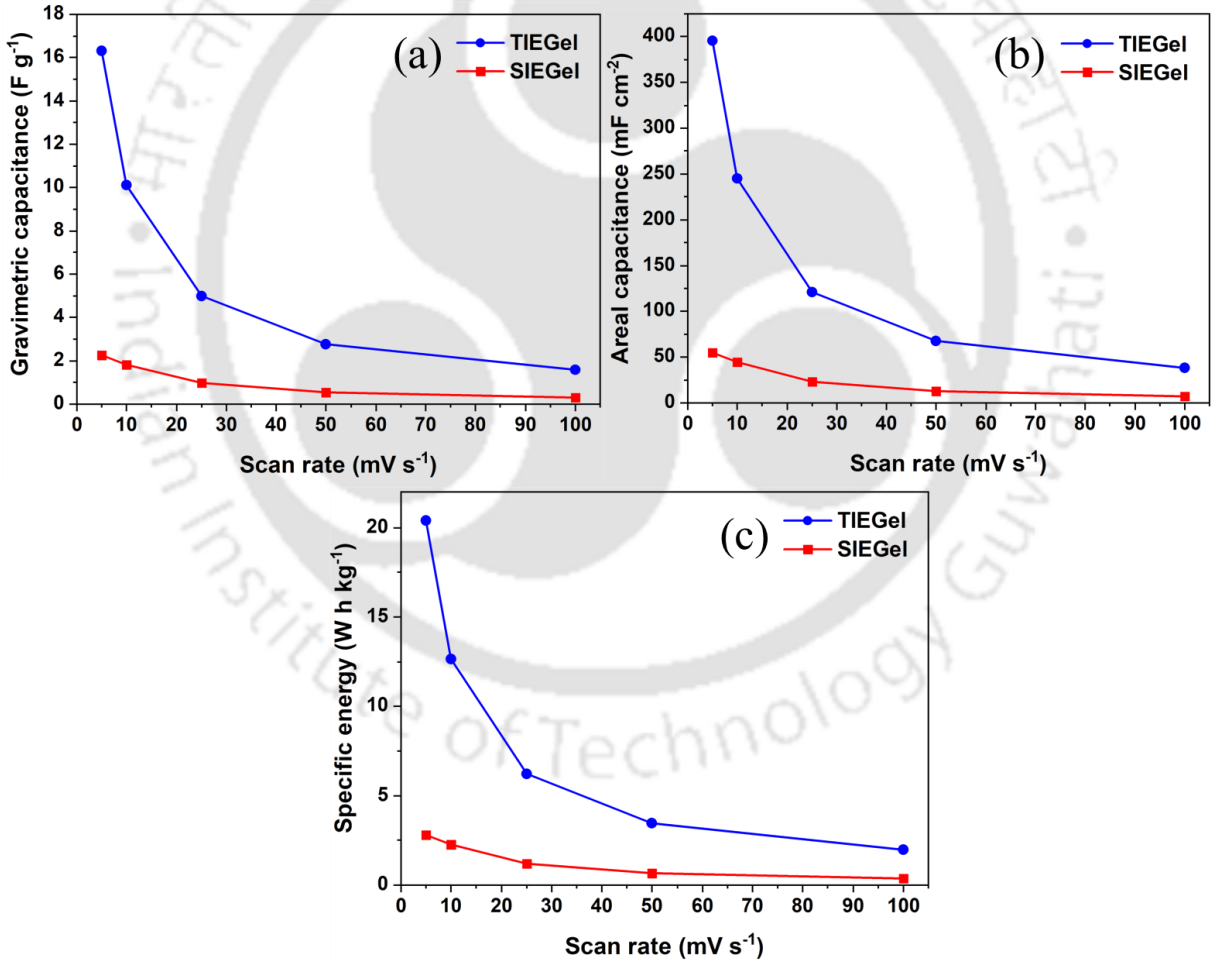

Figure 5.6. (a) Gravimetric capacitance, (b) areal capacitance, and (c) specific energy of TIEGel and SIEGel as a function of scan rate at room temperature.

CV was also performed on TIEGel at controlled temperatures of 25, 50, and 80 °C in the same potential range (-3 V to +3 V) using a second coin cell identical to the one used for the experiments at room temperature. The experiments were conducted at the same five scan rates on a PGSTAT101 Autolab potentiostat (Eco, Chemie, The Netherlands) interfaced to a Nova 2.1 software. The double-layer capacitive behavior and the 3 V OPW of the eutectogel were seen to remain unaltered with no trace of electrolyte degradation at the three temperatures for all five scan rates, revealing a stable performance of the system (**Figure 5.7**a–c). This points to the fact the thermal instability in the gel below 80 °C was largely due to entrapped moisture and volatile impurities. The higher current response at higher temperatures indicates faster kinetics, which is expected for such devices.[44] Elevated temperatures lead to better ionic mobility and dissociation of more ions into the electrode pores. This, in turn, increases the effective area at the electrode/electrolyte interface, resulting in higher specific capacitance.[45] The values of maximum specific capacitance and specific energy obtained at 5 mV s^{-1} and 25 °C were 8.5 F g^{-1} (205.8 mF cm^{-2}) and 10.6 W h kg^{-1}, respectively (**Table 5.4**). At 50 °C, the corresponding values almost doubled to 16.4 F g^{-1} (397.5 mF cm^{-2}) and 20.5 W h kg^{-1}. However, at 80 °C, the values for the same parameters increased by a factor of 3 as compared to those at 25 °C and stood at 25.8 F g^{-1} (625.9 mF cm^{-2}) and 32.3 W h kg^{-1}.

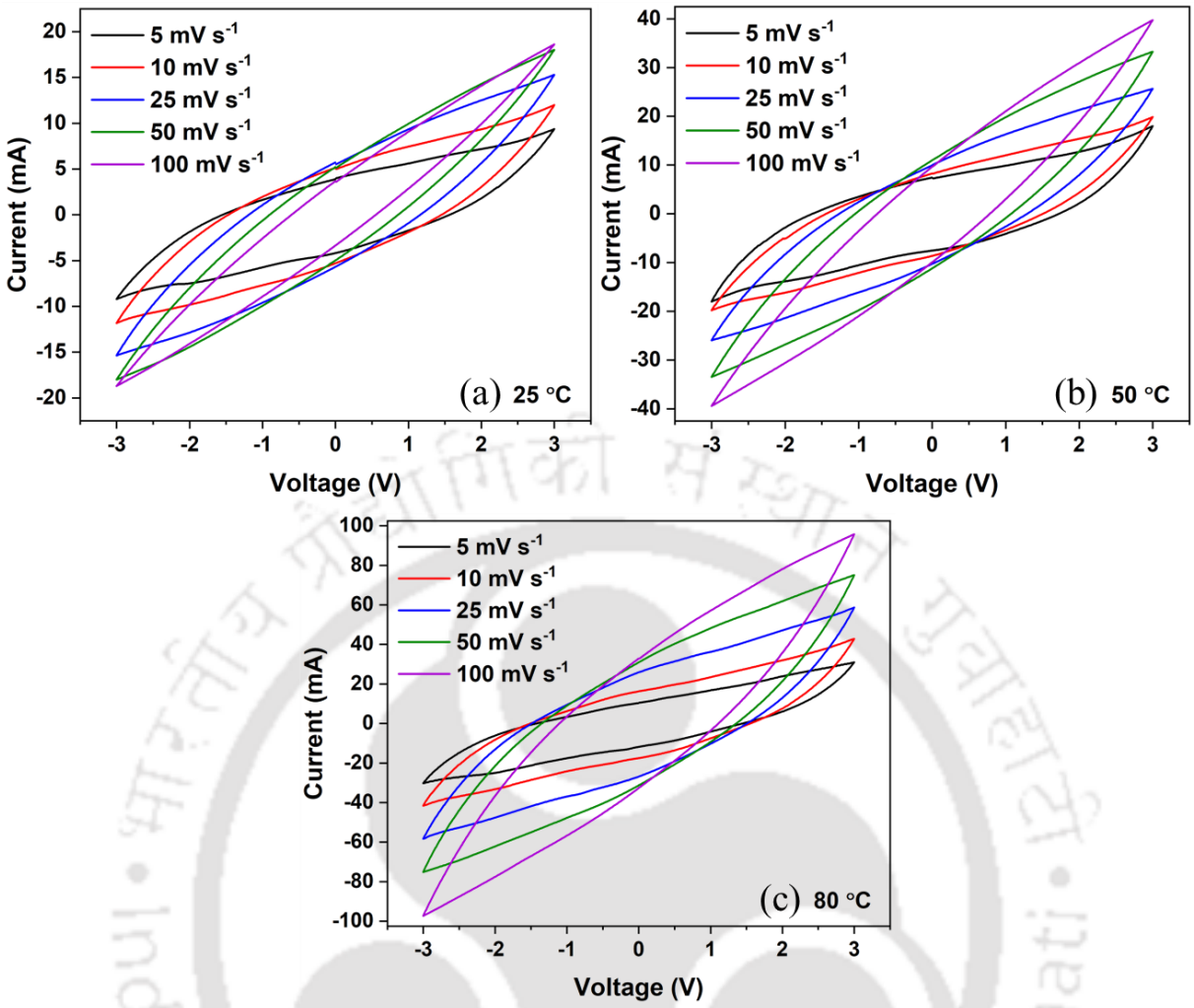

Figure 5.7. Cyclic voltammograms of the TIEGel-based system obtained from CV conducted using the two-electrode coin-cell assembly with rGO electrodes at scan rates of 5, 10, 25, 50, and 100 mV s^{-1} at controlled temperatures of (a) 25 °C, (b) 50 °C, and (c) 80 °C.

Table 5.4. Specific capacitance and specific energy of TIEGel at scan rates of 5, 10, 25, 50, and 100 mV s^{-1} and controlled temperatures of 25, 50, and 80 °C

Temperature (°C)	Scan rate (mV s^{-1})	C_{sp} (F g^{-1})	C_{sp} (mF cm^{-2})	E_{sp} (W h kg^{-1})
25	5	8.49	205.84	10.61
	10	5.34	129.47	6.67
	25	2.33	56.53	2.91
	50	1.03	24.98	1.29
	100	0.35	8.50	0.44
50	5	16.39	397.53	20.49
	10	8.74	212.06	10.93
	25	4.24	102.85	5.30
	50	2.29	55.44	2.86
	100	0.98	23.79	1.23
80	5	25.81	625.97	32.26
	10	18.40	446.39	23.00
	25	10.79	261.80	13.49
	50	6.51	157.82	8.13
	100	3.39	82.13	4.23

At 25 °C, TIEGel delivered specific capacitances of 5.3 (129.5), 2.3 (56.5), 1.0 (24.9), and 0.4 (8.5) F g^{-1} (mF cm^{-2}) with specific energies of 6.7, 2.9. 1.3, and 0.4 W h kg^{-1} at scan rates of 10, 25, 50, and 100 mV s^{-1}, respectively. At 50 °C, it achieved capacitance values of 8.7 (212.1), 4.2 (102.9), 2.3 (55.4), and 0.9 (23.8) F g^{-1} (mF cm^{-2}) with specific energies of 10.9, 5.3, 2.9, and 1.2 W h kg^{-1} for the same respective scan rates. On the other hand, the same system procured specific capacitance values of 18.4 (446.4), 10.8 (261.8), 6.5 (157.8), and 3.4 (82.1) F g^{-1} (mF cm^{-2}) with specific energy of 23.0, 13.5, 8.1, and 4.2 W h kg^{-1} for the

corresponding scan rates at 80 °C. A difference in values of capacitance was observed for the same eutectogel when conducted at room temperature and at a controlled temperature of 25 °C. This may chiefly be attributed to the possible differences in temperatures, mass of sample loaded, and the utilization of two different coin cells. The variation in specific capacitance (gravimetric and areal) and specific energy with scan rate for 25, 50, and 80 °C is represented in **Figure 5.8**a–c. The profiles again show the existence of electrolyte starvation effect in the system at each temperature, leading to a reduced specific capacitance and specific energy at higher scan rates. At 25 °C, the device was able to retain ~63 % and ~4 % of its initial capacitance (and energy) at 10 mV s^{-1} and 100 mV s^{-1}, respectively. It exhibited a capacity (and energy) retention of ~53 % and ~6 % at the same respective scan rates and 50 °C. Interestingly, ~71 % and ~13 % of capacitance (and energy) was retained by the system at 80 °C. The faster decay of capacitance at a higher temperature (50 °C) is in agreement with findings reported previously,[46] and may be attributed to the faster kinetics of the system. Nonetheless, a slower rate of capacitance decay at an even higher temperature of 80 °C is also consistent with previous observations at high temperatures as this.[44] This could be because of the acquisition of better homogeneity of the gel after a certain temperature threshold, leading to better wetting of carbon particles in the electrodes and the formation of a bicontinuous DES/matrix network interface. It may also be noted that the temperature under consideration (80 °C) is quite close to the maximum operational temperature limit of DES5 (~89.9 °C), which leaves the possibility for the domination of the desirable DES properties at that temperature that otherwise remain restricted in gelated form at lower temperatures. Also, at higher temperatures close to 100 °C, a greater amount of unwanted impurities, especially in the form of water and organic residues are susceptible to evaporate, leaving behind a purer gel with the ability to perform better.

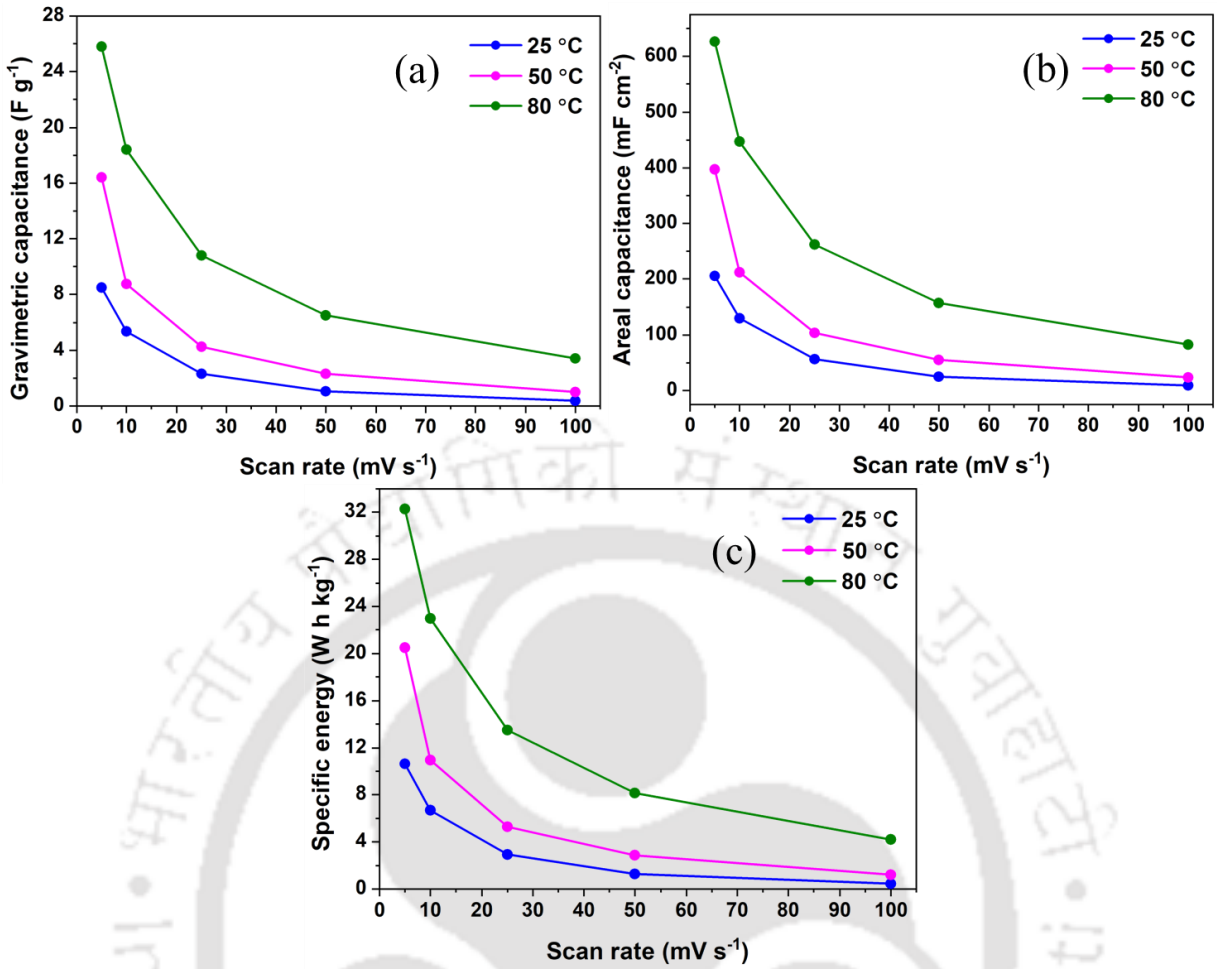

Figure 5.8. (a) Gravimetric capacitance, (b) areal capacitance, and (c) specific energy of TIEGel as a function of scan rate at controlled temperatures of 25, 50, and 80 °C.

5.2.4.2. Electrochemical Impedance Spectroscopy

EIS was performed on TIEGel and SIEGel at the OCP by applying an AC voltage of 5 mV in the frequency range of 0.01 Hz to 100 kHz. The experiments were conducted at room temperature using the rGO-based two-electrode coin-cell system on a Gamry-interfaced CH Instruments, 600 C potentiostat (Gamry). **Figure 5.9** shows the Nyquist plots obtained with the eutectogel samples. Confirming the findings from CV, both eutectogels are seen to exhibit typical EDLC characteristics. The presence of a Warburg element in the plots is a result of the frequency dependence of ion diffusion/transport in the ionogels sandwiched between the porous rGO electrodes.[44] R_s, R_{ct}, and ESR of each eutectogel were determined from its

corresponding Nyquist plot. Thereafter, the ionic conductivity (σ) of the sample and power (P) delivered by the device were calculated using **equations 2.15** (t ~ 0.1 cm) and **1.2**, respectively. The data have been tabulated in **Table 5.5**.

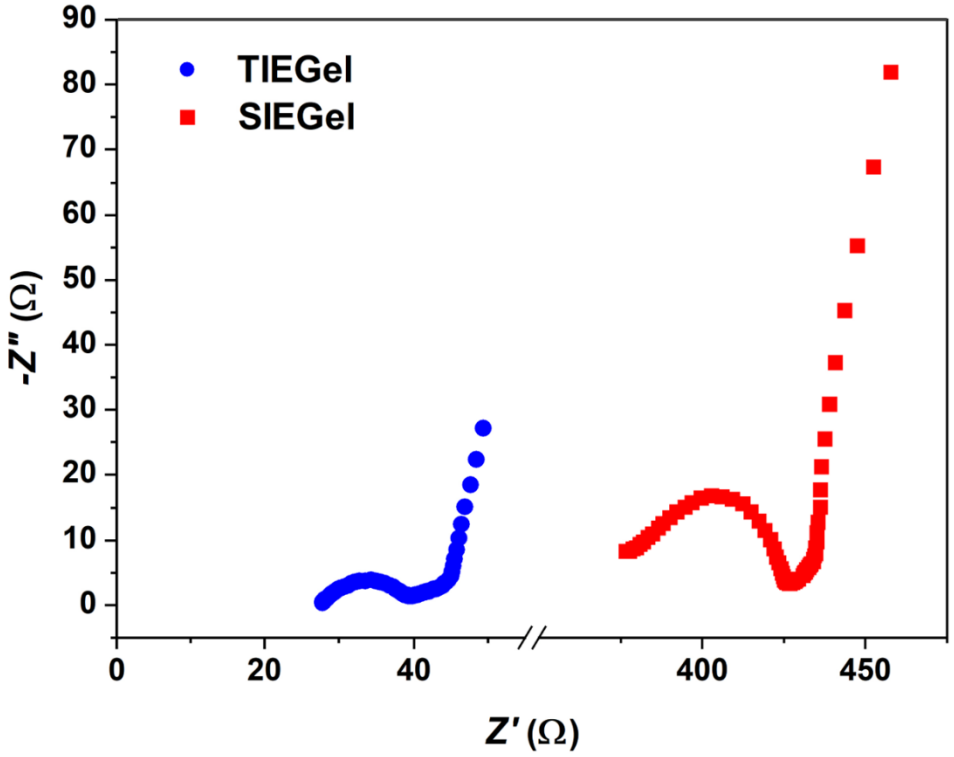

Figure 5.9. Nyquist plots of the systems obtained from EIS conducted on the rGO-based two-electrode coin cell with the TIEGel and SIEGel electrolytes at room temperature.

Table 5.5. Solution resistance, charge-transfer resistance, equivalent series resistance, ionic conductivity, and power associated with TIEGel and SIEGel at room temperature

System	R_s (Ω)	R_{ct} (Ω)	ESR (Ω)	σ (mS cm^{-1})	P (kW kg^{-1})
TIEGel	27.77	11.83	39.60	1.27	3.31
SIEGel	376.66	50.14	426.80	0.09	0.31

Indication of restricted kinetics could be found in both the gels in the form of intrinsic resistance possibly due to interactions between absorbed ions and matrix surface, resulting in low self-diffusivity.[19] TIEGel exhibited a lower ESR (39.6 Ω) with a higher ionic conductivity of 1.3 mS cm^{-1}, the value being in agreement with that reported for other sol-gel-derived IL-based inorganic gels.[26,47] Consequently, the device loaded with the same eutectogel delivered a decent power of 3.3 kW kg^{-1}, which is, however, still higher than that of other non-IL eutectogels experimented with supercapacitors previously.[32–36] The higher dielectric constant of TiO_2 may have facilitated better ionic conduction of TIEGel in the presence of the IL.[42] The SIEGel, however, possessed lower conductivity (~0.1 mS cm^{-1}) and a much higher ESR (426.8 Ω) owing to the high solution resistance in the system (376.7 Ω), suggesting a slower ion transport than that of its titania-based counterpart. These observations are in agreement with those of other sol-gel-derived TiO_2- and SiO_2-confined IL-based gels reported previously.[5,26] Due to the high ESR, the SIEGel-based cell was able to deliver less power comparatively (0.3 kW kg^{-1}). Nonetheless, the values of ionic conductivity and power obtained in either case are still comparable to those of the ionogels explored in Chapter 3 and much higher than those of the titania-based NADES gels discussed in Chapter 4 of this thesis, confirming the advantages of the presence of the IL. This may be attributed to the low room-temperature viscosity of the DES (~15 mPa s)[1] and good wettability of its components,[13,14] in addition to an increased charge distribution owing to delocalization of the $[BMIM]^+$ cation.[21] The findings are consistent with the results obtained from cyclic voltammetry. Despite the unimpressive conductivities of the eutectogels, they exhibit excellent compatibility with the rGO electrodes, allowing for a wide OPW and resulting in high-performance EDLCs.

EIS was further conducted on TIEGel at the controlled temperatures of 25, 50, and 80 °C using a different coin cell, the one used to perform CV on the same eutectogel at the said temperatures. The experiments were conducted on a PGSTAT101 Autolab potentiostat (Eco,

Chemie, The Netherlands) interfaced to a Nova 2.1 software. The Nyquist plots confirm that the system was able to maintain its EDLC nature at each temperature (**Figure 5.10**). This corroborates the fact that the thermal instability in the gel below 80 °C was chiefly due to entrapped moisture and volatile impurities. EIS at the higher temperatures yielded lower solution and charge-transfer resistances, thus reconfirming the occurrence of faster kinetics at higher temperatures. High temperature facilitates the formation of self-assembled ionic channels, thus reducing resistance and enhancing faster transfer of charges.[35,44] The calculated resistances, along with the ionic conductivity and power of the system at each temperature are shown in **Table 5.6**. Lower values of R_s and R_{ct} at 50 and 80 °C confirm faster charge transfer. The ionic conductivity at 25 °C (~0.6 mS cm^{-1}) is almost doubled at 50 °C (~1.1 mS cm^{-1}) and is increased by a factor of 4.4 at 80 °C (2.4 mS cm^{-1}). It is noteworthy that the ESR of the ionogel at 25 °C (111.3 Ω), however, is reduced just by a factor of 1.8 at 50 °C (60.6 Ω) and by a factor of 3.4 at 80 °C (~33 Ω). This indicates that the cell resistance is mainly governed by the diffusion of ions in the electrode pores.[44] The specific power is seen to increase from 1.2 kW kg^{-1} at 25 °C to 2.2 and ~4 kW kg^{-1} at 50 and 80 °C, respectively. Possible differences in temperatures and mass of sample loaded, along with the use of two different coin cells may again be largely accounted for the variation in values of resistances and ionic conductivity of the same eutectogel conducted at room temperature and at a controlled temperature of 25 °C.

Table 5.6. Solution resistance, charge-transfer resistance, equivalent series resistance, ionic conductivity, and power associated with TIEGel at 25, 50, and 80 °C

Temperature (°C)	R_s (Ω)	R_{ct} (Ω)	**ESR** (Ω)	σ (mS cm^{-1})	P (kW kg^{-1})
25	63.64	47.66	111.30	0.55	1.18
50	32.39	28.17	60.56	1.09	2.16
80	14.62	18.34	32.96	2.41	3.97

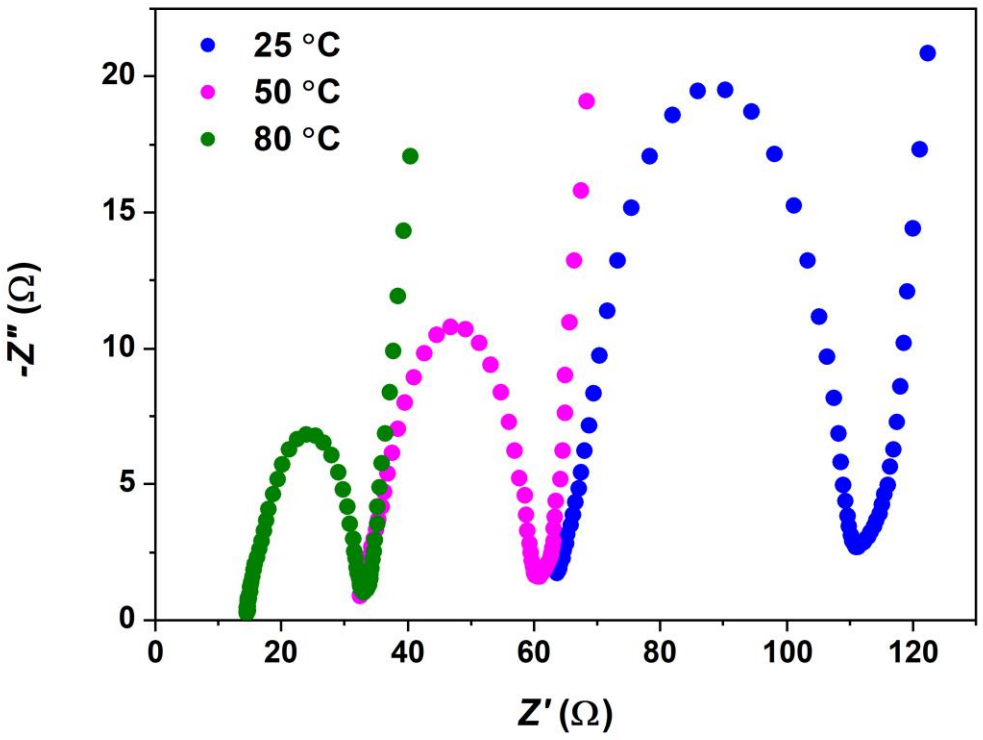

Figure 5.10. Nyquist plots of the system obtained from EIS conducted on the rGO-based two-electrode coin cell with TIEGel electrolyte at 25, 50, and 80 °C.

5.3. Conclusions

The two eutectogels were obtained via a simple sol−gel strategy by the physical confinement of the IL-based hybrid DES ([BMIM][$MeSO_3$] + NMAc) into TiO_2 or SiO_2 derived respectively from TBOT or TEOS. The eutectogels were obtained in amorphous solid form with apparent porosity and interconnected aggregates of titania or silica particles, as confirmed from XRD, FESEM, and FETEM studies. FTIR and Raman analyses indicated that the structural integrity of the DES was not affected by its confinement into the solid matrices, thus confirming gelation through a physical crosslinking. However, marginal shifts in vibrational frequencies of the eutectogels were noticed owing to non-bonded interactions between the pore wall surfaces of the TiO_2 or SiO_2 moieties and DES molecules. TGA analyses showed that the

thermal stability and decomposition temperatures of the DES components tend to alter after gelation, which may again be a consequence of the weak interactions between the DES and the matrices. Nonetheless, the stability windows of the eutectogels are sufficient for potential moderate- to high-temperature applications. The difference in the interactive nature of TiO_2 and SiO_2 with the DES was revealed by the variation in the IR vibrational shifts and degradation temperatures of the two eutectogels.

From the electrochemical perspective, both eutectogels retain the double-layer capacitive behavior of the liquid DES within a wide potential window of 3 V, primarily due to the cationic charge delocalization of the imidazolium IL, which results in an enhanced electrochemical stability. This highlights their good compatibility with rGO electrodes and excellent stability in applications with EDLCs. TIEGel showed higher values for specific capacitance (16.3 F g^{-1} or 395.8 mF cm^{-2}) and specific energy (20.4 W h kg^{-1}) because of the higher dielectric constant of TiO_2, leading to a stronger polarizing effect in the presence of the IL and an increased accumulation of charge density at the electrode/electrolyte interface. As such, the same eutectogel also possesses a lower ESR (39.6 Ω) and a higher ionic conductivity (1.3 mS cm^{-1}). However, decent values for specific power are obtained for both SIEGel and TIEGel due to restricted kinetics and a fairly high intrinsic resistance, with the latter obviously delivering a higher value (3.3 kW kg^{-1}). TIEGel is also able to maintain its OPW and EDLC characteristics at controlled temperatures of 25, 50, and 80 °C while increasing its specific capacitance and ionic conductivity by factors of 3 and 4.4 respectively, at 80 °C.

The characteristics observed herein are fairly comparable to those of relevant ionogels and eutectogels reported previously. Meanwhile, the performance of the two eutectogels discussed in this chapter are at par with that of the ionogels enlisted in Chapter 3 and mostly superior to that of the NADES-based eutectogels studied in Chapter 4 of this thesis, clearly indicating the advantages of the presence of an IL. This is chiefly due to the good

electrochemical stability and better ionicity of the constituent IL, in addition to good wettability and low room-temperature viscosity of the DES. Especially, the acquisition of comparable characteristics with the utilization of lesser quantity of IL as compared to that in ionogels renders these eutectogels more economical. It may thus be concluded that the IL-based eutectogels have the potential to be utilized as cost-effective stable electrolytes in electrochemical storage applications, especially in EDLCs as well as other pertinent realms of electrochemistry. Additionally, the promising characteristics of the gels may provide an appealing route for researchers to undertake further research on the integration of other materials for further enhancement of capacitance and ionic conductivity.

References

(1) Mahanta, U.; Choudhury, S.; Venkatesh, R. P.; SarojiniAmma, S.; Ilangovan, S. A.; Banerjee, T. Ionic-Liquid-Based Deep Eutectic Solvents as Novel Electrolytes for Supercapacitors: COSMO-SAC Predictions, Synthesis, and Characterization. *ACS Sustain Chem Eng* **2020**, *8* (1), 372–381. https://doi.org/10.1021/acssuschemeng.9b05596.

(2) Joos, B.; Vranken, T.; Marchal, W.; Safari, M.; Van Bael, M. K.; Hardy, A. T. Eutectogels: A New Class of Solid Composite Electrolytes for Li/Li-Ion Batteries. *Chemistry of Materials* **2018**, *30* (3), 655–662. https://doi.org/10.1021/acs.chemmater.7b03736.

(3) Vetrivel, V.; Rajendran, K.; Kalaiselvi, V. *Synthesis and Characterization of Pure Titanium Dioxide Nanoparticles by Sol-Gel Method*; 2014; Vol. 7.

(4) Saravanan, S.; Dubey, R. S. Synthesis of SiO2 Nanoparticles by Sol-Gel Method and Their Optical and Structural Properties. *Romanian Journal of Information Science and Technology* **2020**, *23* (1), 105–112.

(5) Wu, F.; Chen, N.; Chen, R.; Zhu, Q.; Tan, G.; Li, L. Self-Regulative Nanogelator Solid Electrolyte: A New Option to Improve the Safety of Lithium Battery. *Advanced Science* **2016**, *3* (1). https://doi.org/10.1002/advs.201500306.

(6) Ji, Y.; Yang, X.; Ji, Z.; Zhu, L.; Ma, N.; Chen, D.; Jia, X.; Tang, J.; Cao, Y. DFT-Calculated IR Spectrum Amide I, II, and III Band Contributions of *N* -Methylacetamide Fine Components. *ACS Omega* **2020**, *5* (15), 8572–8578. https://doi.org/10.1021/acsomega.9b04421.

(7) Furer, V. L. The IR Spectra of N-Methylacetamide Chain Associates. *J Mol Struct* **1997**, *435* (2), 151–155. https://doi.org/10.1016/S0022-2860(97)00171-3.

(8) Gaigeot, M. P.; Vuilleumier, R.; Sprik, M.; Borgis, D. Infrared Spectroscopy of *N* -Methylacetamide Revisited by Ab Initio Molecular Dynamics Simulations. *J Chem Theory Comput* **2005**, *1* (5), 772–789. https://doi.org/10.1021/ct050029z.

(9) Zeeshan, M.; Kulak, H.; Kavak, S.; Polat, H. M.; Durak, O.; Keskin, S.; Uzun, A. Influence of Anion Size and Electronic Structure on the Gas Separation Performance of Ionic Liquid/ZIF-8 Composites. *Microporous and Mesoporous Materials* **2020**, *306*, 110446. https://doi.org/10.1016/j.micromeso.2020.110446.

(10) Verma, Y. L.; Tripathi, A. K.; Shalu; Singh, V. K.; Balo, L.; Gupta, H.; Singh, S. K.; Singh, R. K. Preparation and Properties of Titania Based Ionogels Synthesized Using Ionic Liquid 1-Ethyl-3-Methyl Imidazolium Thiocyanate. *Materials Science and Engineering: B* **2017**, *220*, 37–43. https://doi.org/10.1016/j.mseb.2017.03.010.

(11) Li, X.; Zhang, Z.; Yang, L.; Tachibana, K.; Hirano, S. TiO2-Based Ionogel Electrolytes for Lithium Metal Batteries. *J Power Sources* **2015**, *293*, 831–834. https://doi.org/10.1016/j.jpowsour.2015.06.033.

(12) Li, Z.; Zhang, S.; Jiang, Z.; Cai, D.; Gu, C.; Tu, J. Deep Eutectic Solvent-Immobilized PVDF-HFP Eutectogel as Solid Electrolyte for Safe Lithium Metal Battery. *Mater Chem Phys* **2021**, *267*, 124701. https://doi.org/10.1016/j.matchemphys.2021.124701.

(13) Augé, J.; Sizun, G. Ionic Liquid Promoted Atom Economic Glycosylation under Lewis Acid Catalysis. *Green Chemistry* **2009**, *11* (8), 1179. https://doi.org/10.1039/b904692e.

(14) Herrebout, W. A.; Clou, K.; Desseyn, H. O. Vibrational Spectroscopy of *N* -Methylacetamide Revisited. *J Phys Chem A* **2001**, *105* (20), 4865–4881. https://doi.org/10.1021/jp004396c.

(15) Wang, J.; Zhan, B.; Zhang, S.; Wang, Y.; Yan, L. Freeze-Resistant, Conductive, and Robust Eutectogels of Metal Salt-Based Deep Eutectic Solvents with Poly(Vinyl Alcohol). *ACS Appl Polym Mater* **2022**, *4* (3), 2057–2064. https://doi.org/10.1021/acsapm.1c01899.

(16) Pilathottathil, S.; Thasneema, K. K.; Shahin Thayyil, M.; Pillai, M. P.; Niveditha, C. V. A High Voltage Supercapacitor Based on Ionic Liquid with an Activated Carbon Electrode. *Mater Res Express* **2017**, *4* (7), 075503. https://doi.org/10.1088/2053-1591/aa7116.

(17) Hamsan, M. H.; Aziz, S. B.; Kadir, M. F. Z.; Brza, M. A.; Karim, W. O. The Study of EDLC Device Fabricated from Plasticized Magnesium Ion Conducting Chitosan Based Polymer Electrolyte. *Polym Test* **2020**, *90*, 106714. https://doi.org/10.1016/j.polymertesting.2020.106714.

(18) Shabeeba, P.; Thasneema, K. K.; Thayyil, M. S.; Pillai, M. P.; Niveditha, C. V. A Graphene-Based Flexible Supercapacitor Using Trihexyl(Tetradecyl)Phosphonium Bis(Trifluoromethanesulfonyl)Imide Ionic Liquid Electrolyte. *Mater Res Express* **2017**, *4* (8), 085501. https://doi.org/10.1088/2053-1591/aa7b14.

(19) Chen, N.; Zhang, H.; Li, L.; Chen, R.; Guo, S. Ionogel Electrolytes for High-Performance Lithium Batteries: A Review. *Advanced Energy Materials*. Wiley-VCH Verlag April 25, 2018. https://doi.org/10.1002/aenm.201702675.

(20) López Zavala, M. Á.; González Peña, O. I.; Cabral Ruelas, H.; Delgado Mena, C.; Guizani, M. Use of Cyclic Voltammetry to Describe the Electrochemical Behavior of a Dual-Chamber Microbial Fuel Cell. *Energies (Basel)* **2019**, *12* (18), 3532. https://doi.org/10.3390/en12183532.

(21) Kavanagh, A.; Copperwhite, R.; Oubaha, M.; Owens, J.; McDonagh, C.; Diamond, D.; Byrne, R. Photo-Patternable Hybrid Ionogels for Electrochromic Applications. *J Mater Chem* **2011**, *21* (24), 8687. https://doi.org/10.1039/c1jm10704f.

(22) Espinoza, E. M.; Clark, J. A.; Soliman, J.; Derr, J. B.; Morales, M.; Vullev, V. I. Practical Aspects of Cyclic Voltammetry: How to Estimate Reduction Potentials When Irreversibility Prevails. *J Electrochem Soc* **2019**, *166* (5), H3175–H3187. https://doi.org/10.1149/2.0241905jes.

(23) Horowitz, A. I.; Panzer, M. J. High-Performance, Mechanically Compliant Silica-Based Ionogels for Electrical Energy Storage Applications. *J Mater Chem* **2012**, *22* (32), 16534. https://doi.org/10.1039/c2jm33496h.

(24) Hsia, B.; Marschewski, J.; Wang, S.; In, J. Bin; Carraro, C.; Poulikakos, D.; Grigoropoulos, C. P.; Maboudian, R. Highly Flexible, All Solid-State Micro-

Supercapacitors from Vertically Aligned Carbon Nanotubes. *Nanotechnology* **2014**, *25* (5), 055401. https://doi.org/10.1088/0957-4484/25/5/055401.

(25) Brachet, M.; Gaboriau, D.; Gentile, P.; Fantini, S.; Bidan, G.; Sadki, S.; Brousse, T.; Le Bideau, J. Solder-Reflow Resistant Solid-State Micro-Supercapacitors Based on Ionogels. *J Mater Chem A Mater* **2016**, *4* (30), 11835–11843. https://doi.org/10.1039/C6TA03142K.

(26) Brachet, M.; Brousse, T.; Le Bideau, J. All Solid-State Symmetrical Activated Carbon Electrochemical Double Layer Capacitors Designed with Ionogel Electrolyte. *ECS Electrochemistry Letters* **2014**, *3* (11), A112–A115. https://doi.org/10.1149/2.0051411eel.

(27) Zhu, S.; Taberna, P.-L.; Zhao, N.; Simon, P. Salt-Template Synthesis of Mesoporous Carbon Monolith for Ionogel-Based Supercapacitors. *Electrochem commun* **2018**, *96*, 6–10. https://doi.org/10.1016/j.elecom.2018.09.003.

(28) Liu, X.; Wu, B.; Brandon, N.; Wang, Q. Tough Ionogel-in-Mask Hybrid Gel Electrolytes in Supercapacitors with Durable Pressure and Thermal Tolerances. *Energy Technology* **2017**, *5* (2), 220–224. https://doi.org/10.1002/ente.201600251.

(29) Liu, X.; Wang, B.; Jin, Z.; Wang, H.; Wang, Q. Elastic Ionogels with Freeze-Aligned Pores Exhibit Enhanced Electrochemical Performances as Anisotropic Electrolytes of All-Solid-State Supercapacitors. *J Mater Chem A Mater* **2015**, *3* (30), 15408–15412. https://doi.org/10.1039/C5TA03184B.

(30) Liu, X.; He, B.; Wang, Z.; Tang, H.; Su, T.; Wang, Q. Tough Nanocomposite Ionogel-Based Actuator Exhibits Robust Performance. *Sci Rep* **2014**, *4* (1), 6673. https://doi.org/10.1038/srep06673.

(31) Liu, X.; Taiwo, O. O.; Yin, C.; Ouyang, M.; Chowdhury, R.; Wang, B.; Wang, H.; Wu, B.; Brandon, N. P.; Wang, Q.; Cooper, S. J. Aligned Ionogel Electrolytes for High-Temperature Supercapacitors. *Advanced Science* **2019**, *6* (5). https://doi.org/10.1002/advs.201801337.

(32) Qin, H.; Panzer, M. J. Chemically Cross-Linked Poly(2-hydroxyethyl Methacrylate)-Supported Deep Eutectic Solvent Gel Electrolytes for Eco-Friendly Supercapacitors. *ChemElectroChem* **2017**, *4* (10), 2556–2562. https://doi.org/10.1002/celc.201700586.

(33) Hong, S.; Yuan, Y.; Liu, C.; Chen, W.; Chen, L.; Lian, H.; Liimatainen, H. A Stretchable and Compressible Ion Gel Based on a Deep Eutectic Solvent Applied as a Strain Sensor and Electrolyte for Supercapacitors. *J Mater Chem C Mater* **2020**, *8* (2), 550–560. https://doi.org/10.1039/C9TC05913J.

(34) Li, Z.; Xu, X.; Jiang, Z.; Chen, J.; Tu, J.; Wang, X.; Gu, C. A Silk Protein-Based Eutectogel as a Freeze-Resistant and Flexible Electrolyte for Zn-Ion Hybrid Supercapacitors. *ACS Appl Mater Interfaces* **2022**, *14* (39), 44821–44831. https://doi.org/10.1021/acsami.2c12103.

(35) Wu, Y.; Deng, Y.; Zhang, K.; Qiu, J.; Wu, J.; Yan, L. Ultrahigh Conductive and Stretchable Eutectogel Electrolyte for High-Voltage Flexible Antifreeze Quasi-Solid-State Zinc-Ion Hybrid Supercapacitor. *ACS Appl Energy Mater* **2022**, *5* (3), 3013–3021. https://doi.org/10.1021/acsaem.1c03654.

(36) Yang, H.; Zhang, J.; Yao, J.; Zuo, D.; Xu, J.; Zhang, H. A Gel Polymer Electrolyte Based on Ternary Deep Eutectic Solvent for Flexible, Wide-Temperature Tolerant Zinc-Ion Hybrid Supercapacitors. *J Power Sources* **2022**, *548*, 232070. https://doi.org/10.1016/j.jpowsour.2022.232070.

(37) Khomenko, V.; Raymundo-Piñero, E.; Béguin, F. A New Type of High Energy Asymmetric Capacitor with Nanoporous Carbon Electrodes in Aqueous Electrolyte. *J Power Sources* **2010**, *195* (13), 4234–4241. https://doi.org/10.1016/j.jpowsour.2010.01.006.

(38) Stoller, M. D.; Ruoff, R. S. Best Practice Methods for Determining an Electrode Material's Performance for Ultracapacitors. *Energy Environ Sci* **2010**, *3* (9), 1294. https://doi.org/10.1039/c0ee00074d.

(39) Doblinger, S.; Donati, T. J.; Silvester, D. S. Effect of Humidity and Impurities on the Electrochemical Window of Ionic Liquids and Its Implications for Electroanalysis. *The Journal of Physical Chemistry C* **2020**, *124* (37), 20309–20319. https://doi.org/10.1021/acs.jpcc.0c07012.

(40) Pan, S.; Yao, M.; Zhang, J.; Li, B.; Xing, C.; Song, X.; Su, P.; Zhang, H. Recognition of Ionic Liquids as High-Voltage Electrolytes for Supercapacitors. *Front Chem* **2020**, *8*. https://doi.org/10.3389/fchem.2020.00261.

(41) O'Mahony, A. M.; Silvester, D. S.; Aldous, L.; Hardacre, C.; Compton, R. G. Effect of Water on the Electrochemical Window and Potential Limits of Room-Temperature Ionic Liquids. *J Chem Eng Data* **2008**, *53* (12), 2884–2891. https://doi.org/10.1021/je800678e.

(42) Ketabi, S.; Lian, K. The Effects of SiO 2 and TiO 2 Nanofillers on Structural and Electrochemical Properties of Poly(Ethylene Oxide)–EMIHSO 4 Electrolytes. *Electrochim Acta* **2015**, *154*, 404–412. https://doi.org/10.1016/j.electacta.2014.12.036.

(43) Rana, H. H.; Park, J. H.; Ducrot, E.; Park, H.; Kota, M.; Han, T. H.; Lee, J. Y.; Kim, J.; Kim, J.-H.; Howlett, P.; Forsyth, M.; MacFarlane, D.; Park, H. S. Extreme Properties of Double Networked Ionogel Electrolytes for Flexible and Durable Energy Storage

Devices. *Energy Storage Mater* **2019**, *19*, 197–205. https://doi.org/10.1016/j.ensm.2018.11.008.

(44) Asbani, B.; Douard, C.; Brousse, T.; Le Bideau, J. High Temperature Solid-State Supercapacitor Designed with Ionogel Electrolyte. *Energy Storage Mater* **2019**, *21*, 439–445. https://doi.org/10.1016/j.ensm.2019.06.004.

(45) Xiong, G.; Kundu, A.; Fisher, T. S. Influence of Temperature on Supercapacitor Performance; 2015; pp 71–114. https://doi.org/10.1007/978-3-319-20242-6_4.

(46) Ortega, P. F. R.; Trigueiro, J. P. C.; Silva, G. G.; Lavall, R. L. Improving Supercapacitor Capacitance by Using a Novel Gel Nanocomposite Polymer Electrolyte Based on Nanostructured SiO2, PVDF and Imidazolium Ionic Liquid. *Electrochim Acta* **2016**, *188*, 809–817. https://doi.org/10.1016/j.electacta.2015.12.056.

(47) Wu, F.; Chen, N.; Chen, R.; Zhu, Q.; Qian, J.; Li, L. "Liquid-in-Solid" and "Solid-in-Liquid" Electrolytes with High Rate Capacity and Long Cycling Life for Lithium-Ion Batteries. *Chemistry of Materials* **2016**, *28* (3), 848–856. https://doi.org/10.1021/acs.chemmater.5b04278.

Chapter 6

Research Conclusions and Future Scopes

CHAPTER 6

Research Conclusions and Future Scopes

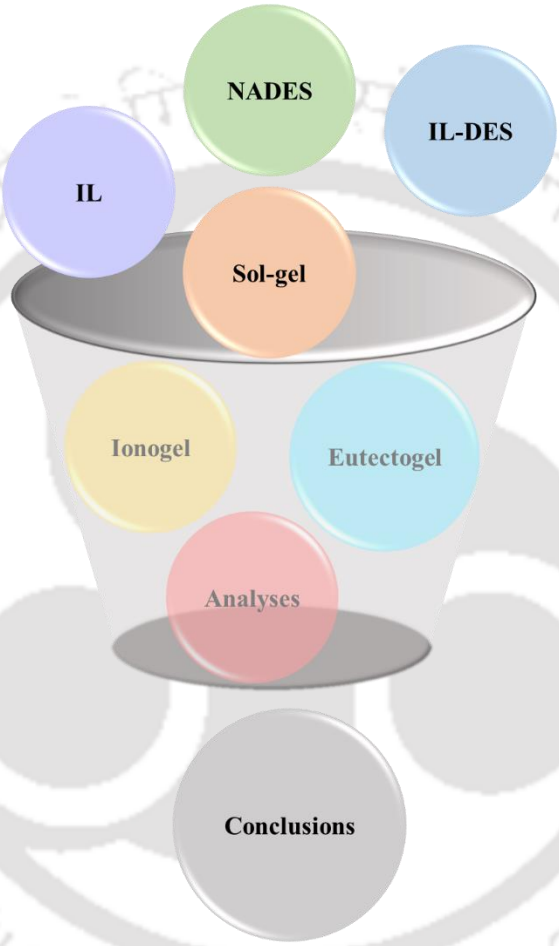

6.1. Introduction

This final chapter aims to emphasize the chief findings of the research. It involves comparing the three primary types of gels examined in this study, offering valuable insights into their prospective suitability for use as solid electrolytes in supercapacitor energy storage technologies. The conclusions are drawn from the results and discussions reported in the preceding chapters. Additionally, the subsequent section delineates potential future directions for this investigation, providing perspectives on possible avenues for further exploration and advancement in the field.

6.2. Overall Conclusions from the Research

The sol-gel encapsulation of the seven ILs considered in this study into TBOT-derived TiO_2 resulted in the formation of seven amorphous, viscoelastic quasi-solid ionogels with porous structures and 3D nanostructured continuous channels, as detailed in Chapter 3 of this thesis. The ten eutectogels prepared similarly by confining the four carboxylic-acid-based NADESs (Chapter 4) and the IL-based DES (Chapter 5) into TiO_2 or SiO_2 derived respectively from TBOT or TEOS were also obtained in amorphous form with apparent porosity and interconnected channels. The synthesis processes for the DESs and the gels utilized a minimal number of precursors, rendering them fast, simple, and cost-effective. The structural integrity of the ILs and the DESs remained intact after their immobilization into the matrix, confirming gelation through physical crosslinking. However, shifts in vibrational frequencies were observed due to non-bonded interactions between the pore wall surfaces of titania or silica moieties and the solvent molecules. As a result, the thermal stability of the ILs and DESs is tampered with after gelation. The ionogels with the $[TFSI]^-$ anion exhibited the best thermal stability among their kind. Nevertheless, the stability windows of all the gels are adequate for potential moderate to high-temperature applications. In the eutectogels, a difference in the

interactive nature of TiO_2 and SiO_2 with the DESs was revealed by the variation in the vibrational shifts and degradation temperatures of the titania- and silica-mediated gels.

Electrochemically, all the seven ionogels demonstrated a double-layer capacitive behavior within a wide potential window of 4 V, owing to the good electrochemical stability and/or hydrophobicity of the host ILs. This underscores their compatibility with rGO electrodes and excellent stability in applications with EDLCs. Consequently, the ionogels achieved specific energy levels comparable to those of polymeric ionogels against rGO and AC electrodes. However, decent values for specific capacitance and specific power were obtained here due to restricted kinetics and higher intrinsic resistance, particularly in TIGels 4, 2, and 7. Despite being comparatively less thermostable, TIGel5 exhibited the best electrochemical performance, delivering the highest specific capacitance (11.5 F g^{-1} or 277.7 mF cm^{-2}), lowest ESR (36.2 Ω), and highest ionic conductivity (1.3 mS cm^{-1}) owing to the high hydrophobicity and low room-temperature viscosity of IL5, combined with increased charge distribution facilitated by the imidazolium-cation delocalization. The maximum energy and power delivered by the system stood at 25.4 W h kg^{-1} and 6.4 kW kg^{-1}. Moreover, the same ionogel maintained its OPW and EDLC characteristics at controlled temperatures of 25 and 50 °C, while showing an increase in specific capacitance and ionic conductivity by factors of 1.6 and 5.9 respectively, at the latter temperature.

The eight NADES gels also exhibited a double-layer capacitive behavior within an impressively wide voltage window of 4 V, a rare observation for DES-based gels. This is attributed to the high hydrophobicity of the DES components. This achievement ensured their excellent compatibility with rGO electrodes and stability in EDLC applications. However, high intrinsic resistance in the systems resulted in specific capacitance and specific energy values reaching only up to 0.9 mF g^{-1} (86.8 µF cm^{-2}) and 2.2 mW h kg^{-1} (SEGel2), respectively. Between the two types, the silica-based gels demonstrated slightly higher specific capacitance

and energy due to the large surface area of SiO_2, facilitating long-range weak dipole interactions between the matrix and the weakly polar NADESs. This further validated the difference in the manner the two matrices interact with the DESs. EIS studies on TEGels confirmed high ESR, leading to low ionic conductivity and specific power, with maximum values reaching only 0.03 mS cm^{-1} and 65.4 mW kg^{-1} (TEGel2), respectively. However, the IL-modified TEGels resulted in retained EDLC characteristics within the 4 V window, coupled with a significant reduction in internal resistance. This led to remarkable improvements in specific capacitance and ionic conductivity, reaching up to 47.7 F g^{-1} (2087 mF cm^{-2}) and 16.3 mS cm^{-1} (TEGel2), respectively. These enhancements are attributed to the formation of a hybrid network of interconnected "ionic" channels with the introduction of the IL, along with its good wettability. Therefore, the standalone eutectogels formed from the NADESs lack the desirable electrochemical properties observed in ionogels due to the absence of an ionic or polar component and the presence of steric hindrance from bulky molecules.

The IL-based DES maintained its double-layer capacitive behavior and 3 V OPW post-confinement, primarily due to the cationic charge distribution of the imidazolium IL, enhancing its electrochemical stability. This again highlights the compatibility of the two corresponding eutectogels with rGO electrodes and their stability in EDLC applications. TIEGel demonstrated higher specific capacitance (16.3 F g^{-1} or 395.8 mF cm^{-2}) and specific energy (20.4 W h kg^{-1}) attributed to the higher dielectric constant of TiO_2, resulting in stronger polarization in the presence of the IL and an increased charge density at the electrode/electrolyte interface. Consequently, TIEGel exhibited lower ESR (39.6 Ω) and higher ionic conductivity (1.3 mS cm^{-1}). However, both the silica- and titania-based gels procured decent values of specific power due to constrained kinetics and relatively high intrinsic resistance, with the latter notably delivering higher power (3.3 kW kg^{-1}). Moreover, TIEGel maintained its OPW and EDLC properties across controlled temperatures of 25, 50, and 80 °C, exhibiting notable improvement

in specific capacitance and ionic conductivity by factors of 3 and 4.4 respectively, at 80 °C. The satisfactory performance of the gels is largely due to the good electrochemical stability and better ionicity of the constituent IL, in addition to good wettability and low room-temperature viscosity of the DES.

Overall, all the gels are double-layer capacitive within a wide potential window. Most of the IL-based ionogels discussed in Chapter 3 exhibit reasonable electrochemical characteristics favorable for supercapacitors. On the other hand, although more cost-effective and electrochemically stable, the NADES-based eutectogels presented in Chapter 4 possess high intrinsic resistance primarily because of the absence of an appropriate ionic medium. The characteristics of the IL-based eutectogels from Chapter 5 are at par with that of the ionogels and mostly superior to that of the NADES-based eutectogels, clearly indicating the advantages of the presence of an IL. **Table 6.1** compares the mass fraction of the inorganic matrix (determined from TGA), OPW (10 mV s^{-1}), specific capacitance (10 mV s^{-1}), specific energy (10 mV s^{-1}), power, and ionic conductivity of TIGel5, TEGel2, SEGel2, TIEGel, and SIEGel at room temperature, revealing the better performance of the IL-based gels. However, the delivery of competent performance with the utilization of lesser quantity of IL as compared to that in ionogels renders the IL-based eutectogels more economical. It may, thus be concluded that these eutectogels offer the best trade-off between cost and performance among the three primary categories of gels studied in this work, supporting their utilization as cost-effective solid electrolytes in supercapacitors. While the NADES-based eutectogels may not possess electrochemical properties as appealing as those of their two other counterparts, their potential for improvement and application in various fields remains significant.

Table 6.1. Comparison of mass fraction of the inorganic matrix, OPW (10 mV s^{-1}), specific capacitance (10 mV s^{-1}), specific energy (10 mV s^{-1}), power, and ionic conductivity of TIGel5, TEGel2, SEGel2, TIEGel, and SIEGel at room temperature

System	TiO_2 / SiO_2 mass fraction (wt%)	OPW (V)	$C_{sp\text{-}10\ mV\ s^{-1}}$ ($F\ g^{-1}$)	$C_{sp\text{-}10\ mV\ s^{-1}}$ ($mF\ cm^{-2}$)	$E_{sp\text{-}10\ mV\ s^{-1}}$ ($W\ h\ kg^{-1}$)	P ($kW\ kg^{-1}$)	σ ($mS\ cm^{-1}$)
TIGel5	20.50	4	8.34	202.31	18.53	6.44	1.34
TEGel2	35.61	4	1.87×10^{-5}	3.58×10^{-3}	4.16×10^{-5}	6.54×10^{-5}	0.03
SEGel2	36.58	4	9.92×10^{-4}	8.68×10^{-2}	2.20×10^{-3}	–	–
TIEGel	34.94	3	10.12	245.41	12.65	3.31	1.27
SIEGel	26.61	3	1.83	44.37	2.29	0.31	0.09

6.3. Future Scopes of the Research

In recent years, the supercapacitor has experienced significant advancements which include the introduction of relatively safer, more robust, and sustainable solid electrolytes. In this context, ionogels and eutectogels have saliently subjugated the realm of such electrolytes. However, restricted kinetics inhibit their efficiency to perform parallelly with their liquid counterparts. In the current study, for instance, although a wide OPW was achieved for the inorganic gels, they exhibited only fair electrochemical characteristics, leaving room for further improvement in the systems. Nevertheless, these electrolytes are still at their nascent stage of development and hence, there are ample scopes for novel research in this area by taking a deeper dive into the correlation between their structural and functional properties. Future research could largely focus on enhancing their capacitance and conductivity through material modifications and exploring new synthesis strategies for improved electrochemical performance.

As a preliminary study, the cycling stability of the current systems may be assessed and their OPW, capacitance, and internal resistances may be corroborated through galvanostatic charge-discharge (GCD) technique. The ratio of the solvent to matrix precursor loading has a notable influence on the properties of the gels. Thus, further research may be directed towards deciphering the effect of variation of loading ratio of TBOT or TEOS on the present systems. Given the advantages of TiO_2 owing to its high dielectric constant, more inorganic ionogels and eutectogels could be synthesized using suitable ILs and DESs and analyzed for properties favorable for supercapacitors. Especially in case of DESs, their low cost, tunability, and ease of synthesis allows for the convenient production of potentially inexpensive eutectogels with elevated capacitance and ionic conductivity. A possible approach could be the replacement of non-ionic and long-chained DES-forming components with ionic and less bulkier ones. Such advancements could position them as a novel and competitive category of solid-state electrolytes for high-performance supercapacitors. Moreover, other novel gels with enhanced thermal and electrochemical properties may be investigated by substituting the two types of matrices considered in this study with other inorganic and/or polymeric scaffolds prepared via a sol-gel or an alternative synthesis route.

The type of electrode also plays an important role on the characteristics of a supercapacitor. Therefore, the properties of the gels explored here may be studied in conjunction with other carbonaceous and/or porous electrodes. Additionally, it may be worth studying the correlation among cations and anions of ILs, HBAs and HBDs of DESs, and the anchoring matrices in context of the properties of the resultant ionogels or eutectogels. In this regard, it may be beneficial to combine experimental and computational approaches, so as to shed light on the rudimentary details of the underlying phenomena considering different aspects such as electrochemical reactions, diffusion of ions, solid electrode/electrolyte interface resistances, material porosity, and byproduct formation. The viability of the current electrolytes

in supercapacitors may be predicted and validated by studying the complex formation mechanism and the interactive forces of the systems through density-functional-theory- (DFT-) based quantum-chemical (QC) calculations, molecular dynamics (MD) simulations, COMSOL-based numerical modelling, etc. However, the theoretical development has still not attained a mature state and needs considerable efforts in upcoming days.

Appendices

APPENDIX A

(CHAPTER 3)

FTIR Table for TIGels 2-7

CV and Nyquist Plots of TIGel5 at 100 °C

Table A1. Vibrational bands of ILs 2–7 and TIGels 2–7 along with their corresponding assignments

Assignment	System											
	Vibrational band (cm^{-1})											
	IL2	**TIGel2**	**IL3**	**TIGel3**	**IL4**	**TIGel4**	**IL5**	**TIGel5**	**IL6**	**TIGel6**	**IL7**	**TIGel7**
$_s\nu_sH-O-H$	–	1716	–	1716	–	1718	–	1718	–	1718	–	1541
δ_aC-H	1560	1562	1573	1573	1571	1564	1571	1568	1573	1568	1492	1492
$\nu C-C$	–	–	1469	1471	–	–	–	–	–	–	–	–
$_s\nu C-N$	1458	1458	–	–	1328	1328	–	–	1328	1328	1327	1327
$P-CH_2-R$ deform	1307	1367	–	–	–	–	–	–	–	–	–	–
ν_aSO_2	–	–	–	–	1348	1348	–	–	1348	1348	1346	1346
$_s\nu C-F$	–	–	–	–	–	–	1296	1296	–	–	–	–
$_s\nu C-N$	1213	1186	1168	1166	–	–	–	–	–	–	–	–
$_s\nu C-F$	–	–	–	–	–	–	1182	1180	–	–	–	–
$_s\nu CF_3$	–	–	–	–	1178	1180	–	–	1178	1182	1176	1178
ν_sSO_2	–	–	–	–	1132	1132	–	–	1132	1132	1132	1132
$_s\nu B-F$	–	–	1033	1055	–	–	–	–	–	–	–	–
$\nu S-N-S$	–	–	–	–	1051	1053	–	–	1051	1053	1051	1053
$_s\nu C-F$	–	–	–	–	–	–	962	962	–	–	–	–
$_s\nu_aC-N$	813	846	–	–	947	910	–	–	842	902	910	900
$_s\nu_sC-N$	900	891	–	–	–	–	–	–	–	–	–	–
$_b\nu_aH-C=C-H$	–	–	–	–	–	–	808	810	–	–	–	–
$_s\nu_sC-S$	–	–	–	–	788	788	–	–	788	788	788	788

Table A1 continues

Assignment	System											
	Vibrational band (cm^{-1})											
	IL2	**TIGel2**	**IL3**	**TIGel3**	**IL4**	**TIGel4**	**IL5**	**TIGel5**	**IL6**	**TIGel6**	**IL7**	**TIGel7**
${}_{b}\nu CF_3$	–	–	–	–	740	738	–	–	740	738	740	738
$\nu_s P{-}C$	719	719	–	–	–	–	–	–	–	–	–	–
${}_{b}\nu_s H{-}C{=}C{-}H$	–	–	–	–	–	–	717	719	–	–	–	–
${}_{s}\nu_a N{-}C{\equiv}N$	663	601	–	–	–	–	–	–	–	–	–	–
${}_{b}\nu C{-}H$	522	513	623	623	509	507	–	–	509	507	511	507
ring deform	–	–	–	–	–	–	615	617	–	–	–	–
$\nu_a SO_2$	–	–	–	–	611	611	–	–	611	611	613	613
${}_{b}\nu PF_3$	–	–	–	–	–	–	495	495	–	–	–	–
${}_{s}\nu_a P{-}F$	–	–	–	–	–	–	430	420	–	–	–	–

${}_{s}\nu_s$: symmetric stretching, δ_a: asymmetric scissoring, ${}_{s}\nu_a$: asymmetric stretching, ${}_{b}\nu_a$: asymmetric bending, ${}_{b}\nu_s$: symmetric bending

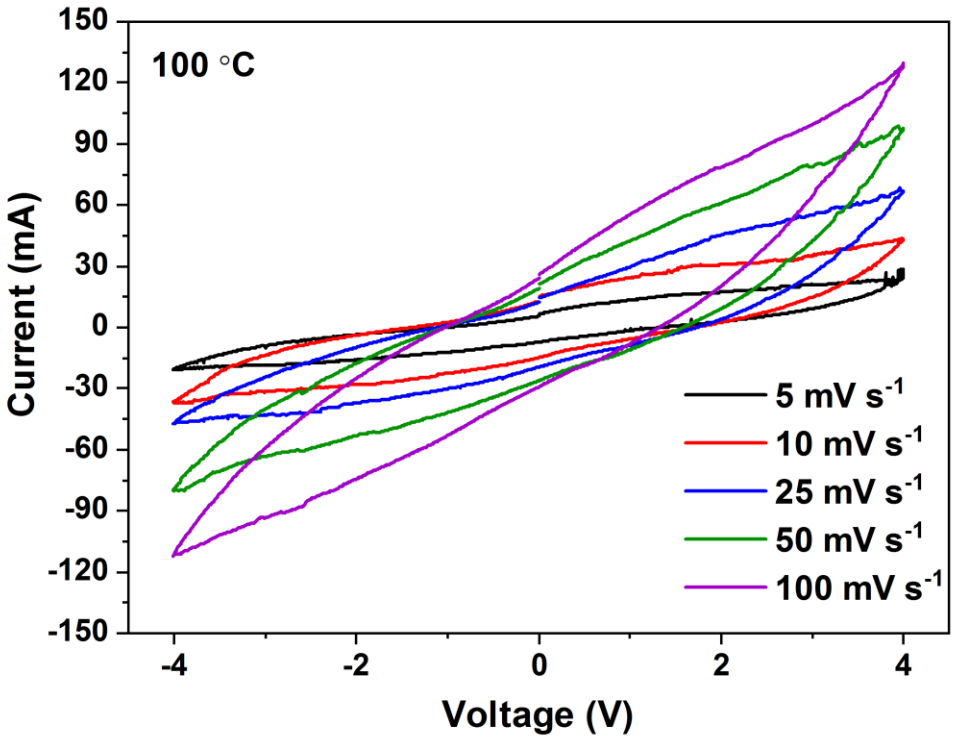

Figure A1. Cyclic voltammograms of the TIGel5-based system obtained from CV conducted using the two-electrode coin-cell assembly with rGO electrodes at scan rates of 5, 10, 25, 50, and 100 mV s^{-1} at 100 °C.

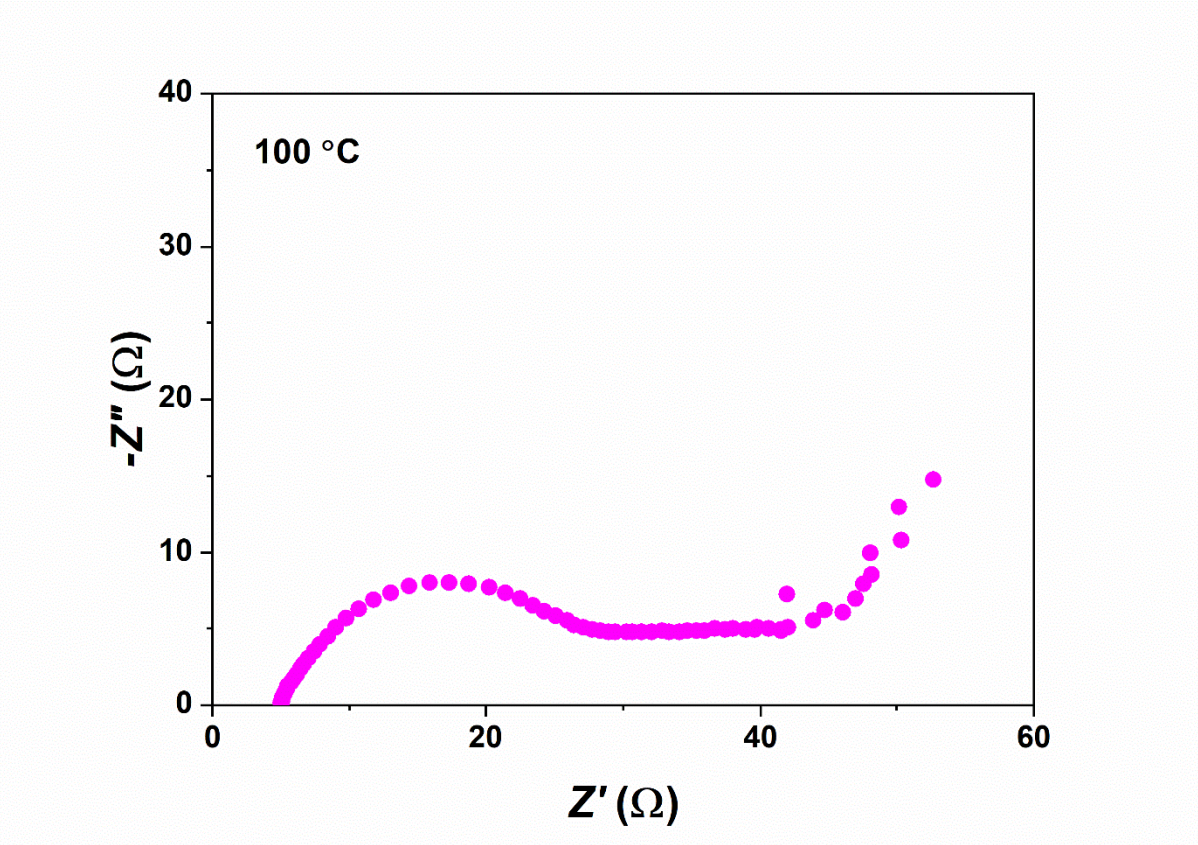

Figure A2. Nyquist plot of the system obtained from EIS conducted on the rGO-based two-electrode coin cell with TIGel5 electrolyte at 100 °C.

APPENDIX B

(CHAPTER 4)

Viscosity of DESs 1–4 as a function of shear rate

Viscosity and water content data of DESs 1–4

^{1}H NMR plots of DESs 1–4

Contact angle of DES3

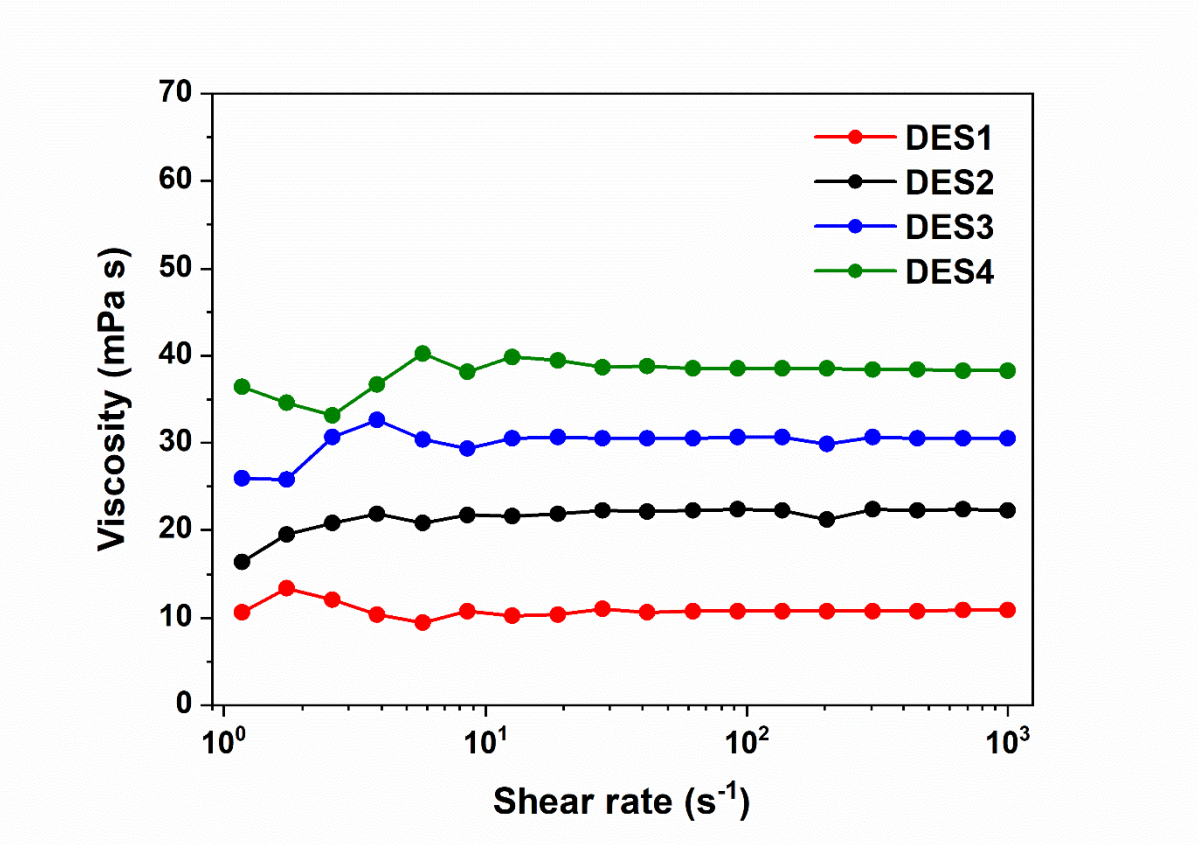

Figure B1. Rhelogical plot depicting viscosity versus shear rate for DESs 1–4 at room temperature.

Table B1. Viscosity and water content of DESs 1–4

DES	Viscosity (Pa s)	Water content (wt%)
DES1 (Decanoic acid + DL-Menthol)	0.011	0.20
DES2 (Lauric acid + DL-Menthol)	0.022	0.12
DES3 (Myristic acid + DL-Menthol)	0.031	0.05
DES4 (Palmitic acid + DL-Menthol)	0.038	0.05

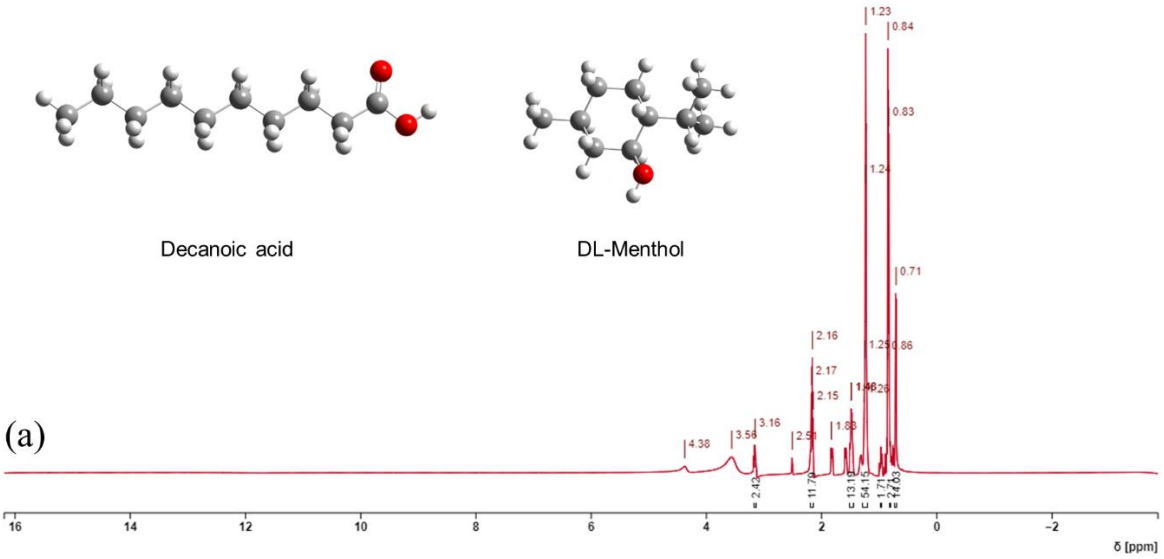

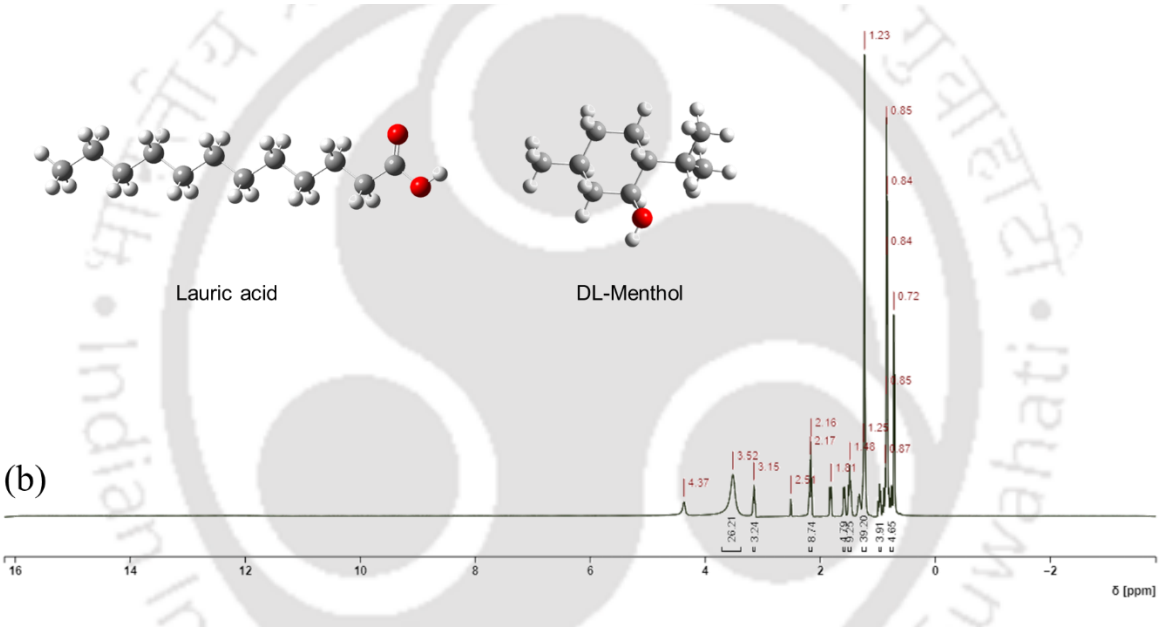

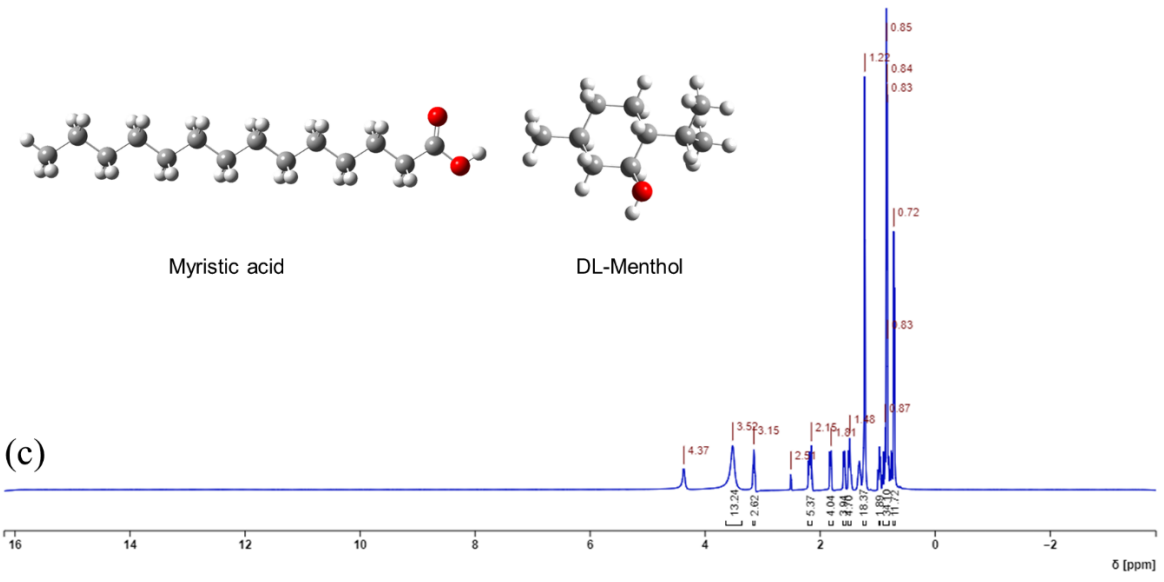

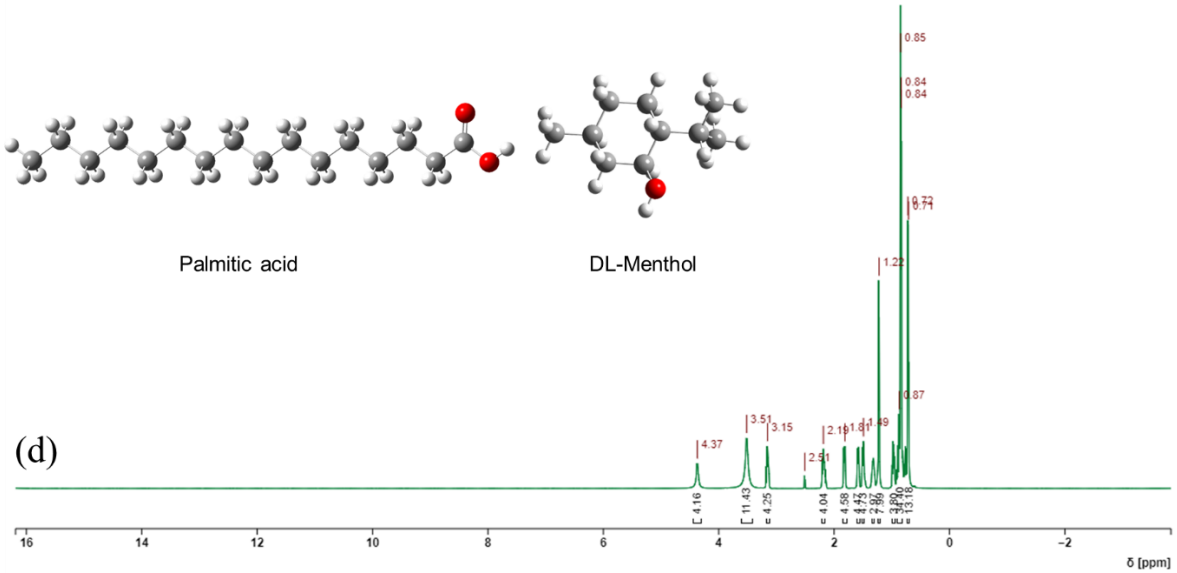

Figure B2. ^{1}H NMR spectra of (a) DES1, (b) DES2, (c) DES3, and (d) DES4.

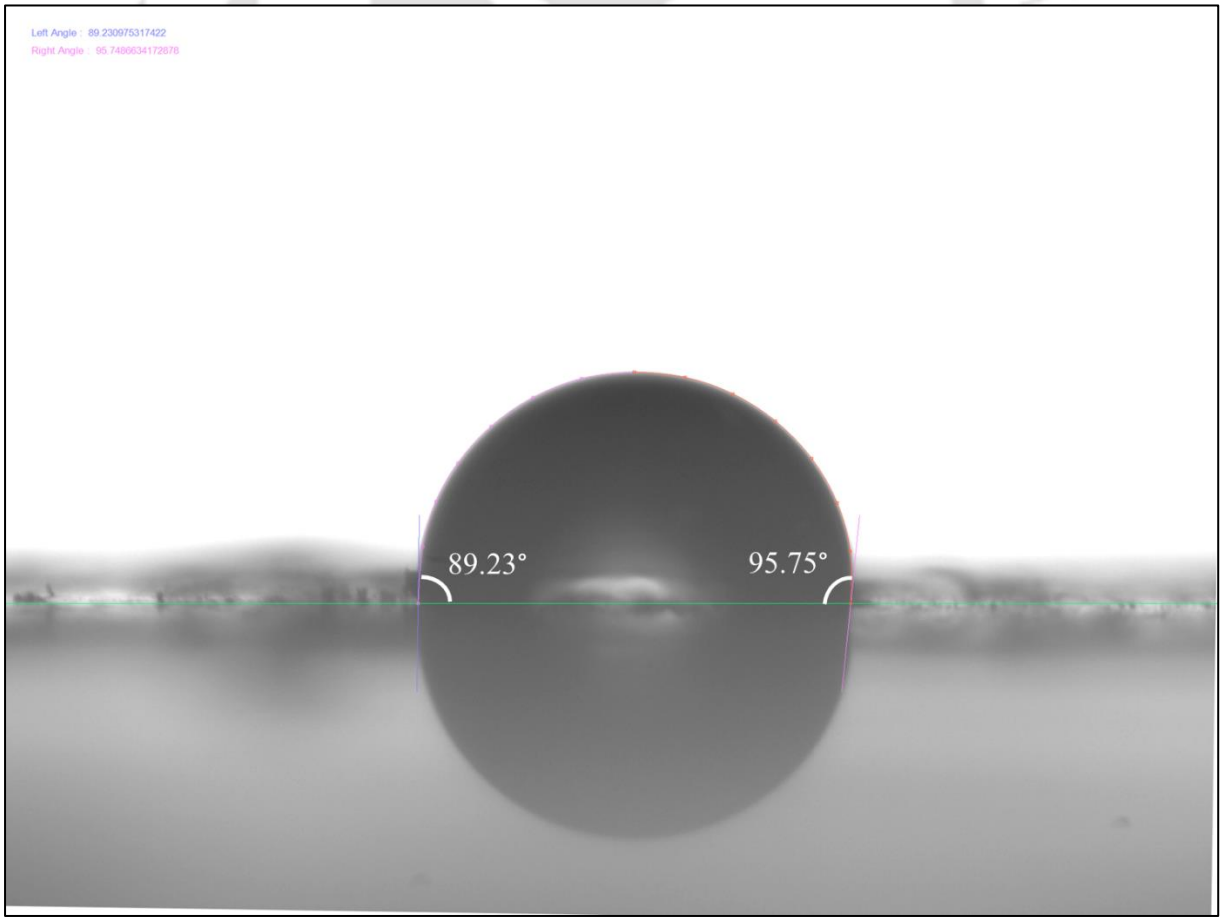

Figure B3. Contact angle of DES3 measured against water.

APPENDIX C

(CHAPTER 5)

^{1}H NMR plot of DES5

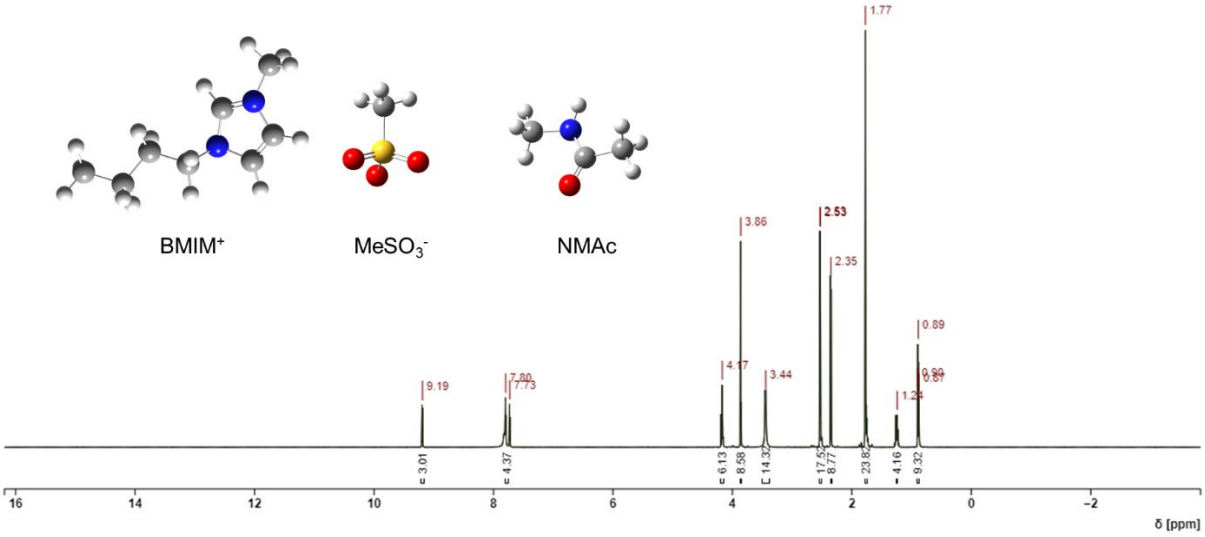

Figure C1. ^{1}H NMR spectrum of DES5.

Research Outputs

Communication of Research Results

Articles Published in Peer-Reviewed Journals

(1) **Dutta, A.**; Mahanta, J.; Banerjee, T. Supercapacitors in the Light of Solid Waste and Energy Management: A Review. *Adv. Sustain. Syst.* **2020**, *4* (12), 2000182. https://doi.org/10.1002/adsu.202000182

(2) **Dutta, A.**; Mitra, S.; Basak, M.; Banerjee, T. A Comprehensive Review on Batteries and Supercapacitors: Development and Challenges since Their Inception. *Energy Storage* **2022**, *5* (1), No. e339. https://doi.org/10.1002/est2.339

(3) **Dutta, A.**; Mishra, D. K.; Kundu, D.; Mahanta, U.; Jiang, S. P.; Silvester, D. S.; Banerjee, T. Examining the Electrochemical Nature of an Ionogel Based on the Ionic Liquid $[P_{66614}][TFSI]$ and TiO_2: Synthesis, Characterization, and Quantum Chemical Calculations. *Ind. Eng. Chem. Res.* **2022**, *61* (25), 8763–8774. https://doi.org/10.1021/acs.iecr.2c00550

(4) **Dutta, A.**; Kundu, D.; Sharma, S.; Paul, N.; Naik, P. K.; Silvester, D. S.; Banerjee, T. Physically Cross-Linked Titania-Supported Novel Eutectogels as Solid-State Electrolytes: An Experimental and Quantum Chemical Investigation. *ACS Sustain Chem Eng* **2023**, *12* (1), 248–262. https://doi.org/10.1021/acssuschemeng.3c05551

Citations as on June 25, 2024: 145 (Google Scholar)

REVIEW

ADVANCED SUSTAINABLE SYSTEMS
www.advsustainsys.com

Supercapacitors in the Light of Solid Waste and Energy Management: A Review

*Arindam Dutta, Jiwajyoti Mahanta, and Tamal Banerjee**

In line with the UN's Sustainable Development Goals (SDGs), the world is witnessing a phenomenal shift toward renewable energy. With this, the demand for energy storage devices has gained immense attention from researchers worldwide over the past decades and so have concerns pertaining to the disposal and management of material and energy wastes from various energy resources. Because of their unique features such as high power density, long cycling stability, and high capacitance, supercapacitors have emerged as a promising technology for storing energy. This review focuses on some of the recent advances in supercapacitors in the wake of solid waste and energy management. First, the utilization of a range of solid waste materials in the fabrication of supercapacitors is summarized. Thereafter, the roles of some of the recently developed "green" electrolytes in curbing the detrimental effects of waste generation from supercapacitors are discussed. Furthermore, different applications of supercapacitors in the field of energy management are highlighted. The strategies for the management of waste generated on account of a supercapacitor's end of life are also reported. The review is concluded by outlining some of the unarticulated challenges as well as the personal outlook of the authors in this area.

1. Introduction

Over the past few decades, the world has witnessed a dramatic upsurge in the demand for energy with the increase in population, urbanization, and modernization. This calls for the generation of higher amount of energy which, in turn, requires the exploitation of energy resources at a faster rate. This, not only results in rapid depletion of the limited sources of energy, but also poses a threat to the environment with the emission of greenhouse gases (GHGs). Therefore, in compliance with the UN's Sustainable Development Goals (SDGs) 7, 12, and 13, in particular, a much-needed shift toward renewable energy has already been seen in the recent years to mitigate these challenges.[1–10] As a result, this has caught tremendous attention of researchers all over the world on the development of efficient and effective energy storage devices. Although these devices overcome the pitfall of energy crisis, however, in many a case, the cost is paid in the form of environmental contamination with the wastes generated from them. This, on the other hand, is gradually snowballing into a major threat to the already disturbed carbon cycle balance.

Lately, supercapacitors, also known as ultracapacitors, have emerged as a class of leading-edge technology for energy storage. These noble devices exhibit a unique combination of favorable characteristics such as high power density, long shelf life, good cyclability, high capacitance, low environmental impact, and intrinsically safe design and operation.[11–17] They can be utilized in a wide range of applications such as electric vehicles (EVs) and hybrid electric vehicles (HEVs), pulsing techniques, digital devices[18–27] as well as in other fields of energy and power quality management.[28–37] Meanwhile, management of material wastes generated from various sources including electrochemical devices has long been a matter of concern. A study by World Bank revealed that food and green wastes account for about 44% of the total waste generated in the world (**Figure 1**a). This is followed by paper and plastic wastes, each contributing 17% and 12% of the total, respectively. The remainder consists of glass, metal, wood, rubber, leather, and other wastes. The trend in the fraction of organic wastes is seen to increase with a decrease in levels of economic development, especially in middle- and low-income countries. Interestingly, only about 19% of the total waste generated worldwide is recovered through recycling and composting while 33% is disposed in open dumps (Figure 1b). In addition to that, about 36.6% ends up in landfills and 11.1% is incinerated for final disposal. In 2016, solid waste treatment and disposal was responsible for the emission of about 1.6 billion tons of carbon dioxide (CO_2) equivalent GHG, which accounted for nearly 5% of global emissions. Besides, financing solid waste management systems stands as a major challenge in combatting the effects of waste generation and its disposal.[38]

Apart from municipal solid wastes, there are several other categories of waste streams such as industrial waste, agricultural waste, construction and demolition waste, hazardous waste, medical waste, and electronic waste (Figure 1c). It is observed that industrial waste generation is about 18 times higher than that of municipal solid waste. The income level of a country or a region is directly proportional to the rise in the

A. Dutta, J. Mahanta, Prof. T. Banerjee
Department of Chemical Engineering
Indian Institute of Technology Guwahati
Guwahati, Assam 781039, India
E-mail: tamalb@iitg.ac.in

The ORCID identification number(s) for the author(s) of this article can be found under https://doi.org/10.1002/adsu.202000182.

DOI: 10.1002/adsu.202000182

Received: 25 November 2021 | Revised: 1 February 2022 | Accepted: 22 March 2022

DOI: 10.1002/est2.339

REVIEW

ENERGY STORAGE WILEY

A comprehensive review on batteries and supercapacitors: Development and challenges since their inception

Arindam Dutta[1] | **Shirsendu Mitra**[2] | **Mitali Basak**[3] | **Tamal Banerjee**[1]

[1]Department of Chemical Engineering, Indian Institute of Technology Guwahati, Guwahati, Assam, India

[2]Discipline of Physics, Indian Institute of Technology Gandhinagar, Palaj, Gujarat, India

[3]Centre for Nanotechnology, Indian Institute of Technology Guwahati, Guwahati, Assam, India

Correspondence
Tamal Banerjee, Department of Chemical Engineering, Indian Institute of Technology Guwahati, Guwahati 781039, Assam, India.
Email: tamalb@iitg.ac.in

Abstract

The chemistry underlying the storage phenomena in batteries and supercapacitors has been known to mankind for quite some time now. Nonetheless, a holistic apprehension of their rudimentary characteristics throughout their lifetime and beyond is imperative to accentuate their maximum potential. Although numerous reviews have addressed many of the facts individually, a consolidated report on the associated history, challenges, and environmental aspects considering the cutting-edge advancements in this field is missing. This review gives a comprehensive insight into the two technologies by drawing a detailed comparison between their governing attributes and potential challenges. First, a brief history of batteries and supercapacitors along with their classifications based on materials and corresponding working mechanisms are delineated. Thereafter, some of the inexorable losses restricting the performance of these systems from reaching their theoretical limits are outlined. A picture of the significance of theoretical modeling of batteries and supercapacitors highlighting the associated challenges in the same is drawn. Furthermore, their fates after retirement as well as their scopes in the future based on their current trends are reported in the ensuing sections. Alongside detailed tutorial background of energy storage literature, this review compares different energy storage devices and the latest developments in this field.

KEYWORDS

battery, classification, parasitic reaction, recycling, supercapacitor, theoretical modeling

1 | INTRODUCTION

The demand for global energy requirement is growing consistently in contemporary society, and so are the concerns about the depletion and associated pollution caused by the high consumption of fossil fuels. Because of this crisis, several research and technological developments have been achieved to date in the areas like renewable energy, energy from alternative sources, energy storage devices, and energy harvesting from waste materials. Among renewable sources of energy, solar energy,[1,2] tidal energy,[3,4] and wind energy[5,6] are appealing alternative options for electricity generation. However, the intermittent and unpredictable characteristics of these sources render electricity competitive only with the parallel development of efficient and effective energy storage systems. The power extracted from whatsoever sources calls for the requirement of storage facilities to accumulate energy for sporadic utilization.[7-11] Also, storage of power is of utmost importance for meeting on-demand power requirements and supply of power in extensively remote areas. Among the various electrochemical technologies in existence today, batteries and supercapacitors have saliently subjugated the domain of energy storage,

I&EC research
Industrial & Engineering Chemistry Research
pubs.acs.org/IECR Article

Examining the Electrochemical Nature of an Ionogel Based on the Ionic Liquid $[P_{66614}][TFSI]$ and TiO_2: Synthesis, Characterization, and Quantum Chemical Calculations

Arindam Dutta, Dhirendra Kumar Mishra, Debashis Kundu, Upasana Mahanta, San Ping Jiang, Debbie S. Silvester, and Tamal Banerjee*

Cite This: Ind. Eng. Chem. Res. 2022, 61, 8763−8774 Read Online

ABSTRACT: With countries and regions setting strict targets for adopting renewable and sustainable technologies, worldwide demand for energy storage has surged dramatically. Novel materials and new storage chemistry solutions are being explored to realize storage technologies for the next generation. This step-change includes fundamental research in the design of new electrolytes. Ionogels are gaining popularity in electrochemical applications because of their ability to overcome the drawbacks of their liquid counterparts while retaining certain beneficial qualities of the latter. The present study reports the preparation of a novel quasi-solid ionogel through the confinement of the ionic liquid (IL) trihexyltetradecylphosphonium bis(trifluoromethylsulfonyl)imide ($[P_{66614}][TFSI]$) into a matrix of titania (TiO_2) by a simple one-pot sol−gel process. The properties of the ionogel have been studied via field emission scanning electron microscopy (FESEM), rheology, Fourier transform infrared (FTIR) spectroscopy, thermogravimetric analysis (TGA), and cyclic voltammetry (CV). The ionogel manifests shear-thinning viscoelastic behavior. The integrity of the IL remains unaffected after its confinement in TiO_2. Thermal stability analysis shows little mass loss of the ionogel up to a temperature of ∼93 °C, favoring its utilization in high-temperature applications. The ionogel demonstrates a double-layer capacitive behavior with an impressive operating potential window (OPW) of 4 V (−4 to +4 V), substantiating its applicability and excellent stability in the electrochemical domain. The formation of the weakly coordinating ionogel is analyzed using density functional theory (DFT). The electronic structures of the precursors and the ionogel are elucidated at the B3LYP/LANL2DZ level of theory. The quantum chemical (QC) calculations reveal that the interaction of the IL with the cross-linker results in some dimensional changes due to alterations in the vibrational frequencies of the respective groups present in the ionogel system.

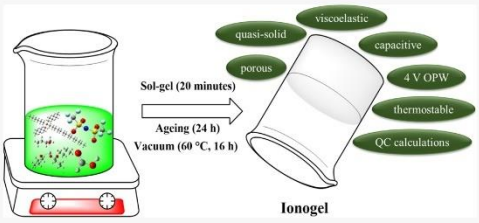

1. INTRODUCTION

Ionic liquids (ILs) have been explored as electrolytes owing to their exceptional properties, such as nonflammability, thermal resilience, good ionic conductivity, and wide electrochemical potential windows.[1−5] Nevertheless, for applications in solid-state systems, the main challenge of using ILs remains in their liquid nature, leading to risks of component corrosion and leakage during packaging and transport. To overcome these difficulties, ILs are being replaced by a new class of quasi-solid electrolyte called ionogels in energy storage devices as well as other electrochemical applications.[6] Not only does this aid the convenience of users but also allows the possibility to widen the scope, durability, and the overall sustainability of the system. Ionogels are composite materials obtained through the immobilization of ILs into a solid matrix with the help of a cross-linking element.[7] Even at reduced pressure, ionogels have been observed to remain highly stable over time. They eliminate the chance of leakage while retaining various favorable properties of their parent ILs.[1,8]

Research on ionogels as potential electrolyte candidates for lithium-ion batteries and supercapacitors has been carried out since the beginning of this century.[1,9] In addition to polymeric materials,[10] different types of inorganic materials such as nonmetal oxides (e.g., SiO_2),[11−15] metal oxides (e.g., TiO_2),[6,15−28] and metal−organic frameworks (MOFs)[29−31] have been used as confining systems for ionogels. A breakthrough was achieved in 2011 with the synthesis of a

Received: February 17, 2022
Revised: April 25, 2022
Accepted: June 6, 2022
Published: June 14, 2022

https://doi.org/10.1021/acs.iecr.2c00550
Ind. Eng. Chem. Res. 2022, 61, 8763−8774

ACS Sustainable Chemistry & Engineering

pubs.acs.org/journal/ascecg Research Article

Physically Cross-Linked Titania-Supported Novel Eutectogels as Solid-State Electrolytes: An Experimental and Quantum Chemical Investigation

Arindam Dutta, Debashis Kundu, Surbhi Sharma, Nabendu Paul, Papu Kumar Naik, Debbie S. Silvester, and Tamal Banerjee*

Cite This: ACS Sustainable Chem. Eng. 2024, 12, 248−262 Read Online

ACCESS | Metrics & More | Article Recommendations | Supporting Information

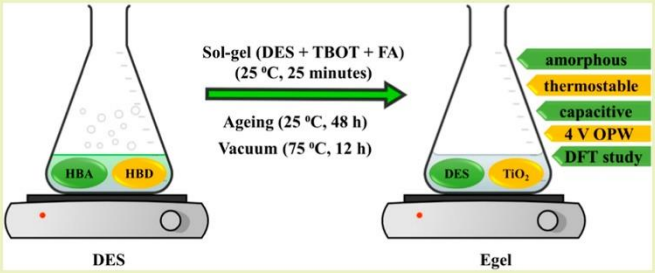

ABSTRACT: Four novel eutectogel (Egel) electrolytes are prepared from the confinement of four hydrophobic deep eutectic solvents (DESs) within a solid matrix of titania (TiO_2) by a nonaqueous sol−gel method. The DESs are composed of decanoic acid, lauric acid, myristic acid, and palmitic acid, each mixed with DL-Menthol in optimal molar ratios. The characteristics of the Egels have been analyzed with the help of field emission scanning electron microscopy, field emission transmission electron microscopy, Fourier transform infrared spectroscopy, X-ray diffraction, thermogravimetric analysis, electrochemical impedance spectroscopy, and cyclic voltammetry characterization techniques. The structural properties of the DESs remain unaffected after their confinement into TiO_2. Thermal stability analyses show almost no mass loss for all the Egels up to a temperature of ∼ 42 °C, with an average initial decomposition temperature of ∼ 150 °C. The gels demonstrate a double-layer capacitive behavior with an operating potential window of about 4 V (−4 to + 4 V) each, proving their potential practicality in electrochemical applications. The nonbonded interactive network facilitated by various noncovalent interactions (H-bonding and van der Waals dispersion) and charge transfer phenomena among the different components of the Egel systems are particularly responsible for their stable and sustainable electrochemical properties suitable for the development of potential electrolytes.

KEYWORDS: *eutectogel, deep eutectic solvent, titania, gel electrolyte, operating potential window*

1. INTRODUCTION

The global demand for energy storage is seeing a dramatic upsurge as the world saliently shifts to renewable and sustainable forms of technology. Newer materials and storage chemistry are being investigated as a part of the process in order to develop next-generation storage solutions. This step-change involves intensive research in the design of novel electrolytes. While liquid electrolytes have been ubiquitously used with storage technologies, one of their limitations lies in their fluid nature inhibiting the convenience of packaging, portability, and leakage.[1−3] With a view to overcoming these difficulties, the concept of solid or quasi-solid electrolytes has recently stimulated significant interest in the electrochemical realm recently. Such electrolytes are obtained by confining a solvent into a polymer, inorganic, or hybrid solid matrix.[4−18] Ionogels prepared from immobilized ionic liquids (ILs) have been studied with several energy storage technologies such as batteries[7,12,15,17] and supercapacitors.[8,16,19,20] These electrolytes are known to retain the excellent electrochemical properties of their host solvents, besides aiding the robust flexibility of the system. However, extensive use of ILs or

Received: August 31, 2023
Revised: December 4, 2023
Accepted: December 5, 2023
Published: December 15, 2023

https://doi.org/10.1021/acssuschemeng.3c05551
ACS Sustainable Chem. Eng. 2024, 12, 248−262

Articles Submitted or in Line for Submission

(1) **Dutta, A.**; Kundu, D.; Naik, P. K.; Silvester, D. S.; Banerjee, T. Synthesis and Properties of Physically Cross-Linked Silica-Mediated Novel Eutectogels Developed from Carboxylic-Acid-Based Natural Deep Eutectic Solvents. (Under review in *Industrial & Engineering Chemistry Research*)

(2) **Dutta A.**; Kundu D.; Sharma S.; Silvester D. S.; Banerjee T. Investigating the Electrochemical Properties of Ionic-Liquid-Mediated Inorganic Eutectogels Derived from Carboxylic-Acid-Based Hydrophobic Deep Eutectic Solvents. (Under review in *Journal of Solution Chemistry*)

(3) **Dutta, A.**; Millar, W.; Silvester, D. S.; Banerjee, T. Novel Eutectogels Derived from an Ionic-Liquid-Based Deep Eutectic Solvent as Electrolytes for Supercapacitors: Synthesis and Characterization. (*In line for submission*)

(4) **Dutta, A.**; Mahanta, J.; Millar, W.; Silvester, D. S.; Banerjee, T. Titania-Confined Novel Ionogels with a Wide Operating Potential Window as Propitious Solid-State Electrolytes for Electrochemical Supercapacitors. (*In line for submission*)

List of Conference Presentations

(1) **Dutta A.**; Mahanta J. Supercapacitor Energy Storage Devices in the Light of Waste Management: A Review. *National Symposium on Sustainable Waste Management (SWM2019)*, Tezpur, India, August 3, 2019. ***(Awarded Best Paper)***

(2) **Dutta A.**; Kundu D.; Sharma S.; Silvester D. S.; Banerjee T. Investigating the Electrochemical Properties of Ionic-Liquid-Mediated Inorganic Eutectogels Derived

from Carboxylic-Acid-Based Hydrophobic Deep Eutectic Solvents. *IIChE – Chemcon 2023*, Kolkata, India, December 27–30, 2023.

List of Workshops Attended

(1) **Workshop on Intellectual Property Rights**. *Indian Institute of Technology Guwahati*, Guwahati, India, March 14–17, 2019.

(2) **Deep Eutectic Solvents for Environmental Remediation and Energy Storage**. *Indian Institute of Technology Guwahati*, Guwahati, India, July 29–30, 2020.

(3) **Ionic Liquids and Deep Eutectic Solvents with Nature**. *Indian Institute of Technology Guwahati*, Guwahati, India, March 10–13, 2021.

(4) **Dynamic Light Scattering Technique & Gas Adsorption Technique**. *Indian Institute of Technology Guwahati*, Guwahati, India, March 7, 2022.